The Dissertation Committee for Yawei Liang Certifies that this is the approved version of the following dissertation:

New Materials for Advanced Applications: Electrochromism, Electrocatalysis, and Bioimaging

Committee:

Richard A. Jones, Supervisor

Emily L. Que

Michael J. Rose

Charles Buddie Mullins

Alan Campion

New Materials for Advanced Applications: Electrochromism, Electrocatalysis, and Bioimaging

by

Yawei Liang, B.S.

Dissertation

Presented to the Faculty of the Graduate School of

The University of Texas at Austin

in Partial Fulfillment

of the Requirements

for the Degree of

Doctor of Philosophy

The University of Texas at Austin

May 2017

Dedication

To my parents,

Thank you for your endless support and love.

Acknowledgements

First, I would like to thank Dr. Bradley J. Holliday for providing me the opportunity to study at UT, and for his support and guidance when I first started at graduate school. I would also like to thank Dr. Richard A. Jones for advising me during the past year and supporting my graduate school career. His generous help, guidance and mentorship have helped me along the way to finish my study at UT, and I always thank him for that. Additionally, I would like to thank my committee: Dr. Alan Campion, Dr. Charles Buddie Mullins, Dr. Michael J. Rose, and Dr. Emily L. Que for their help and support.

I would like to thank Dr. Matthew Raiford, Dr. Minh Nguyen, Dr. Kory Mueller, Dr. Sarah Moench, and Dr. Kristin Suhr for teaching me fundamental skills to perform chemical research when I joined the group. I would also like to thank my lovely labmates-Minh, Kory, Sarah, Kristin, Dan, Leander, Matt, beauty Claudina, beauty' Trang, Rob, Ty, and Weiran. Your friendship makes my every day in lab, and thank you for helping, discussing and criticizing my research.

I would like to thank Dr. Hugo Celio, Dr. Vincent Lynch, and Da Xie for running XPS, X-ray diffraction, and chemistry simulation experiments for me. I would also like to thank the NMR and Mass Spectroscopy facilities in the chemistry department at UT.

I would like to thank Xiang Li for discussing electrochemistry-related problems with me, Ryan Pekarek for helping me with the XPS data, Da and Zhulin for introducing basic simulation concepts to me.

I would like to thank my parents. Dad, thank you for being a super hero when I was a kid. Mom, thank you for being the most beautiful and the bravest female in my heart.

To my best friend and my fiancé-Jiajie, thank you for choosing me to face the life's challenges together with you, and thank you for encouraging me to be a better person.

New Materials for Advanced Applications: Electrochromism, Electrocatalysis, and Bioimaging

Yawei Liang, Ph.D.

The University of Texas at Austin, 2017

Supervisor: Richard A. Jones

Electrochromic materials have the applications in smart-windows, electrochromic mirrors, and electrochromic display devices. Three Fe(II) bis(terpyridine)-based complexes with thiophene (**2.2a**), bithiophene (**2.2b**), and 3,4-ethylenedioxythiophene (**2.2c**) side chains have been synthesized to provide two terminal active sites for electrochemical polymerization. The thin film of **poly-2.2b** has been electrodeposited on ITO/glass substrate and was characterized using electrochemistry, X-ray photoelectron spectroscopy, UV-vis spectroscopy and atomic force microscopy. The film exhibited great optical contrast with a change of transmittance of 40% upon applying voltage to it, and a coloration efficiency of 3823 cm^2C^{-1} with a switching time of 1 s. It also demonstrated commonplace stability and reversibility, with a 10% loss in peak current intensity after 200 cyclic voltammetry (CV) cycles and almost no loss in change of transmittance after 900 potential switches between 1.1 V and 0.4 V (vs Fc^+/Fc).

Lanthanide complexes have unique photophysical properties that can be utilized in areas such as bioimaging, bio-sensors, fluoroimmunoassays, and organic light emitting diodes. Our group has previously synthesized the complex-Eu(III) tris-(2-thenoyltrifluroacetonate) 2,6-bis(pyrazoly)pyridine [Eu(bppy)$(tta)_3$], which has a quantum yield of 60% in dichloromethane solution and 90% in solid state. Various functionalities

were introduced on the original bppy ligand, such as carboxyl, hydroxyl, and amino groups to provide the active sites for bioconjugation purpose. Four Eu(III)(R-bppy)$(tta)_3$ complexes (**3.2a**-**3.2d**) were synthesized and their photophysical properties were fully characterized. Their quantum yields range from 20.2% to 45.4% and lifetimes range from 383.9-417.2 μs.

Efficiently transforming the greenhouse gas CO_2 into liquid fuels or useful synthetic precursors would have a significant impact on balancing the global carbon cycle. A series of mononuclear Re(I) complexes with dipyrido[3,2-a:2',3'-c]phenazine (dppz) derived ligands (**4.2a**-**4.2d**) were synthesized and investigated as homogeneous electrocatalysts for CO_2 reduction. CV studies showed large enhancements of the cathodic currents under CO_2 atmosphere for the Re(I) complexes, indicating the electrocatalytic reduction of CO_2. CO was confirmed as the only gaseous phase product by gas chromatography. Compared to the Lehn catalyst, a benchmark catalyst for reducing CO_2 to CO, the Re(I) dppz complex with a larger degree of conjugation transformed CO_2 into CO at a lower overpotential.

Table of Contents

List of Tables

List of Figures

List of Schemes

Chapter 1: Functional Metal Complexes for Electrochromism, Electrocatalysis, and Bioimaging Studies

1.1 Electrochromic Conducting Metallopolymers

1.1.1 Electrochromic Materials

An electrochromic (EC) material can be characterized by its reversible and stable color change when a voltage is applied. The color of an EC material usually interchanges between a transparent (or bleached) and a colored state, or between two different colored states. The applications of EC materials include controllable light devices for optical information storage, controllable aircraft canopies, glare-reduction systems for offices, and smart windows for intelligent buildings.[1-3] The parameters used for characterizing an EC material include contrast ratio (or optical contrast, ΔT%: change of light transmittance between the bleached and colored states), coloration efficiency (or CE: absorbance change per charge injected per unit area), response time (time taken to observe a color change in the material), and stability or life cycle of the material. These data are obtained from cyclic voltammetry, chronoamperometry, and *in situ* spectroscopy. The solid-state EC device is commonly constructed in a sandwich configuration (Figure 1.1).[4]

Most electrochromic phenomena in early reports were observed in WO_x thin films, and therefore tungsten oxide is the most commonly used material in the smart windows market.[2, 5, 6] Nonetheless, other transition metal oxides such as MoO_x and VO_x display electrochromic properties as well.[7-9] In addition, Prussian blue,[10] viologens,[11, 12] metal phthalocyanines,[3] and conducting polymers[13] have also been studied for their electrochromic behaviors. The commonly accepted electrochromic mechanisms and some of these materials are summarized in Table 1.1.[1, 4, 14, 15]

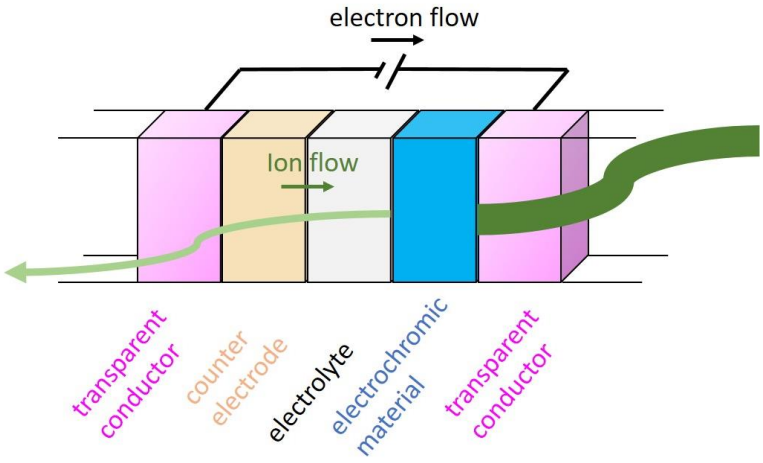

Figure 1.1. Schematic diagram of a solid-state electrochromic device.

Table 1.1. Commonly studied electrochromic materials.

Electrochromic Materials		Coloration Mechanism
WO_3 + $x(Li^+ + e^-)$ → $Li_xW^{VI}_{(1-x)}W^V_xO_3$ transparent → blue	(**1.1**)	intervalence charge transfer (IVCT)
$[Fe^{III}Fe^{II}(CN)_6]^-$ + e^- → $[Fe^{III}Fe^{II}(CN)_6]^{2-}$ blue → transparent	(**1.2**)	intervalence charge transfer (IVCT)
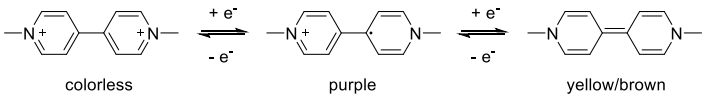 colorless ⇌ purple ⇌ yellow/brown	(**1.3**)	charge transfer (CT)
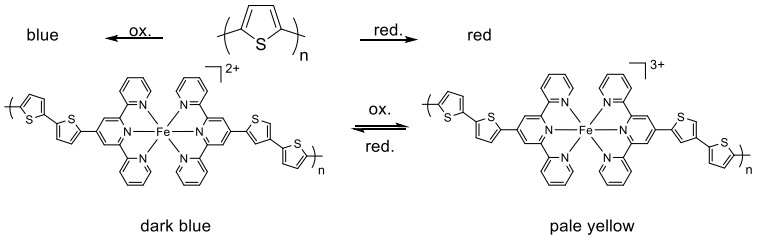 blue ⇌ red dark blue ⇌ pale yellow	(**1.4**) (**1.5**)	doping/undoping metal ligand charge transfer (MLCT)

It should be noted that, conducting metallopolymers (CMPs) encompass a unique class of hybrid materials which contain both the traditional metal complex core structure and the conducting polymer backbones, and have been of great interest to researchers over the years.[16-18] The colors of traditional metal complexes mainly come from the metal to ligand charge transfer (MLCT), intervalence charge transfer (IVCT), intraligand charge

transfer (ICT), and related visible-region electronic transitions. The colors can also be altered or eliminated upon oxidation or reduction of the materials because of the involvement of valence electrons. Based on the electropolymerization of a wide range of metal complex monomers, the resulting CMPs have been applied to electrochromic systems with several advantages, including the catalyst-free polymerization process, direct grafting the doped conducting polymers onto the electrode surface, and easy control of the film thickness by integration of the input charge.[19-30] By altering the metal center in monomers, polymeric thin films in different colors can be obtained after electropolymerization, providing ease of control over the color of the electrochromic materials from a synthetic perspective.[28] More examples of constructing the electrochromic conducting metallopolymers via the electropolymerization method can be found in 1.1.2.

1.1.2 Electrochromic Conducting Metallopolymers

Certain ruthenium(II) complexes are well-documented for near infrared (NIR) electrochromism.[20-24] In 2011 Yao and coworkers reported a reductive electropolymerization of the biscyclometalated ruthenium complex (**1.6**). The metallopolymer exhibited NIR electrochromism with tricolor switching. A 40% contrast ratio at 1165 nm, and a 250 cm^2C^{-1} coloration efficiency was observed as a result of switching the IVCT and MLCT transitions of individual mixed valent dimetallic units.[22] Additionally, other ruthenium(II) complexes with N-N bidentate ligands functionalized with vinyl (**1.7**-**1.9**) or thiophene groups (**1.10a**-**1.10c**) have been electropolymerized and studied for their NIR electrochromic properties.[20-24] Apart from using ruthenium-containing metallopolymers for NIR electrochromic application, a cyclometalated platinum(II) chloride structure with a 4-(diphenylamino)phenyl group (**1.11**) has also been reported by Liu and coworkers in 2015. The resulting metallopolymer exhibited low-

voltage-controlled anodic coloration near-infrared (NIR) electrochromism with a significant optical contrast ratio (ΔT% = 88.8% at 820 nm), a fast response time (1.9 s for the coloration step and 2.3 s for the bleaching step), and a relatively high coloration efficiency (CE = 363.3 cm^2C^{-1}) as a result of reversible switching of the MLCT/ICT and the dication absorption transitions.[19]

A diversity of metal centers have been employed in metallopolymers for visible-region electrochromism. N-heterocyclic carbene (NHC)-based metallopolymers, containing iridium (**1.12a**), gold (**1.12b**), copper (**1.13a**) or silver (**1.12c**, **1.13b**) metal centers with thiophene groups at each end of the monomers have been investigated for visible electrochromism.[25, 26] Additionally, an Fe(II) complex with N-(pyridin-2-ylmethylidene)-2,5-bis(thiophen-2-yl)aniline ligand (**1.14**) was prepared to construct a conducting electrochromic metallopolymer film with a color change from orange to black under applied potential (0.6 V vs Ag).[27] More recently, metallopolymers containing metal bis(terpyridine)-based complexes (metal = Fe, Ru) core structures with substituted electropolymerizable groups [N',N'-disubstituted aminophenyl (**1.15-1.17**) and bithiophene (**1.18**)] have been utilized to make electrochromic thin films as well.[28-30] Remarkably, the resulting metallopolymer from the electropolymerization of **1.18**, reported by Jones and coworkers in 2016, shows an electrochromic behavior at 596 nm with a 40% contrast ratio, a response time of 0.75 s, and a coloration efficiency of 3823 cm^2C^{-1}.[30]

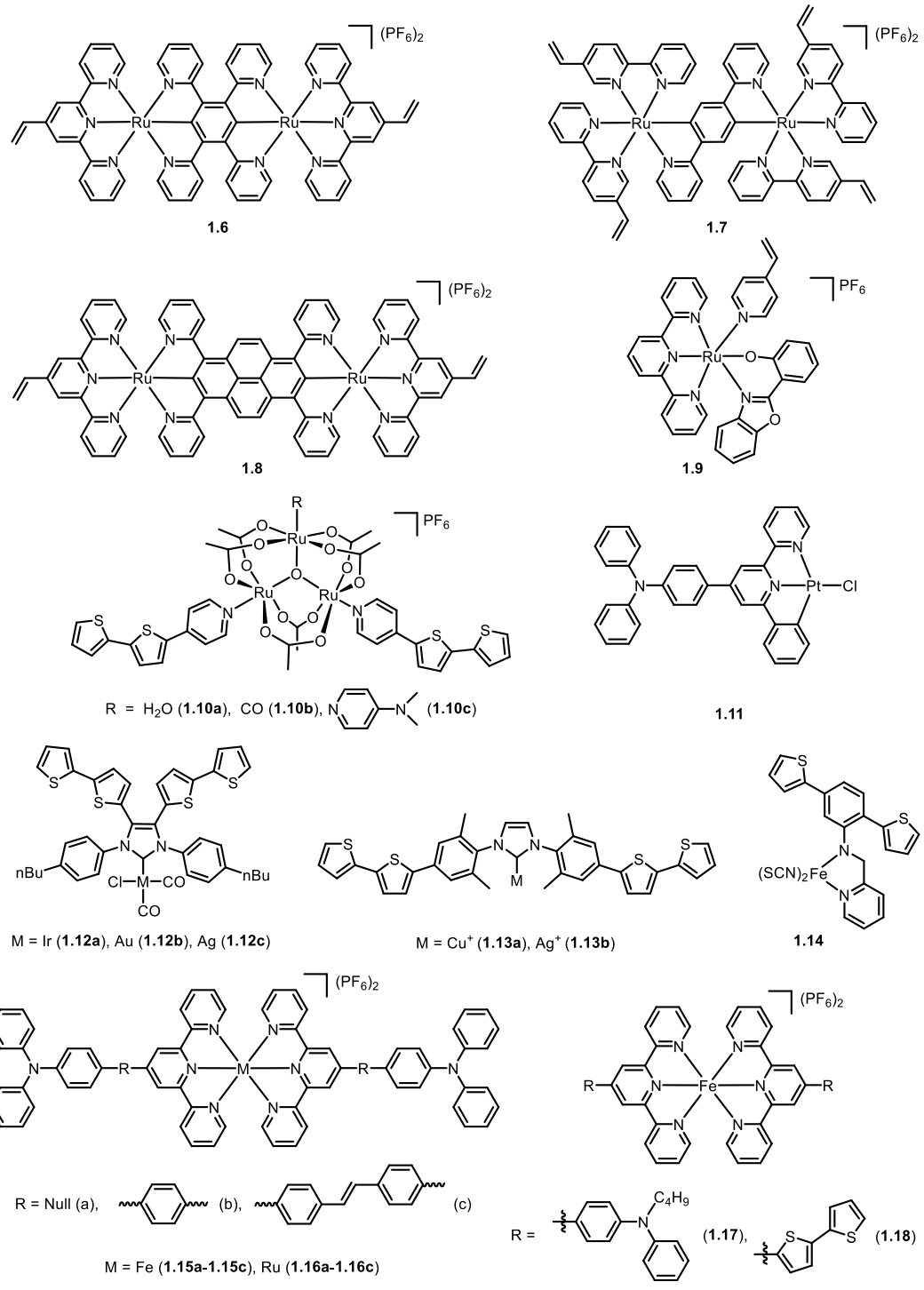

Figure 1.2. Previously reported electropolymerizable metal complexes used for electrochromic materials.

The optical contrasts (ΔT%) of several reported CMPs are listed in Table 1.2, ranging from 20% to 90% at the given wavelengths. The wavelength (NIR or visible) is often chosen at which the electrochrome exhibits the highest value of ΔT%. The surface coverage of the polymeric thin film affects the electrochromism considerably. It was found that too low or too high of a polymer coverage on the working electrode surface would give a lower value of ΔT%. However, films with low contrast ratios normally have relatively short response times.[20] Electrochromic CMPs have CE values on the order of 10^2 to 10^3 cm^2C^{-1} (Table 1.2). Considering that the CE value of MWO_x is generally about 150-200 cm^2C^{-1},[31, 32] electrochromic metallopolymers have a very promising future for industrial applications because of the high optical contrast and coloration efficiency. The response times of electrochromic metallopolymers range from 0.75 to 20 seconds, and their film stabilities vary from only a few to thousands of potential switching cycles, which is considered a major drawback compared to that of the electrochromic metal oxides.

Table 1.2. Common values of ΔT%, CE, and response times reported in the literatures of electropolymerized metallopolymers.

polymer	wavelength (nm)	ΔT%	CE (cm^2C^{-1})	response time (s)
poly-**1.6**	1165	40	250	6
poly-**1.7**	1300	41	200	15-20
poly-**1.8**	2050	35	220	2
poly-**1.11**	820	88.8	363.3	2.1
poly-**1.17**	579	20.3	164	2.2
poly-**1.18**	596	40	3823	0.75

The conducting metallopolymers discussed herein are mainly deposited on transparent ITO/glass surfaces by reductive or oxidative electropolymerizations for

electrochromic applications. The vinyl (**1.6-1.9**), thiophene (**1.10**, **1.12a-1.12c**, **1.13a-1.13b**, **1.14**, **1.18**), and diphenylamine (**1.11**, **1.15a-1.15c**, **1.16a-1.16c**, **1.17**) groups are the most common functionalities in the monomer structures for electropolymerization purposes. Commercialization opportunities for developed electrochromic metallopolymeric films are enormous, such as electrochromic glazing windows for cars and buildings, and multi-purpose electrochromic devices. Recent work is still focusing on the discovery of new metallopolymers with better performances. Future studies need to focus on ways to produce devices with large areas and which can be efficiently prepared using material of low cost, high performance and with long lifetimes.

1.2 Luminescent Europium Complexes for Time-Gated Fluorometry

1.2.1 Luminescent Lanthanide Complexes

The emission wavelengths of the trivalent lanthanide [Ln(III)] ions range from ultraviolet to near-infrared (NIR). Among them, Eu(III) and Tb(III) have been extensively studied, due to their intensive visible emissions. NIR lanthanide emitters such as Sm(III), Dy(III), Pr(III), Ho(III), Yb(III), Nd(III), and Er(III) have attracted attention in recent years, because their longer emission wavelengths are more efficient in penetrating human tissue than visible light.[33] The 4f electrons of Ln(III) are shielded by the $5s^1 5p^6$ sub-shells, resulting in very sharp emission peaks. The 4f-4f electron transitions in Ln(III) ions are forbidden due to the Laporte rule, however, the rule can be relaxed by several mechanisms, such as molecular vibration and *J*-mixing. The low probability of f-f electronic transitions gives the characteristic long lifetimes of Ln(III) luminescence.[34] Their sharp emission peaks and long lifetimes (10-10^3 μs) make Ln(III) ions much more useful as bioimaging probes than the common organic fluorophores.[35]

Ln(III) ions have very low molar absorptivities (ε = 1-10 $M^{-1}cm^{-1}$). Because the f-f electronic transition is forbidden, it is difficult to excite Ln(III) ions by light sources other than powerful lasers. One way of sensitizing Ln(III) is to use chromophores as antenna ligands (ε = 10^4-10^5 $M^{-1}cm^{-1}$) for light absorption, through a process called the "antenna effect". Figure 1.3 illustrates the process which consists of several steps: (i) population of the excited states of the antenna ligands, (ii) subsequent intersystem crossing (ISC) from S_1 to T_1, (iii) energy transfer (ET) from the T_1 energy level of the ligand to the luminescent excited state of the Ln(III). The overall quantum yield (Φ_{tot}) of the Ln(III) complex upon excitation is determined by the efficiency of sensitization (η_{sens}) and the quantum yield (Φ_{Ln}) of the Ln(III) luminescence step (equation 1.1). The efficiency of sensitization (η_{sens}) is regulated by the intersystem crossing and the energy transfer steps. The energy transfer can occur via either Förster or Dexter mechanisms, depending on the position and the nature of the chromophore.[33] In order to have a fast energy transfer, a shorter distance between the chromophore and the Ln(III) metal center is advantageous, which can be achieved by directly coordinating the metal center to the antenna ligand. In addition, in order to have an efficient energy transfer, the energy of the triplet excited state of the chromophore should be at least 1850 cm^{-1} (0.23 eV) higher than the lowest emitting energy level of Ln(III), otherwise back-energy transfer may take place.[33] Figure 1.4 shows some typical ligands forming highly luminescent complexes with Eu(III) or Tb(III) ions.[36]

The quantum yield (Φ_{Ln}) of the Ln(III) luminescence step is determined by the radiative rate constant (k_r) and the non-radiative constant (k_{nr}). Because the lanthanide ion usually possesses a relatively long-lived excited state, it can undergo non-radiative energy transfer to high frequency vibrational oscillators such as O-H, N-H, and to a smaller extent, C-H. As a result, the presence of these functional groups may quench the Ln(III) luminescence.[37, 38]

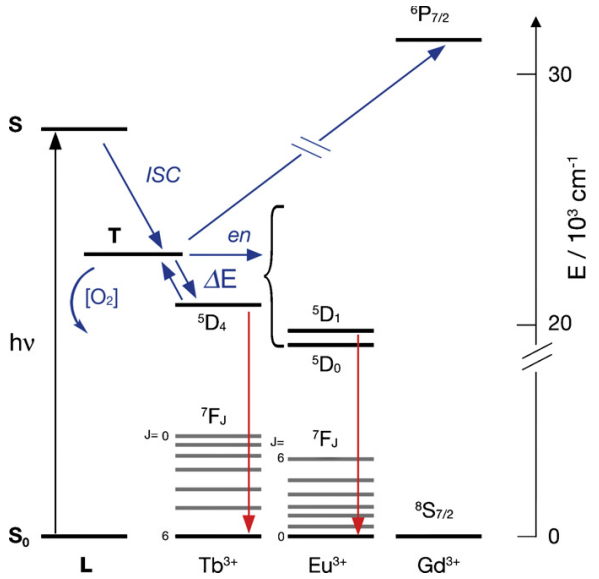

Figure 1.3. The antenna effect for sensitization of the luminescence in some lanthanide cations. Blue lines indicate the non-radiative processes, and red lines indicate the radiative processes. Adapted from Tondello *et al. Coord. Chem. Rev.* **2010**, *254*, 487.

$$\Phi_{tot} = \eta_{sens}\Phi_{Ln} \qquad \text{(eq 1.1)}$$

$$\frac{1}{\tau_R} = A_{MD,0}n^3\left(\frac{I_{tot}}{I_{MD}}\right) \qquad \text{(eq 1.2)}$$

$$\Phi_{Ln} = \frac{k_r}{k_r+k_{nr}} = \frac{\tau_{obs}}{\tau_R} \qquad \text{(eq 1.3)}$$

To quantify the parameters mentioned above, several methods have been developed, especially with Eu(III) complexes.[39] The overall quantum yield (Φ_{tot}) and observed lifetime (τ_{obs}) of Eu(III) luminescence can be directly measured by monitoring the Eu(III) emission peak via fluorometry. The radiative (or natural) lifetime (τ_R), by definition, is not affected by the processes illustrated in Figure 1.3, and can be calculated from equation 1.2 if assuming that both the energy of the $^5D_0 \rightarrow {}^7F_1$ transition and its dipole strength are constant.[39] In that equation, n is the refractive index of the medium (solvent), $A_{MD,0}$ is the spontaneous emission probability for $^5D_0 \rightarrow {}^7F_1$ transition in *vacuo*, and $\frac{I_{tot}}{I_{MD}}$ is the ratio of the total area of the corrected Eu(III) emission spectrum to the area of the

$^5D_0 \rightarrow {}^7F_1$ emission band. The value of $A_{MD,0}$ equals 14.65 s^{-1} from theoretical calculations. The quantum yield of the Ln(III) luminescence step (Φ_{Ln}) can be calculated from the observed lifetime (τ_{obs}) and the radiative lifetime (τ_R) based on equation 1.3.[39]

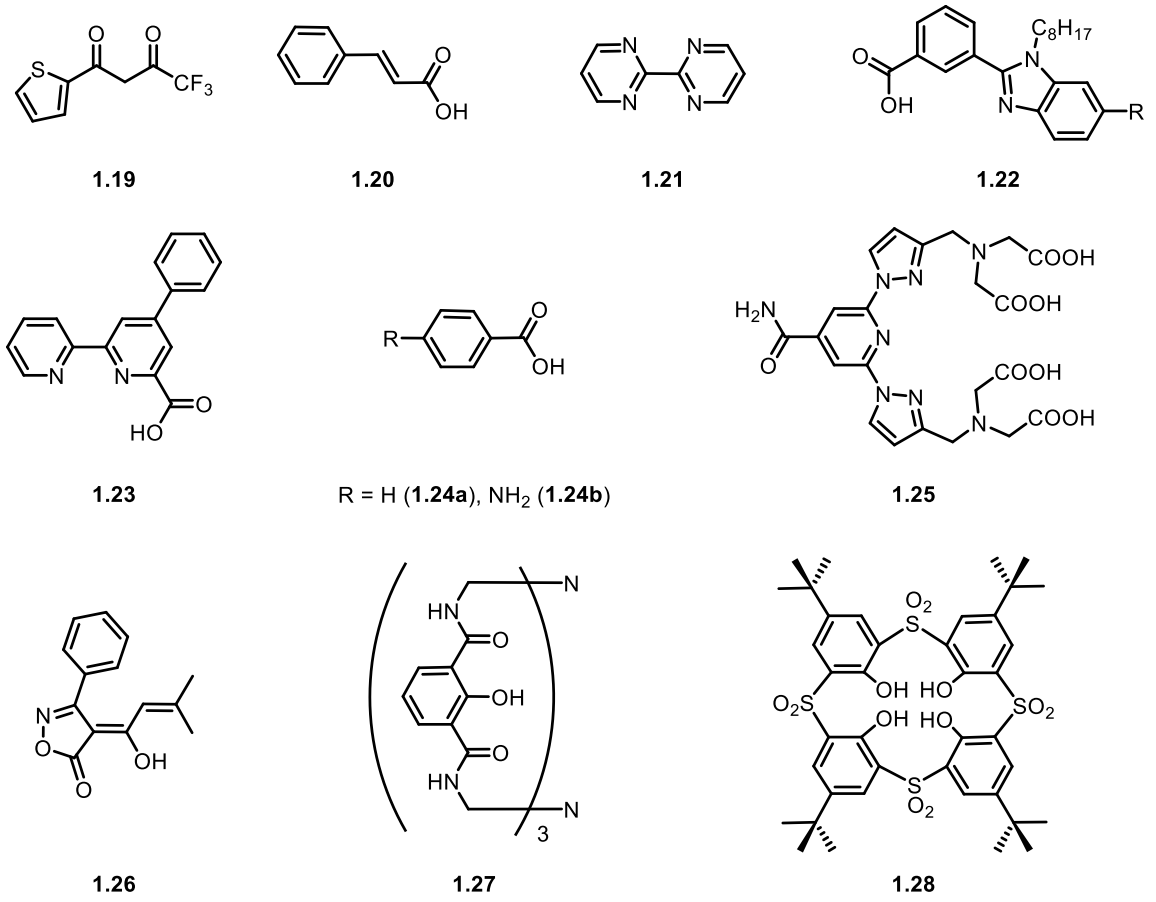

Figure 1.4. Ligands giving luminescent Eu(III) or Tb(III) complexes.

1.2.2 Eu(III) Complex-Based Fluorescence Labels

Because of the large Stokes shifts, sharp emission peaks, long luminescence lifetimes, the lanthanide chelates have broad applications as luminescent probes for highly sensitive, time-gated (or time-resolved) fluoroimmunoassays, DNA hybridization assays, fluorescence microscopy bioimaging, and other analytical techniques.[40-42] The

fluorescence lifetimes of lanthanide complexes vary from 10-10^3 μs, while the decay time of background luminescence is around of 1-20 ns.[43] As a result, by using the luminescent lanthanide chelates as bio-labels for time-gated fluorometry, the nonspecific background luminescence from the biological sample, the cuvette materials, and the scattering light can be effectively eliminated. Therefore, time-gated fluorometers using lanthanide complexes are several orders of magnitude more sensitive than conventional ones. The Eu(III)-containing compounds, usually in chelate form, are one type of the most well-studied lanthanide fluorescent bio-labels for biological studies.[35, 44]

For biological molecule labeling, a labeling reagent should have a good solubility, a high stability in an aqueous environment, and an appropriate coupling group. In addition, an efficient Eu(III) label must have a strong coordination site to the Eu(III) ion in order to saturate the first coordination sphere of the Eu(III) ion, as well as have good energy matching between the antenna ligand and the excited state of Eu(III).[35, 44] Figure 1.5 illustrates a typical luminescent lanthanide label and its basic constituents.

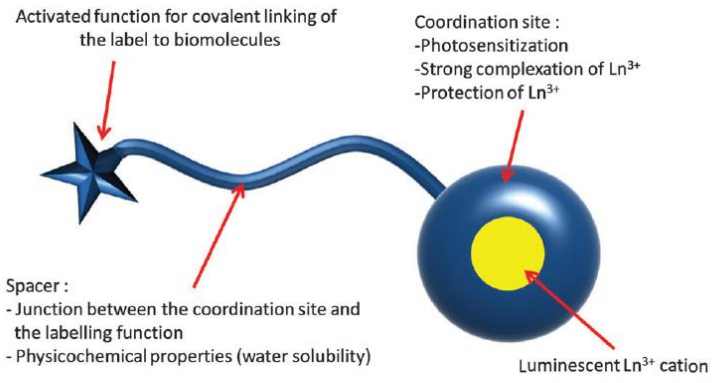

Figure 1.5. Schematic representation of a luminescent lanthanide label and its basic constituents. Adapted from Charbonnière *et al. Chem. Commun.* **2016**, *52*, 5080.

As noted above, the covalent interactions between Eu(III) labels and biological molecules require the introduction of appropriate functional groups in the design of the ligands. The functional groups can be activated *in situ*, or the activated functional group can be achieved during the ligand synthesis.[43, 45, 46] The *in situ* activation methodology may cause undesired cross-coupling reactions (activation of the biological molecules itself), therefore, the latter approach providing an activated function that will react with a specific biological molecule is more preferred. Figure 1.6 shows several most commonly seen activated functional ligands in Eu(III) bio-labels in the literature.[44] The commonly seen functional groups in bioconjugation from the biomolecule side are aliphatic amino and thiol groups, which can be found in the N-terminus of proteins, the amino acids lysine or cysteine.[44] The chlorosulfonyl group is an activated function commonly seen in Eu(III) bio-labels (**1.30c**,[47, 51] **1.31**,[43] **1.32**[48]). The chlorosulfonyl group generating from the reaction of chlorosulfonic acid on aromatic phenyl rings can react with amine, forming sulfonamide bonds. Moreover, N-hydroxysuccinimide groups (NHS or its more water-soluble sulfonated derivative, sulfo-NHS) are very attractive activated functionalities which can react with amine, resulting in amide bonds (**1.34b**).[49] They are acquired from the reaction of a carboxylic acid with N,N'-dicyclohexylcarbodiimide (DCC) or 1-ethyl-3-(3-dimethylaminopropyl)carbodiimide (EDCI) in the presence of N-hydroxysuccinimide.[50, 51] Furthermore, the dichlorotriazine group (**1.36b**,[52] **1.37c**[45]) obtained from the reaction of cyanuric chloride with amines can serve as an activated function in Eu(III) bio-labels as well.[53] Additionally, the isothiocyanate group, generated from the reaction of an aromatic primary amine with thiophosgene, is another well-documented functionality in Eu(III) bio-labels (**1.36a**,[52, 54] **1.37a**[55]). Upon reaction with amines, a strong thiourea bond between the label and the biological molecule can be formed. Last but not the least are thiol functions. They are less common than amino groups

in proteins but are present in cysteine residues. The most commonly seen functionality in bio-labels targeting thiol groups is maleimide (**1.36c**),[56] which can react with thiol though a Michael addition, forming a thioether bond. Other thiol directed labelling functions include methanethiosulfonate groups etc (**1.38**).[57] There are other less common activated functionalities used in bio-labels, which can be found in a recent review.[44]

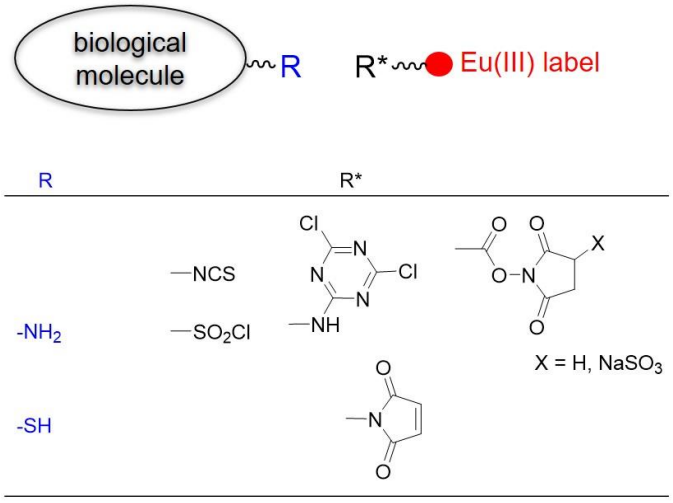

Figure 1.6. Representative examples of Eu(III) labels bearing amine and thiol targeting activated functions.

Since β-diketone is a commonly used antenna ligand to sensitize Eu(III) luminescence, several chlorosulfonylated tetradentate-diketones incorporating two β-diketone subunits were synthesized and were developed their applications for protein labeling and time-resolved fluorescence bioassays (Figure 1.7).[43, 47, 58-60] It has been found that the tetradentate structure increased both the stability of the complex and the fluorescence intensity of the Eu(III) emission, due to the decrease in number of coordinated water molecules in the first coordination sphere of Eu(III) ions.[61] As discussed earlier, the

chlorosulfonylated β-diketone Eu(III) complexes can be conjugated to proteins by the formation of a sulfonamide bond.

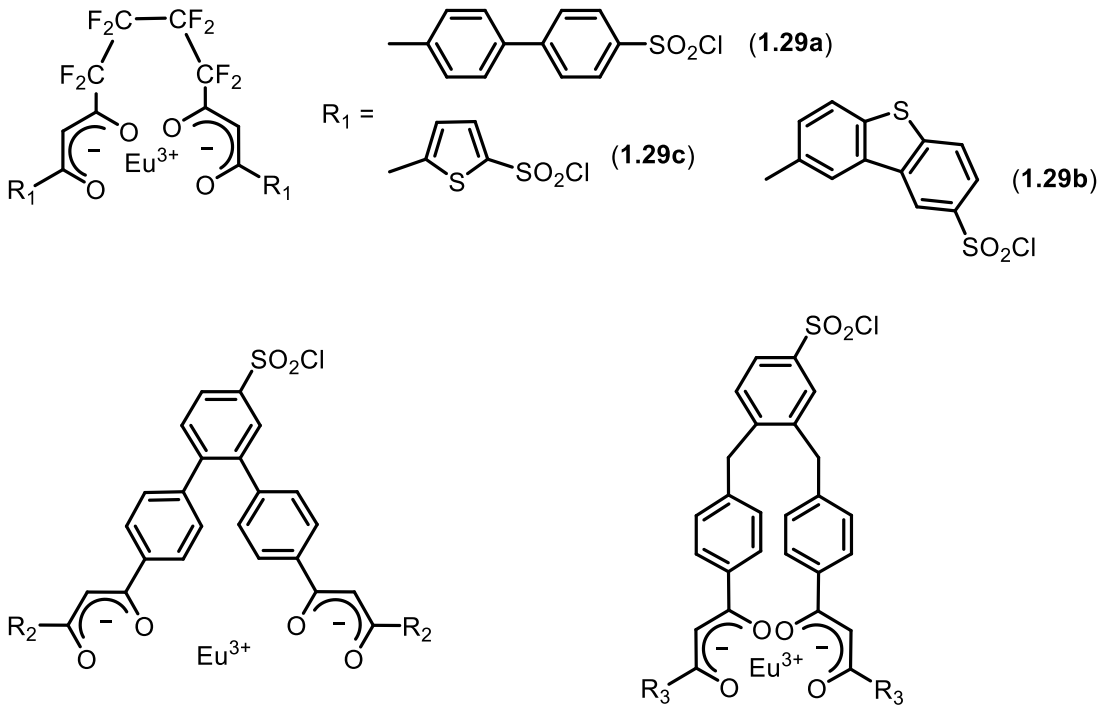

Figure 1.7. Structures of several chlorosulfonylated tetradentate β-diketones Eu(III) bio-labels.

The aromatic amine derivative is another type of ligand which can form highly luminescent complexes with the Eu(III) ion. These ligands mainly derive from the structures of 2,2'-pyridine, 2,2',2''-terpyridine, and 1,10-phenanthroline. The polyacid moiety leads to very soluble Eu(III) complexes in aqueous solutions. The chlorosulfonyl (**1.32**, **1.33**), N-hydroxysuccinimide ester (**1.34a**, **1.34b**), isothiocyanato (**1.36a**,**1.37a**) or (4,6-dichloro-1,3,5-triazin-2-yl)amino group (**1.36b**, **1.37c**) shown in Figure 1.8 can be coupled to proteins or other amino-containing compounds in an aqueous buffer.[44, 45, 48, 49,

[52, 54, 55] The amino-containing labels (**1.35**, **1.37b**) need to be activated firstly using 2,4,6-dichloro-1,3,5-triazine, then the resulting compound with the (4,6-dichloro-1,3,5-triazin-2-yl)amino group can further react with biological molecules (Figure 1.9).[35, 62]

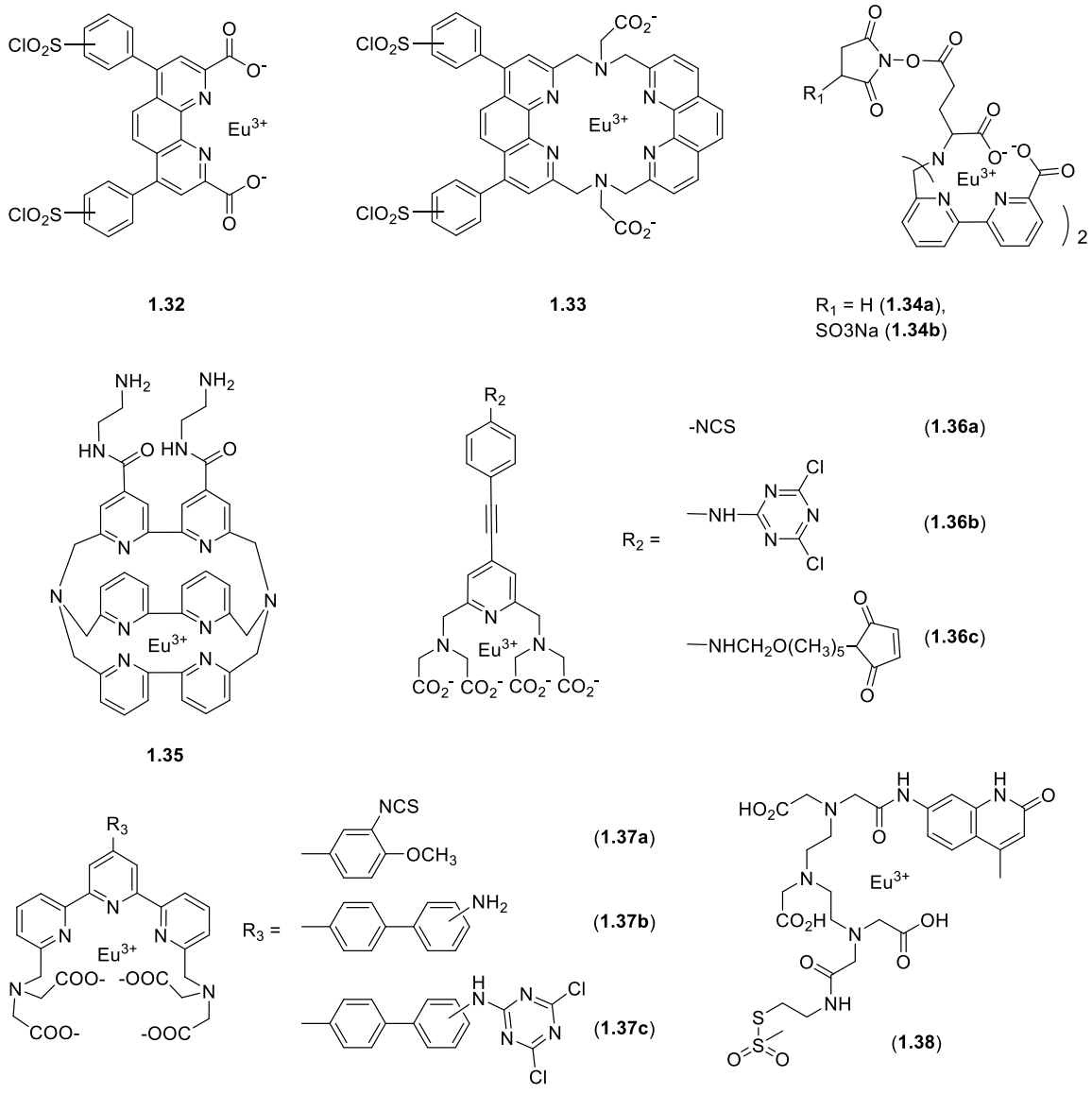

Figure 1.8. Structures of some fluorescent Eu(III) complexes with aromatic amine derivatives than can be used as bio-labels.

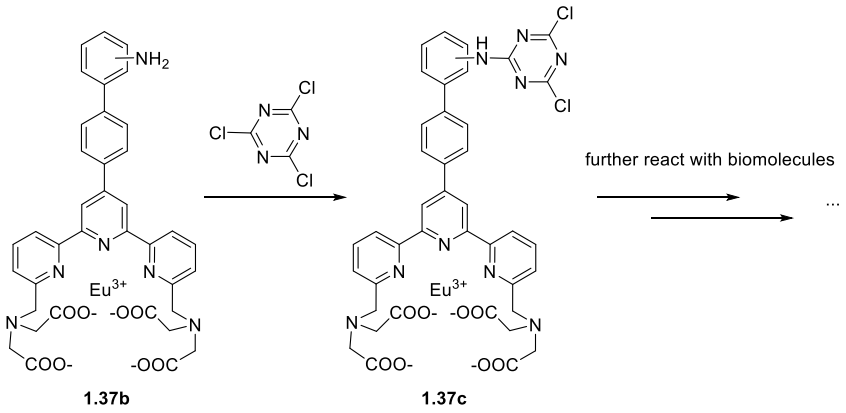

Figure 1.9. Activation of **1.37b** with 2,4,6-dichloro-1,3,5-triazine.

Except for the discrete Eu(III) molecular complexes with bioconjugable groups, there are other methods in the literature to approach the Eu(III)-containing luminescent bio-labels, eliminating the solubility and stability issues by either enclosing the Eu(III) complexes into silicate/protein-based particles[63-65] or utilizing lanthanide-doped luminescent nanocrystals.[66, 67] These topics are not included in this chapter.

The sensitivity, selectivity, and stability of lanthanide complexes are very crucial when using them as bio-labels. These requirements often lead to long-step syntheses of intricate ligands. Furthermore, the resulting complexes must be able to penetrate cells for practical applications of intracellular probes. More work to address all these challenges are expected in the next decades.

1.3. Rhenium Complex Catalyzed Electrochemical Reduction of Carbon Dioxide

1.3.1 Electrochemical Reduction of Carbon Dioxide

The electrochemical reduction of carbon dioxide is the conversion of carbon dioxide into its reduced form using electrical energy. The research in electrochemical and photochemical reduction of CO_2 is growing because of the increasing concentration of CO_2

in the atmosphere and the steady growth in global energy demand. Direct use of CO_2 in industry is very limited, most of which is used as a carbon source in carboxylation reactions and other transformation reactions to produce urea, methanol, and organic carbonates.[68] Therefore, the other strategy to balance the global carbon cycle is to transfer the excess CO_2 into other chemical feedstocks in different applications. Since the carbon atom in the CO_2 molecule is in its most oxidized form and relatively stable, it requires a large amount of energy to convert CO_2 into other chemicals (Figure 1.10). The reduction potential of CO_2 without proton coupling is even higher due to a configuration change from linear to bent after the molecule is reduced to its radical form.

$$CO_2 + 2H^+ + 2e^- \longrightarrow CO + H_2O \qquad E^0 = -0.53\ V \quad \text{eq (1.4)}$$

$$CO_2 + 2H^+ + 2e^- \longrightarrow HCO_2H \qquad E^0 = -0.61\ V \quad \text{eq (1.5)}$$

$$CO_2 + 6H^+ + 6e^- \longrightarrow CH_3OH + H_2O \qquad E^0 = -0.38\ V \quad \text{eq (1.6)}$$

$$CO_2 + 8H^+ + 8e^- \longrightarrow CH_4 + 2H_2O \qquad E^0 = -0.24\ V \quad \text{eq (1.7)}$$

$$CO_2 + e^- \longrightarrow CO_2^{\bullet -} \qquad E^0 = -1.90\ V \quad \text{eq (1.8)}$$

pH 7 in aqueous solution vs normal hydrogen electrode (NHE), 25°C, 1 atm gas pressure, and 1 M for other solutes

Figure 1.10. Thermodynamic potentials for various CO_2 reduction products.

Regarding catalysts for electrochemical reduction of CO_2, there are three types of catalysts researchers are currently focusing on, which are described in Figure 1.11: (1) heterogeneous metallic catalysts; (2) heterogeneous nonmetallic catalysts; (3) homogenous molecular catalysts (coordination and organometallic complexes).[69-73] While appreciating the first two approaches, molecular catalysts have greatly attracted the attention of researchers because the catalyst performance can be sophisticatedly tuned via modification

of the chemical structures, and their detailed catalytic mechanisms are easier to study than others.

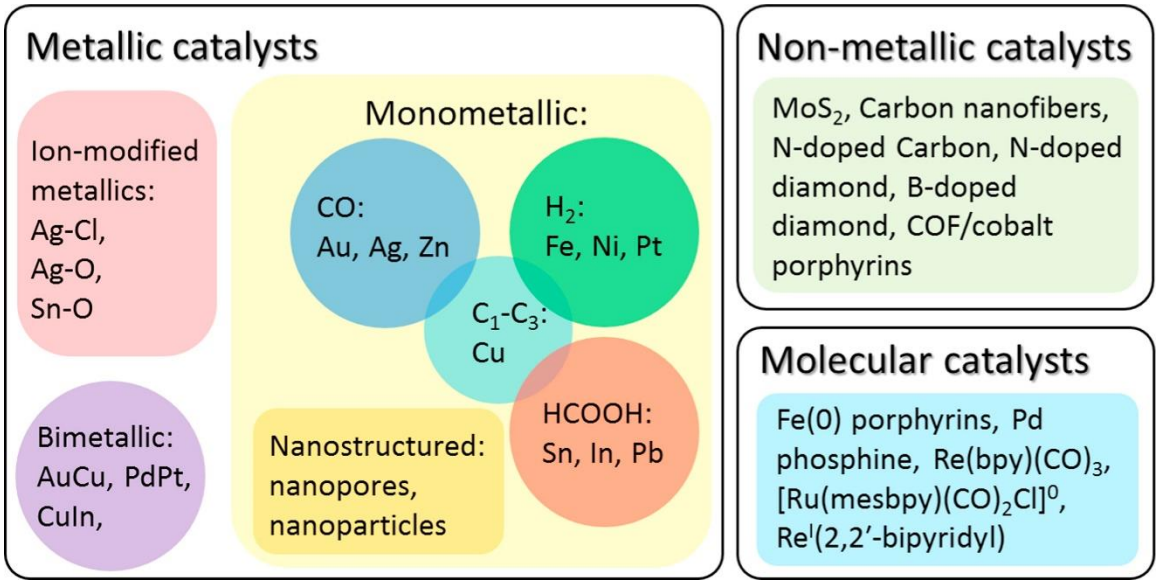

Figure 1.11. Three types of catalysts developed for electrochemical CO_2 reduction. Adapted from Jiao *et al. Nano Energy* **2016**, *29*, 439.

1.3.2 Electrocatalytic Reduction of CO_2 by Rhenium(2,2'-bipyridyl)-Type Catalysts

Electrocatalytic reduction of CO_2 by homogeneous molecular catalysts have been studied intensively in the past few decades.[73-84] To mediate the multi-electron/multi-proton transfer during the electrochemical reduction of CO_2, the molecular catalysts must be able to perform multiple reductions, either by reducing the metal center or by reducing the ligand scaffold. In this context, polypyridine ligands are appropriate to use as ligands for molecular catalysts.[72] Among the many reported homogeneous polypyridine-containing catalysts for CO_2 reduction, [*fac*-Re(bpy)$(CO)_3$X] (bpy = 2,2'-bipyridine; X = Cl, Br, or a coordinating solvent molecule) "Lehn's catalyst" (**1.39**), exhibits relatively high activity and turnover number.[85, 86] The mechanism of electrocatalytic reduction of CO_2 by Lehn's

catalyst was proposed by Meyer and coworkers in 1985, involving two different electrocatalytic pathways. In the two-electron reduction pathway (Scheme 1.1, A), the two-electron reduced intermediate $[Re(bpy)(CO)_3]^-$ with one negative charge is claimed to be the active species for CO_2 binding and reduction to form CO. In the one-electron pathway (Scheme 1.1, B), the proposed neutral intermediate $[Re^0(bpy)(CO)_3]$ is presumably reactive to CO_2.[86-89]

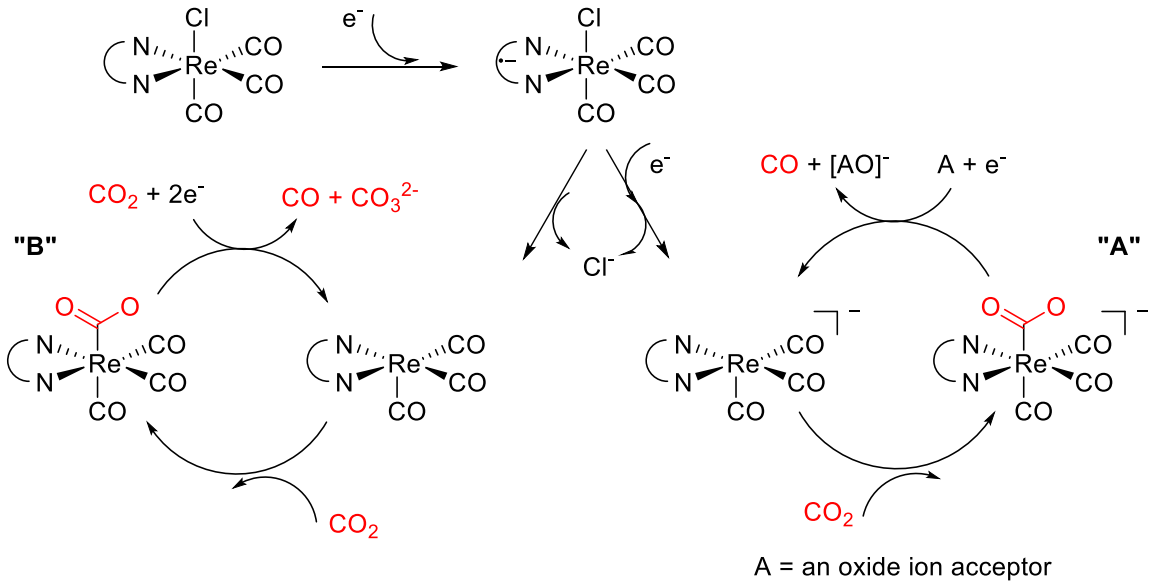

Scheme 1.1. One- and two-electron pathway mechanisms of electrochemical reduction of CO_2 using the Lehn catalyst proposed by Meyer in 1985.

The two-electron reduction pathway is the most accepted mechanism for electrochemical reduction of CO_2 in acetonitrile solution. Both infrared spectroscopy chemistry (IR-SEC) and density function theory (DFT) calculations supported $[Re(bpy)(CO)_3]^-$ as the electrocatalytically-active species.[90-93] Kubiak and coworkers proposed a more detailed two-electron reduction mechanism indicating the non-innocent role of the bpy ligand (Scheme 1.2).[91] The catalytically active species $[Re(bpy)(CO)_3]^-$ was

obtained after two single-electron transfers and a loss of halide. In $[Re(bpy)(CO)_3]^-$, a portion of the electrons in the π^*orbital of bpy weakly overlaps with the Re 5d orbitals, and the HOMO involves both the Re metal center and the ligand. This electronic configuration pushes the selectivity towards the CO_2 reduction over the H^+ reduction through both σ- and π- interactions.[91, 93] Additionally, the redox-active bpy ligand plays a significant role in the electrocatalytic process by storing electrons and stabilizing negative charges on the intermediates. The reduction potential of CO_2 can be tuned by modifying the bpy ligand to alter the steric and electronic effects.[90-95] The bpy moiety also acts as an important sink of electrons during electrocatalysis at sufficiently negative applied potentials.[96]

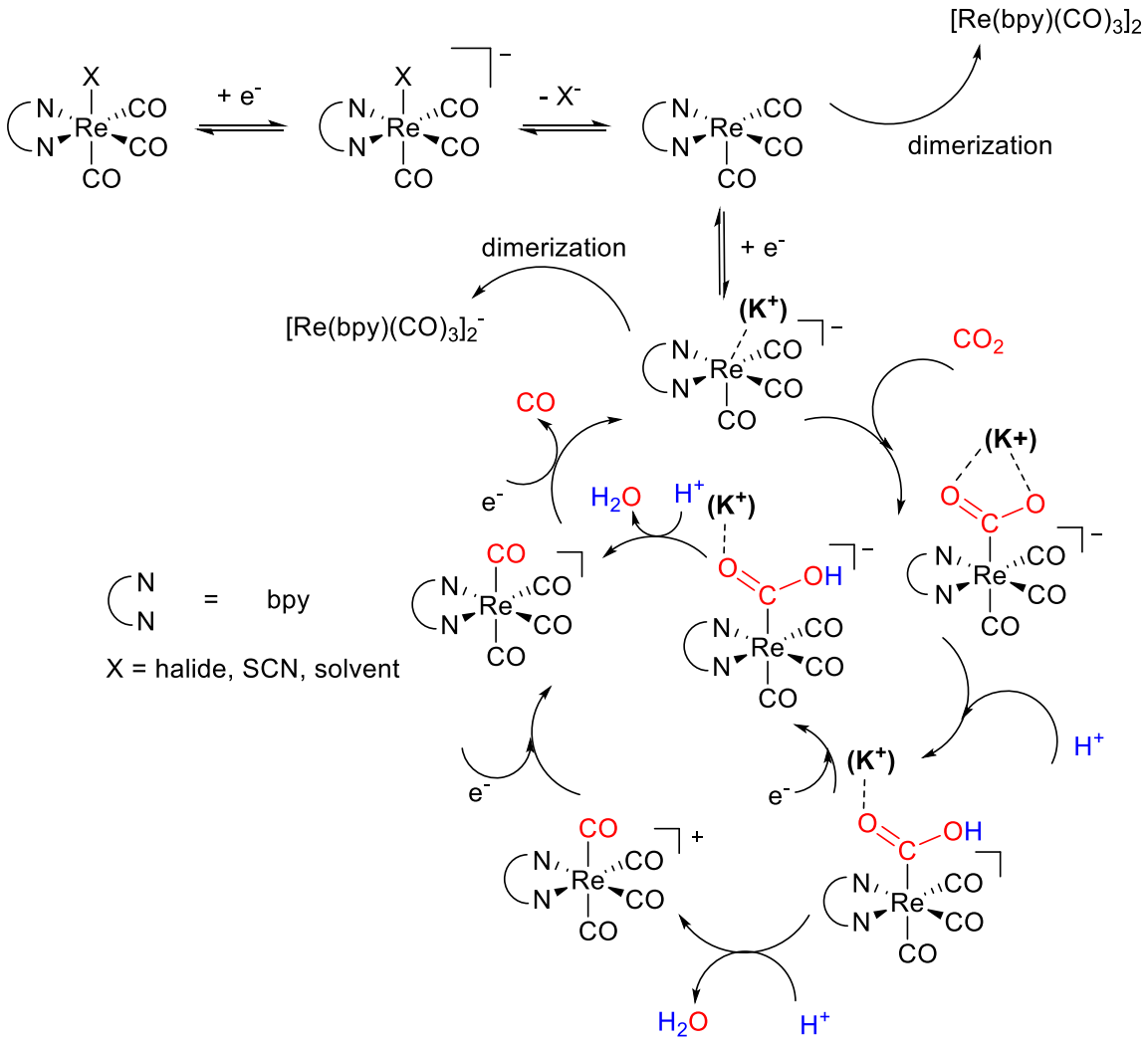

Scheme 1.2. Proposed mechanism of electrochemical reduction of CO_2 using the $Re(N\text{-}N)(CO)_3X$ catalyst reported by Kubiak and Carter in 2013.

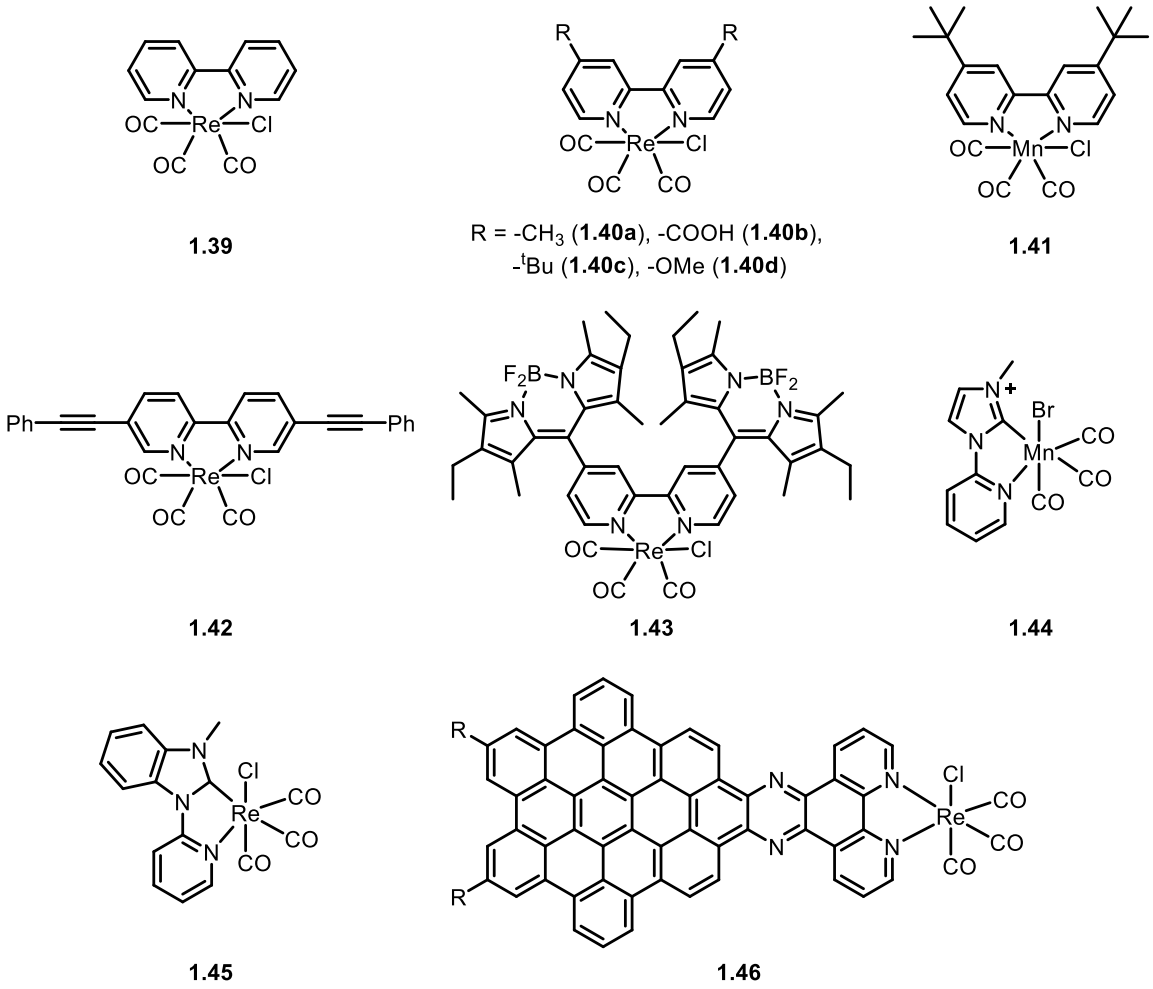

Figure 1.12. Structures of the Lehn catalyst and its analogues.

Inspired by the proposed mechanism, analogues of the Lehn's catalyst have been extensively researched. A systematic study of substituent effects on the 4, 4'- position of the bpy ligand (**1.40a**-**1.40d**) has been reported by Dr. Kubiak and coworkers in 2010.[87] A larger increase in the catalytic current with a more electron-donating substituted catalyst (**1.40c**) was observed, and it was also proposed that the steric hindrance from the *tert*-butyl group suppressed the dimerization deactivation pathway. The hypothesis was in good agreement with the IR-SEC experiment. Efforts were put forth by the same group to

substitute the metal center in the Lehn catalyst with manganese (Mn), an abundant first row transition metal (**1.41**).[97] Unlike the Lehn catalyst, Mn analogues required the addition of Brönsted acids for catalytic turnover. Chemical modification to bpy ligands was also studied intensively, including extension of the conjugated π-electron system (**1.42**) and the addition of redox-active moieties (**1.43**). For investigating the effect of modification on the coordination atoms, the N-heterocyclic carbene (NHC)-containing Mn (**1.44**) or Re (**1.45**) catalysts were also synthesized and studied for electrocatalytic CO_2 reduction.[98, 99] Very recently, a well-defined nanographene-Re complex (**1.46**) was reported where the electron delocalization was over the nanographene and the metal ion. This significantly decreased the electrical potential to drive the CO_2 reduction reaction, suggesting that large conjugated systems can dramatically affect the electrical potential of reduction.[100] The performances of these catalysts are summarized in Table 1.3 for comparison.

Table 1.3. Lehn catalyst and its analogues assessed for electrocatalytic CO_2 reduction.

Catalyst	Solvent	FE_{CO} (%) [a]	$E_{pc, CO2}$ [b]	k ($M^{-1}s^{-1}$) [c]	i_c/i_p [d]	Literature
1.39	DMF-10% H_2O	98	-1.3 V vs NHE	50	3.4	Lehn, 1985
1.40c	MeCN	99	-2.0 V vs SCE	650	18.4	Kubiak, 2010
1.41	MeCN-1.4 M TFE	100	-2.2 V vs SCE	N/A	42	Kubiak, 2013
1.42	MeCN	45 (50 for Lehn)	-1.8 V vs NHE (0.3 V positive than Lehn)	220	8	Sariciftci, 2012
1.43	MeCN	catalyst decomposed	-2.0 V vs SCE	3400 (1100 for Lehn)	4	Rosenthal, 2014
1.44	MeCN-5% H_2O	35	-1.7 V vs SCE	N/A	1.9	Schaefer, 2014
1.45	MeCN	60 (99 for Lehn)	-2.2 V vs Fc^+/Fc	N/A	2.3	Agarwal, 2014
1.46	THF-5% MeOH	96	-0.8 V vs NHE	N/A	N/A	Li, 2017

a. Faradaic efficiency (FE) = moles of CO produced × 2 ÷ moles of electrons input

b. $E_{pc, CO2:}$ the reduction peak potential of CO_2

c. k: second order rate constant

d. i_c/i_p = catalytic current (i_c) under a CO_2 atmosphere ÷ peak current (i_p) under an inert atmosphere around the same potentials

Except for the electrocatalytic properties discussed above, Re(bpy)-based catalysts have also been explored for photochemical reduction of CO_2 since 1984.[85] Triethanolamine (TEOA) is usually added into the reaction system to serve as an electron and proton donor. When performing the reaction, Re catalysts were excited by light forming a triplet metal-to-ligand charged transfer (^{3}MLCT) excited state, which is quenched by TEOA to yield the

catalytically active species $[Re(bpy^{\cdot-})(CO)_3X]$. The complex $[Ru(bpy)_3]^{2+}$ is a commonly used photosensitizer for CO_2 reduction.[101] More examples of photocatalytic reduction of CO_2 have been summarized in a recently published review, and will not be discussed in this chapter.[84]

In summary, a number of Re-polypyridyl complexes have been studied for electrocatalytic CO_2 reduction. CO_2 reduction is favored over proton reduction, and conversion of CO_2 to CO is selective over other products. Mechanistic studies have identified a catalytically active intermediate $[Re(bpy)(CO)_3]^-$. Synthetic modifications on the ligand backbone give opportunities to evaluate the mechanism of CO_2 reduction in detail and tune the properties of electrocatalysis. Most modifications involve electronic/steric tuning of the bpy ligand, while fewer reports use other polypyridyl ligands or other coordination compounds.

1.4 REFERENCES

1. Mortimer, R. J.; Dyer, A. L.; Reynolds, J. R. Electrochromic Organic and Polymeric Materials for Display Applications. *Displays* **2006,** *27*, 2-18.
2. Mortimer, R. J. Electrochromic Materials. *Chem. Soc. Rev.* **1997,** *26*, 147-156.
3. Somani, P. R.; Radhakrishnan, S. Electrochromic Materials and Devices: Present and Future. *Mater. Chem. Phys.* **2003,** *77*, 117-133.
4. Runnerstrom, E. L.; Llordes, A.; Lounis, S. D.; Milliron, D. J. Nanostructured Electrochromic Smart Windows: Traditional Materials and NIR-Selective Plasmonic Nanocrystals. *Chem. Commun.* **2014,** *50*, 10555-10572.
5. Granqvist, C. G. Electrochromic Tungsten Oxide Films: Review of Progress 1993-1998. *Sol. Energy Mater. Sol. Cells* **2000,** *60*, 201-262.
6. Niklasson, G. A.; Granqvist, C. G. Electrochromics for Smart Windows: Thin Films of Tungsten Oxide and Nickel Oxide, and Devices Based on These. *J. Mater. Chem.* **2007,** *17*, 127-156.
7. Fang, G. J.; Liu, Z. L.; Wang, Y.; Liu, Y. H.; Yao, K. L. Synthesis and Structural, Electrochromic Characterization of Pulsed Laser Deposited Vanadium Oxide Thin Films. *J. Vac. Sci. Technol. A* **2001,** *19*, 887-892.

8. Lin, Y.-S.; Tsai, T.-H.; Tien, S.-W. Atmospheric Pressure Plasma Jet-Synthesized Electrochromic Organomolybdenum Oxide Thin Films for Flexible Electrochromic Devices. *Thin Solid Films* **2013,** *529*, 248-252.

9. Gao, Q.; Wang, S.; Fang, H.; Weng, J.; Zhang, Y.; Mao, J.; Tang, Y. One-Dimensional Growth of Moox-Based Organic-Inorganic Hybrid Nanowires with Tunable Photochromic Properties. *J. Mater. Chem.* **2012,** *22*, 4709-4715.

10. Mortimer, R. J.; Reynolds, J. R. In Situ Colorimetric and Composite Coloration Efficiency Measurements for Electrochromic Prussian Blue. *J. Mater. Chem.* **2005,** *15*, 2226-2233.

11. Felderhoff, M.; Heinen, S.; Molisho, N.; Webersinn, S.; Walder, L. Molecular Suppression of the Pimerization of Viologens (=4,4'-Bipyridinium Derivatives) Attached to Nanocrystalline Titanium Dioxide Thin-Film Electrodes. *Helv. Chim. Acta* **2000,** *83*, 181-192.

12. Sydam, R.; Deepa, M.; Joshi, A. G. A Novel 1,1'-Bis[4-(5,6-Dimethyl-1H-Benzimidazole-1-yl)Butyl]-4,4'-Bipyridinium Dibromide (Viologen) for a High Contrast Electrochromic Device. *Org. Electron.* **2013,** *14*, 1027-1036.

13. Beaujuge, P. M.; Reynolds, J. R. Color Control in π-Conjugated Organic Polymers for Use in Electrochromic Devices. *Chem. Rev.* **2010,** *110*, 268-320.

14. Berggren, L.; Jonsson, J. C.; Niklasson, G. A. Optical Absorption in Lithiated Tungsten Oxide Thin Films: Experiment and Theory. *J. Appl. Phys.* **2007,** *102*, 083538.

15. Sonmez, G. Polymeric Electrochromics. *Chem. Commun.* **2005**, 5251-5259.

16. Holliday, B. J.; Swager, T. M. Conducting Metallopolymers: The Roles of Molecular Architecture and Redox Matching. *Chem. Commun.* **2005**, 23-36.

17. Whittell, G. R.; Manners, I. Metallopolymers: New Multifunctional Materials. *Adv. Mater.* **2007,** *19*, 3439-3468.

18. Stanley, J. M.; Holliday, B. J. Luminescent Lanthanide-Containing Metallopolymers. *Coord. Chem. Rev.* **2012,** *256*, 1520-1530.

19. Qiu, D.; Bao, X.; Zhao, Q.; Yang, Q.; Feng, Y.; Wang, H.; Yang, C.; Liu, K. Near-IR Electrochromic Film Prepared by Oxidative Electropolymerization of the Cyclometalated Pt(II) Chloride with a Triphenylamine Group. *Inorg. Chem.* **2015,** *54*, 8264-8270.

20. Nie, H.-J.; Zhong, Y.-W. Near-Infrared Electrochromism in Electropolymerized Metallopolymeric Films of a Phen-1,4-Diyl-Bridged Diruthenium Complex. *Inorg. Chem.* **2014,** *53*, 11316-11322.

21. Yao, C.-J.; Yao, J.; Zhong, Y.-W. Metallopolymeric Films Based on a Biscyclometalated Ruthenium Complex Bridged by 1,3,6,8-Tetra(2-

Pyridyl)Pyrene: Applications in Near-Infrared Electrochromic Windows. *Inorg. Chem.* **2012,** *51*, 6259-6263.

22. Yao, C.-J.; Zhong, Y.-W.; Nie, H.-J.; Abruña, H. D.; Yao, J. Near-IR Electrochromism in Electropolymerized Films of a Biscyclometalated Ruthenium Complex Bridged by 1,2,4,5-Tetra(2-Pyridyl)Benzene. *J. Am. Chem. Soc.* **2011,** *133*, 20720-20723.

23. Matsuse, R.; Abe, M.; Tomiyasu, Y.; Inatomi, A.; Yonemura, H.; Yamada, S.; Hisaeda, Y. Metallopolymer Films Exhibiting Three-Color Electrochromism in the UV/Vis and Near-IR Region: Remarkable Utility of Trimetallic Clusters Bearing Thienyl Pendants and Their Mixed-Valent Charge Transfer Transitions. *J. Inorg. Organomet. Polym. Mater.* **2012,** *23*, 136-146.

24. Zeng, Q.; McNally, A.; Keyes, T. E.; Forster, R. J. Redox Induced Switching Dynamics of a Three Colour Electrochromic Metallopolymer Film. *Electrochim. Acta* **2008,** *53*, 7033-7038.

25. Satheeshkumar, C.; Park, J.-Y.; Jeong, D.-C.; Song, S. G.; Lee, J.; Song, C. Synthesis and Electronic Properties of N-Heterocyclic Carbene-Containing Conducting Polymers with Coinage Metals. *RSC Adv.* **2015,** *5*, 60892-60897.

26. Powell, A. B.; Bielawski, C. W.; Cowley, A. H. Design, Synthesis, and Study of Main Chain Poly(N-Heterocyclic Carbene) Complexes: Applications in Electrochromic Devices. *J. Am. Chem. Soc.* **2010,** *132*, 10184-10194.

27. Djukic, B.; Seda, T.; Gorelsky, S. I.; Lough, A. J.; Lemaire, M. T. π-Extended and Six-Coordinate Iron(II) Complexes: Structures, Magnetic Properties, and the Electrochemical Synthesis of a Conducting Iron(II) Metallopolymer. *Inorg. Chem.* **2011,** *50*, 7334-7343.

28. Fan, C.; Ye, C.; Wang, X.; Chen, Z.; Zhou, Y.; Liang, Z.; Tao, X. Synthesis and Electrochromic Properties of New Terpyridine-Triphenylamine Hybrid Polymers. *Macromolecules* **2015,** *48*, 6465-6473.

29. Bao, X.; Zhao, Q.; Wang, H.; Liu, K.; Qiu, D. Metallopolymer Electrochromic Film Prepared by Oxidative Electropolymerization of a Fe(II) Complex with Arylamine Functionalized Terpyridine Ligand. *Inorg. Chem. Commun.* **2013,** *38*, 88-91.

30. Liang, Y.; Strohecker, D.; Lynch, V.; Holliday, B. J.; Jones, R. A. A Thiophene-Containing Conductive Metallopolymer Using an Fe(II) Bis(Terpyridine) Core for Electrochromic Materials. *ACS Appl. Mater. Interfaces* **2016,** *8*, 34568-34580.

31. Huang, Z.-F.; Song, J.; Pan, L.; Zhang, X.; Wang, L.; Zou, J.-J. Tungsten Oxides for Photocatalysis, Electrochemistry, and Phototherapy. *Adv. Mater.* **2015,** *27*, 5309-5327.

32. Wojcik, P. J.; Pereira, L.; Martins, R.; Fortunato, E. Statistical Mixture Design and Multivariate Analysis of Inkjet Printed a-WO_3/TiO_2/WO_x Electrochromic Films. *ACS Comb. Sci.* **2014,** *16*, 5-16.

33. Armelao, L.; Quici, S.; Barigelletti, F.; Accorsi, G.; Bottaro, G.; Cavazzini, M.; Tondello, E. Design of Luminescent Lanthanide Complexes: From Molecules to Highly Efficient Photo-Emitting Materials. *Coord. Chem. Rev.* **2010,** *254*, 487-505.

34. Hasegawa, Y.; Nakagawa, T.; Kawai, T. Recent Progress of Luminescent Metal Complexes with Photochromic Units. *Coord. Chem. Rev.* **2010,** *254*, 2643-2651.

35. Yuan, J.; Wang, G. Lanthanide Complex-Based Fluorescence Label for Time-Resolved Fluorescence Bioassay. *J. Fluoresc.* **2005,** *15*, 559-568.

36. Bünzli, J.-C. G. Lanthanide Luminescence for Biomedical Analyses and Imaging. *Chem. Rev.* **2010,** *110*, 2729-2755.

37. Dickins, R. S.; Parker, D.; de Sousa, A. S.; Williams, J. A. G. Closely Diffusing O-H, Amide N-H and Methylene C-H Oscillators Quench the Excited State of Europium Comlexes in Solution. *Chem. Commun.* **1996**, 697-698.

38. Beeby, A.; Clarkson, I. M.; Dickins, R. S.; Faulkner, S.; Parker, D.; Royle, L.; S. de Sousa, A.; Williams, J. A. G.; Woods, M. Non-Radiative Deactivation of the Excited States of Europium, Terbium and Ytterbium Complexes by Proximate Energy-Matched OH, NH and CH Oscillators: An Improved Luminescence Method for Establishing Solution Hydration States. *J. Chem. Soc., Perkin Trans.* **1999**, 493-504.

39. Werts, M. H. V.; Jukes, R. T. F.; Verhoeven, J. W. The Emission Spectrum and the Radiative Lifetime of Eu^{3+} in Luminescent Lanthanide Complexes. *PCCP* **2002,** *4*, 1542-1548.

40. Amoroso, A. J.; Pope, S. J. A. Using Lanthanide Ions in Molecular Bioimaging. *Chem. Soc. Rev.* **2015,** *44*, 4723-4742.

41. Heffern, M. C.; Matosziuk, L. M.; Meade, T. J. Lanthanide Probes for Bioresponsive Imaging. *Chem. Rev.* **2014,** *114*, 4496-4539.

42. Soini, E.; Kojola, H. Time-Resolved Fluorometer for Lanthanide Chelates-a New Generation of Nonisotopic Immunoassays. *Clin. Chem.* **1983,** *29*, 65-68.

43. Zhang, L.; Wang, Y.; Ye, Z.; Jin, D.; Yuan, J. New Class of Tetradentate β-Diketonate-Europium Complexes That Can Be Covalently Bound to Proteins for Time-Gated Fluorometric Application. *Bioconjugate Chem.* **2012,** *23*, 1244-1251.

44. Sy, M.; Nonat, A.; Hildebrandt, N.; Charbonniere, L. J. Lanthanide-Based Luminescence Biolabelling. *Chem. Commun.* **2016,** *52*, 5080-5095.

45. Nishioka, T.; Yuan, J.; Yamamoto, Y.; Sumitomo, K.; Wang, Z.; Hashino, K.; Hosoya, C.; Ikawa, K.; Wang, G.; Matsumoto, K. New Luminescent Europium(III) Chelates for DNA Labeling. *Inorg. Chem.* **2006,** *45*, 4088-4096.

46. Deng, W.; Jin, D.; Drozdowicz-Tomsia, K.; Yuan, J.; Goldys, E. M. Europium Chelate (BHHCT-Eu^{3+}) and Its Metal Nanostructure Enhanced Luminescence Applied to Bioassays and Time-Gated Bioimaging. *Langmuir* **2010,** *26*, 10036-10043.

47. Yuan, J.; Matsumoto, K.; Kimura, H. A New Tetradentate β-Diketonate-Europium Chelate That Can Be Covalently Bound to Proteins for Time-Resolved Fluoroimmunoassay. *Anal. Chem.* **1998,** *70*, 596-601.

48. Evangelista, R. A.; Pollak, A.; Allore, B.; Templeton, A. F.; Morton, R. C.; Diamandis, E. P. A New Europium Chelate for Protein Labelling and Time-Resolved Fluorometric Applications. *Clin. Biochem.* **1988,** *21*, 173-178.

49. Claudel-Gillet, S.; Steibel, J.; Weibel, N.; Chauvin, T.; Port, M.; Raynal, I.; Toth, E.; Ziessel, R. F.; Charbonnière, L. J. Lanthanide-Based Conjugates as Polyvalent Probes for Biological Labeling. *Eur. J. Inorg. Chem.* **2008,** *2008*, 2856-2862.

50. Starck, M.; Kadjane, P.; Bois, E.; Darbouret, B.; Incamps, A.; Ziessel, R.; Charbonnière, L. J. Towards Libraries of Luminescent Lanthanide Complexes and Labels from Generic Synthons. *Chem. Eur. J.* **2011,** *17*, 9164-9179.

51. Nchimi-Nono, K.; Wegner, K. D.; Linden, S.; Lecointre, A.; Ehret-Sabatier, L.; Shakir, S.; Hildebrandt, N.; Charbonniere, L. J. Activated Phosphonated Trifunctional Chelates for Highly Sensitive Lanthanide-Based FRET Immunoassays Applied to Total Prostate Specific Antigen Detection. *Org. Biomol. Chem.* **2013,** *11*, 6493-6501.

52. Takalo, H.; Mukkala, V.-M.; Mikola, H.; Liitti, P.; Hemmila, I. Synthesis of Europium(III) Chelates Suitable for Labeling of Bioactive Molecules. *Bioconjugate Chem.* **1994,** *5*, 278-282.

53. de Hoog, P.; Gamez, P.; Driessen, W. L.; Reedijk, J. New Polydentate and Polynucleating N-Donor Ligands from Amines and 2,4,6-Trichloro-1,3,5-Triazine. *Tetrahedron Lett.* **2002,** *43*, 6783-6786.

54. Mitrunen, K.; Pettersson, K.; Piironen, T.; Björk, T.; Lilja, H.; Lövgren, T. Dual-Label One-Step Immunoassay for Simultaneous Measurement of Free and Total Prostate-Specific Antigen Concentrations and Ratios in Serum. *Clin. Chem.* **1995,** *41*, 1115-1120.

55. Saha, A. K.; Kross, K.; Kloszewski, E. D.; Upson, D. A.; Toner, J. L.; Snow, R. A.; Black, C. D. V.; Desai, V. C. Time-Resolved Fluorescence of a New Europium-Chelate Complex: Demonstration of Highly Sensitive Detection of Protein and DNA Samples. *J. Am. Chem. Soc.* **1993,** *115*, 11032-11033.

56. Hovinen, J. Convenient Synthesis of Maleimido-Derivatized Lanthanide(III) Chelates and Their Use in Mercapto Group Conjugation. *Bioconjugate Chem.* **2007,** *18*, 597-600.

57. Ge, P.; Selvin, P. R. Thiol-Reactive Luminescent Lanthanide Chelates: Part 2. *Bioconjugate Chem.* **2003,** *14*, 870-876.

58. Yuan, J.; Matsumoto, K. Synthesis of a New Tetradentate β-Diketonate-Europium Chelate and Its Application for Time-Resolved Fluorimetry of Albumin. *J. Pharm. Biomed. Anal.* **1997,** *15*, 1397-1403.

59. Wu, F.-B.; Han, S.-Q.; Zhang, C.; He, Y.-F. Synthesis of a Highly Fluorescent β-Diketone-Europium Chelate and Its Utility in Time-Resolved Fluoroimmunoassay of Serum Total Thyroxine. *Anal. Chem.* **2002,** *74*, 5882-5889.

60. Wu, F.-B.; Zhang, C. A New Europium β-Diketone Chelate for Ultrasensitive Time-Resolved Fluorescence Immunoassays. *Anal. Biochem.* **2002,** *311*, 57-67.

61. Jingli, Y.; Shinji, S.; Ryosuke, S.; Keiichiro, M.; Kazuko, M. Structure and Luminescence Properties of the Tetradentate β-Diketonate-Europium(III) Complexes. *Chem. Lett.* **2003,** *32*, 492-493.

62. Weibel, N.; Charbonnière, L. J.; Guardigli, M.; Roda, A.; Ziessel, R. Engineering of Highly Luminescent Lanthanide Tags Suitable for Protein Labeling and Time-Resolved Luminescence Imaging. *J. Am. Chem. Soc.* **2004,** *126*, 4888-4896.

63. Tan, M.; Wang, G.; Hai, X.; Ye, Z.; Yuan, J. Development of Functionalized Fluorescent Europium Nanoparticles for Biolabeling and Time-Resolved Fluorometric Applications. *J. Mater. Chem.* **2004,** *14*, 2896-2901.

64. Liu, X.; Ye, Z.; Wei, W.; Du, Y.; Yuan, J.; Ma, D. Artificial Luminescent Protein as a Bioprobe for Time-Gated Luminescence Bioimaging. *Chem. Commun.* **2011,** *47*, 8139-8141.

65. Tian, L.; Dai, Z.; Zhang, L.; Zhang, R.; Ye, Z.; Wu, J.; Jin, D.; Yuan, J. Preparation and Time-Gated Luminescence Bioimaging Applications of Long Wavelength-Excited Silica-Encapsulated Europium Nanoparticles. *Nanoscale* **2012,** *4*, 3551-3557.

66. Zheng, W.; Tu, D.; Huang, P.; Zhou, S.; Chen, Z.; Chen, X. Time-Resolved Luminescent Biosensing Based on Inorganic Lanthanide-Doped Nanoprobes. *Chem. Commun.* **2015,** *51*, 4129-4143.

67. Zheng, W.; Huang, P.; Tu, D.; Ma, E.; Zhu, H.; Chen, X. Lanthanide-Doped Upconversion Nano-Bioprobes: Electronic Structures, Optical Properties, and Biodetection. *Chem. Soc. Rev.* **2015,** *44*, 1379-1415.

68. Mikkelsen, M.; Jorgensen, M.; Krebs, F. C. The Teraton Challenge. A Review of Fixation and Transformation of Carbon Dioxide. *Energy Environ. Sci.* **2010,** *3*, 43-81.

69. Wang, W.-H.; Himeda, Y.; Muckerman, J. T.; Manbeck, G. F.; Fujita, E. CO_2 Hydrogenation to Formate and Methanol as an Alternative to Photo- and Electrochemical CO_2 Reduction. *Chem. Rev.* **2015,** *115*, 12936-12973.

70. Sultana, S.; Sahoo, P. C.; Martha, S.; Parida, K. A Review of Harvesting Clean Fuels from Enzymatic CO_2 Reduction. *RSC Adv.* **2016,** *6*, 44170-44194.

71. Kumar, B.; Brian, J. P.; Atla, V.; Kumari, S.; Bertram, K. A.; White, R. T.; Spurgeon, J. M. New Trends in the Development of Heterogeneous Catalysts for Electrochemical CO_2 Reduction. *Catal. Today* **2016,** *270*, 19-30.

72. Lu, Q.; Jiao, F. Electrochemical CO_2 Reduction: Electrocatalyst, Reaction Mechanism, and Process Engineering. *Nano Energy* **2016,** *29*, 439-456.

73. Benson, E. E.; Kubiak, C. P.; Sathrum, A. J.; Smieja, J. M. Electrocatalytic and Homogeneous Approaches to Conversion of CO_2 to Liquid Fuels. *Chem. Soc. Rev.* **2009,** *38*, 89-99.

74. Qiao, J.; Liu, Y.; Hong, F.; Zhang, J. A Review of Catalysts for the Electroreduction of Carbon Dioxide to Produce Low-Carbon Fuels. *Chem. Soc. Rev.* **2014,** *43*, 631-675.

75. Whipple, D. T.; Kenis, P. J. A. Prospects of CO_2 Utilization Via Direct Heterogeneous Electrochemical Reduction. *J. Phys. Chem. Lett.* **2010,** *1*, 3451-3458.

76. Costentin, C.; Robert, M.; Saveant, J.-M. Catalysis of the Electrochemical Reduction of Carbon Dioxide. *Chem. Soc. Rev.* **2013,** *42*, 2423-2436.

77. Choi, J.; Benedetti, T. M.; Jalili, R.; Walker, A.; Wallace, G. G.; Officer, D. L. High Performance Fe Porphyrin/Ionic Liquid Co-Catalyst for Electrochemical CO_2 Reduction. *Chem. Eur. J.* **2016**, *22*, 14158-14161.

78. Johnson, B. A.; Maji, S.; Agarwala, H.; White, T. A.; Mijangos, E.; Ott, S. Activating a Low Overpotential CO_2 Reduction Mechanism by a Strategic Ligand Modification on a Ruthenium Polypyridyl Catalyst. *Angew. Chem. Int. Ed.* **2016,** *55*, 1825-1829.

79. Portenkirchner, E.; Oppelt, K.; Ulbricht, C.; Egbe, D. A. M.; Neugebauer, H.; Knör, G.; Sariciftci, N. S. Electrocatalytic and Photocatalytic Reduction of Carbon Dioxide to Carbon Monoxide Using the Alkynyl-Substituted Rhenium(I) Complex (5,5'-Bisphenylethynyl-2,2'-Bipyridyl)$Re(CO)_3Cl$. *J. Organomet. Chem.* **2012,** *716*, 19-25.

80. Lim, C.-H.; Holder, A. M.; Musgrave, C. B. Mechanism of Homogeneous Reduction of CO_2 by Pyridine: Proton Relay in Aqueous Solvent and Aromatic Stabilization. *J. Am. Chem. Soc.* **2013,** *135*, 142-154.

81. Froehlich, J. D.; Kubiak, C. P. Homogeneous CO_2 Reduction by Ni(Cyclam) at a Glassy Carbon Electrode. *Inorg. Chem.* **2012,** *51*, 3932-3934.

82. Cole, E. B.; Lakkaraju, P. S.; Rampulla, D. M.; Morris, A. J.; Abelev, E.; Bocarsly, A. B. Using a One-Electron Shuttle for the Multielectron Reduction of CO_2 to Methanol: Kinetic, Mechanistic, and Structural Insights. *J. Am. Chem. Soc.* **2010,** *132*, 11539-11551.

83. Stanton, C. J.; Vandezande, J. E.; Majetich, G. F.; Schaefer, H. F.; Agarwal, J. Mn-NHC Electrocatalysts: Increasing π Acidity Lowers the Reduction Potential and Increases the Turnover Frequency for CO_2 Reduction. *Inorg. Chem.* **2016**.

84. Elgrishi, N.; Chambers, M. B.; Wang, X.; Fontecave, M. Molecular Polypyridine-Based Metal Complexes as Catalysts for the Reduction of CO_2. *Chem. Soc. Rev.* **2017,** *46*, 761-796.

85. Hawecker, J.; Lehn, J.-M.; Ziessel, R. Electrocatalytic Reduction of Carbon Dioxide Mediated by $Re(Bipy)(CO)_3Cl$ (Bipy = 2,2'-Bipyridine). *J. Chem. Soc., Chem. Commun.* **1984**, 328-330.

86. Sullivan, B. P.; Bolinger, C. M.; Conrad, D.; Vining, W. J.; Meyer, T. J. One- and Two-Electron Pathways in the Electrocatalytic Reduction of CO_2 by *fac*-$Re(bpy)(CO)_3Cl$ (bpy = 2,2'-Bipyridine). *J. Chem. Soc., Chem. Commun.* **1985**, 1414-1416.

87. Smieja, J. M.; Kubiak, C. P. $Re(Bipy\text{-}tbu)(CO)_3Cl$−Improved Catalytic Activity for Reduction of Carbon Dioxide: IR-Spectroelectrochemical and Mechanistic Studies. *Inorg. Chem.* **2010,** *49*, 9283-9289.

88. Hayashi, Y.; Kita, S.; Brunschwig, B. S.; Fujita, E. Involvement of a Binuclear Species with the Re−C(O)O−Re Moiety in CO_2 Reduction Catalyzed by Tricarbonyl Rhenium(I) Complexes with Diimine Ligands: Strikingly Slow Formation of the Re−Re and Re−C(O)O−Re Species from $Re(Dmb)(CO)_3S$ (Dmb = 4,4'-Dimethyl-2,2'-Bipyridine, S = Solvent). *J. Am. Chem. Soc.* **2003,** *125*, 11976-11987.

89. Agarwal, J.; Fujita, E.; Schaefer, H. F.; Muckerman, J. T. Mechanisms for CO Production from CO_2 Using Reduced Rhenium Tricarbonyl Catalysts. *J. Am. Chem. Soc.* **2012,** *134*, 5180-5186.

90. Sampson, M. D.; Froehlich, J. D.; Smieja, J. M.; Benson, E. E.; Sharp, I. D.; Kubiak, C. P. Direct Observation of the Reduction of Carbon Dioxide by Rhenium Bipyridine Catalysts. *Energy Environ. Sci.* **2013,** *6*, 3748-3755.

91. Keith, J. A.; Grice, K. A.; Kubiak, C. P.; Carter, E. A. Elucidation of the Selectivity of Proton-Dependent Electrocatalytic CO_2 Reduction by *fac*-$Re(bpy)(CO)_3Cl$. *J. Am. Chem. Soc.* **2013,** *135*, 15823-15829.

92. Benson, E. E.; Kubiak, C. P. Structural Investigations into the Deactivation Pathway of the CO_2 Reduction Electrocatalyst $Re(bpy)(CO)_3Cl$. *Chem. Commun.* **2012,** *48*, 7374-7376.

93. Benson, E. E.; Sampson, M. D.; Grice, K. A.; Smieja, J. M.; Froehlich, J. D.; Friebel, D.; Keith, J. A.; Carter, E. A.; Nilsson, A.; Kubiak, C. P. The Electronic States of Rhenium Bipyridyl Electrocatalysts for CO_2 Reduction as Revealed by X-Ray Absorption Spectroscopy and Computational Quantum Chemistry. *Angew. Chem. Int. Ed.* **2013,** *52*, 4841-4844.

94. Machan, C. W.; Yin, J.; Chabolla, S. A.; Gilson, M. K.; Kubiak, C. P. Improving the Efficiency and Activity of Electrocatalysts for the Reduction of CO_2 through Supramolecular Assembly with Amino Acid-Modified Ligands. *J. Am. Chem. Soc.* **2016,** *138*, 8184-8193.

95. Machan, C. W.; Chabolla, S. A.; Yin, J.; Gilson, M. K.; Tezcan, F. A.; Kubiak, C. P. Supramolecular Assembly Promotes the Electrocatalytic Reduction of Carbon Dioxide by Re(I) Bipyridine Catalysts at a Lower Overpotential. *J. Am. Chem. Soc.* **2014,** *136*, 14598-14607.

96. Teesdale, J. J.; Pistner, A. J.; Yap, G. P. A.; Ma, Y.-Z.; Lutterman, D. A.; Rosenthal, J. Reduction of CO_2 Using a Rhenium Bipyridine Complex Containing Ancillary Bodipy Moieties. *Catal. Today* **2014,** *225*, 149-157.

97. Smieja, J. M.; Sampson, M. D.; Grice, K. A.; Benson, E. E.; Froehlich, J. D.; Kubiak, C. P. Manganese as a Substitute for Rhenium in CO_2 Reduction Catalysts: The Importance of Acids. *Inorg. Chem.* **2013,** *52*, 2484-2491.

98. Agarwal, J.; Shaw, T. W.; Stanton, C. J.; Majetich, G. F.; Bocarsly, A. B.; Schaefer, H. F. NHC-Containing Manganese(I) Electrocatalysts for the Two-Electron Reduction of CO_2. *Angew. Chem. Int. Ed.* **2014,** *53*, 5152-5155.

99. Stanton, C. J.; Machan, C. W.; Vandezande, J. E.; Jin, T.; Majetich, G. F.; Schaefer, H. F.; Kubiak, C. P.; Li, G.; Agarwal, J. Re(I) NHC Complexes for Electrocatalytic Conversion of CO_2. *Inorg. Chem.* **2016,** *55*, 3136-3144.

100. Qiao, X.; Li, Q.; Schaugaard, R. N.; Noffke, B. W.; Liu, Y.; Li, D.; Liu, L.; Raghavachari, K.; Li, L.-S. Well-Defined Nanographene-Rhenium Complex as an Efficient Electrocatalyst and Photocatalyst for Selective CO_2 Reduction. *J. Am. Chem. Soc.* **2017,** *139*, 3934-3937.

101. Takeda, H.; Koike, K.; Inoue, H.; Ishitani, O. Development of an Efficient Photocatalytic System for CO_2 Reduction Using Rhenium(I) Complexes Based on Mechanistic Studies. *J. Am. Chem. Soc.* **2008,** *130*, 2023-2031.

Chapter 2: A Thiophene-Containing Conductive Metallopolymer Using an Iron(II) Bis(terpyridine) Core for Electrochromic Materials[1]

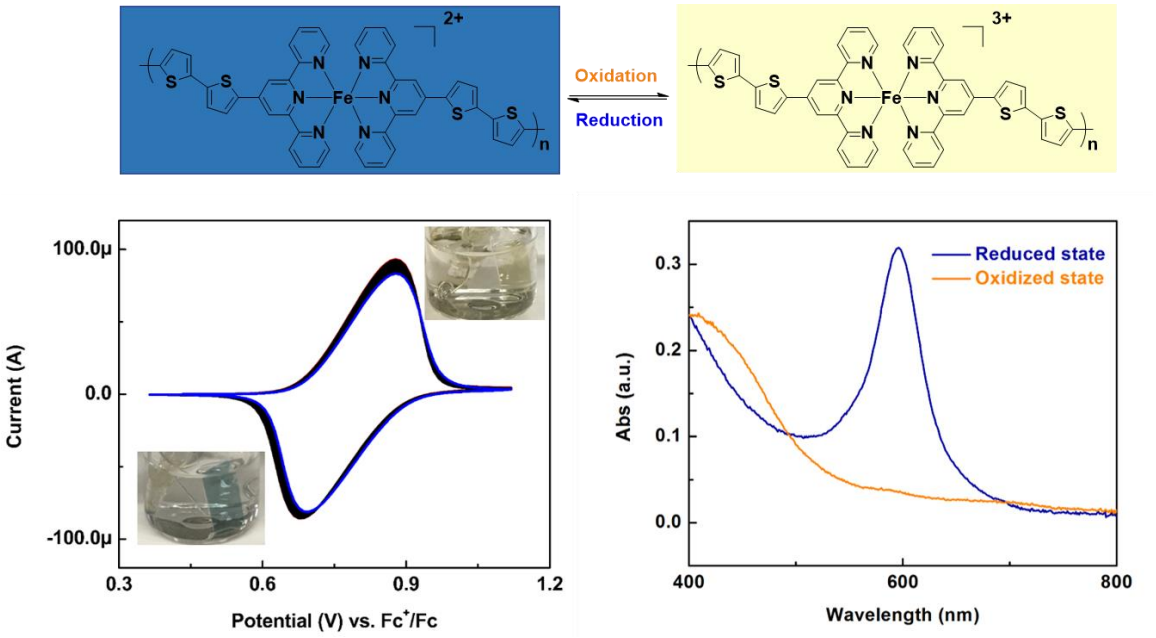

[1] This chapter is based partially on the following published work-
Liang, Y.; Strohecker, D.; Lynch, V.; Holliday, B. J.; Jones, R. A. *ACS Appl. Mater. Interfaces* **2016**, *8*, 34568. DOI: 10.1021/acsami.6b11657.
Author contributions: Y.L. conceived the project and synthesized the compounds investigated in this research. D.S. was responsible for XPS experiment. V.L. performed single crystal X-ray diffraction experiment. Y.L. investigated the electropolymerization process of the compounds and their electrochromic properties. Y.L., D.S., and R. A. J. prepared the manuscript.

ABSTRACT: Three Fe(II) bis(terpyridine)-based complexes with thiophene (**2.2a**), bithiophene (**2.2b**), and 3,4-ethylenedioxythiophene (**2.2c**) side chains were designed and synthesized for the purpose of providing two terminal active sites for electrochemical polymerization. The corresponding metallopolymers (**poly-2.2b**, and **poly-2.2c**) were synthesized on indium tin oxide (ITO)-coated glass substrates via oxidative electropolymerization of the thiophene-substituted monomer and characterized using electrochemistry, X-ray photoelectron spectroscopy, UV-vis spectroscopy and atomic force microscopy. The film **poly-2.2b** was further studied for electrochromic (EC) color-switching properties and fabricated into a solid-state EC device. **Poly-2.2b** films exhibit an intense MLCT absorption band at 596 nm ($\varepsilon = 4.7 \times 10^4\ M^{-1}cm^{-1}$) in the UV-vis spectra without any applied voltage. Upon application of low potentials (between 1.1 V and 0.4 V vs Fc^+/Fc), the obtained electropolymerized film exhibited great contrast with a change of transmittance percentage ($\Delta T\%$) of 40% and a high coloration efficiency of 3823 cm^2C^{-1} with a switching time of 1 s. The film demonstrates commonplace stability and reversibility with a 10% loss in peak current intensity after 200 cyclic voltammetry cycles and almost no loss in change of transmittance change ($\Delta T\%$) after 900 potential switches between 1.1 and 0.4 V (vs Fc^+/Fc) with a time interval of 0.75 s. The electropolymerization of **2.2b** provides a convenient and controllable way of film fabrication. Electrochromic behavior was also achieved in a solid-state device comprised of a **poly-2.2b** film and a polymer-supported electrolyte sandwiched between two ITO-coated glass electrodes.

2.1 INTRODUCTION

Conducting metallopolymers (CMPs) encompass a unique class of hybrid materials which contain both metal centers and conducting polymer backbones and have been a focus of great interest over the past decade.[1-3] With the advantages of beneficial properties of

both organic and inorganic materials, CMPs have found applications in diverse areas such as photoluminescent materials,[4, 5] sensor technologies,[6, 7] templated nanoparticle synthesis,[8, 9] spin-crossover conductors,[10, 11] and valence tautomerism materials.[12] In addition to the interesting applications mentioned above, electrochromism has been studied using electropolymerized conducting metallopolymers.[11, 13, 14] Recently, Fe(II) and Ru(II) bis(terpyridine)-based complexes with *N*',*N*'-disubstituted aminophenyl side chains have also been electropolymerized to make electrochromic films.[15, 16] A color change was observed while applying voltages on these conducting metallopolymer films. However, the aforementioned electrochromic materials based on metallopolymers suffer from problems such as long-term instability, long response time, difficult fabrication and low coloration efficiency.[17-19]

Kurth and co-workers reported an electrochromic thin film of metallo-supramolecular polyelectrolytes based on $Fe(OAc)_2$ and 1,4-bis(2,2':6',2''-terpyridin-4'-yl)benzene which shows a promising color switch between blue and colorless under applied potential.[20] This suggests that the Fe(II) bis(terpyridine) core may be a desirable motif for electrochromism with high coloration efficiency. Furthermore, terpyridine-M^{2+}-terpyridine (M^{2+} = Ru^{2+}, Zn^{2+}, Fe^{2+}, or Co^{2+}) linkages are strictly linear and rigid due to the delocalization of the π-electrons across the conjugated ligands.[13] This can increase the long-term stability of polymers. Among the film processing methods used for Fe(II) bis(terpyridine)-based electrochromic materials, including nanosheet assemblies and coordination-based molecular assemblies,[15, 21, 22] solution-based electropolymerization on a film surface has several advantages, including ease of processability and fine control of film thickness owing to the electropolymerization process.[23] Recently, Tao and co-workers synthesized a series of Fe(II) complexes with functionalized terpyridine ligands and demonstrated successful electropolymerization of the complexes on an indium tin oxide

(ITO) film surface.[15] Electrochromism was observed when a voltage (2 V vs AgCl/Ag) was applied, although this process was not very efficient and did not yield a high-contrast color switch (from purple to dark green). It was suggested that the intrinsic conjugation within the (diphenylamino)phenyl moiety might be detrimental to the coloration efficiency. On the other hand, thiophene and its derivatives have been well-studied and also widely used for electropolymerization.[24-28] In addition, poly(3,4-alkylenedioxythiophene) and its derivatives electrodeposited or spray-coated onto various substrate surfaces demonstrate promising EC properties. Although a full color palette has been achieved in these specific systems, synthetic modification on the polymer backbone and the use of an immobilized counterion such as polystyrenesulfonate (PSS^-) is necessary to tune the color states of the conjugated polymer and to efficiently transport electrons within the resulting polymeric film.[17, 29-33] Therefore, I envisioned that polymeric structures accessed by adding thiophene as the electropolymerizable moiety onto the Fe(II)-bis(terpyridine) core structure might lead to an easy and controllable synthesis of electrochromic metallopolymers with more desirable properties.

Herein, the electropolymerization and electrochromism studies of thiophene-containing Fe(II) bis(terpyridine) complexes (**2.2a**-**2.2c**) are described. By taking advantage of the easy synthesis and fast redox activity of the bis(terpyridine) metal complex unit, the electropolymerization processes of a series of thiophene-containing bis(terpyridine) metal structures were demonstrated and the electrochromic properties of the resulting metallopolymer films were investigated. The ligands 4'-(thiophen-2-yl)-2,2':6',2''-terpyridine (**2.1a**), 4'-([2,2'-bithiophen]-5-yl)-2,2':6',2''-terpyridine (**2.1b**), and 4'-(3,4-ethylenedioxythiophene)-2,2':6',2''-terpyridine (**2.1c**) and their corresponding Fe(II) complexes (**2.2a**-**2.2c**), were synthesized for the purpose of electrochemical polymerization (Scheme 2.1). Although the ligands[34-36] and two complexes, **2.2a** and

2.2c,[37, 38] have been synthesized before, to the best of our knowledge, it is the first that the electropolymerization process and the electrochromic behavior of **2.2a**-**2.2c** have been reported.[39]

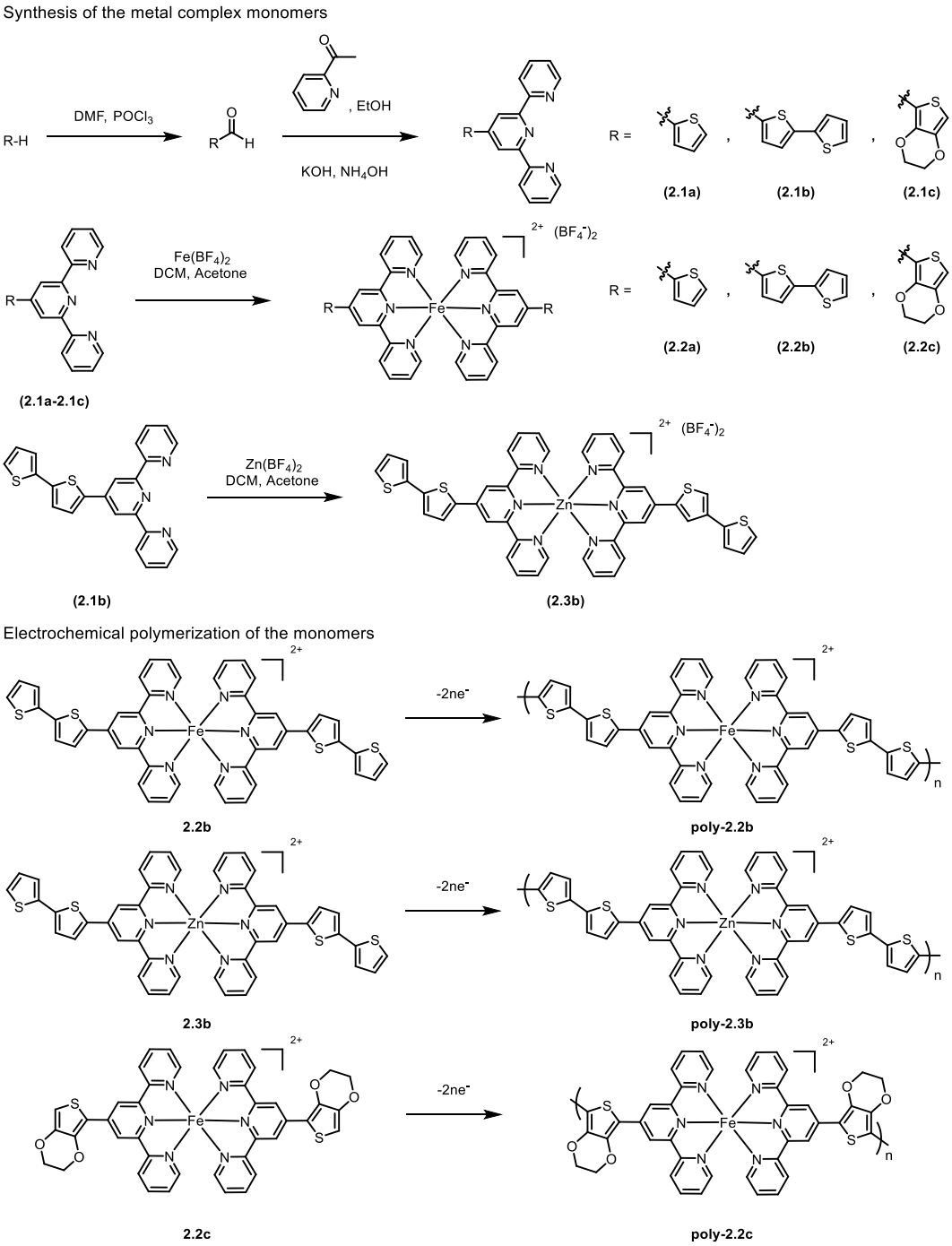

Scheme 2.1. Syntheses of the ligands (**2.1a**-**2.1c**), metal complexes (**2.2a**-**2.2c**, **2.3b**) and the corresponding conducting metallopolymers (**poly-2.2b**, **poly-2.3b**, **poly-2.2c**).

2.2 EXPERIMENTAL SECTION

2.2.1 Materials and Reagents

2,2'-bithiophene-5-carboxaldehyde and 3,4-ethylenedioxythiophene-2-carboxaldehyde were prepared by the Vilsmeier-Haack reaction.[40, 41] 2-thiophenecarboxaldehyde was purchased from Chem Impex. All chemicals for the synthesis of 4'-(thiophen-2-yl)-2,2':6',2"-terpyridine (L1), 4'-(2,2'-bithiophen-5-yl)-2,2':6',2"-terpyridine (L2), 4'-(3,4-ethylenedioxythiophene)-2,2':6',2"-terpyridine (L3) and corresponding complexes $M(Ln)_2$ ($M = Fe^{2+}$, n = 1-3; $M = Zn^{2+}$, n = 2) were purchased from Alfa Aesar, Aldrich or Chem Impex, and used without further purification. Acetonitrile used in electrochemical experiments was obtained from EMD Millipore Corporation and purified via a two-column alumina purification system (Pure Process Technology, NH). Tetrabutylammonium hexafluorophosphate ($TBAPF_6$) was purchased from Oakwood and purified by triplicate recrystallization from hot ethanol before drying under vacuum for three days. ITO glasses (R_s = 70-100 Ω, 7 × 50 × 0.7 mm) were purchased from Delta Technologies, LTD, and were cleaned by sonicating sequentially in acetone and dichloromethane prior to use.

2.2.2 Characterization Methods

Air- and moisture-sensitive reactions were performed with standard Schlenk techniques under an inert nitrogen atmosphere. ^{1}H NMR spectra were recorded using an Agilent 400 MR NMR spectrometer at 400 MHz. Coupling constants are reported in hertz (Hz), and chemical shifts are reported as parts per million (ppm) relative to residual solvent peaks (residual $CDCl_3$ δ_H = 7.26 ppm, residual CD_3CN δ_H = 1.94 ppm). ^{13}C NMR spectra were recorded using an Agilent 400 MR NMR spectrometer at 100 MHz in $CDCl_3$ solution, and chemical shifts are reported as parts per million (ppm) relative to residual $CDCl_3$ δ_C

(77.16 ppm).[42] High resolution mass spectra (HRMS) were obtained on an Agilent Technologies 6530 Accurate Mass Q-TOF LC/MS instrument. Infrared spectra were recorded with a Nicolet IR 200 FTIR spectrophotometer. Absorption spectra were recorded on a Varian Cary 6000i UV-VIS-NIR spectrophotometer using Starna quartz fluorimeter cells with a path length of 10 mm. X-ray photoelectron spectroscopy (XPS) was carried out on a PHI 5700 XPS system equipped with dual Mag X-ray source and monochromatic Al X-ray source complete with depth profile and angle-resolved capabilities. AFM measurements in this work are based on an AFM platform (Park AFM XE70). The contact cantilever (PPPOLY-CONTSCR) was purchased from the same company.

2.2.3 Synthesis of 4'-(thiophen-2-yl)-2,2':6',2''-terpyridine (2.1a), 4'-(2,2'-bithiophen-5-yl)-2,2':6',2''-terpyridine (2.1b) and 4'-(3,4-ethylenedioxythiophene)-2,2':6',2''-terpyridine (2.1c)

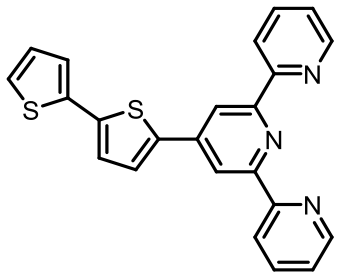

2.1b

4'-(2,2'-bithiophen-5-yl)-2,2':6',2''-terpyridine (2.1b). To a solution of 2,2'-bithiophene-5-carboxaldehyde (0.200 g, 1.03 mmol) in ethanol (15.6 mL) were added 2-acetylpyridine (0.253 g, 2.09 mmol) and potassium hydroxide (0.115 g, 2.06 mmol) successively, resulting in a yellow solution, followed by addition of an aqueous solution of ammonia (28 wt%, 9.3 mL). The resulting mixture was heated to reflux at 75 ℃ for 10 h. After cooling to ambient temperature, the precipitate was filtered and washed with ethanol three times, yielding a green-yellow solid (Yield: 0.104 g, 25%). ^{1}H NMR ($CDCl_3$): 8.74 (2H, d, J = 4.69 Hz), 8.67 (2H, s), 8.64 (2H, d, J = 7.98 Hz), 7.87 (2H, td, J = 7.63, 1.76

Hz), 7.70 (1H, d, J = 3.84 Hz), 7.36 (2H, dd, J = 7.41, 4.71 Hz), 7.28-7.26 (2H, m), 7.23 (1H, d, J = 3.82 Hz), 7.06 (1H, dd, J = 5.01, 3.56 Hz). ^{13}C NMR ($CDCl_3$): 156.24, 156.16, 149.28, 143.17, 140.44, 139.22, 137.22, 136.99, 128.15, 126.70, 125.18, 124.83, 124.41, 124.06, 121.47, 116.82. ^{1}H NMR (CD_3CN): 8.75 (2H, ddd, J = 4.80, 1.81, 0.93 Hz), 8.70 (3H, m), 8.68 (1H, t, J = 1.08 Hz), 7.98 (2H, td, J = 7.66, 1.78 Hz), 7.79 (1H, d, J = 3.86 Hz), 7.47 (2H, ddd, J = 7.51, 4.74, 1.16 Hz), 7.43 (2H, ddd, J = 5.87, 3.63, 1.17 Hz), 7.36 (1H, d, J = 3.85 Hz), 7.12 (1H, dd, J = 5.09, 3.63 Hz). HRMS (ESI): calcd. for $[M+H]^+$ m/z: 398.07800, found: 398.07940. UV-vis [CH_3CN, nm ($M^{-1}cm^{-1}$)]: 357 (2.2×10^4), 284 (1.8×10^4), 238 (2.0×10^4).

4'-(thiophen-2-yl)-2,2':6',2''-terpyridine (**2.1a**) and 4'-(3,4-ethylenedioxythiophene)-2,2':6',2''-terpyridine (**2.1c**). **2.1a** and **2.1c** were synthesized using similar synthetic routes to **2.1b**.[38, 43]

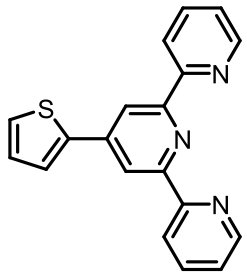

2.1a

4'-(thiophen-2-yl)-2,2':6',2''-terpyridine (2.1a). Yield: 22%. ^{1}H NMR ($CDCl_3$): 8.74 (2H, ddd, J = 4.78, 1.79, 0.93 Hz), 8.70 (2H, s), 8.65 (2H, dt, J = 7.98, 1.09 Hz), 7.88 (2H, m), 7.79 (1H, dd, J = 3.68, 1.15 Hz), 7.45 (1H, dd, J = 5.04, 1.13 Hz), 7.36 (2H, ddd, J = 7.48, 4.81, 1.23 Hz), 7.18 (1H, dd, J = 5.07, 3.7 Hz). ^{13}C NMR ($CDCl_3$): 156.24, 156.22, 149.28, 143.59, 142.06, 136.98, 128.41, 127.23, 125.95, 124.03, 121.48, 117.32. ^{1}H NMR (CD_3CN): 8.74 (2H, m), 8.71 (2H, s), 8.68 (2H, dt, J = 7.97, 1.23 Hz), 7.97 (2H, m), 7.84 (1H, dd, J = 3.63, 1.18 Hz), 7.61 (1H, dd, J = 5.07, 1.11 Hz), 7.46 (2H, ddd, J = 7.56, 4.73, 1.16 Hz), 7.25 (1H, dd, J = 5.09, 3.28 Hz). HRMS (ESI): calcd. for $[M+H]^+$ m/z:

317.09320, found: 317.09380. UV-vis [CH_3CN, nm ($M^{-1}cm^{-1}$)]: 280 (3.6 $\times 10^4$), 249 (2.3 $\times 10^4$), 227 (1.9 $\times 10^4$).

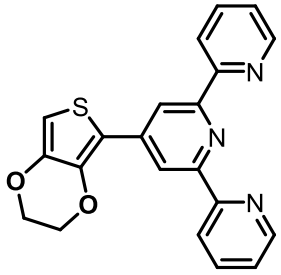

2.1c

4'-(3,4-ethylenedioxythiophene)-2,2':6',2''-terpyridine (2.1c). Yield: 20%. ^{1}H NMR ($CDCl_3$): 8.77 (2H, s), 8.74 (2H, ddd, *J* = 4.81, 1.80, 0.93 Hz), 8.62 (2H, dt, *J* = 7.98, 1.06 Hz), 7.86 (2H, m), 7.34 (2H, ddd, *J* = 7.49, 4.80, 1.23 Hz), 6.48 (1H, s), 4.45 (2H, m), 4.30 (2H, m). ^{13}C NMR ($CDCl_3$): 156.56, 155.97, 149.29, 142.66, 142.49, 141.25, 136.89, 123.82, 121.46, 117.08, 115.56, 100.60, 65.27, 64.60. ^{1}H NMR (CD_3CN): 8.77 (2H, s), 8.72 (2H, ddd, *J* = 4.75, 1.74, 0.89 Hz), 8.66 (2H, d t, *J* = 7.97, 1.00 Hz), 7.96 (2H, td, *J* = 7.67, 1.80 Hz), 7.44 (2H, ddd, *J* = 7.49, 4.77, 1.17 Hz), 6.61 (1H, s), 4.45 (2H, m), 4.32 (2H, m). HRMS (ESI): calcd. for $[M+H]^+$ m/z: 374.09580, found: 374.09620. UV-vis [CH_3CN, nm ($M^{-1}cm^{-1}$)]: 326 (0.77 $\times 10^4$), 287 (1.3 $\times 10^4$), 231 (0.85 $\times 10^4$).

2.2.4 Synthesis of Metal Complexes (2.2a-2.2c, M = Fe^{2+}; 2.3b, M = Zn^{2+}) with Ligands 2.1a-2.1c

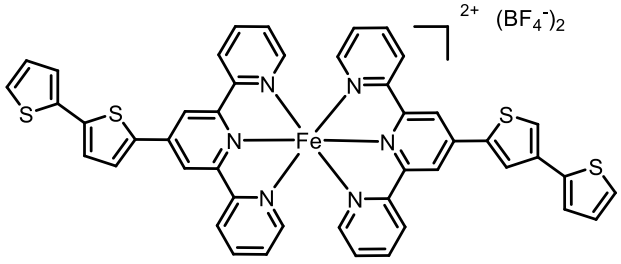

2.2b

Fe(II) Bis(4'-(2,2'-bithiophen-5-yl)-2,2':6',2''-terpyridine) tetrafluoroborate (2.2b). Iron(II) tetrafluoroborate hexahydrate $Fe(BF_4)_2 \cdot 6(H_2O)$ (21.2 mg, 0.063 mmol) and

L2 (50 mg, 0.126 mmol) were stirred in a solvent mixture of acetone (2 mL) and dichloromethane (4 mL) for 1 h. The solvent was then removed under vacuum, giving a dark purple-colored solid (quant.). ^{1}H NMR (CD_3CN): 9.06 (4H, s), 8.61 (4H, d, J = 8.02 Hz), 8.25 (2H, d, J = 3.92 Hz), 7.91 (4H, t, J = 6.91 Hz), 7.60 (2H, d, J = 3.89 Hz), 7.55 (4H, d, J = 4.31 Hz), 7.21 (6H, m), 7.09 (4H, t, J = 6.66 Hz). HRMS (ESI): calcd. for $[M\text{-}2BF_4]^{2+}$ m/z: 425.03770, found: 425.03890. UV-vis [CH_3CN, nm ($M^{-1}cm^{-1}$)]: 589 (4.7 $\times 10^4$), 389 (6.1 $\times 10^4$), 322 (4.6 $\times 10^4$), 277 (4.6 $\times 10^4$). IR (solid, cm^{-1}): 3072.45w, 1606.69m, 1560.21w, 1535.23w, 1508.94w, 1468.83m, 1449.42m, 1430.93m, 1313.89w, 1279.72w, 1241.96m, 1163.80w, 1033.78s, 861.64w, 859.68w, 839.45w, 798.74w, 789.16m, 753.47m, 728.13w, 698.00m, 652.20w, 628.05w.

The complexes Fe(II) Bis(4'-(thiophen-2-yl)-2,2':6',2''-terpyridine) tetrafluoroborate (**2.2a**), Fe(II) Bis(4'-(3,4-ethylenedioxythiophene)-2,2':6',2''-terpyridine) tetrafluoroborate (**2.2c**) and Zn(II) Bis(4'-(2,2'-bithiophen-5-yl)-2,2':6',2''-terpyridine) tetrafluoroborate (**2.3b**) were synthesized in a similar manner to Fe(II) Bis(4'-(2,2'-bithiophen-5-yl)-2,2':6',2''-terpyridine) tetrafluoroborate (**2.2b**).

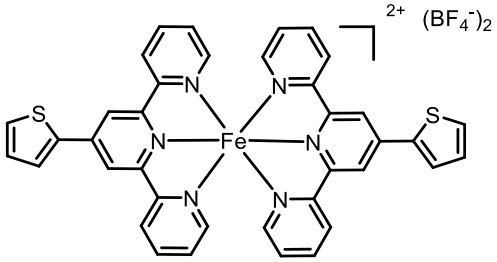

2.2a

Fe(II) Bis(4'-(thiophen-2-yl)-2,2':6',2''-terpyridine) tetrafluoroborate (2.2a). ^{1}H NMR (CD_3CN): 9.11 (4H, s), 8.64 (4H, d, J = 7.83 Hz), 8.32 (2H, dd, J = 3.72, 1.12 Hz), 7.92 (6H, m), 7.49 (2H, dd, J = 5.12, 3.71 Hz), 7.22 (4H, m), 7.10 (4H, m). HRMS (ESI): calcd. for $[M\text{-}2BF_4]^{2+}$ m/z 343.05000, found: 343.05110. UV-vis [CH_3CN, nm ($M^{-1}cm^{-1}$)]: 573 (1.9 $\times 10^4$), 323 (4.0 $\times 10^4$), 280 (4.0 $\times 10^4$). IR (solid, cm^{-1}): 3085.91w,

1615m, 1540.5w, 1470.01m, 1432.14m, 1401.58w, 1339.77w, 1247.68m, 1164.28w, 1059.75s, 856.12w, 790.69m, 755.35w, 727.01w, 655.29w, 633.22w.

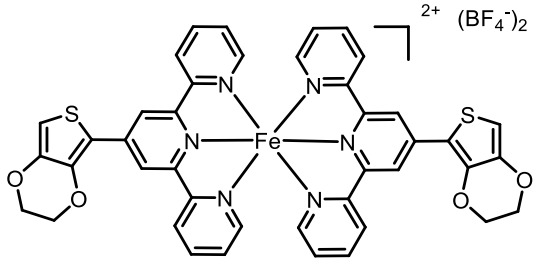

2.2c

Fe(II) Bis(4'-(3,4-ethylenedioxythiophene)-2,2':6',2''-terpyridine) tetrafluoroborate (2.2c). ^{1}H NMR (CD_3CN): 9.12 (4H, s), 8.54 (4H, dt, J = 7.97, 1.07 Hz), 7.87 (4H, td, J = 7.77, 1.39 Hz), 7.18 (4H, m), 7.06 (4H, ddd, J = 7.38, 5.63, 1.29 Hz), 6.92 (2H, s), 4.65 (4H, m), 4.44 (4H, m). HRMS (ESI): calcd. for $[M\text{-}2BF_4]^{2+}$ m/z: 401.05550, found: 401.05740. UV-vis [CH_3CN, nm ($M^{-1}cm^{-1}$)]: 582 (2.3×10^4), 350 (3.2×10^4), 317 (3.6×10^4), 283 (3.6×10^4), 275 (3.1×10^4). IR (solid, cm^{-1}): 3111.89w, 1610.94m, 1533.97w, 1497.82m, 1481.88w, 1450.12w, 1427.78m, 1364.07m, 1282.94w, 1166.75w, 1068.38s, 954.80w, 910.22w, 792.98w, 757.67w, 723.03w, 695.33w, 653.83w, 613.43w.

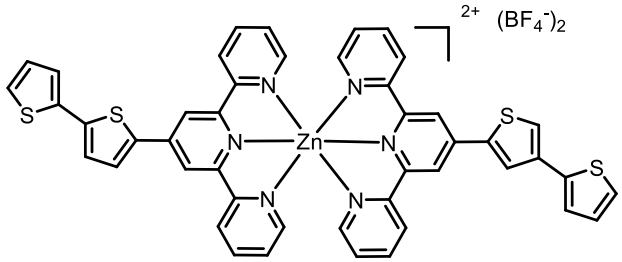

2.3b

Zn(II) Bis(4'-(2,2'-bithiophen-5-yl)-2,2':6',2''-terpyridine) tetrafluoroborate (2.3b). ^{1}H NMR (CD_3CN): 8.81 (4H, s), 8.69 (4H, d, J = 7.95 Hz), 8.16 (6H, m), 7.84 (4H, d, J = 4.41 Hz), 7.54 (6H, m), 7.40 (4H, m), 7.20 (2H, t, J = 4.35 Hz). HRMS (ESI): calcd. for $[M\text{-}2BF_4]^{2+}$ m/z: 429.03480, found: 429.03620. UV-vis [CH_3CN, nm ($M^{-1}cm^{-1}$)]: 393

(7.2 $\times 10^4$), 320 (5.5 $\times 10^4$), 278 (6.7 $\times 10^4$), 234 (7.6 $\times 10^4$). IR (solid, cm^{-1}): 3074.40w, 1600.90m, 1570.64w, 1549.72w, 1510.98w, 1476.46m, 1449.01m, 1424.95m, 1371.75w, 1252.88w, 1164.09w, 1049.40s, 1025.13s, 1011.88s, 884.10w, 864.20w, 839.42w, 822.59w, 788.63m, 777.84m, 744.26w, 726.01w, 689.53m, 675.20w, 656.67w, 639.24w.

2.2.5 Electrochemistry

Electrochemical studies were performed in a glovebox under a nitrogen atmosphere using GPES software from Eco. Chemie B. V. and an Autolab Potentiostat (PGSTAT30). All electrochemical experiments were performed in acetonitrile with 0.1 M $TBAPF_6$ as supporting electrolyte. All cyclic voltammetry (CV) experiments were carried out with ITO-coated glass electrode, a Pt wire coil counter electrode and a $AgNO_3$/Ag reference electrode (Ag wire dipped in a 0.01 M $AgNO_3$ solution with 0.1 M $TBAPF_6$ in dry acetonitrile). Unless stated otherwise, potentials are reported relative to the ferrocenium/ferrocene couple (Fc^+/Fc), which was used as an external standard to calibrate the $AgNO_3$/Ag reference electrode. For electrochemical impedance spectroscopy (EIS) measurements, Autolab Potentiostat (PGSTAT128) and NOVA software were used. The EIS spectra of a bare ITO film (R_s = 4-10 Ω, 1 cm^2) and the same ITO film after 5, 10, 15, 20 and 25 potential sweeping cycles, respectively, were measured in the frequency range of 10^6 to 10^{-1} Hz with 0.01 V amplitude. EIS measurements were carried out at 0.7 V vs $AgNO_3$/Ag during temporary interruptions of the polymerization process as described below.

2.2.6 Electropolymerization of The Metallopolymer Films

The preparation of polymeric films (**poly-2.2b**, **poly-2.3b**, and **poly-2.2c**) was achieved via electrochemical polymerization, which was conducted in a three-electrode cell by CV in dry acetonitrile or $BF_3 \cdot Et_2O$ solution containing monomers and 0.1 M

$TBAPF_6$ as supporting electrolyte at a scan rate of 100 mV/s. By successively scanning the working electrode from -0.5 V to 1.5 V vs a $AgNO_3$/Ag reference electrode for a set number of CV cycles, the monomer was sequentially electropolymerized onto the ITO working electrode surface to create a layer of film. The resulting films were washed three times with dry acetonitrile to remove residual monomer and electrolyte, then characterized and tested for electrochromic properties.

2.2.7 UV-vis-NIR Spectroelectrochemistry

The spectroelectrochemical measurements were obtained using the previously-described cell arrangement and performed on polymeric films deposited on ITO-coated glass substrates which also functioned as the working electrode, a platinum wire coil as the counter electrode, and $AgNO_3$/Ag as reference electrode. Experiments were carried out in an optical cuvette inside the glovebox. Absorption spectra were recorded on a Varian Cary 6000i UV-vis-NIR spectrophotometer within the NIR/visible spectra ($1300 \geq \lambda \geq 365$ nm) under several applied potentials.

2.2.8 Single Crystal X-ray Structure Determination

Crystals of **2.2a**, **2.2c** and **2.3b** were grown though slow evaporation from acetone. Crystals of **2.2b** grew as purple needles by vapor diffusion of diethyl ether into an acetone solution of **2.2b**. Crystals suitable for data collection were covered with hydrocarbon oil and mounted on thin nylon loops. X-ray experimental details can be found in the Appendix.

2.2.9 Preparation of Solid-State Electrochromic Devices

The gel electrolyte [acetonitrile (ACN) : poly-propylene carbonate (PC) : poly-methyl methacrylate (PMMA) : $(CF_3SO_2)_2N^-Li^+$ 70:20:7:3 wt% composition] was drop cast onto the **poly-2.2b**/ITO film, covered with another ITO film and then dried under vacuum overnight. The ITO films used for the device have a R_s value of 4-10 Ω, and were

purchased from Delta Technologies, LTD. The layered structures of the device are described in the following discussion.

2.3 Results and Discussion

2.3.1 Structure of the Metal Complexes

Ligands **2.1a**-**2.1c** were synthesized according to literature procedures, and characterization data for them is consistent with literature values.[38, 43, 44] The homoleptic complexes, **2.2a**-**2.2c**, were prepared by the reaction of iron(II) tetrafluoroborate hexahydrate and the corresponding ligand with a 1:2 ratio in a mixture of dichloromethane and acetone under a nitrogen atmosphere over the course of 1 h. **2.3b** was synthesized using zinc(II) tetrafluoroborate hydrate and **2.1b** in a similar manner. The ^{1}H NMR spectra of the complexes, as recorded in CD_3CN, have revealed well-resolved signals in the aromatic region. In comparison to the NMR peaks of the ligands, the signals of the terpyridine units shift upon metalation, indicating successful complexation between ligand and metal.[35, 45] All the complexes showed IR absorptions around 1050 cm^{-1} (Figure 2.1), indicating the B-F stretching mode from the counter ion BF_4^-.[46] Single crystal X-ray structures of all complexes were obtained. As shown in Figure 2.2, X-ray diffraction experiments revealed the monomeric structures of **2.2a**-**2.2c**, and **2.3b**, demonstrating pseudo-octahedral geometry of all the complexes. Crystal structure data have been uploaded to the Cambridge Structural Database; CCDC 1494014-1494017 contain the supplementary crystallographic data for this chapter. The data can be obtained free of charge from The Cambridge Crystallographic Data Centre via www.ccdc.cam.ac.uk/structures.

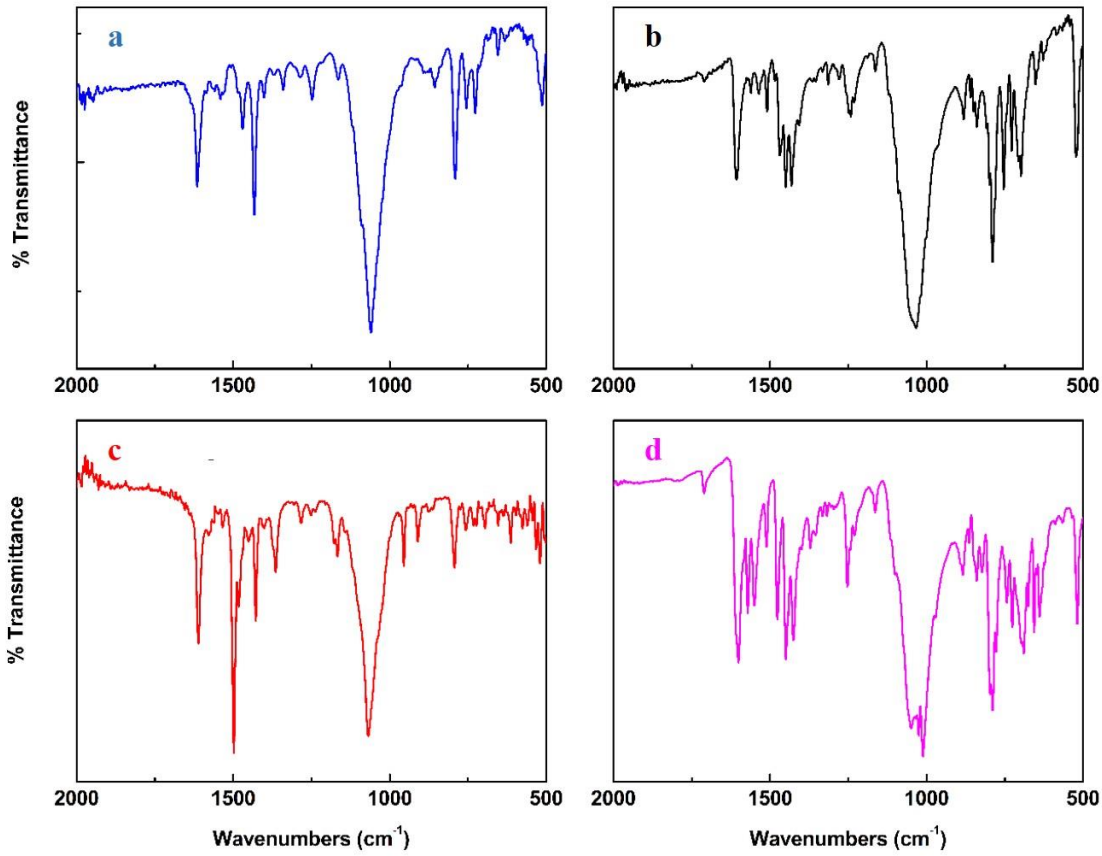

Figure 2.1. FTIR spectra of metal complexes **2.2a** (a), **2.2b** (b), **2.2c** (c), and **2.3b** (d).

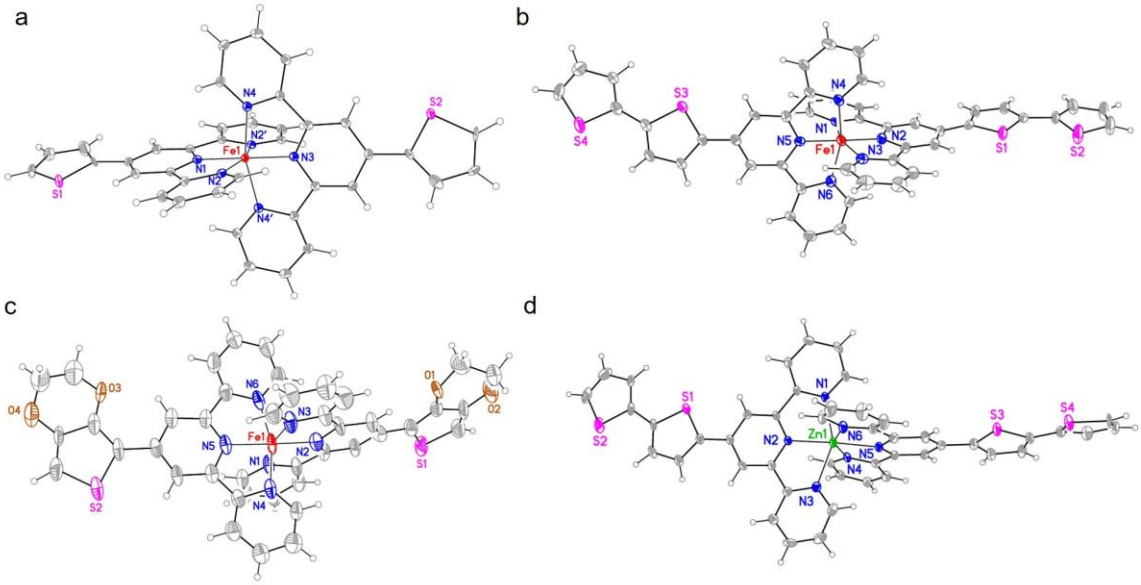

Figure 2.2. Views of the **2.2a** (a), **2.2b** (b), **2.2c** (c) and **2.3b** (d) complexes showing the heteroatom labeling scheme. Displacement ellipsoids are scaled to the 50% probability level.

2.3.2 Electropolymerization Growth of the Polymeric Films

The electrochemical polymerization procedure is described in the Experimental Section 2.2.6. Complex **2.2b** was electropolymerized on the surface of ITO-coated glass in dry acetonitrile solution, while **2.2c** was electropolymerized on the ITO surface in $BF_3{\cdot}Et_2O$ solution to form the films (**poly-2.2b**, and **poly-2.2c**). Complex **2.2a** failed to electropolymerize in either acetonitrile or $BF_3{\cdot}Et_2O$ solutions. This solvent effect has been observed by Forster and co-workers before, resulting from the stability of the cation radical formed during the electropolymerization process.[35] The electrochemical polymerization mechanism of polythiophene is known to display a 95+% preference for α,α-coupling.[47] Thus, it seems reasonable to assume that the thiophene-containing metal-bis(terpyridine) complex underwent oxidative electropolymerization by linking the α-carbons of the outermost thienyl groups of each complex to the outermost α-carbons of the neighboring complex, as illustrated in Scheme 2.2.[48]

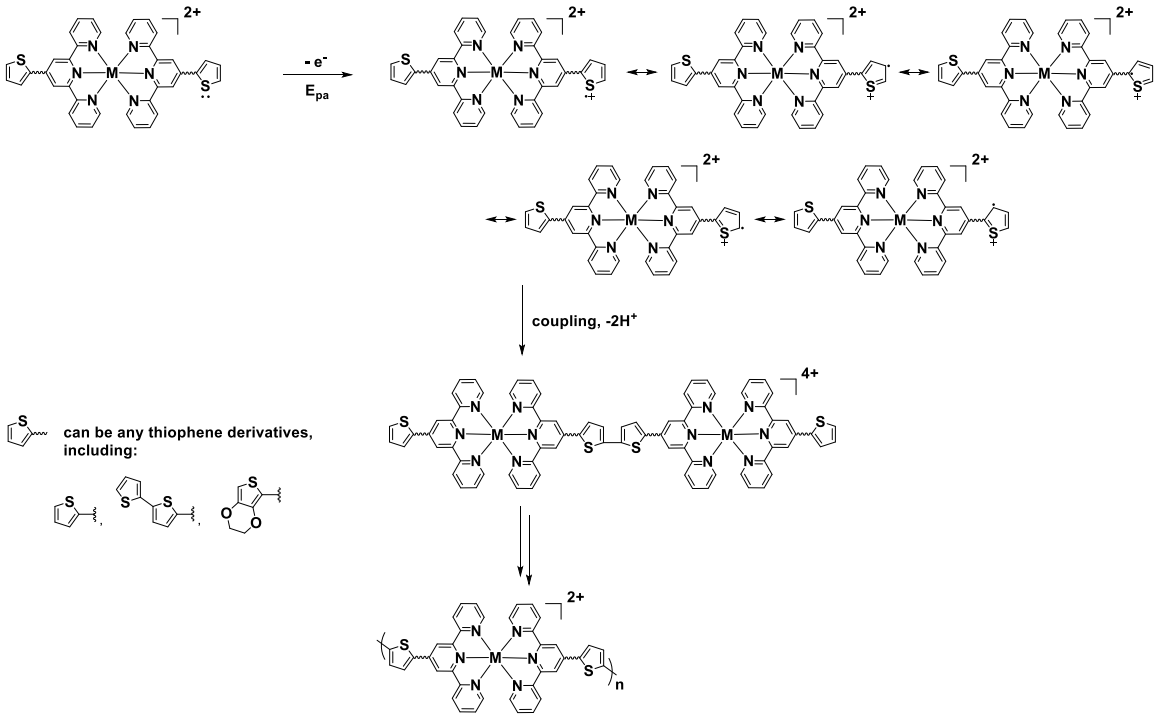

Scheme 2.2. Electrochemical polymerization mechanism of the thiophene-containing metal-bis(terpyridine) complex.

For the electropolymerization of **2.2b** on the ITO surface, the linear increase of redox current at $E_{1/2}$ = 0.77 V (Figure 2.3) indicates that the amount of deposited polymer on the ITO surface was increased with successive CV scans. The irreversible redox behavior at 1.12 V can be attributed to the oxidation of the bithiophene moiety.[49] The sharp irreversible peak at 0.6 V before the oxidation wave (Fe^{2+} to Fe^{3+}) was previously reported as a charge trapping event in a very similar electropolymerizable system with Os^{2+} as the metal center.[35] After being rinsed with acetonitrile three times to remove unreacted monomer and oligomeric species, a blue-colored film of insoluble material (i.e., **poly-2.2b**) was observed on the ITO surface. The cyclic voltammogram of the resulting film tested in a monomer-free acetonitrile electrolyte solution demonstrated one reversible redox process at 0.77 V (Figure 2.3, inset), which corresponds to the half wave potential reported for

Fe^{3+}/Fe^{2+} redox couple.[21] Additionally, the CV curves of the **poly-2.2b** film were measured under various scan rates. The peak currents were linearly proportional to the scan rates (Figure 2.3, inset), evidencing a thin film absorption redox behavior on the ITO surface.[50] When testing the redox properties of the **poly-2.2b** film in a monomer-free acetonitrile solution, the irreversible peak at 0.6 V only appeared at the first scan and was completely diminished over subsequent scans (Figure 2.4a). Also, the intensity of this peak largely decreased when the potential window was shifted toward more positive potentials (Figure 2.4b). Such evidence corroborates the charge-trapping property of the irreversible peak at 0.6 V. EIS measurements were conducted on an ITO electrode modified with **poly-2.2b** in the frequency of 10^6 to 10^{-1} Hz with an amplitude of 0.01 V during temporary interruptions of the electropolymerization process. Nyquist plots derived from the impedance spectra show depressive semicircles; the diameter of the semicircle increases with polymer growth (Figure 2.5). The diameter of the semicircle is responsible for the resistance of electron transfer in the polymer film.[51] These observations reveal the successful electropolymerization process of **2.2b** on the ITO surface. To confirm the onset oxidation potential of the bithiophene moiety within **poly-2.2b**, a redox-inert **2.3b** complex was synthesized and electrochemically polymerized on the ITO surface. The first CV scan of **2.3b** solution shows an irreversible oxidation peak at 1 V (Figure 2.6, red line), and the current of the anodic peak at 1.2 V increases linearly as the scan number increases (Figure 2.6, inset), verifying that the oxidative polymerization of the bithiophene component within **2.2b** or **2.3b** occurs when the potential reached 1.2 V. After the resulting **poly-2.3b** film was rinsed with acetonitrile three times, the current drops drastically from 150 μA to 15 μA. The current drop is attributed to delamination, suggesting that the **poly-2.3b** film growth is not as stable as the **poly-2.2b** film on the ITO surface. Such delamination of the **poly-2.3b** film from the ITO substrate is not surprising because the adhesion between the

electropolymerized (or electrodeposited) film and the electrode surface is mostly due to noncovalent interactions.[52, 53] Redox matching of the metal-centered electroactivity with that of the electropolymerizable backbone also plays a crucial role in the resulting properties of the electropolymerized films, such as stability and conductivity.[1]

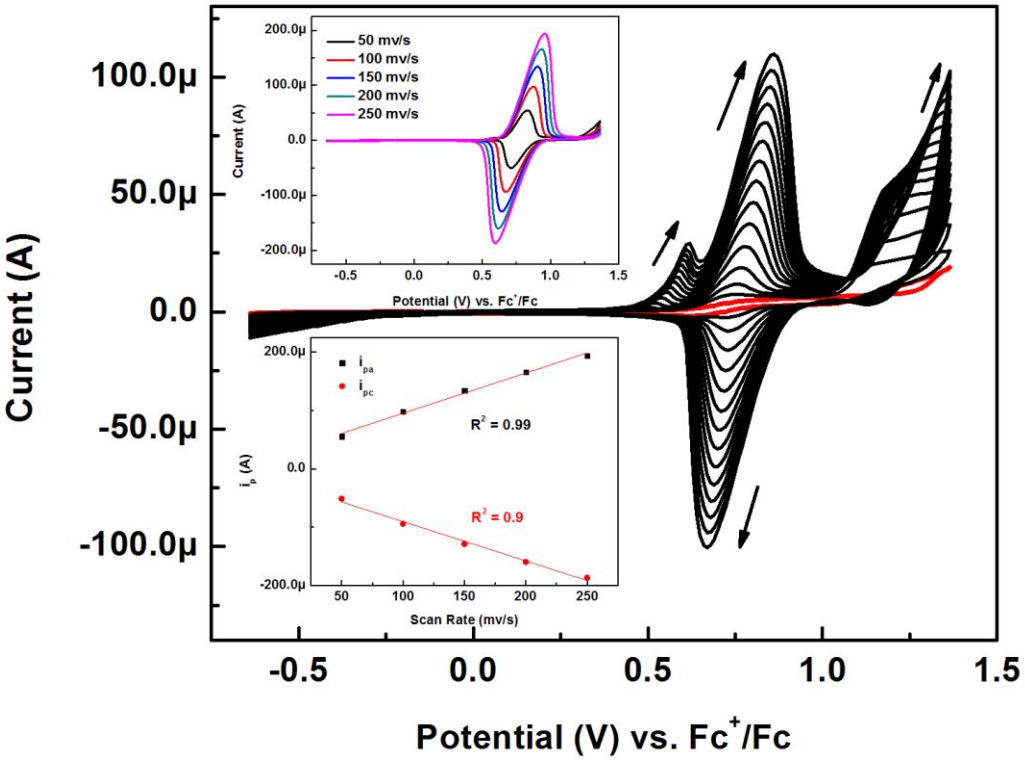

Figure 2.3. Overlay of continuous cyclic voltammograms of **poly-2.2b** over time on the ITO surface in acetonitrile solution of 0.1 mM **2.2b** with 0.1 M $TBAPF_6$ electrolyte at a scan rate of 100 mV/s. The red curve indicates the initial CV scan. The inset graphs indicate that both the anodic and cathodic peak currents ($E_{1/2}$ = 0.77 V) of the **poly-2.2b** film increase linearly as the scan rate increases (50, 100, 150, 200, and 250 mV/s) in a monomer-free acetonitrile solution with 0.1 M $TBAPF_6$ as the supporting electrolyte.

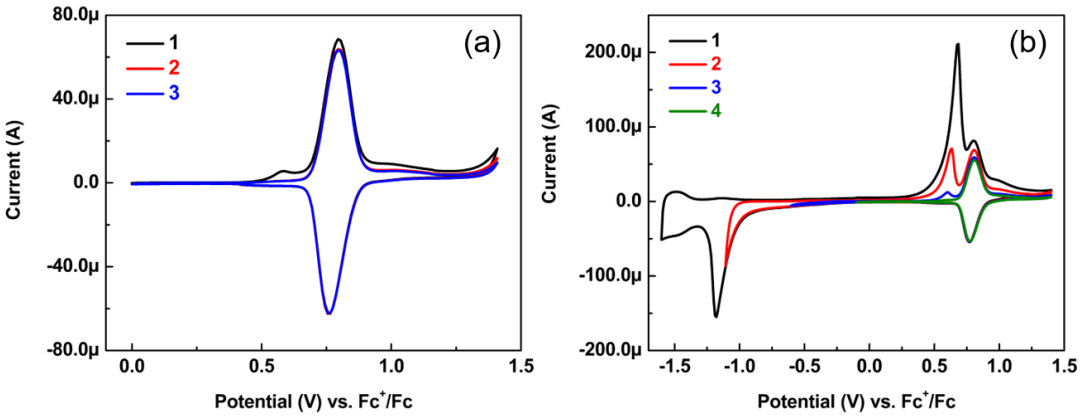

Figure 2.4. (a) Overlay of the first (1), second (2) and third (3) CV scans of **poly-2.2b** electropolymerized on an ITO surface in a monomer-free acetonitrile solution with 0.1 M $TBAPF_6$ as supporting electrolyte at a scan rate of 100 mV/s. (b) CV scans of **poly-2.2b** electropolymerized on ITO surface in a monomer-free acetonitrile solution with different potential sweeping windows.

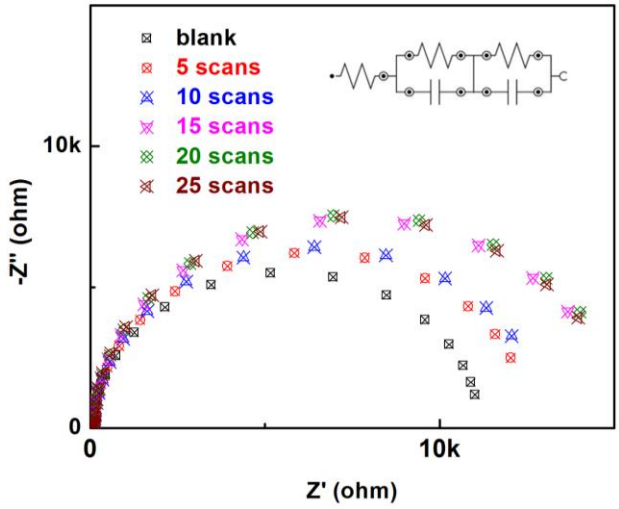

Figure 2.5. Fitted Nyquist plots (-Z'' vs Z') measured on a bared ITO electrode (blank) and **poly-2.2b** modified on the same ITO electrode after potential sweeping of 5, 10, 15, 20, and 25 cycles during electropolymerization process. Inset shows equivalent circuit.

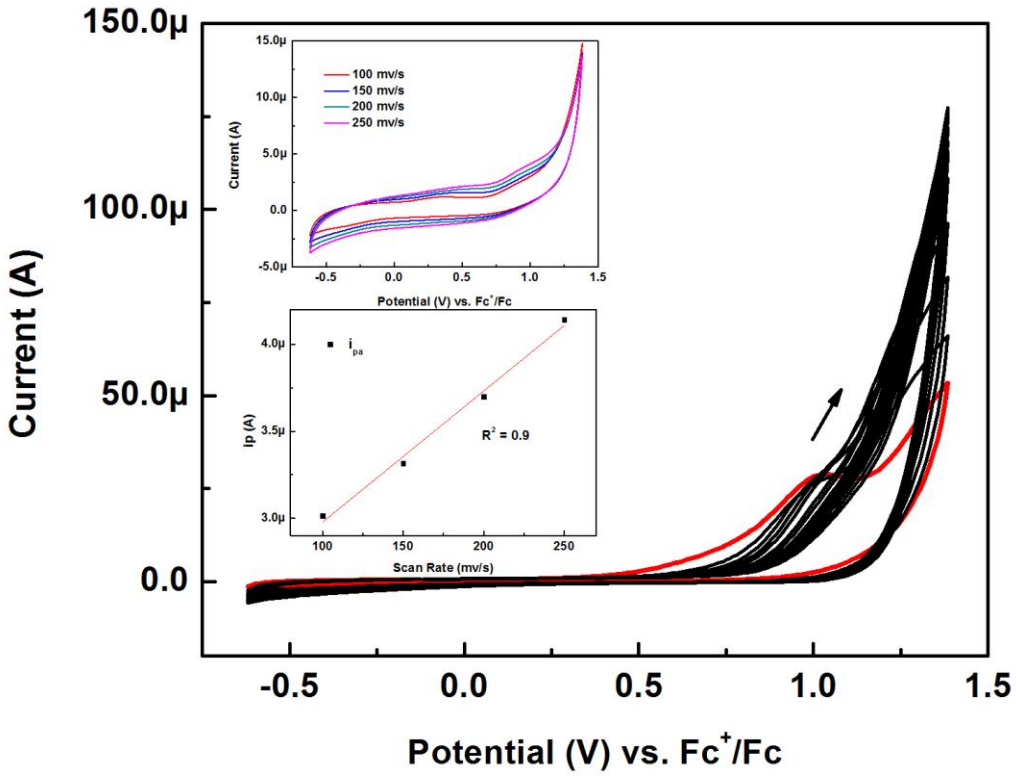

Figure 2.6. Overlay of continuous cyclic voltammograms of **poly-2.3b** over time on the ITO surface in acetonitrile solution of 0.1 mM **2.3b** with 0.1 M $TBAPF_6$ electrolyte at a scan rate of 100 mV/s. The red curve indicates the first CV scan. The inset graphs indicate that the anodic peak current (at 1.2 V) increases linearly as the scan rate increases (100, 150, 200, and 250 mV/s) in a monomer-free acetonitrile solution with 0.1 M $TBAPF_6$ as the supporting electrolyte.

Complex **2.2c** failed to polymerize on the ITO substrate in acetonitrile but did demonstrate a peak current increase in a $BF_3{\cdot}Et_2O$ solution (Figure 2.7). The current amplitudes of the cathodic and anodic peaks at $E_{1/2}$ = 0.85 V attributed to the Fe^{3+}/Fe^{2+} redox couple increase with continuous CV scans, indicating the growth of an electroactive film. The value of $E_{1/2}$ for the Fe^{3+}/Fe^{2+} redox couple in **2.2c** higher than that in **2.2b** may be attributed to the different solvents used during electropolymerization processes. The CV

current of the **poly-2.2c** film remained at a steady value after being rinsed with acetonitrile, suggesting a fairly stable film. In addition, the CV curve of the **poly-2.2c** film in a monomer-free electrolyte solution was tested under different scan rates. The peak currents were linearly proportional to the scan rates (Figure 2.7, inset), again confirming a thin film redox behavior at the ITO surface.

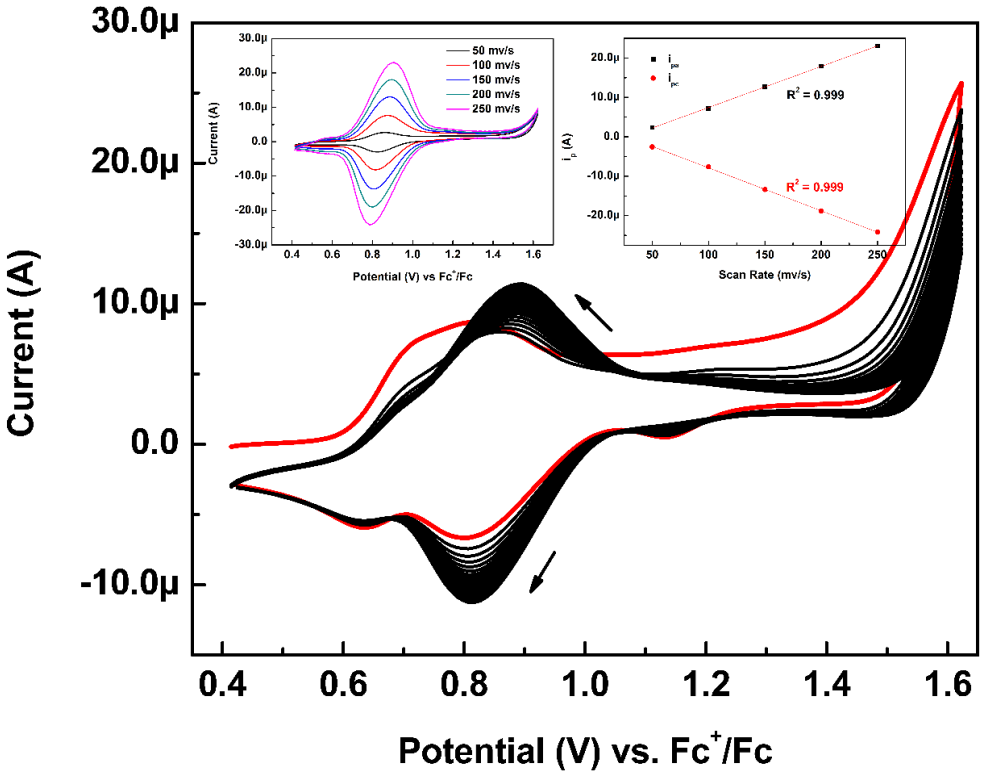

Figure 2.7. Overlay of continuous cyclic voltammograms of **poly-2.2c** over time on the ITO surface in $BF_3{\cdot}Et_2O$ solution of 0.3 mM **2.2c** with 0.1 M $TBAPF_6$ electrolyte at a scan rate of 100 mV/s. The red curve indicates that the first CV scan. The inset graphs indicate that both the anodic and cathodic peak currents ($E_{1/2}$ = 0.85 V) of the **poly-2.2c** film increase linearly as the scan rate increases (50, 100, 150, 200, and 250 mV/s) in a monomer-free acetonitrile solution with 0.1 M $TBAPF_6$ as the supporting electrolyte.

The different behavior of iron complexes **2.2a**-**2.2c** in electropolymerization can be attributed to the electronic distribution of the electrochemically formed cation radical in

thiophene-containing systems.[35] Preliminary DFT calculations show that the SOMO orbital in which the radical cation resides is almost exclusively positioned on the electropolymerizable groups of **2.2b** and **2.2c** (Figure 2.8). The electropolymerization of **2.2c** required more stringent anhydrous conditions and exclusion of other nucleophilic impurities for successful electropolymerization. The radical cation generated upon oxidation of **2.2a** is shown to be delocalized across the thiophene moiety in addition to the terpyridine portion of the ligand and metal center, resulting in lessened reactivity toward electropolymerization. Even though the electropolymerization of **2.2c** is achievable in $BF_3 \cdot Et_2O$ solvent, it is still not as effective as that of **2.2b**, as indicated by the lower current response after performing the same number of CV scans (Figures 2.3 and 2.7). As a result, a colored film could be barely noticed on the ITO surface by the naked eye after electropolymerzing **2.2c**. In contrast, a thick and stable film can be grown from **2.2b** electrochemically on an ITO surface, which is evidence of suitability for electrochromic material applications.

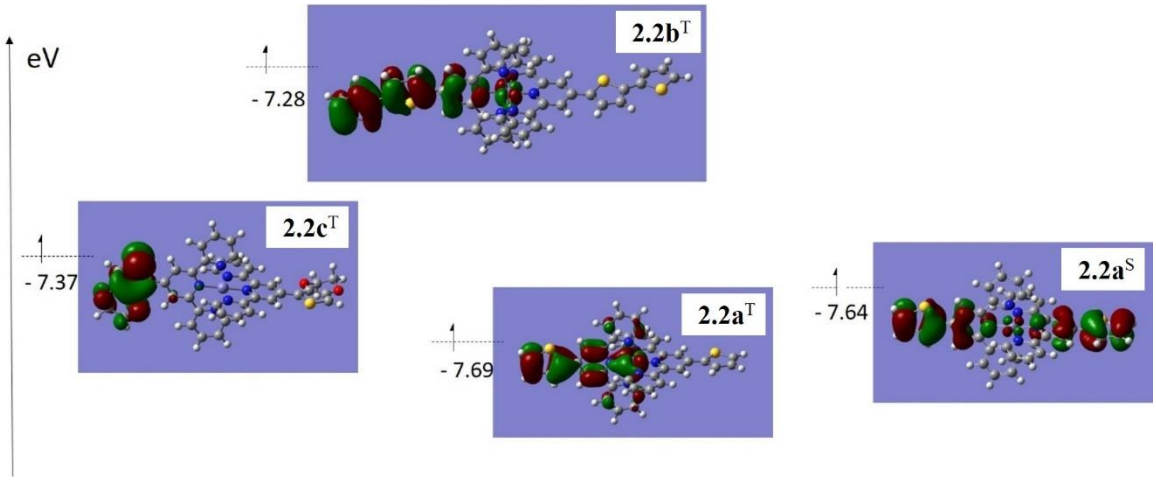

Figure 2.8. Calculated SOMOs of the two-electron oxidized forms of **2.2a**-**2.2c** in triplet state configurations. Calculated SOMO of the two-electron oxidized form of **2.2a** in singlet state configuration is also included.

2.3.3 Optical Properties of Metal Complexes (2.2a-2.2c, and 2.3b) and Metallopolymers (poly-2.2b)

Ligands **2.1a**-**2.1c** and the corresponding Fe(II) complexes **2.2a**-**2.2c** were investigated using UV-vis spectroscopy in acetonitrile solution (Figure 2.9a). The molar absorptivity of the most red-shifted π-π^* ligand energy transfer peak and the corresponding metal-ligand charge transfer (MLCT) peak are summarized in Table 2.1. The lowest energy absorption band is at 280 nm for **2.1a**, 328 nm for **2.1c**, and 356 nm for **2.1b**, suggesting that the bathochromic shift of the $\pi \rightarrow \pi^*$ absorption peak is due to the increasing conjugation of the ligand. The corresponding Fe(II) complexes, **2.2a**-**2.2c**, differ from the color of the ligands, appearing dark purple in color upon coordination. The drastic color change is assigned to the metal-ligand charge transfer (MLCT) at ca. 585 nm wavelength, which is common for Fe(II)-bis(terpyridine) complexes.[15, 20-22] The **2.2a**, **2.2c** and **2.2b** complexes have MLCT absorptions at 573, 581 and 589 nm, respectively. Different chemical modifications on the terpyridine ligand appear to shift the MLCT band within a range of 16 nm. It also demonstrates a trend toward the bathochromic shift of the MLCT absorption with increasing conjugation. Because the electropolymerization of **2.2b** onto the ITO substrate is efficient enough to observe a dark blue-colored film by naked eye, the absorption profile of the **poly-2.2b** film was analyzed. The MLCT peak of **poly-2.2b** was observed at 596 nm, red-shifted from the MLCT transition of the monomer (589 nm) due to extended conjugation after polymerization.[54]

The absorption profile of **2.3b** in acetonitrile is similar to that of **2.2b** with regard to the ligand-based absorption features from 220 to 450 nm (Figure 2.9b). Additionally, no MLCT absorption is observed due to the d^{10} electron configuration of the Zn^{2+} ion. Compared to the absorption peaks of **2.1b**, both **2.2b** and **2.3b** display a red-shift of the ligand-based absorption peaks after metalation. The similar ligand-based absorption

features of the Fe(II) and Zn(II) complexes suggest that both complexes have similar pseudo-octahedral coordination environments, which matches well with the single crystal structures.[55, 56]

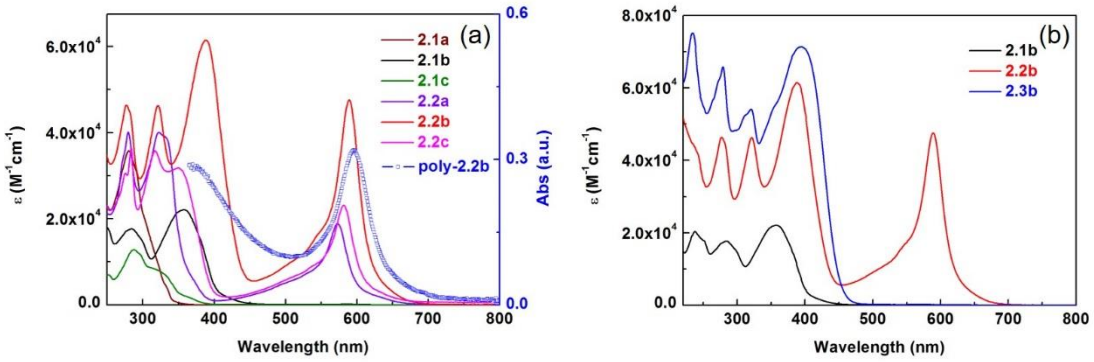

Figure 2.9. (a) Molar absorptivity of ligands **2.1a**-**2.1c** and complexes **2.2a**-**2.2c** in acetonitrile. The absorption profile of **poly-2.2b** is labeled as a blue line with square symbol. (b) Molar absorptivity of **2.1b** and its corresponding **2.2b** and **2.3b** complexes in acetonitrile.

Table 2.1. UV-vis properties of **2.1a**-**2.1c** and **2.2a**-**2.2c** in acetonitrile, and **poly-2.2b** in solid film state on ITO substrate.

Ligand	$\lambda_{\pi-\pi^*}$ (nm), $\varepsilon(10^4 M^{-1}cm^{-1})$	Fe(II) complexes	λ_{MLCT} (nm), $\varepsilon(10^4 M^{-1}cm^{-1})$	Polymers	λ_{MLCT} (nm)
2.1a	280, 3.6	**2.2a**	573, 1.9	**poly-2.2a**	---
2.1b	356, 2.2	**2.2b**	589, 4.7	**poly-2.2b**	596
2.1c	328, 0.7	**2.2c**	581, 2.3	**poly-2.2c**	---
		Fe(terpyridine-triphenylamine)$_2$ [a.]	576, 2.4		

a. Literature reported data.[15]

2.3.4 XPS and AFM Study of the Poly-2.2b Film

The composition of the polymer, **poly-2.2b**, electropolymerized on the ITO film surface was investigated by quantitative XPS. The binding energy of the Fe $2p_{1/2}$ core level

of **poly-2.2b** was found at 721.7 eV, and the binding energy of Fe $2p_{3/2}$ was observed at 709 eV. Moreover, the binding energy of the N 1s XPS peak was observed at 400.2 eV; the S $2p_{1/2}$ peak at 165.6 eV, and the S $2p_{3/2}$ peak at 164.4 eV (Figure 2.10). These results are consistent with the energy levels of Fe 2p and N 1s orbitals of $[Fe(tpy)_2](BF_4)_2 \cdot H_2O$ previously reported (708 and 399.7 eV, respectively),[21] confirming that the complexation between ligand **2.1b** and the Fe (II) precursors is complete. Elemental abundance was calculated, giving the elemental ratios Fe:N:S of 1:6.8:4.1. These ratios are in good agreement with the theoretical ratios (1: 6: 4 in **2.2b**).

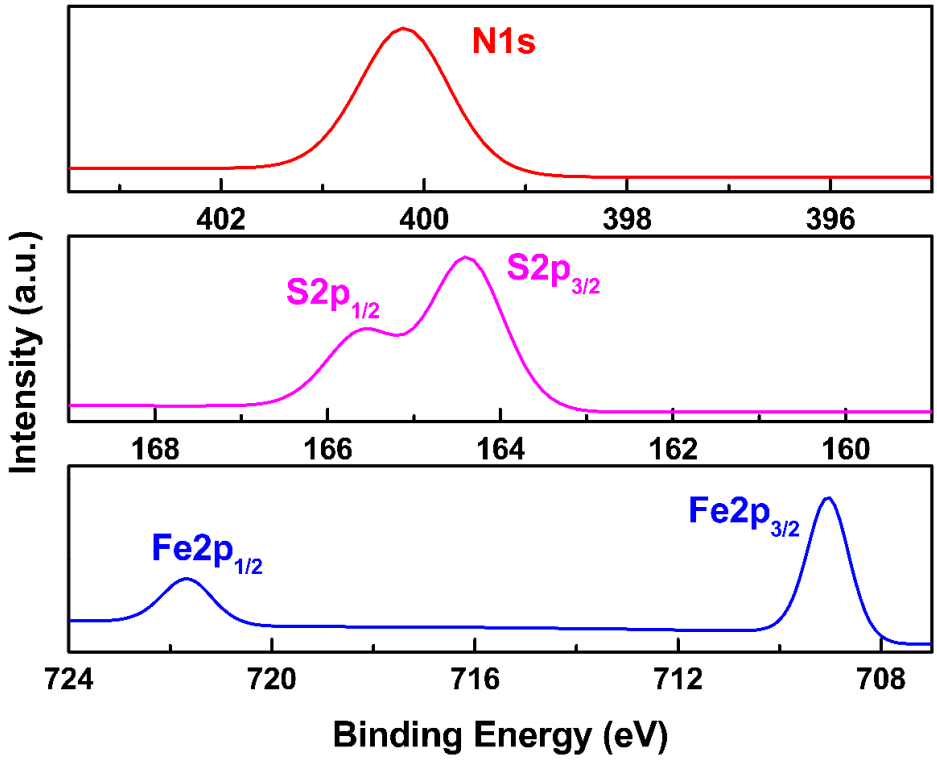

Figure 2.10. XP spectra of **poly-2.2b** on ITO-coated glass surface focusing on N 1s, S 2p, and Fe 2p core levels, respectively.

AFM was used to measure the thickness of the **poly-2.2b** film electropolymerized on ITO after 50 CV cycles of sweeping an applied potential from -0.5 V to 1.5 V (vs

$AgNO_3$/Ag) in a **2.2b** monomer solution. A 3D AFM image and an AFM image are shown in Figure 2.11a and Figure 2.11b. A height of 150 nm was measured at the cross section (labeled "1" in Figure 2.11b) in Figure 2.11c.

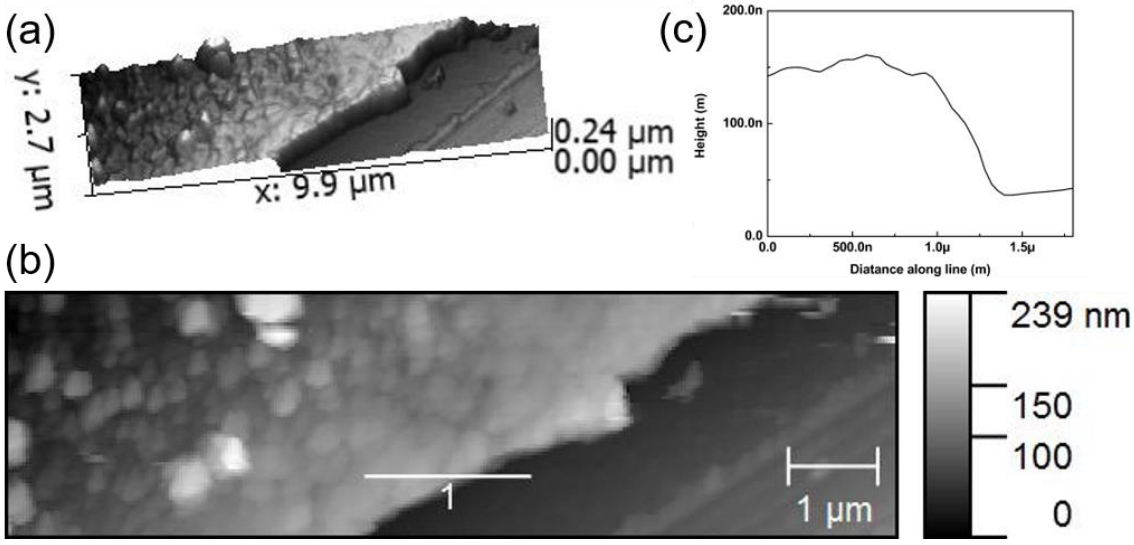

Figure 2.11. (a) 3D-AFM image of surface morphology of **poly-2.2b** film grown after 50 CV scans in the monomer solution on an ITO substrate surface. (b) AFM image and cross-section analysis of **poly-2.2b** on ITO substrate surface. (c) Height measurement of the **poly-2.2b** film at the cross-section (labeled "1" in b).

2.3.5 Electrochromic Behavior of the Poly-2.2b Film

Because the growth of **poly-2.2b** results in sufficient thickness to see a colored film on the ITO surface by the naked eye, **poly-2.2b** was further studied to quantify the observed electrochromic response properties. Cyclic voltammetry experiments of **poly-2.2b** on ITO were performed in a monomer-free acetonitrile solution with 0.1 M $TBAPF_6$ supporting electrolyte (Figure 2.12). One reversible redox event was observed at $E_{1/2}$ = 0.77 V (vs Fc^+/Fc), which was assigned to the $Fe^{3+/}Fe^{2+}$ redox couple within the Fe-bis(terpyridine) moiety, as the value of $E_{1/2}$ is in good agreement with other reported Fe-bis(terpyridine) complexes.[21] This particular electrochemical activity is accompanied by a noticeable

electrochromic behavior. The UV-vis spectrum of **poly-2.2b** film on ITO surface shows a MLCT absorption peak at λ = 596 nm under no applied voltage (Figure 2.13a); however, when **poly-2.2b** was gradually electrochemically oxidized from 0 to 1.2 V, the intensity of the MLCT band decreased significantly, and was completely diminished as the applied voltage achieved passed 0.8 V (Figure 2.13a). Elimination of this MLCT absorption changes the film color from deep blue to pale yellow once oxidized (Figure 2.12, inset). The optical response was recorded and the absorbance change (Δabs.) was calculated as 0.3. When the oxidized film was reduced back to 0.7 V, the MLCT band at 596 nm was reestablished (Figure 2.13b), and the original dark blue color returned (Figure 2.12, inset). Additionally, no electrochromism of **poly-2.3b** was observed, proving that the MLCT absorption within **poly-2.2b** is crucial for the electrochromic behavior observed.

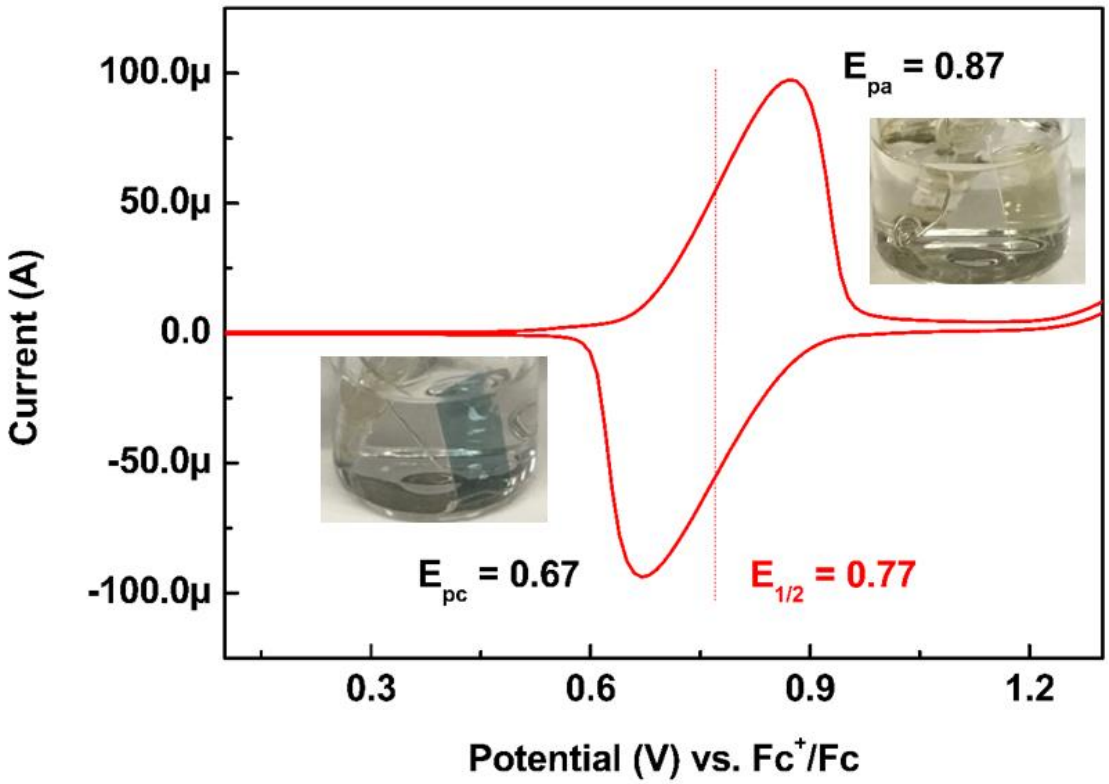

Figure 2.12. Cyclic voltammetry plot of **poly-2.2b** electropolymerized on the ITO surface in a monomer-free acetonitrile solution with 0.1 M $TBAPF_6$ as supporting electrolyte.

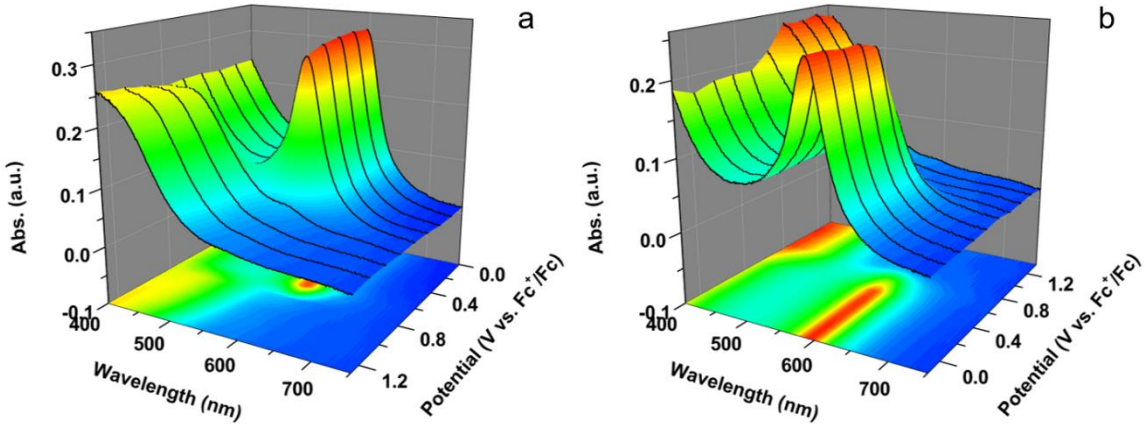

Figure 2.13. Spectroelectrochemistry of **poly-2.2b** measured on an ITO-coated glass surface in acetonitrile with 0.1 M $TBAPF_6$ as supporting electrolyte at a potential sweep from 0 to 1.20 V (a) and from 1.20 to 0 V (b).

The redox states of iron between Fe^{3+} and Fe^{2+} within the **poly-2.2b** film were alternated by switching potentials between 1.1 and 0.4 V while varying switching times and concomitantly monitoring change in percentage transmittance (Figure 2.14a). When the potential switching time was below 0.75 s, the value of ΔT% increased as the increase of the switching time (Figure 2.14b). The value of ΔT% reached a saturation level of 40% when the switching time was above 0.75 s, indicating completion of the oxidation reaction from Fe^{2+} to Fe^{3+} within the **poly-2.2b** film. Coloration efficiency (CE) values correspond to the power efficiency of the electrochromic materials, and imply the change in optical density per unit charge injected/ejected per unit area of the electrode. The value of CE was calculated using the following equation.[57, 58]

$$\mathrm{CE} = \frac{\Delta OD}{Q} = \frac{A_b - A_c}{Q} = \frac{log\frac{T_b}{T_c}}{Q} = \frac{log\frac{T_b}{T_c}}{i \times \mathrm{t}}$$

The area of polymerized **poly-2.2b** was measured with a ruler (Figure 2.15). The length of the film $l = 0.7\ cm$ and the height $h = 2.1\ cm$. Therefore, $\mathrm{Aear} = \mathrm{l} \times \mathrm{h} = 0.7\ \mathrm{cm} \times 2.1\ \mathrm{cm} = 1.47\ cm^2$.

From Figure 2.14, T_b = 89 %, T_c = 49 % $\frac{T_b}{T_c} = \frac{89\ \%}{49\ \%}$ = 1.82 (λ = 596 nm).

From Figure 2.16, current $i = 10^{-4}\ A$

Therefore,

$$\mathrm{CE} = \frac{\Delta OD}{Q} = \frac{A_b - A_c}{Q} = \frac{log\frac{T_b}{T_c}}{Q} = \frac{log\frac{T_b}{T_c}}{i \times \frac{t}{Area}} = \frac{log\ 1.82}{10^{-4} A \times \frac{1\ s}{1.47 cm^2}} = 3823\ cm^2 C^{-1}$$

This CE value is much higher than most values reported for electrochromic metal complexes in the literature, as most achieve CE values on the magnitude of 10^2 to 10^3.[22, 59]

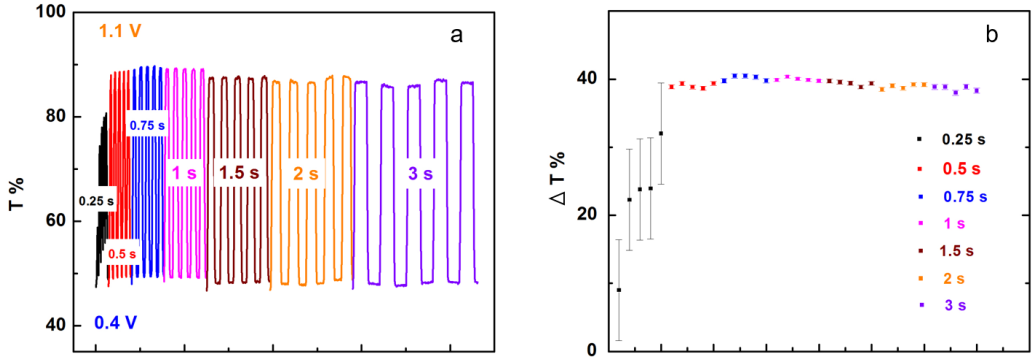

Figure 2.14. T% (a) and Δ T% with error bars (b) at 596 nm for **poly-2.2b** electropolymerized on ITO film surface when switching potentials between 1.1 V and 0.4 V (vs Fc^{+}/Fc) utilizing different interval times.

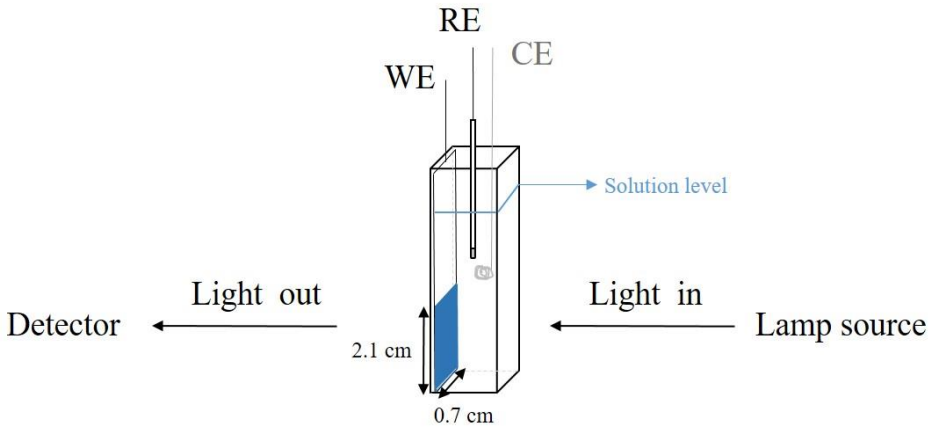

Figure 2.15. Spectroelectrochemistry measurement setup. The blue area indicates the area of electropolymerized **poly-2.2b** film.

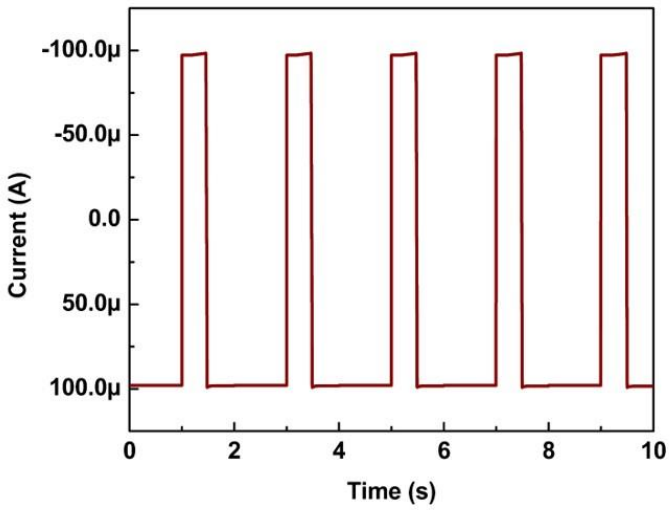

Figure 2.16. Current monitored with potential switching between 1.1 to 0.4 V (vs Fc^{+}/Fc) applied on **poly-2.2b**/ITO film with a time interval of 1 s.

2.3.6 Stability of the Electrochromic Poly-2.2b Film

The notable electrochemical stability of the material was demonstrated by performing CV scans on the **poly-2.2b** film between 0.4 and 1.1 V for 200 cycles (Figure 2.17a). A loss of 10% of the oxidation peak current intensity and a loss of 5% of the reduction peak current intensity were observed after 200 redox cycles (Figure 2.17b). In addition, T% of the **poly-2.2b** film electropolymerized on the ITO glass surface was also monitored by spectroelectrochemistry measurement during 900 cycles of potential switching between 1.1 and 0.4 V with a time interval of 0.75 s (Figure 2.18a). The value of ΔT% remains almost unchanged during the process (Figure 2.18b), which shows good stability of the **poly-2.2b**/ITO film under applied potentials. The stability of the **poly-2.2b** film may be attributed to the extended delocalization of electrons and positive charges throughout the conducting polymer backbone.[22] Additionally, the intramolecular charge transfer from the thiophene group (donor) to the metallic terpyridine group (acceptor) can

also effectively stabilize the oxidized state (i.e., Fe^{3+}) of the metallic terpyridine.[15] The stability might also be due to the method of fabrication of the film. Compared to other molecular assembly methods, electropolymerization involves only the active material without the need of using other assembly materials such as a counter layer, which can disrupt film uniformity.[22, 60]

The feasibility of a solid-state **poly-2.2b**-based device was demonstrated by covering the electropolymerized **poly-2.2b** film with a gel electrolyte (ACN:PC:PMMA:$(CF_3SO_2)_2N^-Li^+$ 70:20:7:3 wt% composition) and a second top ITO electrode (Figure 2.19a). Electrochromic switching between the blue and pale yellow states was observed with this solid-state setup using potential steps of -2.5 to 2.5 V with a pulse width of 10 s (Figure 2.19b).

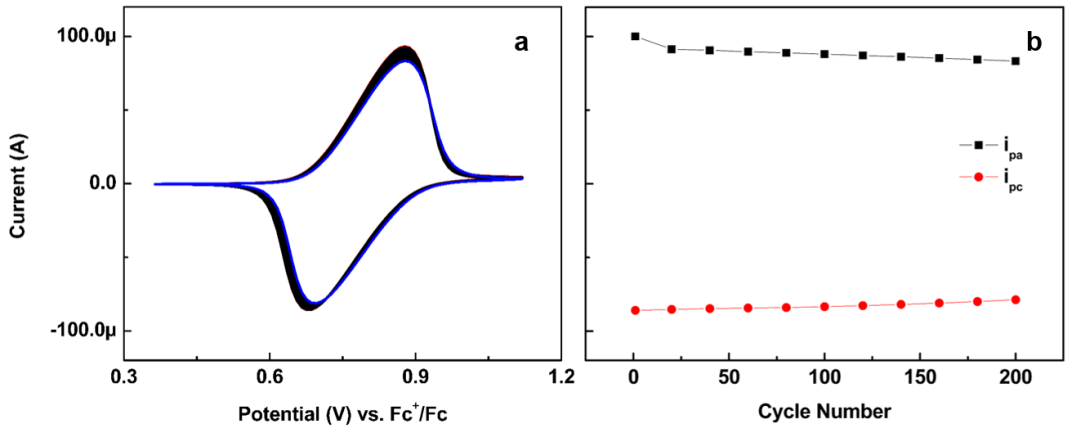

Figure 2.17. Electrochemical stability of **poly-2.2b** film. (a) The polymer film on ITO can perform 200 electrochemical cycles with minimal current loss and switches color between dark blue and pale yellow. (b) Peak oxidation and reduction current as monitored over 200 electrochemical redox cycles.

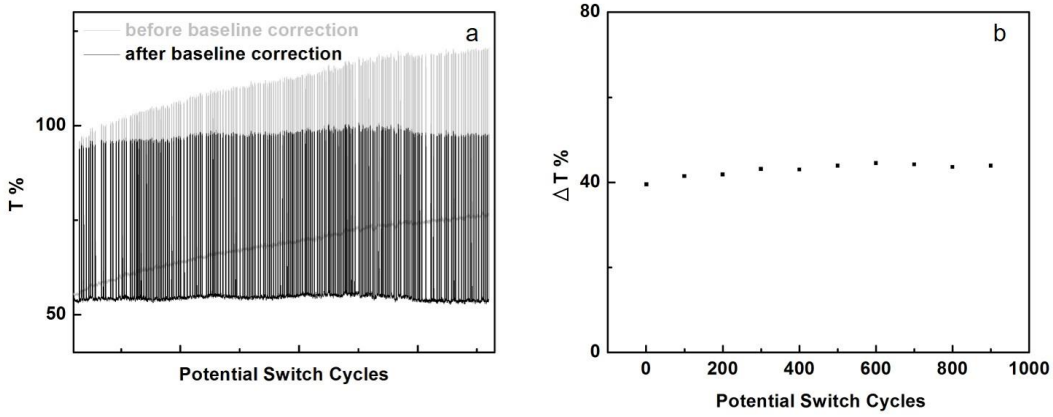

Figure 2.18. T% (a) and ΔT% (b) monitored during 900 potential switches between 1.1 to 0.4 V (vs Fc^{+}/Fc) at 0.75 s intervals applied on the **poly-2.2b** film electrodeposited on the ITO glass surface.

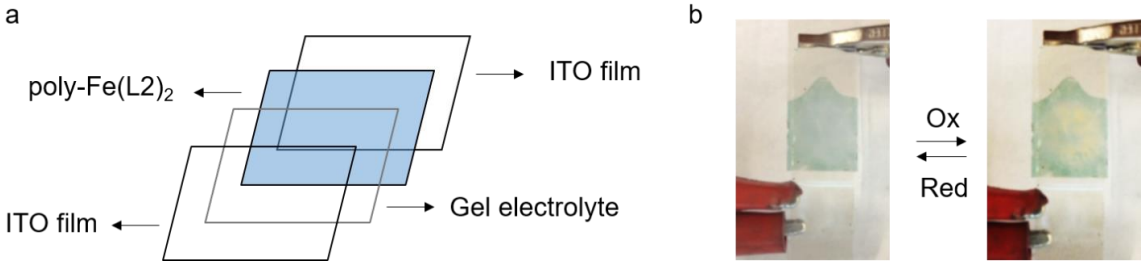

Figure 2.19. Solid-state electrochromic device architecture and performance. (a) Structure of electrochromic device composed of **poly-2.2b**. (b) Photographs showing the device operation. Potential windows of -2.5 to 2.5 V were applied with a pulse width of 10 s.

2.4 CONCLUSION

Three Fe(II)-bis(terpyridine)-based complexes containing thiophene (**2.2a**), bithiophene (**2.2b**) and 3,4-ethylenedioxythiophene (**2.2c**) groups have been synthesized and characterized spectroscopically as well as by single crystal X-ray crystallography. The ligands **2.1a**-**2.1c**, containing thiophene groups, provide a feasible and controllable way to process large areas of polymers via electropolymerization. The electrochromic behavior of the Fe(II)-bis(terpyridine) core structure is preserved, despite the increase in conjugation

upon introducing the thiophene rings. In 2005, Forster and co-workers reported that the choice of solvent exerts an influence on the electropolymerization process.[35] In this study, a similar solvent effect was observed: complex **2.2b** electropolymerized in acetonitrile solution successfully and most efficiently; **2.2c** did not electropolymerize in acetonitrile but did in $BF_3 \cdot Et_2O$ solution, and **2.2a** did not show electropolymerization either in acetonitrile or in $BF_3 \cdot Et_2O$ solution. The **poly-2.2b** electropolymerized on ITO surface has enough thickness to observe a colored film. The electrochromism of **poly-2.2b** was examined by UV-vis spectroscopy and spectroelectrochemistry. Under very low voltages applied between 1.1 and 0.4 V (vs Fc^+/Fc), the obtained electropolymerized film exhibits remarkable electrochromic behavior in 1 s. The high molar absorptivity of the MLCT band ($\varepsilon = 4.7 \times 10^4\ M^{-1}cm^{-1}$) results in a high contrast ratio ($\Delta T\% = 40\%$) and extremely high coloration efficiency (3823 cm^2C^{-1}). Additionally, negligible change of $\Delta T\%$ is noticed after 900 potential switches applied on the electrochromic **poly-2.2b** film, and minimal peak current loss (5%) is observed after subjecting the film to 200 CV cycles. Furthermore, a simple **poly-2.2b**-based solid state electrochromic device was constructed which also demonstrated a color switch from blue to pale yellow. Thus it has been determined that thiophene-containing conducting metallopolymers using Fe(II)-terpyridine as the core structure are potentially useful materials for generating electrochromic devices. Future directions will focus on employing other electropolymerizable groups, as well as Co^{2+} and Ru^{2+} to obtain tunable electrochromic phenomenon at other visible or near-infrared wavelengths.

2.5 REFERENCES

1. Holliday, B. J.; Swager, T. M. Conducting Metallopolymers: The Roles of Molecular Architecture and Redox Matching. *Chem. Commun.* **2005**, 23-36.
2. Whittell, G. R.; Manners, I. Metallopolymers: New Multifunctional Materials. *Adv. Mater.* **2007,** *19*, 3439-3468.

3. Stanley, J. M.; Holliday, B. J. Luminescent Lanthanide-Containing Metallopolymers. *Coord. Chem. Rev.* **2012,** *256*, 1520-1530.

4. Chen, X.-Y.; Yang, X.; Holliday, B. J. Photoluminescent Europium-Containing Inner Sphere Conducting Metallopolymer. *J. Am. Chem. Soc.* **2008,** *130*, 1546-1547.

5. Koga, Y.; Yoshida, N.; Matsubara, K. PL and EL Behavior of Near-Red Luminescent Metallopolymer Easily Prepared from Phosphine-Containing Copolymer and Chloro{Bis(1-Phenylisoquinolinato-N,$C^{2'}$)}Iridium(III), and Its Monomeric Analog. *J. Polym. Sci., Part A: Polym. Chem.* **2009,** *47*, 4366-4378.

6. Holliday, B. J.; Stanford, T. B.; Swager, T. M. Chemoresistive Gas-Phase Nitric Oxide Sensing with Cobalt-Containing Conducting Metallopolymers. *Chem. Mater.* **2006,** *18*, 5649-5651.

7. Smith, R. C.; Tennyson, A. G.; Won, A. C.; Lippard, S. J. Conjugated Metallopolymers for Fluorescent Turn-on Detection of Nitric Oxide. *Inorg. Chem.* **2006,** *45*, 9367-9373.

8. Mejía, M. L.; Agapiou, K.; Yang, X.; Holliday, B. J. Seeded Growth of CdS Nanoparticles within a Conducting Metallopolymer Matrix. *J. Am. Chem. Soc.* **2009,** *131*, 18196-18197.

9. Edelman, K. R.; Stevenson, K. J.; Holliday, B. J. Conducting Metallopolymers as Precursors to Fabricate Palladium Nanoparticle/Polymer Hybrids for Oxygen Reduction. *Macromol. Rapid Commun.* **2012,** *33*, 610-615.

10. Djukic, B.; Lemaire, M. T. Hybrid Spin-Crossover Conductor Exhibiting Unusual Variable-Temperature Electrical Conductivity. *Inorg. Chem.* **2009,** *48*, 10489-10491.

11. Djukic, B.; Seda, T.; Gorelsky, S. I.; Lough, A. J.; Lemaire, M. T. π-Extended and Six-Coordinate Iron(II) Complexes: Structures, Magnetic Properties, and the Electrochemical Synthesis of a Conducting Iron(II) Metallopolymer. *Inorg. Chem.* **2011,** *50*, 7334-7343.

12. O'Sullivan, T. J.; Djukic, B.; Dube, P. A.; Lemaire, M. T. A Conducting Metallopolymer Featuring Valence Tautomerism. *Chem. Commun.* **2009**, 1903-1905.

13. Satheeshkumar, C.; Park, J.-Y.; Jeong, D.-C.; Song, S. G.; Lee, J.; Song, C. Synthesis and Electronic Properties of N-Heterocyclic Carbene-Containing Conducting Polymers with Coinage Metals. *RSC Adv.* **2015,** *5*, 60892-60897.

14. Powell, A. B.; Bielawski, C. W.; Cowley, A. H. Design, Synthesis, and Study of Main Chain Poly(N-Heterocyclic Carbene) Complexes: Applications in Electrochromic Devices. *J. Am. Chem. Soc.* **2010,** *132*, 10184-10194.

15. Fan, C.; Ye, C.; Wang, X.; Chen, Z.; Zhou, Y.; Liang, Z.; Tao, X. Synthesis and Electrochromic Properties of New Terpyridine-Triphenylamine Hybrid Polymers. *Macromolecules* **2015,** *48*, 6465-6473.

16. Bao, X.; Zhao, Q.; Wang, H.; Liu, K.; Qiu, D. Metallopolymer Electrochromic Film Prepared by Oxidative Electropolymerization of a Fe(II) Complex with Arylamine Functionalized Terpyridine Ligand. *Inorg. Chem. Commun.* **2013,** *38*, 88-91.

17. Beaujuge, P. M.; Reynolds, J. R. Color Control in π-Conjugated Organic Polymers for Use in Electrochromic Devices. *Chem. Rev.* **2010,** *110*, 268-320.

18. Groenendaal, L.; Zotti, G.; Aubert, P. H.; Waybright, S. M.; Reynolds, J. R. Electrochemistry of Poly(3,4-Alkylenedioxythiophene) Derivatives. *Adv. Mater.* **2003,** *15*, 855-879.

19. Niklasson, G. A.; Granqvist, C. G. Electrochromics for Smart Windows: Thin Films of Tungsten Oxide and Nickel Oxide, and Devices Based on These. *J. Mater. Chem.* **2007,** *17*, 127-156.

20. Han, F. S.; Higuchi, M.; Kurth, D. G. Metallosupramolecular Polyelectrolytes Self-Assembled from Various Pyridine Ring-Substituted Bisterpyridines and Metal Ions: Photophysical, Electrochemical, and Electrochromic Properties. *J. Am. Chem. Soc.* **2008,** *130*, 2073-2081.

21. Takada, K.; Sakamoto, R.; Yi, S.-T.; Katagiri, S.; Kambe, T.; Nishihara, H. Electrochromic Bis(Terpyridine)Metal Complex Nanosheets. *J. Am. Chem. Soc.* **2015,** *137*, 4681-4689.

22. Shankar, S.; Lahav, M.; van der Boom, M. E. Coordination-Based Molecular Assemblies as Electrochromic Materials: Ultra-High Switching Stability and Coloration Efficiencies. *J. Am. Chem. Soc.* **2015,** *137*, 4050-4053.

23. Friebe, C.; Hager, M. D.; Winter, A.; Schubert, U. S. Metal-Containing Polymers Via Electropolymerization. *Adv. Mater.* **2012,** *24*, 332-345.

24. Scheuble, M.; Goll, M.; Ludwigs, S. Branched Terthiophenes in Organic Electronics: From Small Molecules to Polymers. *Macromol. Rapid Commun.* **2015,** *36*, 115-137.

25. Link, S. M.; Scheuble, M.; Goll, M.; Muks, E.; Ruff, A.; Hoffmann, A.; Richter, T. V.; Navarrete, J. T. L.; Delgado, M. C. R.; Ludwigs, S. Electropolymerized Three-Dimensional Randomly Branched EDOT-Containing Copolymers. *Langmuir* **2013,** *29*, 15463-15473.

26. McEntee, G. J.; Skabara, P. J.; Vilela, F.; Tierney, S.; Samuel, I. D. W.; Gambino, S.; Coles, S. J.; Hursthouse, M. B.; Harrington, R. W.; Clegg, W. Synthesis and Electropolymerization of Hexadecyl Functionalized Bithiophene and Thieno[3,2-b]Thiophene End-Capped with EDOT and EDTT Units. *Chem. Mater.* **2010,** *22*, 3000-3008.

27. Segura, J. L.; Gómez, R.; Reinold, E.; Bäuerle, P. Synthesis and Electropolymerization of a Perylenebisimide-Functionalized 3,4-Ethylenedioxythiophene (EDOT) Derivative. *Org. Lett.* **2005,** *7*, 2345-2348.

28. Akoudad, S.; Roncali, J. Modification of the Electrochemical and Electronic Properties of Electrogenerated Poly(3,4-Ethylenedioxythiophene) by Hydroxymethyl and Oligo(Oxyethylene) Substituents. *Electrochem. Commun.* **2000,** *2*, 72-76.

29. Amb, C. M.; Dyer, A. L.; Reynolds, J. R. Navigating the Color Palette of Solution-Processable Electrochromic Polymers. *Chem. Mater.* **2011,** *23*, 397-415.

30. Dyer, A. L.; Thompson, E. J.; Reynolds, J. R. Completing the Color Palette with Spray-Processable Polymer Electrochromics. *ACS Appl. Mater. Interfaces* **2011,** *3*, 1787-1795.

31. Heuer, H. W.; Wehrmann, R.; Kirchmeyer, S. Electrochromic Window Based on Conducting Poly(3,4-Ethylenedioxythiophene)-Poly(Styrene Sulfonate). *Adv. Funct. Mater.* **2002,** *12*, 89-94.

32. Ponder, J. F.; Österholm, A. M.; Reynolds, J. R. Designing a Soluble PEDOT Analogue without Surfactants or Dispersants. *Macromolecules* **2016,** *49*, 2106-2111.

33. Kumar, A.; Welsh, D. M.; Morvant, M. C.; Piroux, F.; Abboud, K. A.; Reynolds, J. R. Conducting Poly(3,4-Alkylenedioxythiophene) Derivatives as Fast Electrochromics with High-Contrast Ratios. *Chem. Mater.* **1998,** *10*, 896-902.

34. Naseri, Z.; Nemati Kharat, A.; Banavand, A.; Bakhoda, A.; Foroutannejad, S. First Row Transition Metal Complexes of Thienyl Substituted Terpyridine: Structural, Photophysical and Biological Studies. *Polyhedron* **2012,** *33*, 396-403.

35. Hjelm, J.; Handel, R. W.; Hagfeldt, A.; Constable, E. C.; Housecroft, C. E.; Forster, R. J. Conducting Polymers Containing in-Chain Metal Centers: Electropolymerization of Oligothienyl-Substituted {M(Tpy)2} Complexes and in Situ Conductivity Studies, M = Os(II), Ru(II). *Inorg. Chem.* **2005,** *44*, 1073-1081.

36. Beley, M.; Delabouglise, D.; Houppy, G.; Husson, J.; Petit, J. P. Preparation and Properties of Ruthenium (II) Complexes of 2,2':6',2"-Terpyridines Substituted at the 4'-Position with Heterocyclic Groups. *Inorg. Chim. Acta* **2005,** *358*, 3075-3083.

37. Constable, E. C.; Handel, R.; Housecroft, C. E.; Neuburger, M.; Schofield, E. R.; Zehnder, M. Efficient Syntheses of 4'-(2-Thienyl)- and 4'-(3-Thienyl)-2,2':6',2"-Terpyridine: Preparation and Characterization of Fe(II), Ru(II), Os(II) and Co(II) Complexes. *Polyhedron* **2004,** *23*, 135-143.

38. Fillaud, L.; Trippé-Allard, G.; Lacroix, J. C. Synthesis of π-Conjugated 2,2:6',2"-Terpyridine-Substituted Oligomers Based on 3,4-Ethylenedioxythiophene. *Org. Lett.* **2013,** *15*, 1028-1031.

39. Liang, Y.; Strohecker, D.; Lynch, V.; Holliday, B. J.; Jones, R. A. A Thiophene-Containing Conductive Metallopolymer Using an Fe(II) Bis(Terpyridine) Core for Electrochromic Materials. *ACS Appl. Mater. Interfaces* **2016,** *8*, 34568-34580.

40. Raimundo, J.-M.; Blanchard, P.; Gallego-Planas, N.; Mercier, N.; Ledoux-Rak, I.; Hierle, R.; Roncali, J. Design and Synthesis of Push−Pull Chromophores for Second-Order Nonlinear Optics Derived from Rigidified Thiophene-Based π-Conjugating Spacers. *J. Org. Chem.* **2002,** *67*, 205-218.

41. Firstenberg, M.; Shivananda, K. N.; Cohen, I.; Solomeshch, O.; Medvedev, V.; Tessler, N.; Eichen, Y. Harnessing "Click"-Type Chemistry for the Preparation of Novel Electronic Materials. *Adv. Funct. Mater.* **2011,** *21*, 634-643.

42. Gottlieb, H. E.; Kotlyar, V.; Nudelman, A. NMR Chemical Shifts of Common Laboratory Solvents as Trace Impurities. *J. Org. Chem.* **1997,** *62*, 7512-7515.

43. Kharat, A. N.; Bakhoda, A.; Hajiashrafi, T. Catalytic Oxidation of Organosulfides to Sulfoxides Using Two Novel Cu(II) and Ni(II) Complexes with Aqueous H_2O_2: Effect of TMAO Promoter on Oxidation of Organosulfides. *J. Mol. Catal. A: Chem.* **2010,** *333*, 94-99.

44. Klemens, T.; Switlicka-Olszewska, A.; Machura, B.; Grucela, M.; Schab-Balcerzak, E.; Smolarek, K.; Mackowski, S.; Szlapa, A.; Kula, S.; Krompiec, S.; Lodowski, P.; Chrobok, A. Rhenium(I) Terpyridine Complexes - Synthesis, Photophysical Properties and Application in Organic Light Emitting Devices. *Dalton Trans.* **2016,** *45*, 1746-1762.

45. Presselt, M.; Dietzek, B.; Schmitt, M.; Popp, J.; Winter, A.; Chiper, M.; Friebe, C.; Schubert, U. S. Zinc(II) Bisterpyridine Complexes: The Influence of the Cation on the π-Conjugation between Terpyridine and the Lateral Phenyl Substituent. *J. Phys. Chem. C* **2008,** *112*, 18651-18660.

46. Hunt, R. L.; Ault, B. S. Spectroscopic Influences of Ion Pairing: Infrared Matrix Isolation Spectra of the $M^+BF^-_4$ Ion Pair and Its Chlorine-Fluorine Analogs. *Spectrochim. Acta Mol. Biomol. Spectros.* **1981,** *37*, 63-69.

47. Roncali, J. Conjugated Poly(Thiophenes): Synthesis, Functionalization, and Applications. *Chem. Rev.* **1992,** *92*, 711-738.

48. Muenmart, D.; Tarsang, R.; Jungsuttiwong, S.; Keawin, T.; Sudyoadsuk, T.; Promarak, V. Synthesis and Properties of Fluorene-Oligothiophenes Perylenediimide Triads and Their Electropolymerizations. *J. Mater. Chem.* **2012,** *22*, 14579-14586.

49. Caraway, J. D.; Nguyen, M. T.; Mitchell, L. A.; Holliday, B. J. Incorporation of Thieno[3,2-b]Thiophene Moieties as Novel Electropolymerizable Groups in a Conducting Metallopolymer and Study of the Effect on Photostability. *Macromol. Rapid Commun.* **2015,** *36*, 665-670.

50. Yang, R.; Ruan, C.; Dai, W.; Deng, J.; Kong, J. Electropolymerization of Thionine in Neutral Aqueous Media and H_2O_2 Biosensor Based on Poly(Thionine). *Electrochim. Acta* **1999,** *44*, 1585-1596.

51. Qiu, D.; Zhao, Q.; Bao, X.; Liu, K.; Wang, H.; Guo, Y.; Zhang, L.; Zeng, J.; Wang, H. Electropolymerization and Characterization of an Alternatively Conjugated Donor-Acceptor Metallopolymer: Poly-[Ru(4'-(4-(Diphenylamino)Phenyl)-2,2':6",2"-Terpyridine)$_2$]$^{2+}$. *Inorg. Chem. Commun.* **2011,** *14*, 296-299.

52. Chu, P. K.; Liu, X., *Biomaterials Fabrication and Processing Handbook*. CRC press: 2008; p 339.

53. Marzocchi, M.; Gualandi, I.; Calienni, M.; Zironi, I.; Scavetta, E.; Castellani, G.; Fraboni, B. Physical and Electrochemical Properties of PEDOT:PSS as a Tool for Controlling Cell Growth. *ACS Appl. Mater. Interfaces* **2015,** *7*, 17993-18003.

54. Abd-El-Aziz, A. S.; Manners, I., *Frontiers in Transition Metal-Containing Polymers*. Wiley: Hoboken, NY, 2007.

55. Munzert, S. M.; Schwarz, G.; Kurth, D. G. Kinetic Studies of the Coordination of Mono- and Ditopic Ligands with First Row Transition Metal Ions. *Inorg. Chem.* **2016,** *55*, 2565-2573.

56. Collin, J.-P.; Dixon, I. M.; Sauvage, J.-P.; Williams, J. A. G.; Barigelletti, F.; Flamigni, L. Synthesis and Photophysical Properties of Iridium(III) Bisterpyridine and Its Homologues: A Family of Complexes with a Long-Lived Excited State. *J. Am. Chem. Soc.* **1999,** *121*, 5009-5016.

57. Bechinger, C.; Burdis, M. S.; Zhang, J. G. Comparison between Electrochromic and Photochromic Coloration Efficiency of Tungsten Oxide Thin Films. *Solid State Commun.* **1997,** *101*, 753-756.

58. Yao, D. D.; Rani, R. A.; O'Mullane, A. P.; Kalantar-zadeh, K.; Ou, J. Z. Enhanced Coloration Efficiency for Electrochromic Devices Based on Anodized Nb_2O_5/Electrodeposited MoO_3 Binary Systems. *J. Phy. Chem. C* **2014,** *118*, 10867-10873.

59. Nunes, M.; Araújo, M.; Fonseca, J.; Moura, C.; Hillman, R.; Freire, C. High-Performance Electrochromic Devices Based on Poly[Ni(Salen)]-Type Polymer Films. *ACS Appl. Mater. Interfaces* **2016,** *8*, 14231-14243.

60. Schott, M.; Szczerba, W.; Kurth, D. G. Detailed Study of Layer-by-Layer Self-Assembled and Dip-Coated Electrochromic Thin Films Based on Metallo-Supramolecular Polymers. *Langmuir* **2014,** *30*, 10721-10727.

Chapter 3. Highly Luminescent Europium(III) Complexes with Bis(pyrazolyl)pyridine Antenna Ligands[2]

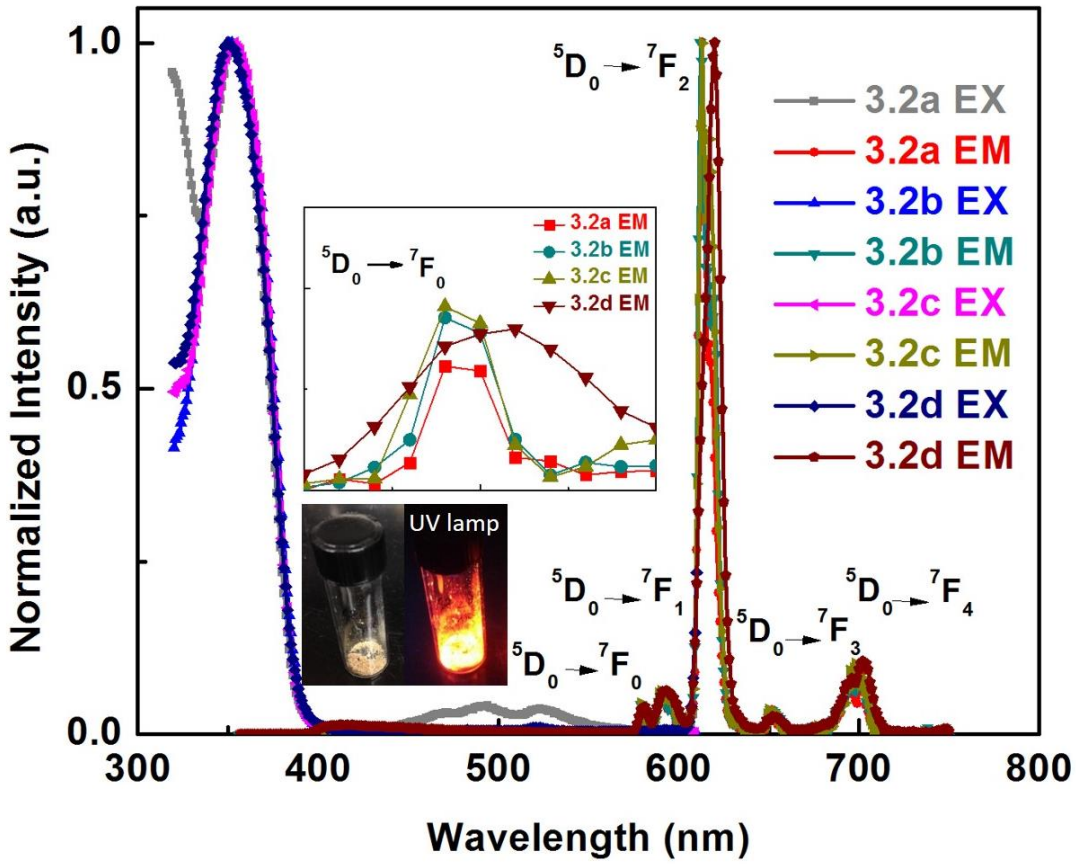

2 This chapter is based partially on the following manuscript-
Liang, Y.; Holliday, B. J.; Jones, R. A.
Highly Luminescent Europium(III) Complexes with Bis(pyrazolyl)pyridine Antenna Ligands, manuscript in preparation

ABSTRACT: Our group has previously synthesized the europium(III) tris-(2-thenoyltrifluroacetonate) 2,6-bis(pyrazoly)pyridine complex [Eu(bppy)(tta)$_3$] giving the quantum yields of 60% in dichloromethane and 93% in the solid state which, to the best of our knowledge, are the highest numbers reported in literature so far. Aiming to expand the family of bppy ligands, various functional groups were introduced to the aromatic ring of the bis(pyrazoly)pyridine (bppy) ligand. By using a general synthetic route, modified bppy ligands with carboxyl (**3.1a**, **3.1c**), hydroxyl (**3.1b**), and amino groups (**3.1d**) were synthesized for the first time. After metalation of the bppy ligands with the europium(III) precursor-Eu(tta)$_3$(H_2O)$_2$, the resulting complexes exhibited bright red luminescence with lifetimes of 383.3 (**3.2a**), 417.2 (**3.2b**), 383.9 (**3.2c**), and 399.5 μs (**3.2d**). Remarkably, complex **3.2b** with tetraethylene glycoxy pendant is strongly luminescent, with a quantum yield of 45.4% in dichloromethane solution. An energy transfer process in complexes **3.2a-3.2d** was proposed based on the photophysical data. It is proposed that the antenna (tta) and ancillary (bppy) ligands complement one another to produce europium(III) complexes with high quantum yields. This study accessed luminescent europium complexes with bioconjugable groups (-COOH or -NH_2), which still retained their high quantum yields and long lifetimes.

3.1 INTRODUCTION

Lanthanide complexes have unique photophysical properties that can be utilized in areas such as bioimaging, bio-sensors, fluoroimmunoassays, and organic light emitting diodes (OLED).[1-3] Direct excitation of the lanthanide center (f-f transition) is Laporte forbidden and inefficient.[4] For this reason, use of antenna molecules or ligands is required to indirectly excite lanthanide metal centers in order to give large Stokes shifts, which is different from conventional organic dyes.[5] The shielding effect of f-orbitals in lanthanides

results in narrow emission peaks and long radiative lifetimes.[5, 6] Many luminescent lanthanide [Eu(III), Tb(III), Sm(III), Dy(III), etc.] chelates have been developed, and ligand families such as bipyridine, terpyridine, beta-diketone are often used as chromophores.[5] By using luminescent lanthanide chelates as labels in microsecond time-resolved luminescence detection, the background auto-luminescence (from biological samples and the instrument, usually in nanosecond) can be effectively eliminated.[7, 8] Current lanthanide-based biolabels are mostly based on Eu(III) and Tb(III) complexes ligated with β-diketone and aromatic amine derivatives since they emit in the visible part of the spectrum.[9-11]

Dr. Hornyák and coworkers reported in 1997 that by adding phenanthroline (Phen) to Eu(III)/2-thenoyltrifluoroacetonate (tta) complexes, the luminescence intensity of Eu(III) was increased 16 times compared to the system without addition of Phen. They attributed the phenomenal increase of luminescence intensity to intramolecular energy transfer from the excited states of both tta and Phen ligands to the emitting states of the Eu(III) ion.[12] Both the chromophores are chemically linked to the metal center, therefore allowing very efficient and rapid energy transfer to the ligand-bound Eu(III). Moreover, bis(pyrazolyl)pyridine (bppy) has been employed as an analogue of Phen and incorporated into Eu(III) tris(β-diketonate) complexes to achieve higher quantum yields.[13-19] Dr. Julie M. Stanley, a former member in our group, developed a series of highly luminescent nine-coordinated Eu(III) tris(β-diketonate) bis(pyrazolyl)pyridine complexes showing exceptionally high quantum yields of Eu(III) emission ranging from 42%-80% in solution and 77-93% in the solid state, respectively.[19] Remarkably, among all the reported Eu(III) complexes in literature, Eu(III) tris-(2-thenoyltrifluoroacetonate) bis(pyrazolyl)pyridine [Eu(bppy)$(tta)_3$] has the highest quantum yield: (60% in dichloromethane and 93% in solid state, respectively).[19]

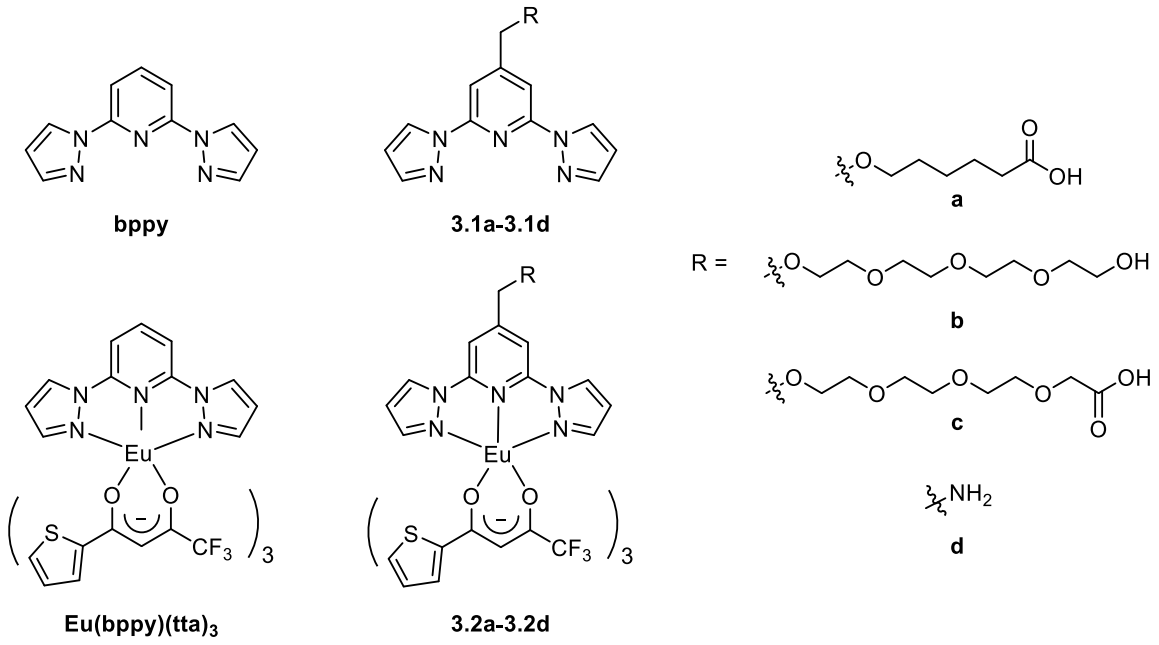

Scheme 3.1. Structures of bppy, Eu(bppy)(tta)$_3$, bppy ligands with different linkers **3.1a**-**3.1d** and their corresponding Eu(R-bppy)(tta)$_3$ complexes **3.2a**-**3.2d** reported in this chapter.

This chapter describes a general synthetic approach to a family of substituted bppy ligands (**3.1a**-**3.1d**) and their corresponding Eu(III) tris-(2-thenoyltrifluoroacetonate) complexes (**3.2a**-**3.2d**). Complexes **3.2a**-**3.2d**, which incorporate both **3.1a**-**3.1d** and tta ligands as highly efficient sensitizers, exhibit long radiative lifetimes and high quantum yields of emission. The functional groups on bppy ligands have promising application to chemically connect the highly luminescent europium(III) chelates to biomolecules by virtue of well-developed biological conjugation protocols.[9, 11, 20] A coupling reaction was performed between **3.2d** and 2,4,6-trichloro-1,3,5-triazinyl (CyC) which is a common reagent in bioconjugation reactions.[11]

3.2 EXPERIMENTAL SECTION

3.2.1 Materials and Reagents

The reported compounds (2,6-di(1H-pyrazol-1-yl)pyridin-4-yl)methanol (bppyCH_2OH), 4-(bromomethyl)-2,6-di(1H-pyrazol-1-yl)pyridine (bppyCH_2Br) and diaquatris(thenoyltrifluoroacetonate)europium(III) ($Eu(tta)_3(H_2O)_2$) were synthesized according to literature procedures.[21, 22] All chemicals for the synthesis of ethyl 6-((2,6-di(1H-pyrazol-1-yl)pyridin-4-yl)methoxy)hexanoate (**3.1a'**), 6-((2,6-di(1H-pyrazol-1-yl)pyridin-4-yl)methoxy)hexanoic acid (**3.1a**), 1-(2,6-di(1H-pyrazol-1-yl)pyridin-4-yl)-2,5,8,11-tetraoxatridecan-13-ol (**3.1b**), 1-(2,6-di(1H-pyrazol-1-yl)pyridin-4-yl)-2,5,8,11-tetraoxatridecan-13-oic acid (**3.1c**), 2-((2,6-di(1H-pyrazol-1-yl)pyridin-4-yl)methyl)isoindoline-1,3-dione (**3.1d'**) and (2,6-di(1H-pyrazol-1-yl)pyridin-4-yl)methanamine (**3.1d**) were purchased from Alfa Aesar, Aldrich or Oxchem, and used without further purification. Dry solvents used in the synthesis was obtained from EMD Millipore Corporation and purified via a two-column alumina purification system (Pure Process Technology, NH).

3.2.2 Characterization Methods

Air- and moisture-sensitive reactions were performed with standard Schlenk techniques under an inert nitrogen atmosphere. ^{1}H NMR spectra were recorded using an Agilent 400 MR NMR spectrometer at 400 MHz. Coupling constants are reported in hertz (Hz), and chemical shifts are reported as parts per million (ppm) relative to residual solvent peaks (residual $CDCl_3$ δ_H = 7.26 ppm). ^{13}C NMR spectra were recorded using an Agilent 400 MR NMR spectrometer at 100 MHz in $CDCl_3$ solution, and chemical shifts are reported as parts per million (ppm) relative to residual solvent peaks ($CDCl_3$ δ_C = 77.16 ppm).[23] High resolution mass spectra (HRMS) were obtained on an Agilent Technologies

6530 Accurate Mass Q-TOF LC/MS instrument. Infrared spectra were recorded with a Nicolet IR 200 FTIR spectrophotometer. Absorption spectra were recorded on a Varian Cary 6000i UV-VIS-NIR spectrophotometer using Starna quartz fluorimeter cells with a path length of 10 mm. Luminescent measurements were recorded on a Photon Technology International QM 4 spectrophotometer equipped with a 6-inch diameter K Sphere-B integrating sphere. For quantum yield measurements, the integrating sphere was used. Quantum yields were calculated by dividing the area under the emission peak of the complex by the difference between the area under the excitation peak of the sample and that of a blank solution (A_{em} sample/(A_{ex} blank-A_{ex} sample), where A = area under peak).[17]

3.2.3 Synthesis of 3.1a', 3.1d' and 3.1a-3.1d

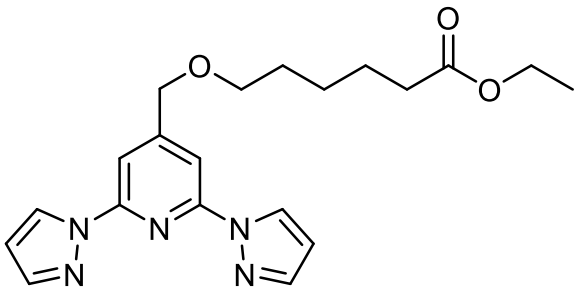

3.1a'

Ethyl 6-((2,6-di(1H-pyrazol-1-yl)pyridin-4-yl)methoxy)hexanoate (3.1a'). To a well stirred solution of bppyCH_2OH (500 mg, 2 mmol) and NaH (200 mg, 8.2 mmol) in dry dimethylformamide (60 mL), ethyl 6-bromohexanoate (1386 mg, 6.2 mmol) in dry dimethylformamide (6 mL) was added dropwise. The reaction was continuously stirred under nitrogen at room temperature for 12 hours. After the completion of the reaction, methanol (10 mL) was added to the flask to react with the excess of NaH. The solvent was removed under reduced pressure. The residue was dissolved in dichloromethane (150 mL), washed with DI water (4×100 mL), dried over anhydrous Na_2SO_4, and the solvent was removed under reduced pressure. Column chromatography afforded the product as a white

solid using a mixture of hexane and ethyl acetate (Hex:EA v:v = 4:1) as eluent (Yield: 351 mg, 44%). ^{1}H NMR ($CDCl_3$): 8.57 (2H, dd, *J* = 2.61, 0.73 Hz); 7.84 (2H, t, *J* = 0.7 Hz); 7.76 (2H, m); 6.49 (2H, dd, *J* = 2.61, 1.68 Hz); 4.62 (2H, t, *J* = 0.71 Hz); 4.12 (2H, q, *J* = 7.15 Hz); 3.56 (2H, t, *J* = 6.53 Hz); 2.32 (2H, t, *J* = 7.43 Hz); 1.68 (4H, m); 1.44 (2H, m); 1.25 (3H, t, *J* = 7.13 Hz). ^{13}C NMR ($CDCl_3$): 173.69; 154.47; 150.18; 142.30; 127.11; 107.89; 107.41; 71.20; 71.01; 60.18; 34.24; 29.33; 25.70; 24.75; 14.23. HRMS (CI): calcd. for $[M+H]^+$ m/z: 384.2036, found: 384.2034. Melting Point: 55-57 ℃.

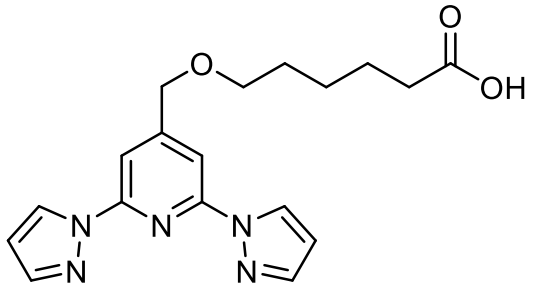

3.1a

6-((2,6-di(1H-pyrazol-1-yl)pyridin-4-yl)methoxy)hexanoic acid (3.1a). To a solution of **3.1a'** (130.5 mg, 0.34 mmol) in ethanol (1.4 mL) was added 10% NaOH aqueous solution (1.4 mL) at room temperature. After stirring for 26 hours, the mixture was adjusted to pH = 1 with 1 M H_3PO_4. The organic layer was washed with DI water (3×3mL), and dried over anhydrous Na_2SO_4. The organic solvent was removed under reduced pressure. Column chromatography afforded the product as a white solid firstly using the mixture of hexane and ethyl acetated (Hex:EA v:v = 4:1) to remove impurities, then using acetone to remove the desired product from the column (Yield: 91.6 mg, 76%). ^{1}H NMR ($CDCl_3$): 8.58 (2H, dd, *J* = 2.58, 0.58 Hz); 7.85 (2H, s); 7.81 (2H, dd, *J* = 1.58, 0.58 Hz); 6.51 (2H, dd, *J* = 2.59, 1.72 Hz); 4.63 (2H, s); 3.62 (2H, t, *J* = 5.86 Hz); 2.42 (2H, t, *J* = 6.61 Hz); 1.73 (4H, m); 1.61 (2H, m). ^{13}C NMR ($CDCl_3$): 177.32; 154.93;

150.17; 142.52; 127.52; 108.10; 107.63; 71.21; 70.54; 34.10; 29.00; 25.16; 24.44. HRMS (CI): calcd. for $[M+H]^+$ m/z: 356.1723, found: 356.1722. Melting Point: 115-117 ℃. FTIR (cm^{-1}): 3103.20w, 2933.68m, 2864.87w, 1723.68s, 1622.46m, 1575.61m, 1519.45m, 1465.62s, 1403.67s, 1366.48w, 1297.38w. UV-vis [CH_2Cl_2, nm ($M^{-1}cm^{-1}$)]: 247 (29,763); 267 nm (10,863); 303 nm (15,179).

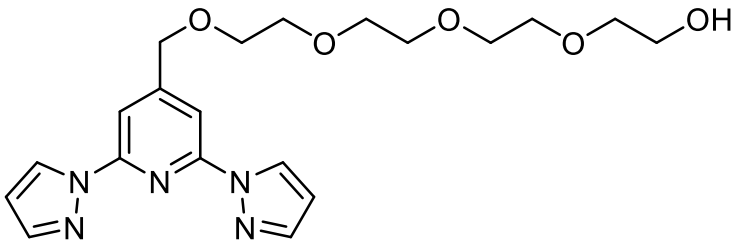

3.1b

1-(2,6-di(1H-pyrazol-1-yl)pyridin-4-yl)-2,5,8,11-tetraoxatridecan-13-ol (3.1b). A suspension of tetraethylene glycol (1.1 mL, 6.37 mmol) and NaH (76 mg, 3.17 mmol) in THF (15 mL) was stirred for 1 hour and then a solution of bppyBr (182 mg, 0.6 mmol) in THF (5 mL) was added dropwise. The resulting light yellow solution was stirring overnight at room temperature. Saturated aqueous NH_4Cl solution was added to the reaction, to bring the pH to 7. The organic phase was dried over Na_2SO_4 after extraction with dichloromethane (60 mL) and water (30 mL). The organic solvent was removed under vacuum, yielding yellow oil as crude product. Column chromatography afforded the product as a colorless oil at room temperature using 3% methanol in dichloromethane as eluent (Yield: 225 mg, 90%). ^{1}H NMR ($CDCl_3$): 8.56 (2H, dd, *J* = 2.61, 0.73 Hz); 7.84 (2H, t, *J* = 0.71 Hz); 7.75 (2H, dd, *J* = 1.66, 0.71 Hz); 6.48 (2H, dd, *J* = 2.61, 1.67 Hz); 4.70 (2H, t, *J* = 0.72 Hz); 3.71 (10H, m); 3.66 (4H, m); 3.59 (2H, m); 2.36 (1H, bs). ^{13}C NMR ($CDCl_3$): 154.18, 150.14, 142.30, 127.16, 107.91, 107.42, 72.47, 71.53, 70.60, 70.53, 70.46, 70.32, 70.21, 30.90. HR-MS (ESI): calcd. for $[M+H]^+$ m/z: 440.19040, found:

440.19040. FTIR (cm^{-1}): 3421.55m, 3124.63w, 2866.95s, 1728.48w, 1617.33s, 1573.53s, 1520.83m, 1460.57s, 1396.02s, 1361.44w, 1284.28w, 1259.25w, 1205.56m, 1098.48s. UV-vis [CH_2Cl_2, nm ($M^{-1}cm^{-1}$)]: 247 (29,778); 267 (10,891); 303 (15,222).

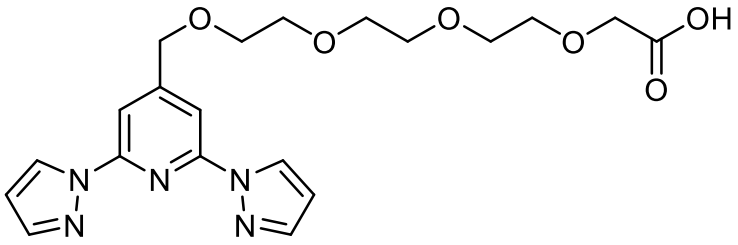

3.1c

1-(2,6-di(1H-pyrazol-1-yl)pyridin-4-yl)-2,5,8,11-tetraoxatridecan-13-oic acid (3.1c). A solution of CrO_3 (85 mg, 0.85 mmol), DI water (0.85 mL) and sulfuric acid (0.13 mL) was added to a cooled (0 ºC) solution of **3.1b** (207.7 mg, 0.5 mmol) in acetone (1.6 mL). The reaction mixture was stirred at 4 ºC overnight and then quenched with isopropanol (0.5 mL). Column chromatography afforded the product as a colorless oil using 5% methanol in dichloromethane as eluent (Yield: 49 mg, 23%). ^{1}H NMR ($CDCl_3$): 8.51 (dd, 2.62, 0.71 Hz, 2H); 7.77 (2H, s); 7.72 (2H, dd, *J* = 1.64, 0.73 Hz); 6.45 (2H, dd, *J* = 2.60, 1.62 Hz); 4.65 (2H, s); 3.90 (2H, s); 3.64 (12 H, m).; 2.35 (1H, bs). ^{13}C NMR ($CDCl_3$): 177.71, 154.33, 152.00, 150.11, 127.14, 107.88, 107.42, 71.46, 70.27, 70.17, 69.93, 46.79. HRMS (ESI): calcd. for $[M+Na]^+$ m/z: 454.16970, found: 454.17020. FTIR (cm^{-1}): 3444.02w, 3125.13w, 2871.37w, 1729.86w, 1617.77s, 1574.51s, 1521.53m, 1463.80s, 1397.55s, 1322.87w,1287.83w, 1259.86w, 1206.01m, 1181.56w, 1101.33s, 1042.89m. UV-vis [CH_2Cl_2, nm ($M^{-1}cm^{-1}$)]: 247 (16,919); 268 (6,537); 305 (8,470).

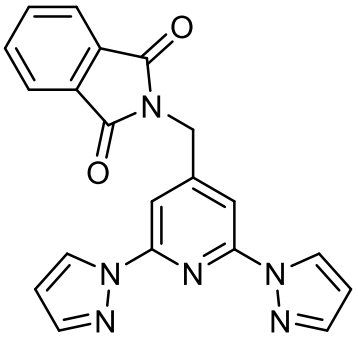

3.1d'

2-((2,6-di(1H-pyrazol-1-yl)pyridin-4-yl)methyl)isoindoline-1,3-dione (3.1d'). Compound bppyBr (0.2921 g, 0.96 mmol) was dissolved in DMF (6.3 mL) with the addition of potassium phthalimide (0.269 g, 1.44 mmol). The reaction mixture was heated at 75 ºC and stirred for 12 hours. The resulting solution was extracted with ethyl acetate (30mL) and water (20 mL). The organic layer was dried over anhydrous Na_2SO_4. The organic solvent was removed under vacuum, affording the product as a white solid (Yield: 0.290 g, 82%). The product was used for the next step without further purification. ^{1}H NMR ($CDCl_3$): 8.54 (2H, dd, *J* = 2.62, 0.72 Hz); 7.89 (3H, m); 7.83 (2H, m); 7.76 (3H, m); 6.48 (2H, dd, *J* = 2.61, 1.65 Hz); 4.98 (2H, t, *J* = 0.68 Hz). HRMS (ESI): calcd. for $[M+Na]^+$ m/z: 393.10700, found: 393.10720. Melting Point: 178-180 ℃.

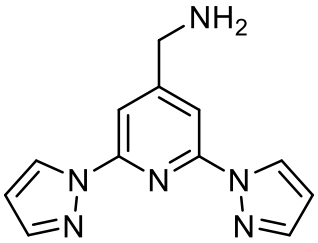

3.1d

(2,6-di(1H-pyrazol-1-yl)pyridin-4-yl)methanamine (3.1d). 3.1d' (179.8 mg, 0.485 mmol) was dissolved in dichloromethane (0.4 mL) and ethanol (1.5 mL) followed by hydrazine hydrate (0.043 mL). The reaction mixture was heated at 55 ºC for 12 hours.

The resulting solution was quenched with water (2 mL), and the product was extracted with dichloromethane (15 mL) and water (8 mL). The organic phase was dried over anhydrous Na_2SO_4, and the solvent was removed under vacuum. The crude product was washed with pentane for three times (3×8 mL), yielding a pale yellow solid (Yield: 58.6 mg, 50%). ^{1}H NMR ($CDCl_3$): 8.57 (2H, dd, *J* = 2.60, 0.48 Hz); 7.84 (2H, s); 7.76 (2H, dd, *J* = 1.54, 0.50 Hz); 6.50 (2H, dd, *J* = 2.57, 1.68 Hz); 4.03 (2H, s). ^{13}C NMR ($CDCl_3$): 150.29, 142.29, 127.15, 107.92, 107.47, 45.67. HRMS (ESI): calcd. for $[M+H]^+$ m/z: 241.11960, found: 241.11970. Melting Point: 79-81 ℃. FTIR (cm^{-1}): 3308.10s, 1621.21m, 1466.77m, 1404.51w, 1208.93w, 1047.37w. UV-vis [CH_2Cl_2, nm ($M^{-1}cm^{-1}$)]: 247 (27,083); 268 (9,868); 303 (13,687).

3.2.4 Synthesis of the Europium(III) Complexes 3.2a-3.2d

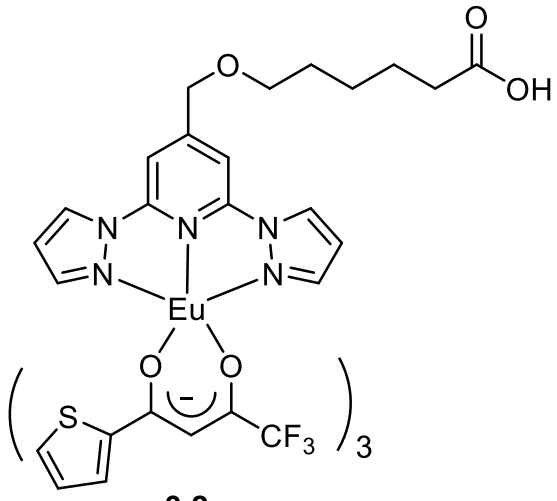

3.2a

3.2a. The europium precursor $Eu(tta)_3(H_2O)_2$ (157.1 mg, 0.184 mmol) and the ligand **3.1a** (65.4 mg, 0.184 mmol) were added to a round-bottom flask with toluene (33 mL). The flask was put into a preheated oil bath at 110 ℃ with continuous stirring. After 24 hours, the solvent was removed under reduced pressure and the product was dried under

nitrogen, affording a light yellow solid (Yield: quantitative). HRMS (ESI): calcd. for [M-tta]$^+$ m/z: 950.06190, found: 950.06020; calcd. for [M-H+2Na]$^+$ m/z: 1216.02200, found: 1216.01990. Melting Point: 169-171 ℃. FTIR (cm^{-1}): 3125.63m, 2962.14m, 1707.64w, 1602.73s, 1575.14w, 1534.20m, 1500.07w, 1455.71m, 1410.42s, 1354.28m. UV-vis [CH_2Cl_2, nm ($M^{-1}cm^{-1}$)]: 247 (22,370); 272 (29,369); 316 (32,935); 345 (38,042). Elemental Analysis: calculated (found) for **3.2a**, $C_{42}H_{33}EuF_9N_5O_9S_3$: C, 43.08 (43.03); H, 2.84 (3.10); N, 5.98 (5.64).

Other europium (III) complexes **3.2b**, **3.2c**, and **3.2d**, were synthesized in a similar manner to **3.2a**.

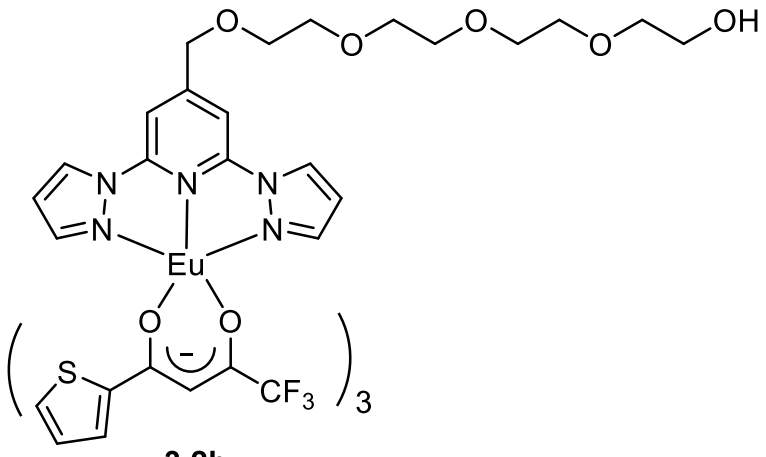

3.2b

3.2b. HRMS (ESI): calcd. for [M-tta]$^+$ m/z: 1013.10230, found: 1013.10140. Melting Point: 46-48 ℃. FTIR (cm^{-1}): 3411.10w, 3123.20w, 2920.45m, 2868.66m, 1601.57s, 1534.18m, 1500.12w, 1455.70s, 1410.39m, 1352.56w, 1299.37s, 1243.76w, 1228.81w, 1179.08m, 1127.72s, 1082.83w, 1056.85m. UV-vis [CH_2Cl_2, nm ($M^{-1}cm^{-1}$)]: 247 (15,045); 271 (17,010); 315 (17,423); 344 (22,734). Elemental Analysis: calculated (found) for **3.2b**, formula: C, 42.86 (44.71); H, 3.19 (4.24); N, 5.68 (4.45).

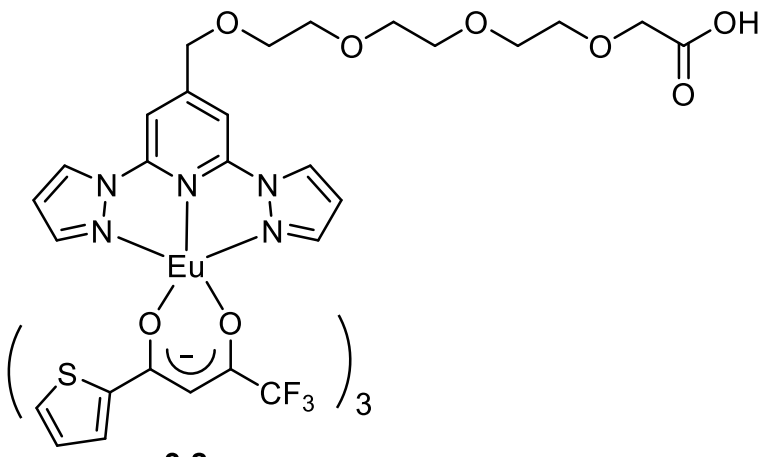

3.2c

3.2c. HRMS (ESI): calcd. for $[M\text{-tta}]^+$ m/z: 1013.10230, found: 1013.10140. Melting Point: 185-187 ℃. FTIR (cm^{-1}): 3412.75w, 3107.49w, 2958.83w, 2923.71w, 2873.03w, 1693.57w, 1600.98s, 1534.20s, 1500.67w, 1455.94m, 1410.60s, 1353.07m, 1298.73s, 1244.29w, 1259.07w, 1179.96m, 1127.84s, 1082.32w, 1057.14m, 1014.82w. UV-vis [CH_2Cl_2, nm ($M^{-1}cm^{-1}$)]: 248 (19,065); 273 (27,470); 320 (34,091); 346 (40,976). Elemental Analysis: calculated (found) for **3.2c**, formula: C, 42.38 (42.99); H, 2.99 (3.37); N, 5.62 (4.35).

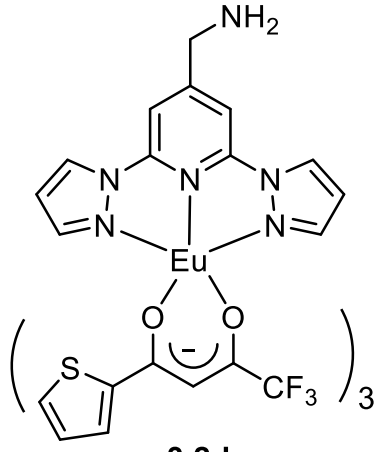

3.2d

3.2d. HRMS (ESI): calcd. for $[M+Na]^+$ m/z: 1076.98660, found: 1076.98410. Melting Point: 115-117 ℃. FTIR (cm^{-1}): 3112.11m, 2923.03m, 2853.15m, 1721.25w,

1684.31w, 1656.80w, 1600.68s, 1535.31s, 1459.23s, 1409.74s, 1353.61m, 1289.58s, 1243.36m, 1228.59m, 1178.18s, 1129.43s, 1082.71w, 1057.04s, 1031.93w. UV-vis [CH_2Cl_2, nm ($M^{-1}cm^{-1}$)]: 248 (27,599); 274 (31,463); 314 (30,421); 346 (33,668). Elemental Analysis: calculated (found) for **3.2d**, formula: C, 40.96 (37.31); H, 2.29 (2.15); N, 7.96 (8.11).

3.3 Results and Discussion

3.3.1 Photophysical Properties of Ligands 3.1a-3.1d and Eu(III) Complexes 3.2a-3.2d

Ligands **3.1a**-**3.1d** and Eu(III) complexes **3.2a**-**3.2d** were prepared according to the steps outlined in Scheme 3.2. **3.1a**-**3.1d** were analyzed via ^{1}H NMR, ^{13}C NMR, HRMS, FTIR and UV-vis spectroscopy. **3.2a**-**3.2d** were characterized by HRMS, FTIR, UV-vis, and elemental analysis. The UV-vis spectrum of **3.2a** displayed absorption peaks at 247, 272, and 315 nm, which is similar to the absorption profile of **3.1a**. The peak at 345 nm is attributed to the absorption of the tta ligand. The UV-vis peak shifts from 303 nm in **3.1a** to 315 nm in **3.2a**, indicating successful metalation between **3.1a** and $Eu(tta)_3(H_2O)_2$ (Figure 3.1, blue and red lines). This observation is similar to what has been reported for the unsubstituted bppy ligand and complex $Eu(bppy)(tta)_3$.[19] Similar bathochromic shifts of the $\pi \rightarrow \pi^*$ energy transfer bands in ligands were observed in **3.2c**-**3.2d** also (Figure 3.2). The UV-vis absorption spectra of **3.1a**-**3.1d**, and **3.2a**-**3.2d** in dichloromethane were also measured, and the results are summarized in Table 3.1.

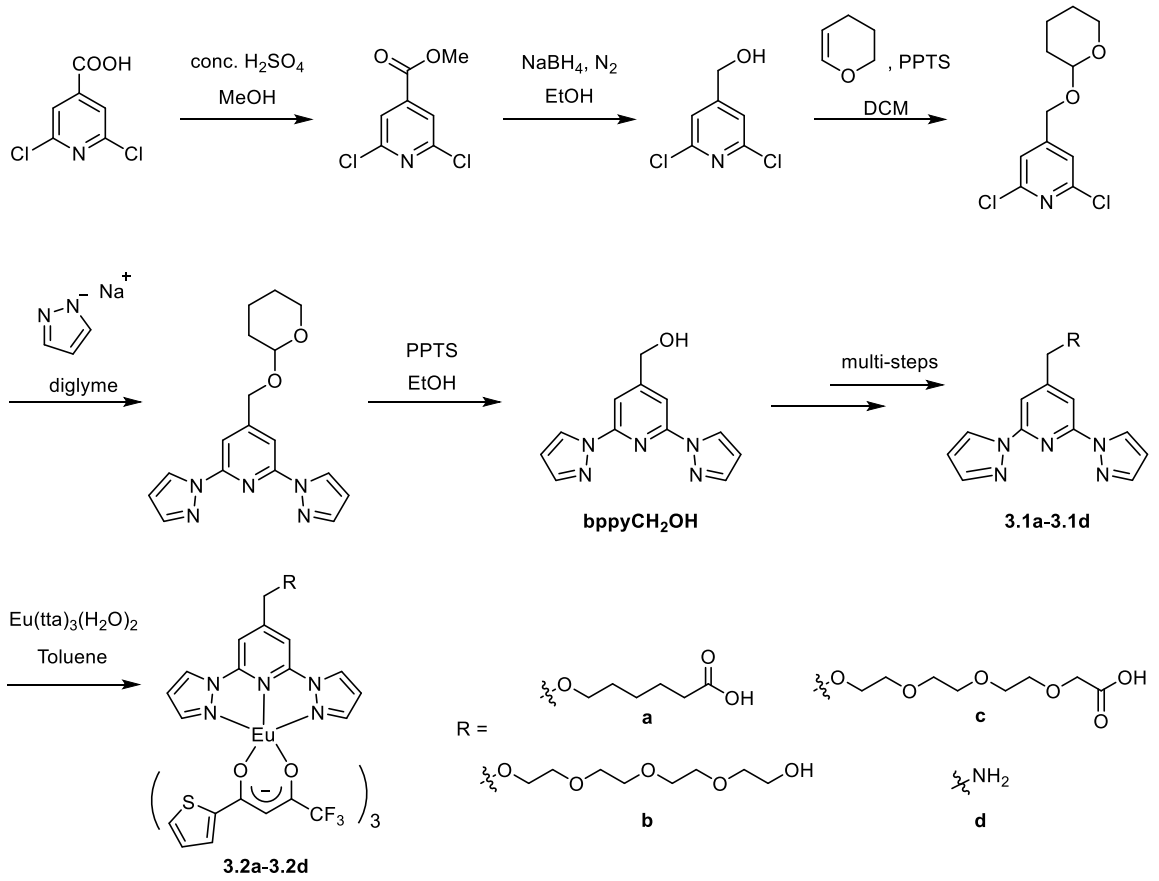

Scheme 3.2. Synthesis of the substituted bppy ligands **3.1a**-**3.1d** and the corresponding Eu(III) tris-(2-thenoyltrifluoroacetonate) complexes **3.2a**-**3.2d**.

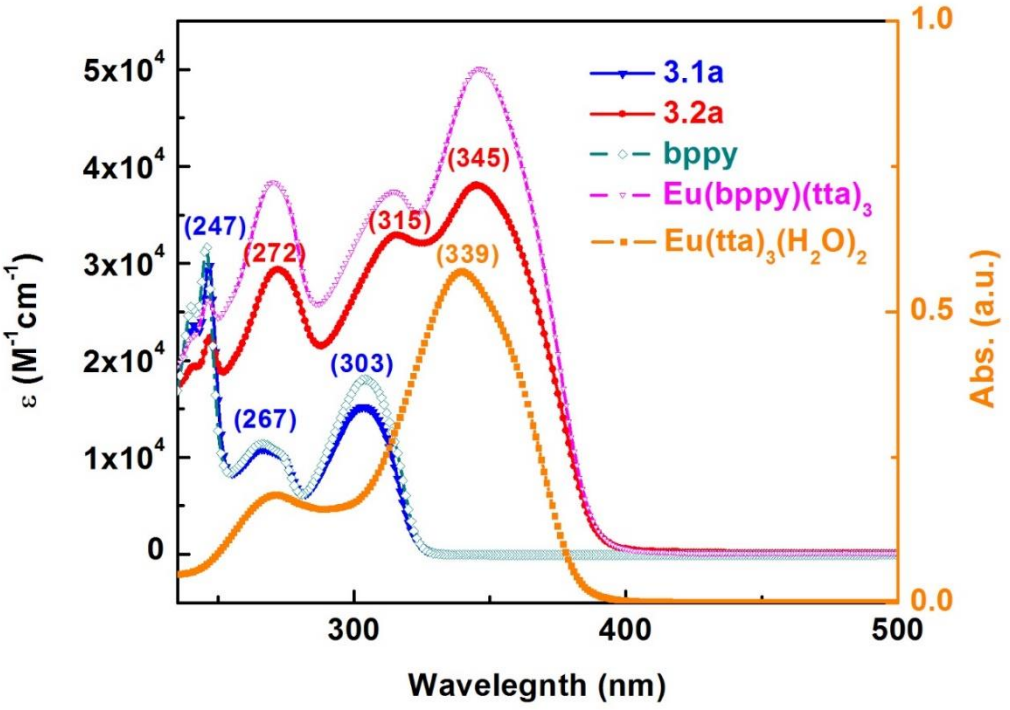

Figure 3.1. UV-vis spectra of **3.1a** and **3.2a** in dichloromethane solutions. UV-vis profiles of bppy, $Eu(bppy)(tta)_3$, and $Eu(tta)_3(H_2O)_2$ included for comparison.

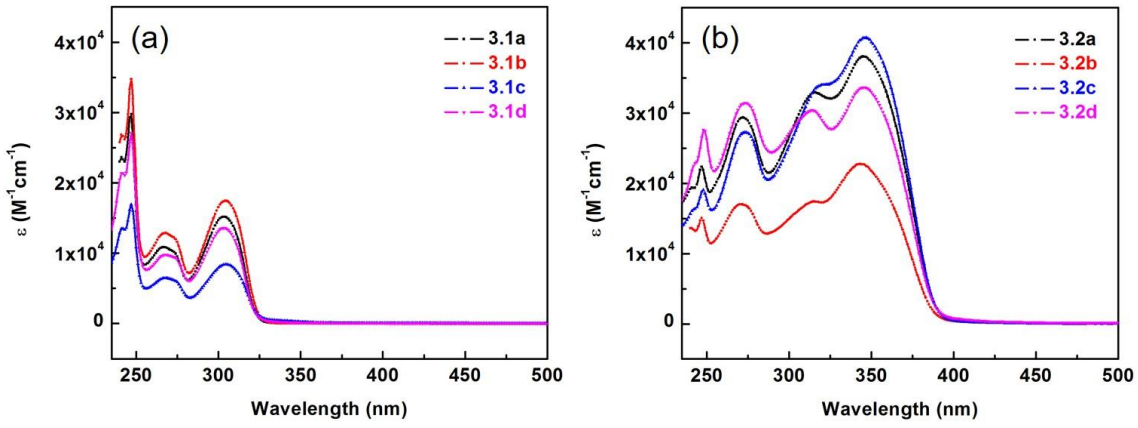

Figure 3.2. UV-vis spectra of **3.1a-3.1d** (a) and **3.2a-3.2d** (b) in dichloromethane solutions.

Table 3.1. Molar absorptivity [λ (nm), $\varepsilon \times 10^{-4}$ $M^{-1}cm^{-1}$] of **3.1a-3.1d** and **3.2a-3.2d**.

compound	λ (nm), ε (10^{-4} $M^{-1}cm^{-1}$)			
3.1a	247, 3.0	267, 1.1	303, 1.5	---
3.1b	247, 3.5	267, 1.3	304, 1.7	---
3.1c	247, 1.7	267, 0.7	305, 0.8	---
3.1d	247, 2.7	268, 1.0	303, 1.4	---
3.2a	247, 2.2	272, 2.9	316, 3.3	345, 3.8
3.2b	247, 1.5	271, 1.7	314, 1.7	343, 2.3
3.2c	248, 1.9	273, 2.7	319, 3.4	346, 4.1
3.2d	248, 2.8	273, 3.1	314, 3.0	346, 3.4

The emission profiles of **3.1a-3.1d** are very similar, with a broad band ranging from 320 to 400 nm (λ_{max} = 336 nm) at room temperature (Figure 3.3, red lines). This feature corresponds to the ligand fluorescence, supported by the small Stokes shift with a short-excited state lifetime. The large overlap between the emission peaks of **3.1a-3.1d** and absorption peak of tta from 308 to 390 nm (Figure 3.4) suggests that the radiation from **3.1a-3.1d** can be absorbed by the tta moiety. To demonstrate this energy transfer process, the phosphorescence spectra of ligands **3.1a-3.1d** were measured at 77 K (Figure 3.3, purple lines). Upon cooling the samples to 77 K in a glassy solvent (a 2:2:1:1 mixture of ethyl iodide-diethyl ether-ethanol-toluene), previously absent vibrational features and ligand phosphorescence were observed. These observations are attributed to the reduction of thermal nonradiative pathways which are responsible for energy loss. The singlet (S_1) and triplet (T_1) excited state energy levels of **3.1a-3.1d** were calculated according to data from Figure 3.3 and are summarized in Table 3.2.[24]

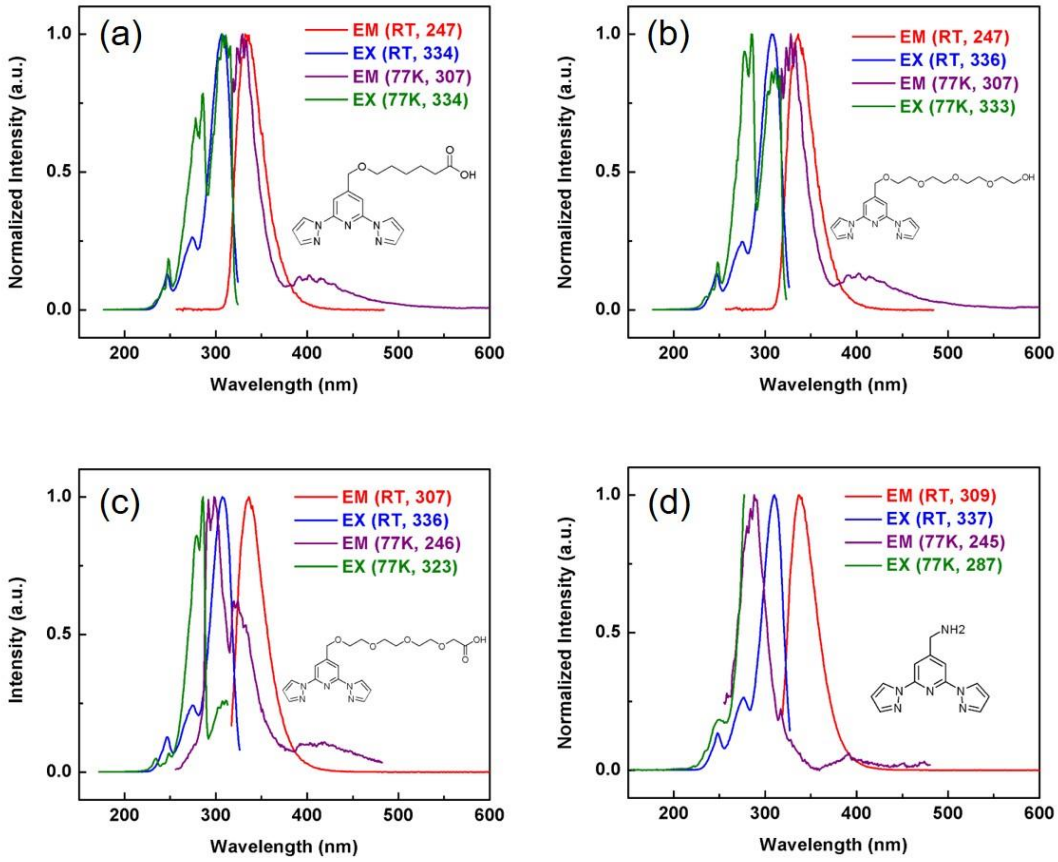

Figure 3.3. Excitation (EX) and emission (EM) spectra of **3.1a** (a), **3.1b** (b), **3.1c** (c), and **3.1d** (d) in dichloromethane solutions at room temperature (RT) and 77K. The number followed by temperature in parentheses is the EX or EM wavelength (nm).

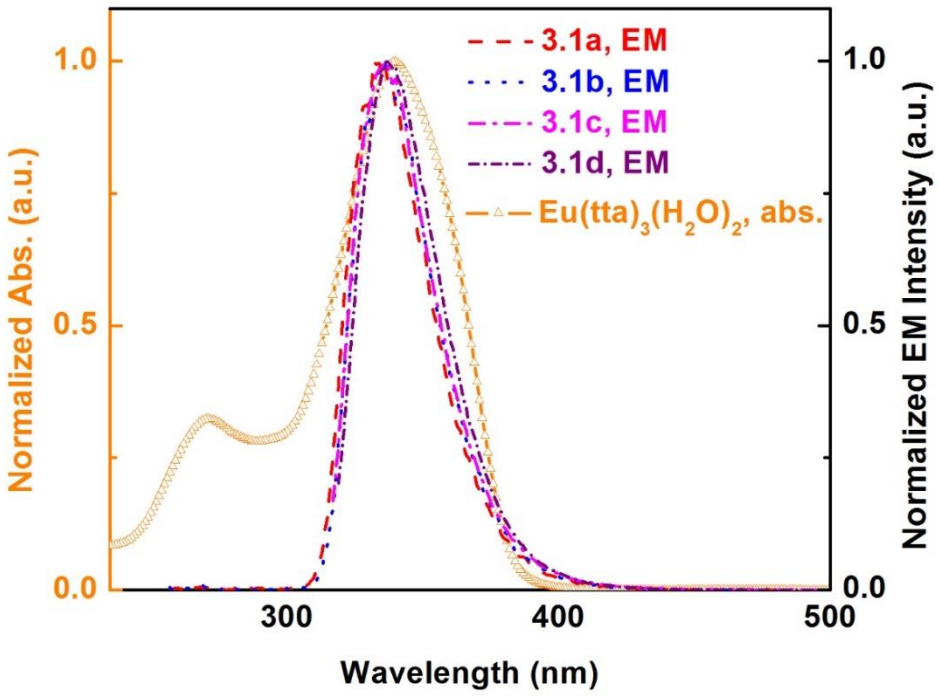

Figure 3.4. Absorption spectrum of $Eu(tta)_3(H_2O)_2$ and the photoluminescence spectra of **3.1a-3.1d** in dichloromethane solutions.

Table 3.2. Singlet and triplet state energy levels of the ligands.

Compound	S_1 (eV)	T_1 (eV)
3.1a	3.72	3.08
3.1b	3.69	3.07
3.1c	3.69	3.03
3.1d	3.67	3.17
tta[25]	3.12	2.35

The excitation spectra of **3.2a-3.2d** demonstrated that the energy transfer from ligands to the Eu(III) ion become the most efficient when the excitation wavelength was at

350 nm (Figure 3.5), which also aligns with the major absorption peak of the tta ligand (Figure 3.4).[17, 19, 25] The emission spectra of **3.2a**-**3.2d** displayed very strong Eu(III) emissions from 580 to 700 nm which are attributed to the $^5D_0 \rightarrow {}^7F_{0\text{-}4}$ transitions. The symmetry of the coordination environment around the Eu(III) ion was low in solution, confirmed by the domination of the spectra by the hypersensitive $^5D_0 \rightarrow {}^7F_2$ transition. The absence of splitting in the $^5D_0 \rightarrow {}^7F_0$ emission peak indicated that there is only one coordination environment around the Eu(III) ion in the system (Figure 3.5, inset), reaffirming the complete complexation between the Eu(III) precursor-Eu(tta)$_3$(H_2O)$_2$ and the substituted bppy ligands.[26] The excited state lifetimes of luminescent **3.2a**-**3.2d** were measured by monitoring the Eu(III) $^5D_0 \rightarrow {}^7F_2$ transition in dichloromethane solution, ranging from 383 (**3.2a**) to 417 (**3.2b**) μs. The long lifetime is not unusual in lanthanide complexes, resulting from the antenna ligand effect.[1, 5, 6] The absolute quantum yields of **3.2a**-**3.2d** were also measured via a calibrated integrating sphere and ranged from 20.2% (**3.2c**) to 45.4% (**3.2b**).[17, 19] The Eu(III) excited state energy can dissipate through O-H or N-H oscillators in the ligands **3.1a**-**3.1d**, which is probably responsible for the lower quantum yields of **3.2a**-**3.2d** compared to the unsubstituted Eu(bppy)(tta)$_3$.

The calculated radiative lifetime (τ_R), radiative process rate constant (k_r), nonradiative process rate constant (k_{nr}), luminescent step quantum yield (Φ_{Ln}), and sensitization efficiency (η_{sens}) are summarized in Table 3.3.[27] The highest total quantum yield (Φ_{tot}) of **3.2b** resulted from its highest values of $\Phi_{Ln}$and η_{sens} among **3.2a**-**3.2d**. Energy of the excited state Eu(III) can dissipate through non-radiative pathways caused by the O-H bond vibration of the carboxylic acid moiety, leading to a larger k_{nr} for **3.2a** and **3.2c**.[28]

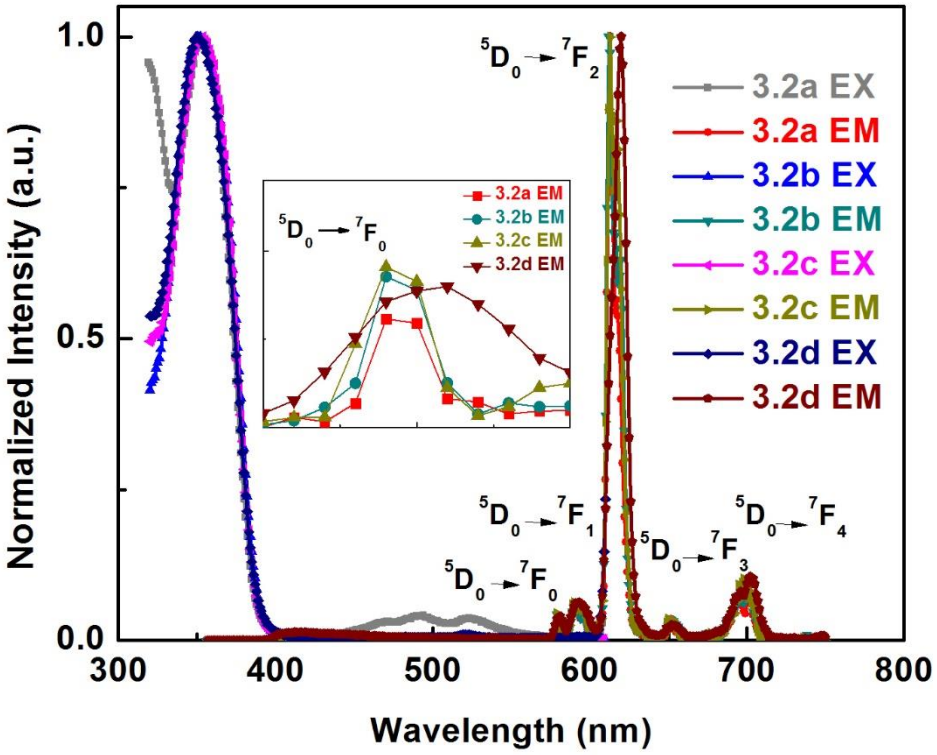

Figure 3.5. Excitation and emission spectra of Eu(III) complexes **3.2a**, **3.2b**, **3.2c**, and **3.2d** at room temperature.

Table 3.3. Luminescent properties of **3.2a-3.2d** in dichloromethane solutions.

Complex	Ex. (nm)	Em. (nm)	$\tau_{obs,RT}$ (μs)	Φ_{tot} (%)	τ_R (μs)	k_r (s^{-1})	k_{nr} (s^{-1})	Φ_{Ln} (%)	η_{sens} (%)
3.2a	354	613	383.3	37.1	895	1117	1492	42.8	86.8
3.2b	352	612	417.2	45.4	803	1245	1152	51.9	87.5
3.2c	354	613	383.9	20.2	898	1113	1491	42.7	47.3
3.2d	350	620	399.5	27.5	873	1146	1357	45.8	60.0

a. Calculations of τ_R, k_r, k_{nr}, Φ_{Ln}, and η_{sens} per Verhoeven *et al.*[27]

Figure 3.6 details the proposed energy transfer process, showing the energy levels of the tta ligand, $^5D_0$ excited state of Eu(III),[17, 25] and the substituted bis(pyrazolyl)pyridine ligands from Table 3.2. The S_1 energy levels of **3.1a-3.1d** match those of the tta and $^5D_0$ energy level of Eu(III). The energy absorbed by both tta and **3.1a-3.1d** can be transferred to the T_1 energy level of tta then to the excited state of Eu(III). On the other hand, the T_1 energy levels between **3.1a-3.1d** and tta have a larger difference (0.73, 0.72, 0.68, 0.82 eV, respectively) than the minimum energy gap requirement (0.23 eV) for an efficient energy transfer process with minimal back energy transfer.[25] Part of the T_1 energy transferred from the S_1 excited states of **3.1a-3.1d** can be transferred to the T_1 excited state of tta, and further to the Eu(III) excited state. This supports previous findings in the literature that the antenna and ancillary ligands complement one another to produce luminescent europium complexes with high quantum yields.[19] Additionally, without incorporation of bppy ligands, the $Eu(tta)_3(H_2O)_2$ complex displayed a shorter emission lifetime (0.23 ms) and a lower luminescent step quantum yield (27%), implying the significance of bppy ligands in the energy transfer process.[29, 30] The difference between the quantum yields of **3.2a-3.2d** is attributed to the well-known facts of O-H (**3.2a**, **3.2c**) and N-H (**3.2d**) bond vibrations

quenching the fluorescence of Eu(III), indicated from their longer nonradiative lifetimes.[31, 32] The quenching occurs through exchange of the Eu(III) electronic excitation energy and the high-frequency vibrational overtones of X-H (X = O, N) bonds.[33]

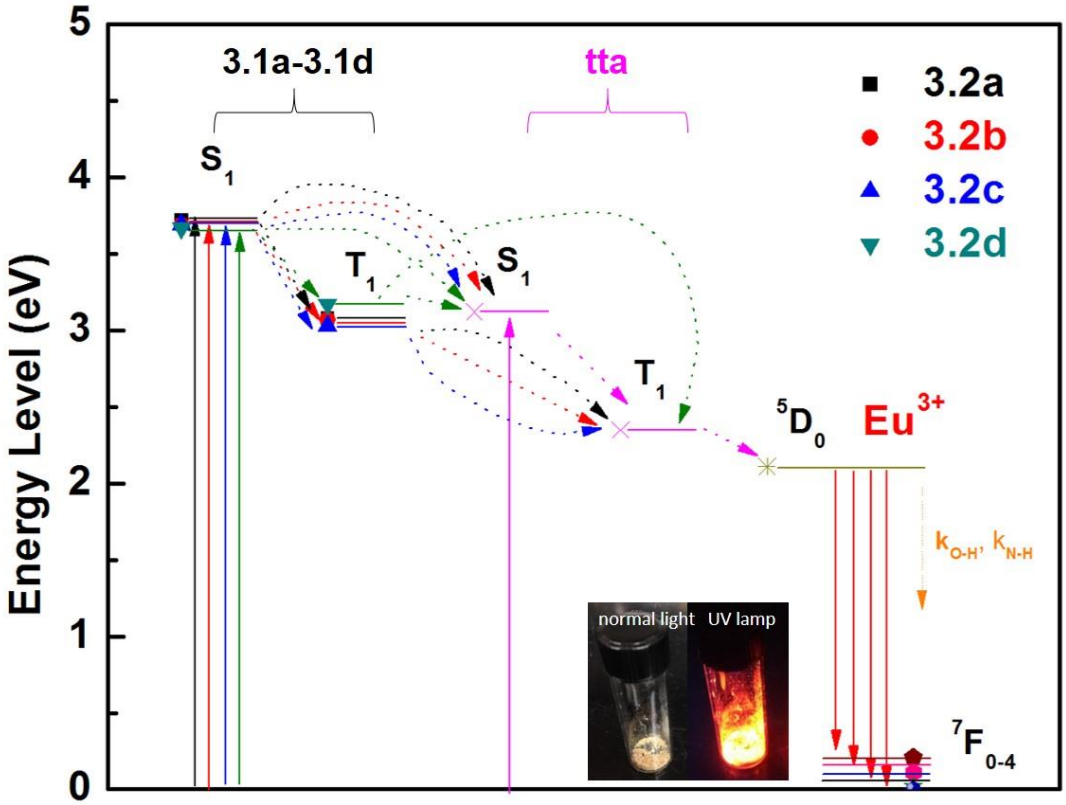

Figure 3.6. Schematic energy level diagram and the energy transfer processes in Eu(III) complexes **3.2a**-**3.2d** in dichloromethane solutions.

3.3.2 Water Solubility of 3.1b

The **3.1b** molecule contains four units of -CH_2CH_2O-, making it highly water-soluble. The UV-vis absorption peaks of **3.1b** exhibit hypsochromic shifts in water compared to those in dichloromethane (DCM) (Figure 3.7a). This observation is commonly seen due to increasing polarity of solvent (ε_{H_2O} = 80.1, ε_{DCM} = 8.93).[34] Unfortunately, it

was not possible to investigate the luminescence of **3.2b** in water due to the fact that it lost water solubility after metalation with $Eu(tta)_3(H_2O)_2$.

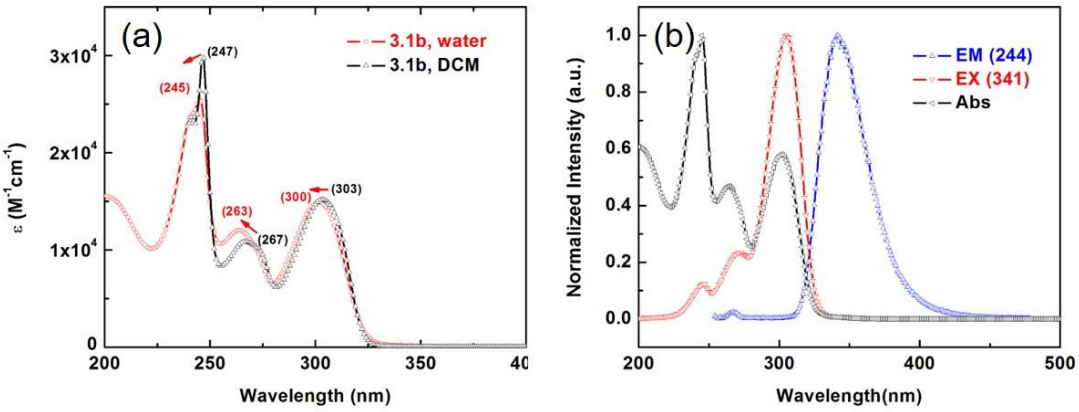

Figure 3.7. (a) UV-vis spectra of **3.1b** in H_2O and DCM, (b) emission, excitation, and absorption spectra of **3.1b** in H_2O.

3.3.3 Coupling Reaction Between 2,4,6-trichloro-1,3,5-triazine and 3.2d

As expected, the coupling reaction between **3.2d** and 2,4,6-trichloro-1,3,5-triazine (CyC), which is commonly used in DNA labeling,[11] gave the desired product **3.2e** via filtration and extraction with DCM/H_2O from the crude product. The formation of **3.2e** was confirmed by HRMS [obs. m/z 1225.92200, calc. m/z 1225.92560 for $(M+Na)^+$], IR, and UV-vis spectroscopy. Compound **3.2e** shows a characteristic broad infrared band at 3409 cm^{-1} indicating the presence of an amino group (Figure 3.9a). The almost identical UV-vis absorption profiles before and after the coupling reaction is not surprising (Figure 3.9b), considering little structural change occurs in the Eu(III) complex. One downside factor regarding the Eu(III) complexes synthesized in this study is that they have poor solubility in water, making them very hard to conjugate with water-soluble biological samples. However, an improvement in water solubility should be achievable by virtue of a variety of methods which people have developed for synthesizing water-soluble bppy ligands.[35]

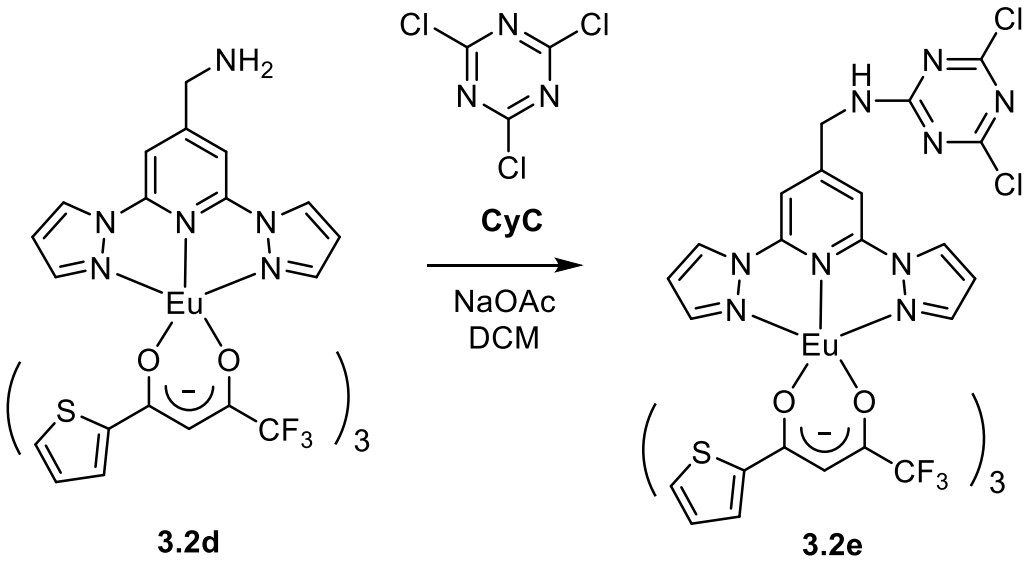

Scheme 3.3. Coupling reaction between **3.2d** and CyC.

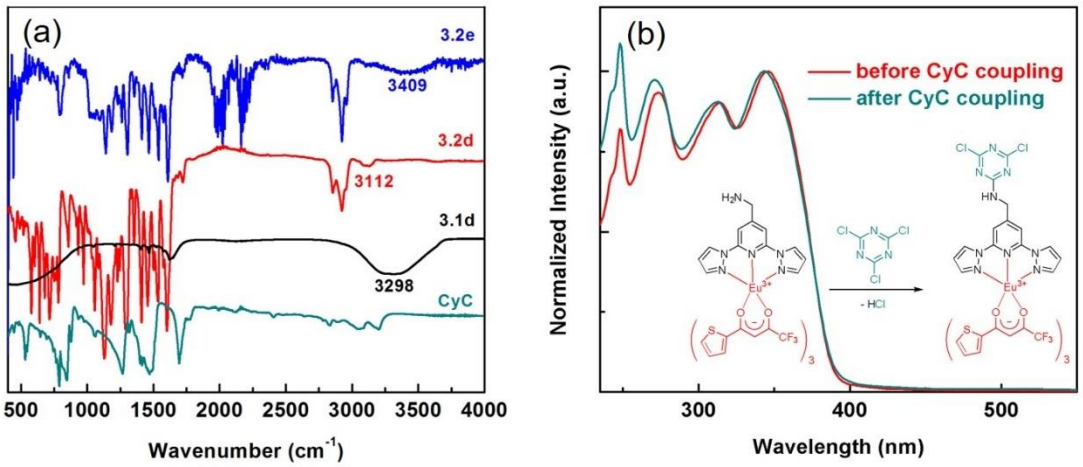

Figure 3.8. (a) Infrared spectroscopy of CyC, **3.1d**, **3.2d**, and **3.2e**. (b) UV-vis spectra of **3.2d** before and after CyC coupling in dichloromethane.

3.4 CONCLUSION

A general synthetic route was designed to prepare novel substituted bis(pyrazolyl)pyridine ligands **3.1a**-**3.1d** and the corresponding Eu(III) complexes **3.2a**-

3.2d, and their photophysical properties were fully characterized. Of particular note is, the quantum yield and sensitization efficiency of complex **3.2b** is 45.4% and 87.5%, respectively, which is the highest among **3.2a**-**3.2d**. The evidence from this study shows that **3.1a**-**3.1d** not only saturate the coordination sites of the Eu(III) ion, but also improve the efficiency of energy transfer between ligands and the Eu(III) excited state. The proposed energy transfer process suggests that the antenna and ancillary ligands complement one another to produce highly luminescent Eu(III) complexes. However, there are limitations for **3.2a**-**3.2d** in direct biological applications due to their relatively low water solubility.

3.5 REFERENCES

1. de Sá, G. F.; Malta, O. L.; de Mello Donegá, C.; Simas, A. M.; Longo, R. L.; Santa-Cruz, P. A.; da Silva Jr, E. F. Spectroscopic Properties and Design of Highly Luminescent Lanthanide Coordination Complexes. *Coord. Chem. Rev.* **2000,** *196*, 165-195.
2. Binnemans, K. Lanthanide-Based Luminescent Hybrid Materials. *Chem. Rev.* **2009,** *109*, 4283-4374.
3. Stanley, J. M.; Holliday, B. J. Luminescent Lanthanide-Containing Metallopolymers. *Coord. Chem. Rev.* **2012,** *256*, 1520-1530.
4. Schrader, B. F. Albert Cotton: Chemical Applications of Group Theory, 3rd Ed. John Wiley & Sons: New York, 1990.
5. Armelao, L.; Quici, S.; Barigelletti, F.; Accorsi, G.; Bottaro, G.; Cavazzini, M.; Tondello, E. Design of Luminescent Lanthanide Complexes: From Molecules to Highly Efficient Photo-Emitting Materials. *Coord. Chem. Rev.* **2010,** *254*, 487-505.
6. Lis, S.; Elbanowski, M.; Mkowska, B.; Hnatejko, Z. Energy Transfer in Solution of Lanthanide Complexes. *J. Photochem. Photobiol. A* **2002,** *150*, 233-247.
7. Faulkner, S.; Pope, S. J. A.; Burton-Pye, B. P. Lanthanide Complexes for Luminescence Imaging Applications. *Appl. Spectrosc. Rev.* **2005,** *40*, 1-31.
8. Thibon, A.; Pierre, V. C. Principles of Responsive Lanthanide-Based Luminescent Probes for Cellular Imaging. *Anal. Bioanal. Chem.* **2009,** *394*, 107-120.

9. Zhang, L.; Wang, Y.; Ye, Z.; Jin, D.; Yuan, J. New Class of Tetradentate β-Diketonate-Europium Complexes That Can Be Covalently Bound to Proteins for Time-Gated Fluorometric Application. *Bioconjugate Chem.* **2012,** *23*, 1244-1251.

10. Yuan, J.; Wang, G. Lanthanide Complex-Based Fluorescence Label for Time-Resolved Fluorescence Bioassay. *J. Fluoresc.* **2005,** *15*, 559-568.

11. Nishioka, T.; Yuan, J.; Yamamoto, Y.; Sumitomo, K.; Wang, Z.; Hashino, K.; Hosoya, C.; Ikawa, K.; Wang, G.; Matsumoto, K. New Luminescent Europium(III) Chelates for DNA Labeling. *Inorg. Chem.* **2006,** *45*, 4088-4096.

12. Erostyák, J.; Buzády, A.; Kaszás, A.; Kozma, L.; Hornyák, I. Time-Resolved Study of Intramolecular Energy Transfer in Eu^{3+}, Tb^{3+}/β-Diketone/o-Phenanthroline Complexes in Aqueous Micellar Solutions. *J. Lumin.* **1997,** *72*, 570-571.

13. Halcrow, M. A. The Synthesis and Coordination Chemistry of 2,6-Bis(Pyrazolyl)Pyridines and Related Ligands-Versatile Terpyridine Analogues. *Coord. Chem. Rev.* **2005,** *249*, 2880-2908.

14. Narayana, Y. S. L. V.; Basak, S.; Baumgarten, M.; Müllen, K.; Chandrasekar, R. White-Emitting Conjugated Polymer/Inorganic Hybrid Spheres: Phenylethynyl and 2,6-Bis(Pyrazolyl)Pyridine Copolymer Coordinated to $Eu(tta)_3$. *Adv. Funct. Mater.* **2013,** *23*, 5875-5880.

15. Narayana, Y. S. L. V.; Chandrasekar, R. Triple Emission from Organic/Inorganic Hybrid Nanovesicles in a Single Excitation. *ChemPhysChem* **2011,** *12*, 2391-2396.

16. Basak, S.; Chandrasekar, R. Multiluminescent Hybrid Organic/Inorganic Nanotubular Structures: One-Pot Fabrication of Tricolor (Blue–Red–Purple) Luminescent Parallepipedic Organic Superstructure Grafted with Europium Complexes. *Adv. Funct. Mater.* **2011,** *21*, 667-673.

17. Stanley, J. M.; Zhu, X.; Yang, X.; Holliday, B. J. Europium Complexes of a Novel Ethylenedioxythiophene-Derivatized Bis(Pyrazolyl)Pyridine Ligand Exhibiting Efficient Lanthanide Sensitization. *Inorg. Chem.* **2010,** *49*, 2035-2037.

18. Starck, M.; Kadjane, P.; Bois, E.; Darbouret, B.; Incamps, A.; Ziessel, R.; Charbonnière, L. J. Towards Libraries of Luminescent Lanthanide Complexes and Labels from Generic Synthons. *Chem. Eur. J.* **2011,** *17*, 9164-9179.

19. Stanley, J. M.; King, A. W.; Rack, J. J.; Holliday, B. J. Femtosecond Interligand Dynamics in Highly Luminescent Lanthanide Complexes. *in preparation*.

20. Deng, W.; Jin, D.; Drozdowicz-Tomsia, K.; Yuan, J.; Goldys, E. M. Europium Chelate (BHHCT-Eu^{3+}) and Its Metal Nanostructure Enhanced Luminescence Applied to Bioassays and Time-Gated Bioimaging. *Langmuir* **2010,** *26*, 10036-10043.

21. Elhaïk, J.; Pask, C. M.; Kilner, C. A.; Halcrow, M. A. Synthesis of 2,6-Di(Pyrazol-1-yl)-4-Bromomethylpyridine, and Its Conversion to Other 2,6-Di(Pyrazol-1-yl)Pyridines Substituted at the Pyridine Ring. *Tetrahedron* **2007,** *63*, 291-298.

22. Kai, J.; Parra, D. F.; Brito, H. F. Polymer Matrix Sensitizing Effect on Photoluminescence Properties of Eu^{3+}-β-Diketonate Complex Doped into Poly-β-Hydroxybutyrate (PHB) in Film Form. *J. Mater. Chem.* **2008,** *18*, 4549-4554.

23. Gottlieb, H. E.; Kotlyar, V.; Nudelman, A. NMR Chemical Shifts of Common Laboratory Solvents as Trace Impurities. *J. Org. Chem.* **1997,** *62*, 7512-7515.

24. Lakowicz, J. R., Principles of Fluorescence Spectroscopy. 3rd ed.; Springer: New York, 2006.

25. Xu, H.; Wang, L.-H.; Zhu, X.-H.; Yin, K.; Zhong, G.-Y.; Hou, X.-Y.; Huang, W. Application of Chelate Phosphine Oxide Ligand in Eu(III) Complex with Mezzo Triplet Energy Level, Highly Efficient Photoluminescent, and Electroluminescent Performances. *J. Phys. Chem. B* **2006,** *110*, 3023-3029.

26. Carlos, L. D.; Videira, A. L. L. Emission Spectra and Local Symmetry of the Eu^{3+} Ion in Polymer Electrolytes. *Phys. Rev. B* **1994,** *49*, 11721-11728.

27. Werts, M. H. V.; Jukes, R. T. F.; Verhoeven, J. W. The Emission Spectrum and the Radiative Lifetime of Eu^{3+} in Luminescent Lanthanide Complexes. *Phys. Chem. Chem. Phys.* **2002,** *4*, 1542-1548.

28. Haas, Y. G. S. Radiative and Nonradiative Pathways in Solutions. Excited States of the Europium(III) Ion. *J. Phys. Chem.* **1972,** *76*, 1093-1104.

29. Teotonio, E. E. S.; Brito, H. F.; Felinto, M. C. F. C.; Kodaira, C. A.; Malta, O. L. Luminescence Investigations on Eu(III) Thenoyltrifluoroacetonate Complexes with Amide Ligands. *J. Coord. Chem.* **2003,** *56*, 913-921.

30. Lourenço, A. V. S.; Kodaira, C. A.; Ramos-Sanchez, E. M.; Felinto, M. C. F. C.; Goto, H.; Gidlund, M.; Malta, O. L.; Brito, H. F. Luminescent Material Based on the $[Eu(tta)_3(H_2O)_2]$ Complex Incorporated into Modified Silica Particles for Biological Applications. *J. Inorg. Biochem.* **2013,** *123*, 11-17.

31. Kazakov, V. P.; Voloshin, A. I.; Ostakhov, S. S.; Shavaleev, N. M. The Anomalous Influence of Water on the Intensity and Lifetime of Fluorescence in Tris(Benzoyltrifluoroacetonate)Europium(III). *Mendeleev Commun.* **1998,** *8*, 47-49.

32. Beeby, A.; M. Clarkson, I.; S. Dickins, R.; Faulkner, S.; Parker, D.; Royle, L.; S. de Sousa, A.; Williams, A. G. J.; Woods, M. Non-Radiative Deactivation of the Excited States of Europium, Terbium and Ytterbium Complexes by Proximate Energy-Matched OH, NH and CH Oscillators: An Improved Luminescence Method for Establishing Solution Hydration States. *J. Chem. Soc., Perkin Trans 2* **1999,** 493-504.

33. Kropp, J. L.; Windsor, M. W. Luminescence and Energy Transfer in Solutions of Rare-Earth Complexes. I. Enhancement of Fluorescence by Deuterium Substitution. *J. Chem. Phys.* **1965,** *42*, 1599-1608.

34. Leung, P. K.; Steig, R. P., Dielectric Constant Measurements: A New, Rapid Method to Characterize Shale at the Wellsite. Society of Petroleum Engineers. Society of Petroleum Engineers: New Orleans, 1992.

35. Halcrow, M. A. Recent Advances in the Synthesis and Applications of 2,6-Dipyrazolylpyridine Derivatives and Their Complexes. *New J. Chem.* **2014,** *38*, 1868-1882.

Chapter 4: Electrocatalytic Reduction of CO_2 Using Rhenium Complexes with Dipyrido[3,2-a:2',3'-c]phenazine Ligands[3]

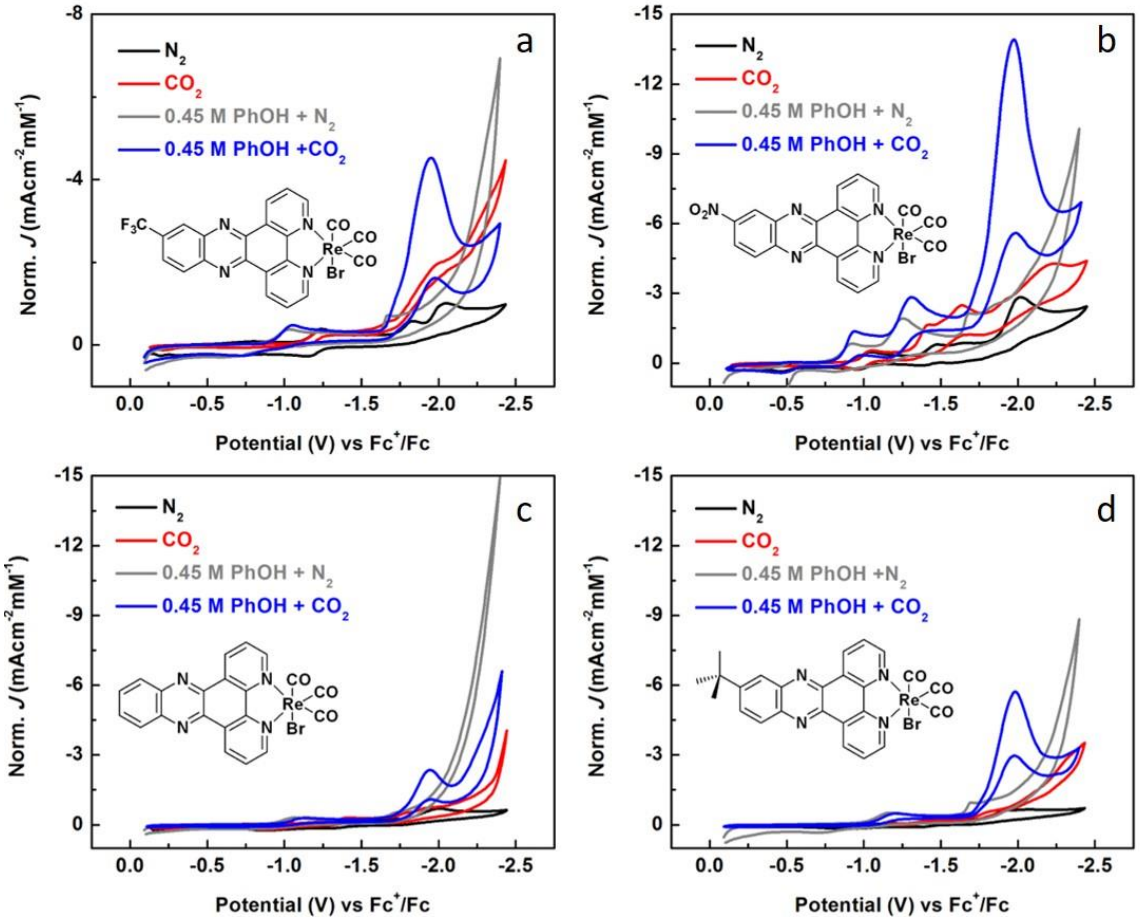

3 This chapter is based partially on the following manuscript-
Liang, Y.; Nguyen, M. T.; Holliday, B. J.; Jones, R. A.
Electrocatalytic Reduction of CO_2 Using Rhenium Complexes with Dipyrido[3,2-a:2',3'-c]phenazine Ligands, submitted

ABSTRACT: The rhenium(I) tricarbonyl diimine complex Re(N-N)$(CO)_3$X (X = Cl, Br or SCN) is a well-documented type of molecular catalyst for the electrochemical reduction of CO_2. Recent developments in this type of catalyst reveal the diimine ligand as playing a significant role in the catalytic reactions. The aim of this study was to extend the scope of diimine ligands used in the Re(I) electrocatalyst for CO_2 reduction. A series of rhenium(I) tricarbonyl dipyrido[3,2-a:2',3'-c]phenazine (dppz) complexes was synthesized, characterized and analyzed as electrocatalysts for CO_2 reduction. Cyclic voltammetry studies show that the rhenium(I) complexes **4.2a**-**4.2d** exhibit dppz ligand-based and metal center-based quasi-reversible reductions. Under a CO_2 atmosphere, complexes **4.2a**-**4.2d** display electrocatalytic an response consistent with $CO_2 \rightarrow CO$ reduction with the presence of the gaseous product CO confirmed by gas chromatography (GC). Additionally, *fac*-Re(2,2'-bipyridine)$(CO)_3$Br, a benchmark catalyst for reducing CO_2 to CO, was also prepared and tested for electrocatalytic properties for comparison. The results show that chemical modifications on the dppz ligand can be used to tailor the electrocatalytic performance of the rhenium(I) complexes, and with the trifluoromethyl substituent, it moves the reduction potential of CO_2 more positive by 200 mV.

4.1 INTRODUCTION

The demand for energy is steadily increasing due to the growth of the population and modern industry. This, in turn, has caused more CO_2 emission, which contributes to issues involving climate change. Therefore, efficiently transforming the greenhouse gas CO_2 into liquid fuels or a useful synthetic precursor, such as CO, would have a great impact on both the global climate change and addressing global energy demands. Researchers are making progress on enzymatic, thermochemical, photochemical and electrochemical reduction of CO_2 catalyzed by metallic, non-metallic and molecular catalysts.[1-5] Among all

the techniques, electrocatalytic reduction of CO_2 by homogeneous molecular catalysis has been studied by many research groups in the past few decades.[5-15] Of many reported homogeneous catalysts for CO_2 reduction, [*fac*-Re(2,2'-bipyridine)$(CO)_3$X], reported by J. M. Lehn and coworkers, exhibits high activities and turnover numbers (Lehn's catalyst).[16, 17] The electrocatalytic reduction of CO_2 by this catalyst has been interpreted in terms of two different electrocatalytic pathways for the reduction of CO_2, a unimolecular $[Re(bpy)]^-$ /$2e^-$ pathway, or a bimolecular 2[Re(bpy)]/[$1e^-$ + $1e^-$].[17-20] There is a considerable amount of literature describing analogues of the Lehn's catalyst for their electrocatalytic properties.[21-28] Kubiak and coworkers have reported a series of Re(I) complexes for electrocatalyzing CO_2 reduction. Their findings suggest that the redox-active 2,2'-bipyridine (bpy) ligand plays an active role in the electrocatalytic reduction by storing electrons and stabilizing negative charges on the proposed intermediate $[Re(bpy)(CO)_3]^-$. Moreover, the reduction potential can be tuned by modifying the bipyridine ligand with various functional groups.[29-34] Furthermore, studies from other groups also imply that the redox-active moiety on the bpy ligand can serve as an electron reservoir for the catalysis.[22] These results inspired us to design rhenium(I) complexes with an N-N bidentate ligand having a high degree of conjugation. This should stabilize the radical intermediate, as well as reserve electrons within the catalyst structure to facilitate the CO_2 reduction process. The employment of the dppz ligand was chosen for several reasons: (i) the dppz ligand has a coordinating bpy end, which can coordinate to the Re(I) center in a similar manner to Lehn's catalyst;[35-37] (ii) the large conjugated ligand can lead to a lower energy of the lowest unoccupied molecular orbital (LUMO) of the Re(I) complex, therefore, decreasing the energy needs to move the Fermi level of the electrode above this unoccupied state;[38] (iii) the electronic properties of the Re(I) complexes can be altered by varying substituents on the aromatic ring using well-known synthetic methodology;[39] and (iv) the photophysical

properties of the rhenium(I) dppz complexes have been thoroughly studied by Gordon and co-workers, indicating the promising application for photocatalysis.[35, 40] Herein, a series of dppz ligands **4.1a**-**4.1d**, with various substituents, from electron-donating (i.e., -^{t}Bu) to electron-withdrawing (i.e., -CF_3), from redox-active (i.e., -NO_2) to redox-inert (i.e., -H) and their corresponding tricarbonyl rhenium(I) bromide complexes **4.2a**-**4.2d** have been synthesized and studied as electrocatalysts for CO_2 reduction.

4.2 EXPERIMENTAL SECTION

4.2.1 Materials and Reagents

The ligands, 11-(trifluoromethyl)dipyrido[3,2-a:2',3'-c]phenazine (**4.1a**), 11-nitrodipyrido[3,2-*a*:2',3'-c]phenazine (**4.1b**), dipyrido[3,2-*a*:2',3'-c]phenazine (**4.1c**) and 11-(tert-butyl)dipyrido[3,2-a:2',3'-c]phenazine (**4.1d**), were prepared by the Schiff base condensation of 1,10-phenanthroline-5,6-dione with the appropriate diamino compound in ethanol under reflux according to known procedures.[39-42] The resulting compounds were purified by recrystallization in methanol, and are identical in all aspects to those reported in the literature. All chemicals for the synthesis of dppz ligands and their corresponding tricarbonyl rhenium(I) bromide complexes were purchased from Sigma-Aldrich, and Alfa Aesar. Acetonitrile used in electrochemical experiments was obtained from EMD Millipore Corporation and purified via a two-column alumina purification system (Pure Process Technology, NH). Tetrabutylammonium hexafluorophosphate ($TBAPF_6$) was purchased from Oakwood and purified by triplicate recrystallization from hot ethanol before drying under vacuum for three days.

4.2.2 Characterization Methods

Air- and moisture-sensitive reactions were performed with standard Schlenk techniques under an inert nitrogen atmosphere. ^{1}H NMR and ^{19}F NMR spectra were

recorded using an Agilent 400 MR NMR spectrometer at 400 MHz for ^{1}H nuclei and 376.5 MHz for ^{19}F nuclei. Coupling constants are reported in hertz (Hz), and chemical shifts are reported as parts per million (ppm) relative to residual solvent peaks (residual $CDCl_3$ δH = 7.26 ppm, residual CD_2Cl_2 δH = 5.32 ppm).[43] High resolution mass spectra (HRMS) were obtained on an Agilent Technologies 6530 Accurate Mass Q-TOF LC/MS instrument. Infrared spectra were recorded with a Nicolet IR 200 FTIR spectrophotometer. Melting points were recorded with an OptiMelt Automated Melting Point System with digital image processing technology from Stanford Research System (SRS, Sunnyvale, CA). Elemental analyses were performed by Midwest Microlab, LLC, Indianapolis, IN (http://midwestlab.com/).

4.2.3 Synthesis of Ligands 4.1a-4.1d and Rhenium(I) dppz Complexes 4.2a-4.2d

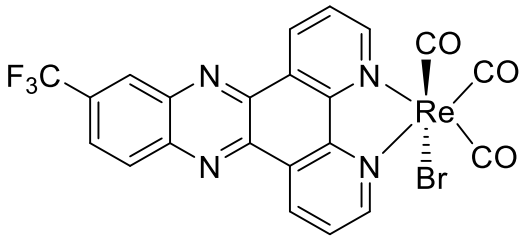

4.2a

ReBr(11-(trifluoromethyl)dipyrido[3,2-a:2',3'-c]phenazine)$(CO)_3$ (4.2a). Pentacarbonyl rhenium(I) bromide, $Re(CO)_5Br$ (58 mg, 0.14 mmol), was added to a Schlenk flask with ligand **4.1a** (50 mg, 0.14 mmol) in a dry box. Then dry methanol (10 mL) was cannula transferred to the flask. After refluxing under nitrogen for 8 hours, an orange yellow solid was collected after hot filtration and a diethyl ether wash (Yield: 69 mg, 69%). ^{1}H NMR ($CDCl_3$): 9.85 (2H, ddd, J = 8.90, 7.43, 1.49), 9.51 (2H, dt, J = 5.23, 1.44), 8.79 (1H, m), 8.60 (1H, d, J = 8.91), 8.21 (1H, dd, J = 8.99, 1.98), 8.06 (2H, ddd, J = 8.24, 5.25, 1.88). ^{19}F NMR ($CDCl_3$): 62.99 (s). HRMS (ESI): calcd. for $[M + Na]^+$ *m/z*:

722.92430, found: 722.92340. FTIR: (cm^{-1}) 2024, 1920, 1890. Melting point: 337-338 ºC. Elemental anal. calculated (found) for **4.2a**, $C_{22}H_9BrF_3N_4O_3Re$: C, 37.72 (37.95); H, 1.30 (1.50); N, 8.00 (7.92).

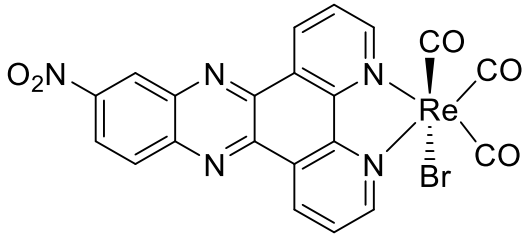

4.2b

ReBr(11-nitrodipyrido[3,2-*a*:2',3'-c]phenazine)(CO)$_3$ (4.2b). Pentacarbonyl rhenium(I) bromide $Re(CO)_5Br$ (81 mg, 0.2 mmol) was added to a Schlenk flask with ligand **4.1b** (65 mg, 0.2 mmol) in a dry box. Then dry methanol (15 mL) was cannula transferred to the flask. After refluxing under nitrogen for 8 hours, an orange yellow solid was collected after hot filtration and a diethyl ether wash (Yield: 91 mg, 67%). ^{1}H NMR (CD_2Cl_2): 9.86 (2H, dt, *J* = 8.25, 1.54), 9.54 (2H, dt, *J* = 5.18, 1.33), 9.38 (1H, d, *J* = 2.52), 8.81 (1H, dd, *J* = 9.35, 2.51), 8.64 (1H, d, *J* = 9.33), 8.08 (2H, m). HRMS (ESI): calcd. for $[M + Na]^+$ *m/z*: 699.92200, found: 699.92090. FTIR: 2025, 1943, 1869 (cm^{-1}). Melting point: 329-331 ºC. Elemental anal. calculated (found) for **4.2b**, $C_{21}H_9BrN_5O_5Re$: C, 37.23 (37.13); H, 1.34 (1.39); N, 10.34 (10.15).

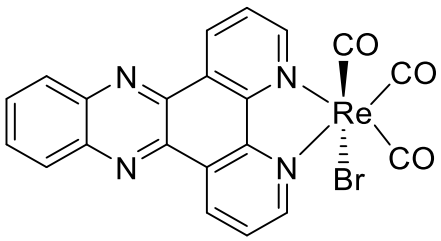

4.2c

ReBr(dipyrido[3,2-*a*:2',3'-c]phenazine)(CO)$_3$ (4.2c). $Re(CO)_5Br$ (81 mg, 0.2 mmol) was added to a Schlenk flask with ligand **4.1c** (56 mg, 0.2 mmol) in a dry glove

box. Then dry methanol (15 mL) was cannula transferred under N_2. After refluxing under nitrogen for 8 hours, a yellow solid was collected after hot filtration and a diethyl ether wash (Yield: 73 mg, 58%). ^{1}H NMR (CD_2Cl_2): 9.88 (2H, dd, *J* = 8.24, 1.48), 9.45 (2H, dd, *J* = 5.23, 1.48), 8.48 (2H, dd, *J* = 6.61, 3.44), 8.07 (m, 4H). HRMS (ESI): calcd. for $[M + Na]^+$ *m/z*: 654.93690, found: 654.93630. FTIR (cm^{-1}): 2021, 1926, 1888. Melting point: 339-340 ºC. Elemental anal. calculated (found) for **4.2c**, $C_{21}H_{10}BrN_4O_3Re$: C, 39.88 (40.25); H, 1.59 (2.17); N, 8.86 (8.09).

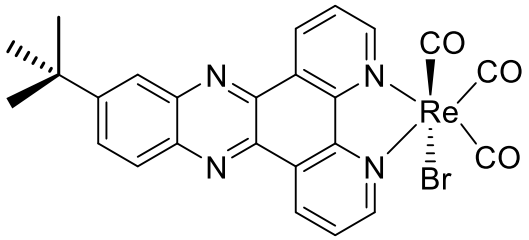

4.2d

ReBr(11-(tert-butyl)dipyrido[3,2-a:2',3'-c]phenazine)(CO)$_3$ (4.2d). $Re(CO)_5Br$ (60 mg, 0.15 mmol) was added to a Schlenk flask with ligand **4.1d** (50 mg, 0.15 mmol) in a dry ox. Then dry methanol (5 mL) was cannula transferred under N_2. After refluxing under nitrogen for 8 hours, a yellow solid was collected after hot filtration and a diethyl ether wash (Yield: 68 mg, 67%). ^{1}H NMR ($CDCl_3$): 9.85 (2H, ddd, *J* = 8.11, 3.57, 1.37), 9.47 (2H, dd, *J* = 5.19, 2.61, 1.47), 8.37 (2H, m), 8.16 (1H, dd, *J* = 9.03, 2.17), 8.01 (ddd, 2H, *J* = 8.18, 5.16, 1.56), 1.55 (9H, s). HRMS (ESI): calcd. for $[M + Na]^+$ *m/z*: 710.99950, found: 710.99800. FTIR (cm^{-1}): 2021.01, 1893.71. Melting point: 315-317 ºC. Elemental anal. calculated (found) for **4.2d**, $C_{25}H_{18}N_4O_3Re$: C, 43.61 (43.72); H, 2.64 (2.84); N, 8.14 (8.09).

4.2.4 Electrochemistry

Electrochemical studies were performed in a glovebox under a nitrogen atmosphere using GPES software from Eco. Chemie B. V. and an Autolab Potentiostat (PGSTAT30).

All electrochemical experiments were performed with 0.1 M tetrabutylammonium hexafluorophosphate ($TBAPF_6$) as the supporting electrolyte. The electrolyte was purified via three recrystallizations from hot ethanol before drying under dynamic vacuum for three days. All cyclic voltammetry experiments were carried out with a glassy carbon electrode (3 mm in diameter), a Pt wire coil counter electrode and a $Ag/AgNO_3$ reference electrode (silver wire dipped in a 0.01 M silver nitrate solution with 0.1 M $TBAPF_6$ in dry acetonitrile). All potentials were reported relative to the ferrocenium/ferrocene couple (Fc^+/Fc), which was used as an external standard to calibrate the reference electrode. All cyclic voltammetry experiments with CO_2 were performed at gas saturation (about 0.25 M) in 3 mL dry acetonitrile solutions with electrolyte by purging with CO_2 for 5 minutes before CVs were taken.[44, 45] Electrocatalytic studies were performed by cycling three times between around -0.2 V and -2.5 V (vs Fc^+/Fc) at a scan rate of 100 mV/s. The value of normalized current density [Norm. J ($mA \cdot cm^{-2} \cdot mM^{-1}$)] was calculated by dividing the current density by the concentration of the catalyst.

4.2.5 Controlled Potential Electrolysis

The controlled potential electrolysis experiments were conducted in a customer-built cell (Figure 4.1). A glassy carbon electrode (3 mm in diameter) was used as the working electrode. The counter electrode was a platinum mesh (0.6 cm x 0.7 cm) and the reference electrode was a $Ag/AgNO_3$ electrode separated from solution by a Teflon tip. The supporting electrolyte was composed of 0.1 M $TBAPF_6$ in acetonitrile. Before each electrolysis, the cell was purged by CO_2 for 30 minutes. All electrolysis experiments were performed with vigorous stirring. After the completion of a run, 3 mL of headspace was sampled with a gas-tight syringe (Valco Instruments Co. Inc.) and injected into a Gas Chromatography Fuel Cell Analyzer (Shimadzu 2014).

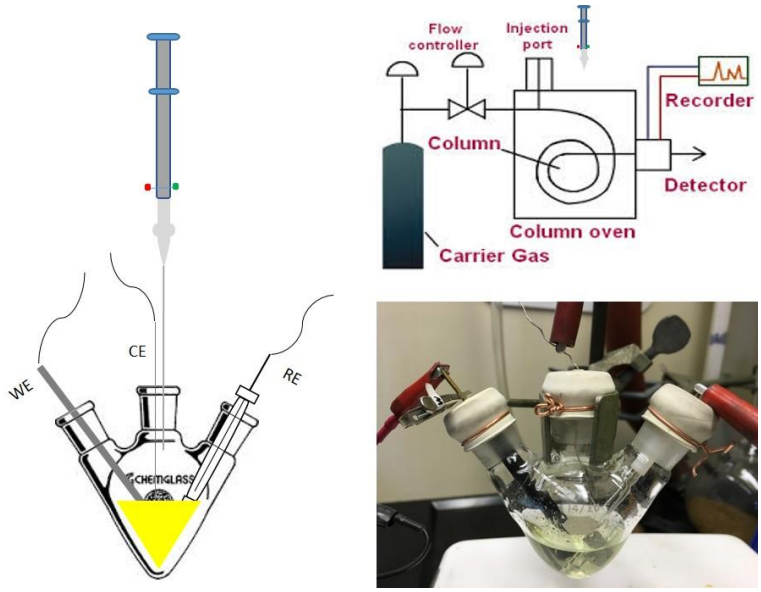

Figure 4.1. Customer-built electrochemical cell using for controlled potential electrolysis experiments.

4.2.6 Single Crystal Structure Determination

Crystals of **4.2b** and **4.2c** were grown by slow evaporation from dichloromethane solutions. Crystals suitable for data collection were covered with hydrocarbon oil and mounted on thin nylon loops. X-ray experimental details can be found in the Appendix.

4.3 Results and Discussion

4.3.1 Synthesis and Structure Determination of the Re(I) dppz Complexes

Complexes **4.2a**-**4.2d**, with varying substituents in the 11-position of dppz ligand, have been synthesized from $Re(CO)_5Br$ and the corresponding ligands **4.1a**-**4.1d** (Scheme 4.1). Single crystals, suitable for X-ray analysis, were grown from the slow evaporation of **4.2b** and **4.2c** in dichloromethane. Attempts at growing suitable crystals for X-ray diffraction of the other complexes were not successful. The X-ray structures revealed that **4.2b** and **4.2c** have octahedral coordination geometries and a *facial* orientation of the three CO ligands (Figure 4.2), as commonly seen in Lehn's catalyst and its analogues. Crystal

structure data have been uploaded to the Cambridge Structural Database; CCDC 1536555-1536556 contain the supplementary crystallographic data for this chapter. The data can be obtained free of charge from The Cambridge Crystallographic Data Centre via www.ccdc.cam.ac.uk/structures.

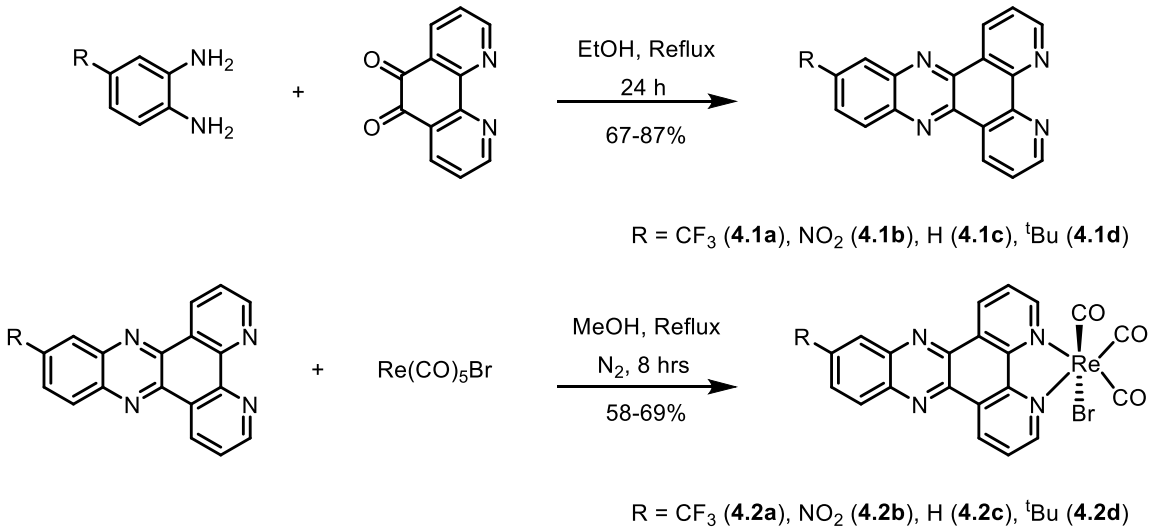

Scheme 4.1. Synthesis of ligands **4.1a**-**4.1d**, and Re(I) complexes **4.2a**-**4.2d**.

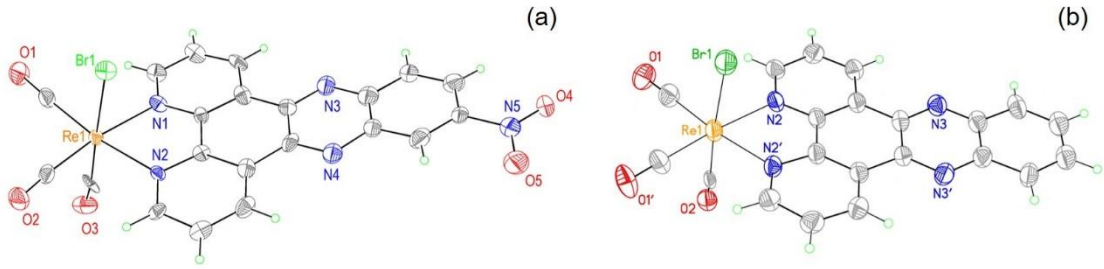

Figure 4.2. Crystal structures of Re(I) complexes **4.2b** (a) and **4.2c** (b).

Ligands **4.1a**-**4.1d** and Re(I) complexes **4.2a**-**4.2b** were studied by UV-vis spectroscopy in acetonitrile solution (Figure 4.3). The absorbance spectra of **4.2a**-**4.2d** contained two predominant transitions: a $\pi \rightarrow \pi^*$ band around 270 nm, and a lower energy

absorption region around 350-380 nm which is assigned to a mixture of metal to ligand charge transfer ($MLCT_{d(Re)} \rightarrow \pi^*_{(dppz)}$) and ligand to ligand charge transfer ($LLCT_{(dppz)}$).[46] Table 4.1 lists the UV-vis spectra peaks and the corresponding molar absorptivity constants of **4.1a**-**4.1d** and **4.2a**-**4.2d**.

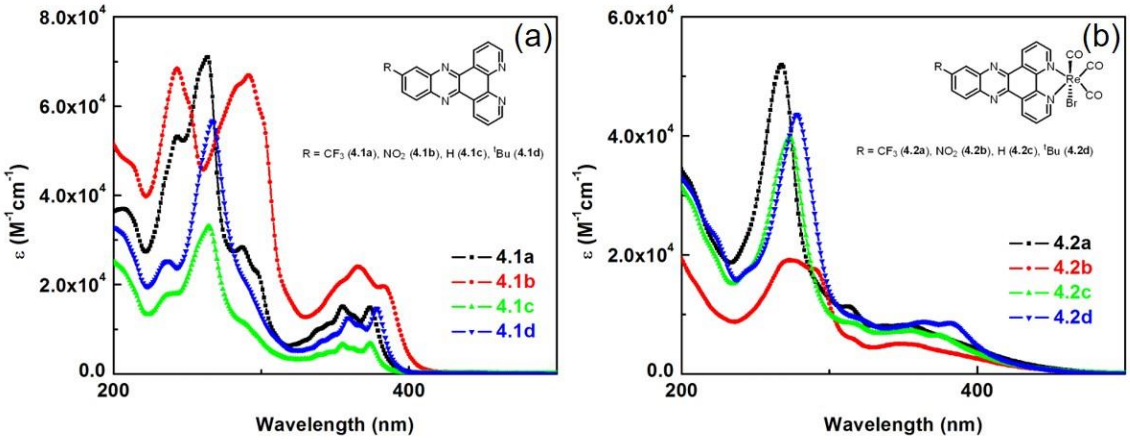

Figure 4.3. UV-vis spectra of **4.1a**-**4.1d** (a) and **4.2a**-**4.2d** (b) in acetonitrile solutions.

Table 4.1. UV-vis properties of ligands **4.1a**-**4.1d** and Re(I) complexes **4.2a**-**4.2d** in acetonitrile.

Compound	λ_{max} [nm ($\varepsilon/10^4 M^{-1}cm^{-1}$)]
4.1a	243 (5.3), 263 (7.1), 288 (2.9), 355 (1.6), 374 (1.5)
4.1b	243 (6.9), 284 (6.5), 291 (6.7), 353 (2.0), 366 (2.4), 383 (2.0)
4.1c	247 (1.8), 265 (3.3), 289 (1.1), 355 (0.7), 374 (0.7)
4.1d	236 (2.5), 267 (5.7), 292 (1.9), 359 (1.3), 378 (1.5)
4.2a	268 (5.2), 314 (1.1), 336 (0.8), 353 (0.8)
4.2b	272 (1.9), 290 (1.8), 315 (0.6), 350 (0.5)
4.2c	272 (4.0), 317 (0.8), 355 (0.7), 374 (0.6)
4.2d	278 (4.4), 319 (1.0), 364 (0.9), 381 (0.9)

4.3.2 Electrochemical Properties of Ligands 4.1a-4.1d and Complexes 4.2a-4.2d

Electrochemical studies were performed on ligands **4.1a-4.1d** and complexes **4.2a-4.2d** to determine their redox activities. The Lehn catalyst, *fac*-Re(2,2'-bipyridine)$(CO)_3Br$ [Re(bpy)$(CO)_3Br$], was also synthesized and studied for comparison. Figure 4.4 presents the cyclic voltammograms (CVs) of **4.1a-4.1d, 4.2a-4.2d**, and the Lehn catalyst under a nitrogen atmosphere in acetonitrile with 0.1 M $TBAPF_6$ as supporting electrolyte. The CVs of **4.2a-4.2d** exhibited redox features similar to those of the Lehn catalyst in the potential range from -1.7 V to -2.0 V vs Fc^+/Fc (Figure 4.4, black dot-dash lines), in agreement with the Re-bipyridine moiety reduction.[16] The phenazine moiety of the ligands gave rise to the redox peaks in the -1.0 to -1.5 V potential range. Complex **4.2b** demonstrated a more complicated redox behavior than the others because of the redox-active nitro group involved. The nitro group is attributed to the reversible redox activity at -1.0 V vs Fc^+/Fc.[47] Table 4.2 illustrates the reduction potentials of **4.1a-4.1d** and **4.2a-4.2d**.

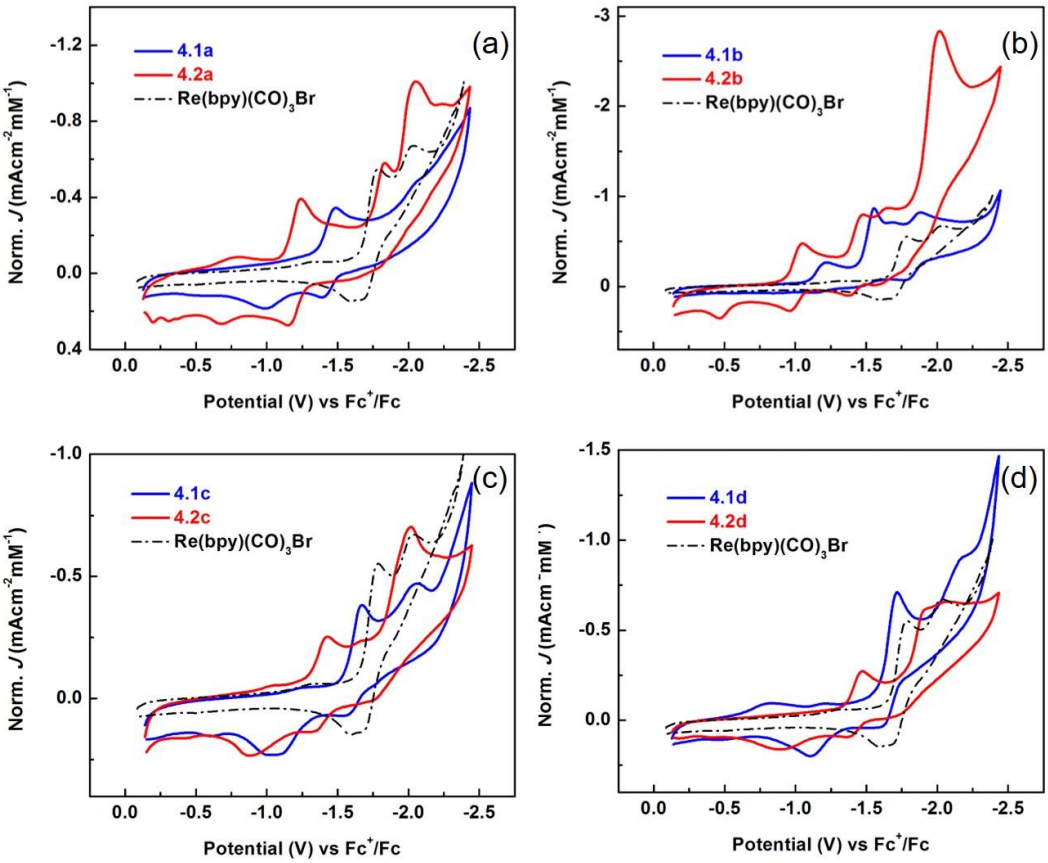

Figure 4.4. Cyclic voltammograms of dppz ligands **4.1a**-**4.1d**, and their corresponding Re(I) complexes **4.2a**-**4.2d** at the scan rate of 100 mV/s in acetonitrile under nitrogen with 0.1 M $TBAPF_6$ as supporting electrolyte. CV of $Re(bpy)(CO)_3Br$ included for comparison.

The peak currents in the CV curves followed a scan rate (υ) dependence which was linear with $\upsilon^{1/2}$, indicating a diffusion-limited electron transfer process (Figure 4.5).[38] In addition, the CV peaks of Re(I) complexes around -2.0 V became more reversible at high scan rates, suggesting a chemical reaction occurred after the electrochemical step. As proposed by Schaefer and coworkers, the latter observation points to Re-Re dimerization during the electrochemical process, a common deactivation pathway for most of the Re complex catalyzing CO_2 reductions.[23]

Table 4.2. Reduction potentials (vs Fc^{+}/Fc) of **4.1a**-**4.1d** and **4.2a**-**4.2d** in acetonitrile.

Compound	1st	2nd	3rd	4th
4.1a	-1.48	-2.06	---	---
4.2a	-1.24	-1.87	-2.03	---
4.1b	-1.22	-1.55	-1.70	-1.88
4.2b	-1.05	-1.48	-1.64	-2.02
4.1c	-1.67	-2.06	---	---
4.2c	-1.42	-1.67	-2.01	---
4.1d	-1.71	-2.19	---	---
4.2d	-1.47	-1.92	-2.07	---
Lehn catalyst [a]	-1.78	-2.03	---	---

a. The Lehn catalyst *fac*-Re(2, 2'-bipyridine)$(CO)_3Br$ was synthesized and used as a reference compound in this study.

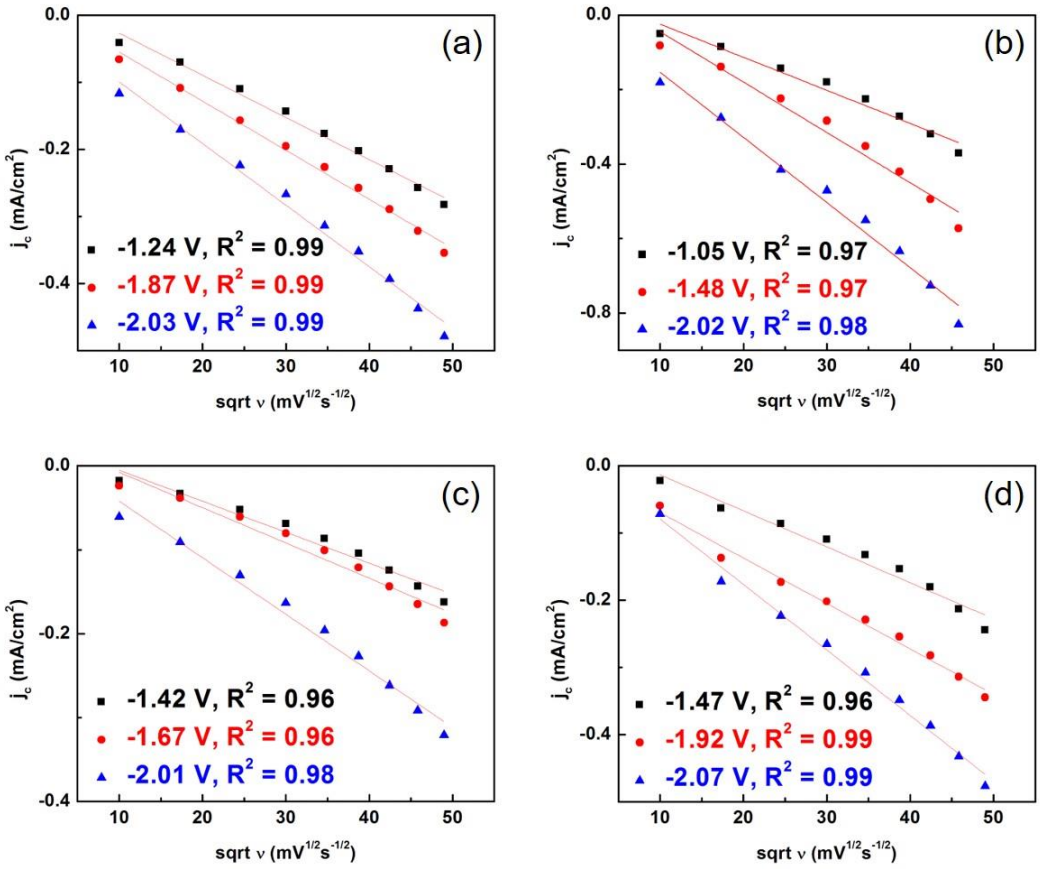

Figure 4.5. Scan rate dependence of the reduction waves of Re(I) complexes at different potentials: **4.2a** (a), **4.2b** (b), **4.2c** (c), and **4.2d** (d).

4.3.3 Electrochemical Catalysis of CO_2 Reduction Using Complexes 4.2a-4.2d

Two control experiments were performed before the electrocatalytic test for complexes **4.2a**-**4.2d**. Firstly, the CV of the Lehn catalyst $Re(bpy)(CO)_3Br$ was studied under both N_2 and CO_2 atmospheres. The cathodic current of the Lehn catalysts showed a 2.2-fold increase at -2.09 V vs Fc^+/Fc under CO_2 compared to the current under an N_2 atmosphere (Figure 4.6a). Secondly, CV curves of a blank electrolyte solution were measured under N_2 and CO_2 atmospheres (Figure 4.6b). Under a CO_2 atmosphere, the blank solution displayed a flat cathodic current until the voltage reached to 1.9 V or 2.3 V

vs Fc^+/Fc with or without the addition of proton source (i.e., PhOH), suggesting no CO_2 reduction occurred before the potential of the working electrode reached to these values.

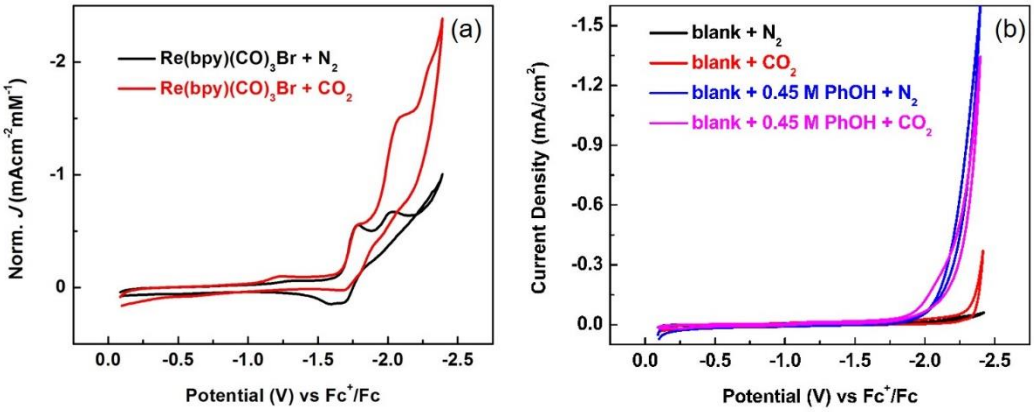

Figure 4.6. Cyclic voltammograms of (a) Lehn catalyst under N_2 and CO_2 saturation and (b) a blank MeCN solution with 0.1 M $TBAPF_6$ as supporting electrolyte under N_2 and CO_2 atmosphere with and without phenol (0.45 M) as a proton source.

Figure 4.7 presents the CVs of **4.2a**-**4.2d** recorded under N_2 and CO_2 with and without phenol as the additional brønsted acid. When acetonitrile solutions of **4.2a**-**4.2d** were saturated with CO_2, differences were observed in the CO_2 reduction wave from complex to complex. Complex **4.2a**, in a CO_2-saturated solution, showed a 2.7-fold increase in current at -2.0 V vs Fc^+/Fc with a complete loss of reversibility, which is consistent with an electrocatalytic response.[16] With the addition of phenol (0.45 M PhOH), the current density increased by more than double with a significant potential shift of 30 mV in the positive direction (Figure 4.7a). This behavior implies the interaction of protons with the reduced species of **4.2a**, which helps the electrocatalytic reduction of CO_2 in acetonitrile solution proposed by Keith and coworkers.[30] Complexes **4.2c** and **4.2d** displayed similar CV features to **4.2a** on the negative sweep with the cathodic currents increasing (around -2.0 V vs Fc^+/Fc) to different extents (Figure 4.7c, Figure 4.7d). Unlike

the others, **4.2b** showed current enhancement not only at the potential of -2.0 V, but also at -1.3 V without a proton source, and at -0.9 V with the addition of a proton source (Figure 4.7b). The current increases at lower voltages may be attributed to the involvement of the redox-active nitro group, although a detailed explanation has not been found yet. Figure 4.8 illustrates the comparison between catalytic currents of **4.2a**-**4.2d** and of the Lehn catalyst at CO_2 reduction potentials. Table 4.3 summarizes the turn over frequency (TOF) of **4.2a**-**4.2d** calculated by a previously reported method.[48] Apart from a little higher TOF of **4.2a** compared to the Lehn catalyst, the CO_2 reduction peak potentials of **4.2a**-**4.2d** are slightly lower than that of the Lehn catalyst due to the higher degree of conjugation.[49] The highest TOF turns from **4.2a** to **4.2b** with the addition of a proton source, and again the detailed reason is not yet completely understood.

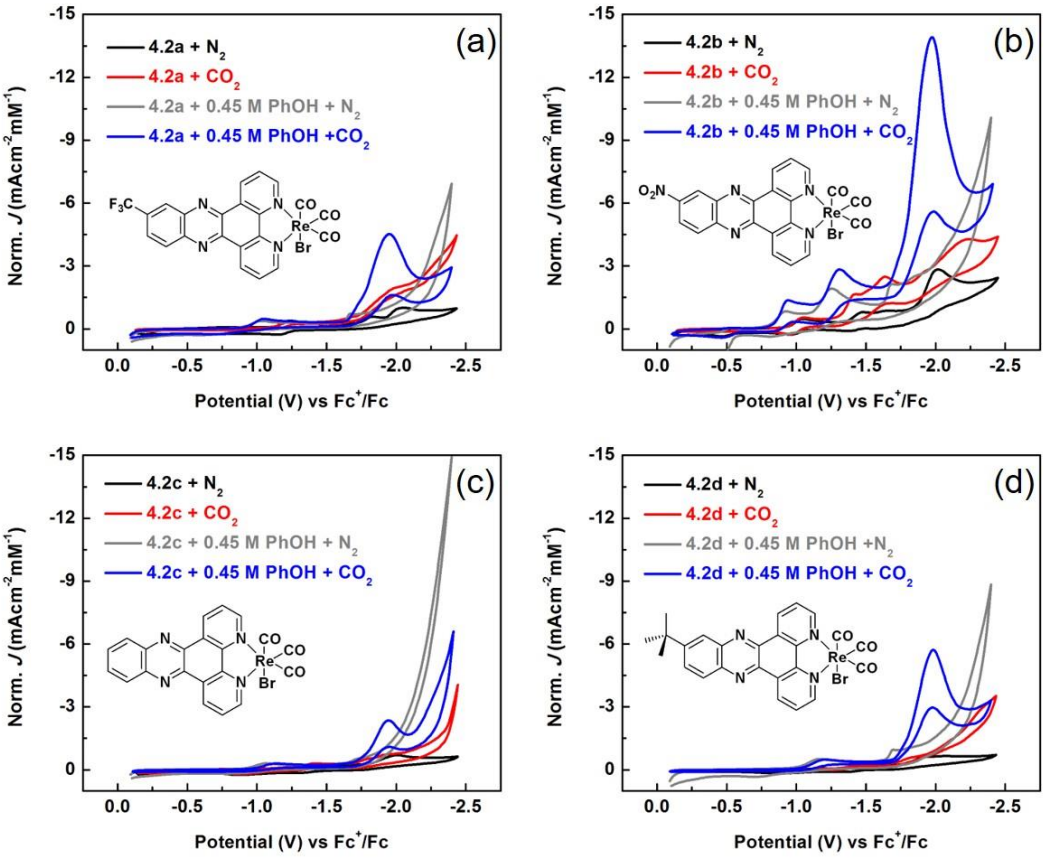

Figure 4.7. Cyclic voltammograms of **4.2a**-**4.2d** (0.1 mM) under N_2 and CO_2 saturation in MeCN with 0.1 M $TBAPF_6$ as supporting electrolyte. The concentrations of Re(I) complexes have been corrected after purging the solution with CO_2 for 5 minutes.

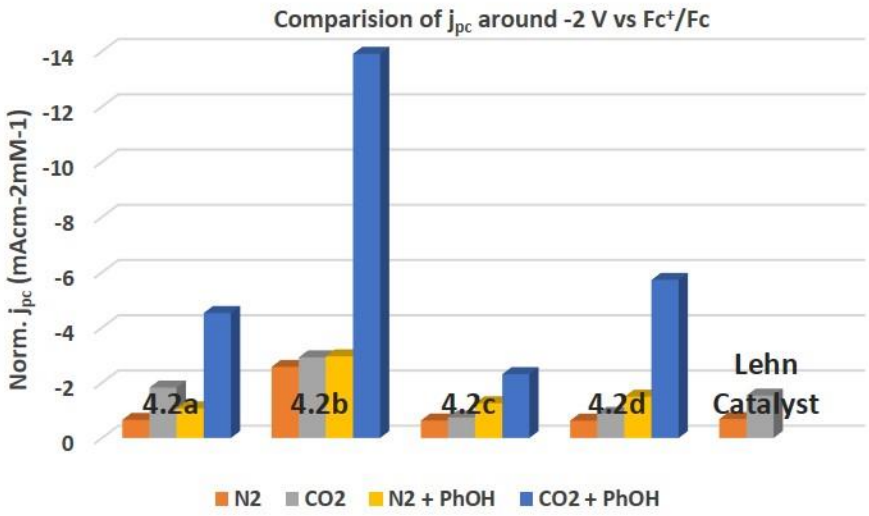

Figure 4.8. Comparison of the cathodic peak currents around -2.0 V of the Re(I) complexes under N_2 and CO_2 atmosphere with and without the addition of 0.45 M phenol (PhOH) in acetonitrile solutions.

Table 4.3. Comparison of i_{cat}/i_p values of **4.2a**-**4.2d** in acetonitrile solutions saturated with CO_2 (ca. 0.25 M).

Re(I) Complexes	No brønsted acid		With 0.45 M PhOH	
	i_{cat}/i_p	TOF (s^{-1}) [a]	i_{cat}/i_p	TOF (s^{-1}) [a]
4.2a	2.7	1.5	4.2	3.6
4.2b	1.1	0.3	4.7	4.4
4.2c	1.2	0.3	1.8	0.7
4.2d	1.4	0.4	3.8	2.9
Lehn Catalyst	2.2	1.0	---	---

a. TOF calculation per Smieja *et.al*.[48]

4.3.4 Identification of Gaseous Phase Product

To identify the electrocatalytic reduction product of CO_2 with **4.2a**-**4.2d** in acetonitrile without the addition of brønsted acid, controlled potential electrolysis experiments were carried out in a one compartment cell at the CO_2 reduction peak potentials displayed in Figure 4.7. Gas chromatography (GC) analysis confirmed the only gaseous product to be CO with a faradaic efficiency ranging from 19% to 53% for different Re(I) complexes (Table 4.4). Furthermore, the reduction peak remained at approximately the same current during the controlled potential electrolysis, indicating good stability for the catalyst. Additionally, there is no significant change in the CV curve or UV-vis spectra of **4.2a**, taken before and after the electrolysis, reaffirming the catalyst stability (Figure 4.9).

Table 4.4. Faradaic efficiency of **4.2a**-**4.2d** and the Lehn catalyst catalyzing CO production measured in this study.

Re(I) Complex	Operating Potential (V vs Fc^+/Fc)	Faradaic efficiency (%)	
		Absolute	Calibrated
4.2a	-1.9	19	59
4.2b	-2.1	53	166
4.3c	-2.0	48	151
4.3d	-2.0	27	84
Lehn Catalyst	-2.1	32 ± 7	100

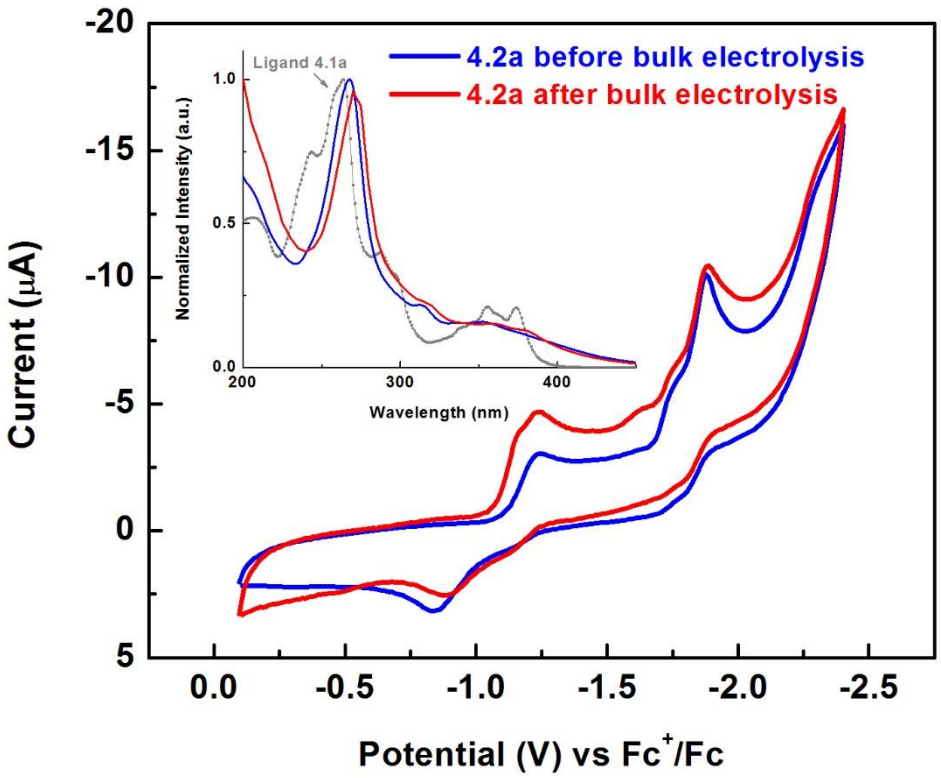

Figure 4.9. CV and UV-vis spectra of compound **4.2a** before and after the controlled potential electrolysis experiment in acetonitrile solution. The UV-vis spectrum of ligand **4.1a** included for comparison.

4.4 CONCLUSION

In conclusion, four new rhenium(I) complexes **4.2a**-**4.2d** with different substituents on the dppz backbone were synthesized and investigated as electrocatalysts for CO_2 reduction. X-ray diffraction studies revealed the *facial* orientation of the three CO ligands in the synthesized Re(I) complexes **4.2b** and **4.2c**. Compared to the Lehn catalyst, $Re(bpy)(CO)_3Br$, which is a benchmark for electrocatalytic reduction of CO_2, **4.2a**-**4.2d** with higher degree of conjugation can lower the energy barrier for the CO_2 reduction process. CO was detected as the only gaseous phase product of **4.2a**-**4.2d** catalyzing CO_2

reduction in acetonitrile with a faradaic efficiency ranging from 19 to 53 %. The extended conjugation within the catalyst provides a possible approach to lower the overpotential of CO_2 reduction, supporting by the fact that **4.2a** catalyzed CO_2 reduction with a smaller overpotential compared to that of using the less-conjugated Lehn catalyst. This work has important implications for the development of more efficient catalysts for the electrocatalysis of CO_2 reduction.

4.5 REFERENCES

1. Wang, W-H.; Himeda, Y.; Muckerman, J. T.; Manbeck, G. F.; Fujita, E. CO_2 Hydrogenation to Formate and Methanol as an Alternative to Photo- and Electrochemical CO_2 Reduction. *Chem. Rev.* **2015,** *115*, 12936-12973.
2. Sultana, S.; Sahoo, P. C.; Martha, S.; Parida, K. A Review of Harvesting Clean Fuels from Enzymatic CO_2 Reduction. *RSC Adv.* **2016,** *6*, 44170-44194.
3. Kumar, B.; Brian, J. P.; Atla, V.; Kumari, S.; Bertram, K. A.; White, R. T.; Spurgeon, J. M. New Trends in the Development of Heterogeneous Catalysts for Electrochemical CO_2 Reduction. *Catal. Today* **2016,** *270*, 19-30.
4. Lu, Q.; Jiao, F. Electrochemical CO_2 Reduction: Electrocatalyst, Reaction Mechanism, and Process Engineering. *Nano Energy* **2016,** *29*, 439-456.
5. Benson, E. E.; Kubiak, C. P.; Sathrum, A. J.; Smieja, J. M. Electrocatalytic and Homogeneous Approaches to Conversion of CO_2 to Liquid Fuels. *Chem. Soc. Rev.* **2009,** *38*, 89-99.
6. Qiao, J.; Liu, Y.; Hong, F.; Zhang, J. A Review of Catalysts for the Electroreduction of Carbon Dioxide to Produce Low-Carbon Fuels. *Chem. Soc. Rev.* **2014,** *43*, 631-675.
7. Whipple, D. T.; Kenis, P. J. A. Prospects of CO_2 Utilization Via Direct Heterogeneous Electrochemical Reduction. *J. Phys. Chem. Lett.* **2010,** *1*, 3451-3458.
8. Costentin, C.; Robert, M.; Saveant, J.-M. Catalysis of the Electrochemical Reduction of Carbon Dioxide. *Chem. Soc. Rev.* **2013,** *42*, 2423-2436.
9. Choi, J.; Benedetti, T. M.; Jalili, R.; Walker, A.; Wallace, G. G.; Officer, D. L. High Performance Fe Porphyrin/Ionic Liquid Co-Catalyst for Electrochemical CO_2 Reduction. *Chem. Eur. J.* **2016,** *22*, 14158-14161.
10. Johnson, B. A.; Maji, S.; Agarwala, H.; White, T. A.; Mijangos, E.; Ott, S. Activating a Low Overpotential CO_2 Reduction Mechanism by a Strategic Ligand

Modification on a Ruthenium Polypyridyl Catalyst. *Angew. Chem. Int. Ed.* **2016,** *55*, 1825-1829.

11. Portenkirchner, E.; Oppelt, K.; Ulbricht, C.; Egbe, D. A. M.; Neugebauer, H.; Knör, G.; Sariciftci, N. S. Electrocatalytic and Photocatalytic Reduction of Carbon Dioxide to Carbon Monoxide Using the Alkynyl-Substituted Rhenium(I) Complex (5,5′-Bisphenylethynyl-2,2′-Bipyridyl)Re(CO)$_3$Cl. *J. Organomet. Chem.* **2012,** *716*, 19-25.

12. Lim, C.-H.; Holder, A. M.; Musgrave, C. B. Mechanism of Homogeneous Reduction of CO_2 by Pyridine: Proton Relay in Aqueous Solvent and Aromatic Stabilization. *J. Am. Chem. Soc.* **2013,** *135*, 142-154.

13. Froehlich, J. D.; Kubiak, C. P. Homogeneous CO_2 Reduction by Ni(Cyclam) at a Glassy Carbon Electrode. *Inorg. Chem.* **2012,** *51*, 3932-3934.

14. Cole, E. B.; Lakkaraju, P. S.; Rampulla, D. M.; Morris, A, J.; Abelev, E.; Bocarsly, A. B. Using a One-Electron Shuttle for the Multielectron Reduction of CO_2 to Methanol: Kinetic, Mechanistic, and Structural Insights. *J. Am. Chem. Soc.* **2010,** *132*, 11539-11551.

15. Stanton, C. J.; Vandezande, J. E.; Majetich, G. F.; Schaefer, H. F.; Agarwal, J. Mn-NHC Electrocatalysts: Increasing π Acidity Lowers the Reduction Potential and Increases the Turnover Frequency for CO_2 Reduction. *Inorg. Chem.* **2016,** *55*, 9509-9512.

16. Hawecker, J.; Lehn, J.-M.; Ziessel, R. Electrocatalytic Reduction of Carbon Dioxide Mediated by Re(Bipy)(CO)$_3$Cl (Bipy = 2,2'-Bipyridine). *J. Chem. Soc., Chem. Commun.* **1984**, 328-330.

17. Sullivan, B. P.; Bolinger, C. M.; Conrad, D.; Vining, W. J.; Meyer, T. J. One- and Two-Electron Pathways in the Electrocatalytic Reduction of CO_2 by *fac*-Re(bpy)(CO)$_3$Cl (bpy = 2,2'-Bipyridine). *J. Chem. Soc., Chem. Commun.* **1985**, 1414-1416.

18. Smieja, J. M.; Kubiak, C. P. Re(bipy-^{t}bu)(CO)$_3$Cl−Improved Catalytic Activity for Reduction of Carbon Dioxide: IR-Spectroelectrochemical and Mechanistic Studies. *Inorg. Chem.* **2010,** *49*, 9283-9289.

19. Hayashi, Y.; Kita, S.; Brunschwig, B. S.; Fujita, E. Involvement of a Binuclear Species with the Re−C(O)O−Re Moiety in CO_2 Reduction Catalyzed by Tricarbonyl Rhenium(I) Complexes with Diimine Ligands: Strikingly Slow Formation of the Re−Re and Re−C(O)O−Re Species from Re(DMB)(CO)$_3$S (DMB = 4,4'-Dimethyl-2,2'-bipyridine, S = Solvent). *J. Am. Chem. Soc.* **2003,** *125*, 11976-11987.

20. Agarwal, J.; Fujita, E.; Schaefer, H. F.; Muckerman, J. T. Mechanisms for CO Production from CO_2 Using Reduced Rhenium Tricarbonyl Catalysts. *J. Am. Chem. Soc.* **2012,** *134*, 5180-5186.

21. Portenkirchner, E.; Oppelt, K.; Ulbricht, C.; Egbe, D. A. M.; Neugebauer, H.; Knör, G.; Sariciftci, N. S. Electrocatalytic and Photocatalytic Reduction of Carbon Dioxide to Carbon Monoxide Using the Alkynyl-Substituted Rhenium(I) Complex (5,5′-Bisphenylethynyl-2,2′-Bipyridyl)Re(CO)$_3$Cl. *J. Organomet. Chem.* **2012,** *716*, 19-25.

22. Teesdale, J. J.; Pistner, A. J.; Yap, G. P. A.; Ma, Y.-Z.; Lutterman, D. A.; Rosenthal, J. Reduction of CO_2 Using a Rhenium Bipyridine Complex Containing Ancillary Bodipy Moieties. *Catal. Today* **2014,** *225*, 149-157.

23. Agarwal, J.; Shaw, T. W.; Stanton, C. J.; Majetich, G. F.; Bocarsly, A. B.; Schaefer, H. F. NHC-Containing Manganese(I) Electrocatalysts for the Two-Electron Reduction of CO_2. *Angew. Chem. Int. Ed.* **2014,** *53*, 5152-5155.

24. Clark, M. L.; Grice, K. A.; Moore, C. E.; Rheingold, A. L.; Kubiak, C. P. Electrocatalytic CO_2 Reduction by M(bpy-R)(CO)$_4$ (M = Mo, W; R = H, ^{t}bu) Complexes. Electrochemical, Spectroscopic, and Computational Studies and Comparison with Group 7 Catalysts. *Chem. Sci.* **2014,** *5*, 1894-1900.

25. Franco, F.; Cometto, C.; Ferrero Vallana, F.; Sordello, F.; Priola, E.; Minero, C.; Nervi, C.; Gobetto, R. A Local Proton Source in a [Mn(bpy-R)(CO)$_3$Br]-Type Redox Catalyst Enables CO_2 Reduction Even in the Absence of Bronsted Acids. *Chem. Commun.* **2014,** *50*, 14670-14673.

26. Riplinger, C.; Sampson, M. D.; Ritzmann, A. M.; Kubiak, C. P.; Carter E. A. Mechanistic Contrasts between Manganese and Rhenium Bipyridine Electrocatalysts for the Reduction of Carbon Dioxide. *J. Am. Chem. Soc.* **2014,** *136*, 16285-16298.

27. Sampson, M. D.; Kubiak, C. P. Electrocatalytic Dihydrogen Production by an Earth-Abundant Manganese Bipyridine Catalyst. *J. Am. Chem. Soc.* **2015,** *54*, 6674-6676.

28. Stanton, C. J.; Machan, C. W.; Vandezande, J. E.; Jin, T.; Majetich, G. F.; Schaefer, H. F.; Kubiak, C. P.; Li, G.; Agarwal, J. Re(I) NHC Complexes for Electrocatalytic Conversion of CO_2. *Inorg. Chem.* **2016,** *55*, 3136-3144.

29. Machan, C. W.; Yin, J.; Chabolla, S. A.; Gilson, M. K.; Kubiak, C. P. Improving the Efficiency and Activity of Electrocatalysts for the Reduction of CO_2 through Supramolecular Assembly with Amino Acid-Modified Ligands. *J. Am. Chem. Soc.* **2016,** *138*, 8184-8193.

30. Keith, J. A.; Grice, K. A.; Kubiak, C. P.; Carter, E. A. Elucidation of the Selectivity of Proton-Dependent Electrocatalytic CO_2 Reduction by *fac*-Re(bpy)(CO)$_3$Cl. *J. Am. Chem. Soc.* **2013,** *135*, 15823-15829.

31. Benson, E. E.; Kubiak, C. P. Structural Investigations into the Deactivation Pathway of the CO_2 Reduction Electrocatalyst Re(bpy)(CO)$_3$Cl. *Chem. Commun.* **2012,** *48*, 7374-7376.

32. Benson, E. E.; Sampson, M. D.; Grice, K. A.; Smieja, J. M.; Froehlich, J. D.; Friebel, D.; Keith, J. A.; Carter, E. A.; Nilsson, A.; Kubiak, C. P. The Electronic States of Rhenium Bipyridyl Electrocatalysts for CO_2 Reduction as Revealed by X-Ray Absorption Spectroscopy and Computational Quantum Chemistry. *Angew. Chem. Int. Ed.* **2013,** *52*, 4841-4844.

33. Sampson, M. D.; Froehlich, J. D.; Smieja, J. M.; Benson, E. E.; Sharp, I. D.; Kubiak, C. P. Direct Observation of the Reduction of Carbon Dioxide by Rhenium Bipyridine Catalysts. *Energy Environ. Sci.* **2013,** *6*, 3748-3755.

34. Machan, C. W.; Chabolla, S. A.; Yin, J.; Gilson, M. K.; Tezcan, F. A.; Kubiak, C. P. Supramolecular Assembly Promotes the Electrocatalytic Reduction of Carbon Dioxide by Re(I) Bipyridine Catalysts at a Lower Overpotential. *J. Am. Chem. Soc.* **2014,** *136*, 14598-14607.

35. Waterland, M. R.; Gordon, K. C. Electronic Absorption, Resonance Raman and Excited-State Resonance Raman Spectroscopy of Rhenium(I) and Copper(I) Complexes, with Substituted Dipyrido[3,2-a:2′,3′-c]Phenazine Ligands, and Their Electron Reduced Products. *J. Raman Spectrosc.* **2000,** *31*, 243-253.

36. van der Salm, H.; Larsen, C. B.; McLay, J. R. W.; Fraser, M. G.; Lucas, N. T.; Gordon, K. C. Stretching the Phenazine MO in dppz: The Effect of Phenyl and Phenyl-Ethynyl Groups on the Photophysics of Re(I) dppz Complexes. *Dalton Trans.* **2014**, 17775-17785.

37. Kurz, P.; Probst, B.; Spingler, B.; Alberto, R. Ligand Variations in [ReX(Diimine)$(CO)_3$] Complexes: Effects on Photocatalytic CO_2 Reduction. *Eur. J. Inorg. Chem.* **2006,** *2006*, 2966-2974.

38. Bard, A. J.; Faulkner, L. R., *Electrochemical Methods: Fundamentals and Applications*. John Wiley & Sons: New York, 2001; Vol. Chapter 3.

39. Butsch, K.; Gust, R.; Klein, A.; Ott, I.; Romanski, M. Tuning the Electronic Properties of dppz-Ligands and Their Palladium(II) Complexes. *Dalton Trans.* **2010,** *39*, 4331-4340.

40. Waterland, M. R.; Gordon, K. C.; McGarvey, J. J.; Jayaweera, P. M. Spectroscopic and Electrochemical Studies of a Series of Copper(I) and Rhenium(I) Complexes with Substituted Dipyrido[3,2-a:2',3'-c]Phenazine Ligands. *J. Chem. Soc., Dalton Trans.* **1998**, 609-616.

41. Jones, J. E.; Jenkins, R. L.; Hicks, R. S.; Hallett, A. J.; Pope, S. J. A. Water-Soluble, Luminescent Iridium(III)-Ytterbium(III) Complexes Using Dipyrido[3,2-a:2',3'-c]Phenazine Derivatives as Bridging Units. *Dalton Trans.* **2012,** *41*, 10372-10381.

42. Ben-David, H.; Iron, M. A.; Neumann, R. Platinum Complexes of Cationic Ligands for the Aerobic Oxidation of "Inert" Perfluoro-Substituted Alcohols. *Chem. Commun.* **2013,** *49*, 1720-1722.

43. Gottlieb, H. E.; Kotlyar, V.; Nudelman, A. NMR Chemical Shifts of Common Laboratory Solvents as Trace Impurities. *J. Org. Chem.* **1997,** *62*, 7512-7515.

44. Fujita, E.; Szalda, D. J.; Creutz, C.; Sutin, N. Carbon Dioxide Activation: Thermodynamics of Carbon Dioxide Binding and the Involvement of Two Cobalt Centers in the Reduction of Carbon Dioxide by a Cobalt(I) Macrocycle. *J. Am. Chem. Soc.* **1988,** *110*, 4870-4871.

45. Gennaro, A.; Isse, A. A.; Vianello, E. Solubility and Electrochemical Determination of CO_2 in Some Dipolar Aprotic Solvents. *J. Electroanal. Chem. Interfacial Electrochem.* **1990,** *289*, 203-215.

46. Sousa, S. F.; Sampaio, R. N.; Barbosa Neto, N. M.; Machado, A. E. H.; Patrocinio, A. O. T. The Photophysics of *fac*-[$Re(CO)_3(NN)(bpa)$]+ Complexes: A Theoretical/Experimental Study. *Photochem. Photobiol. Sci.* **2014,** *13*, 1213-1224.

47. Dreyse, P.; Isaacs, M.; Calfumán, K.; Cáceres, C.; Aliaga, A.; Aguirre, M. J.; Villagra, D. Electrochemical Reduction of Nitrite at Poly-[$Ru(5\text{-}NO_2\text{-}Phen)_2Cl$] Tetrapyridylporphyrin Glassy Carbon Modified Electrode. *Electrochim. Acta* **2011,** *56*, 5230-5237.

48. Smieja, J. M.; Sampson, M. D.; Grice, K. A.; Benson, E. E.; Froehlich, J. D.; Kubiak, C. P. Manganese as a Substitute for Rhenium in CO_2 Reduction Catalysts: The Importance of Acids. *Inorg. Chem.* **2013,** *52*, 2484-2491.

49. Qiao, X.; Li, Q.; Schaugaard, R. N.; Noffke, B. W.; Liu, Y.; Li, D.; Liu, L.; Raghavachari, K.; Li, L.-S. Well-Defined Nanographene–Rhenium Complex as an Efficient Electrocatalyst and Photocatalyst for Selective CO_2 Reduction. *J. Am. Chem. Soc.* **2017,** *139*, 3934-3937.

Appendix: Crystal Tables

X-RAY EXPERIMENTAL FOR 2.2A [$(C_{19}H_{13}N_3S)_2Fe(BF_4)_2(H_2O)_2$]

Crystals grew as large, black prisms by slow evaporation from acetone. The data crystal was cut from a larger crystal and had approximate dimensions: 0.50 x 0.43 x 0.20 mm. The data were collected at -173 °C on a Nonius Kappa CCD diffractometer using a Bruker AXS Apex II detector and a graphite monochromator with MoKα radiation (λ = 0.71073Å). Reduced temperatures were maintained by use of an Oxford Cryosystems 600 low-temperature device. A total of 1674 frames of data were collected using ω-scans with a scan range of 0.5° and a counting time of 23 seconds per frame. Details of crystal data, data collection and structure refinement are listed in Table A.1. Data reductions were performed using SAINT V8.27B.[1] The structure was solved by direct methods using SHELXT[2] and refined by full-matrix least-squares on F^2 with anisotropic displacement parameters for the non-H atoms using SHELXL-2014/7.[3] Structure analysis was aided by use of the programs PLATON98[4] and WinGX.[5] The hydrogen atoms bound to carbon atoms were calculated in idealized positions. The hydrogen atoms on the water molecule were observed in a ΔF map and refined with isotropic displacement parameters.

The Fe complex lies on a crystallographic two-fold rotation axis at 3/4, y, 1/2. Both thiophene rings are disordered around this two-fold rotation axis. The disordered thiophene rings were assigned site occupancy factors of 1/2 and refined with their geometry restrained to be equivalent using bond lengths obtained from comparable thiophene rings found in the Cambridge Crystallographic Database. In addition, both tetrafluoroborate anions were also disorder about crystallographic two-fold rotation axes. The geometry of these anions was restrained to be equivalent.

The function, $\Sigma w (|F_O|^2 - |F_C|^2)^2$, was minimized, where $w = 1/[(\sigma(F_O))^2 + (0.0457*P)^2 + (2.8507*P)]$ and $P = (|F_O|^2 + 2|F_C|^2)/3$. $R_W(F^2)$ refined to 0.0826, with R(F)

equal to 0.0307 and a goodness of fit, S, = 1.07. Definitions used for calculating R(F), $R_W(F^2)$ and the goodness of fit, S, are given below.[6] The data were checked for secondary extinction but no correction was necessary. Neutral atom scattering factors and values used to calculate the linear absorption coefficient are from the International Tables for X-ray Crystallography (1992).[7] All figures were generated using SHELXTL/PC.[8] Tables of positional and thermal parameters, bond lengths and angles, torsion angles and figures are found elsewhere.

X-RAY EXPERIMENTAL FOR 2.2B [$(C_{23}H_{15}N_3S_2)_2FE(BF_4)_2$ - ½ C_4H_8O]

Crystals grew as purple needles by vapor diffusion of diethyl ether into an acetone solution of **2.2b**. The data crystal was cut from a larger crystal and had approximate dimensions; 0.3 x 0.1 x 0.1 mm. The data were collected at -173 °C on a Nonius Kappa CCD diffractometer using a Bruker AXS Apex II detector and a graphite monochromator with MoKα radiation (λ = 0.71075Å). Reduced temperatures were maintained by use of an Oxford Cryosystems 600 low-temperature device. A total of 903 frames of data were collected using ω-scans with a scan range of 0.9° and a counting time of 74 seconds per frame. Details of crystal data, data collection and structure refinement are listed in Table A.2. Data reductions were performed using SAINT V8.27B.[1] The structure was solved by direct methods using SIR97[9] and refined by full-matrix least-squares on F^2 with anisotropic displacement parameters for the non-H atoms using SHELXL-2014/7.[3] Structure analysis was aided by use of the programs PLATON98[4] and WinGX.[5]

A molecule of diethyl ether was badly disordered. Attempts to model the disorder were unsatisfactory. The contributions to the scattering factors due to these solvent molecules were removed by use of the utility SQUEEZE[10] in PLATON98.

The function, $\Sigma w (|F_O|^2 - |F_C|^2)^2$, was minimized, where $w = 1/[(\sigma(F_O))^2 + (0.088*P)^2 + (3.9198*P)]$ and $P = (|F_O|^2 + 2|F_C|^2)/3$. $R_W(F^2)$ refined to 0.197, with R(F) equal to 0.0677 and a goodness of fit, S, = 1.00. Definitions used for calculating R(F), $R_W(F^2)$ and the goodness of fit, S, are given below.[6] The data were checked for secondary extinction but no correction was necessary. Neutral atom scattering factors and values used to calculate the linear absorption coefficient are from the International Tables for X-ray Crystallography (1992).[7] All figures were generated using SHELXTL/PC.[8] Tables of positional and thermal parameters, bond lengths and angles, torsion angles and figures are found elsewhere.

X-RAY EXPERIMENTAL FOR 2.2C [$(C_{21}H_{15}N_3O_2S)_2Fe(BF_4)_2$]

Crystals grew as dark red plates by slow evaporation from acetone. The data crystal was cut from a larger crystal and had approximate dimensions; 0.56 x 0.49 x 0.13 mm. The data were collected at -167 °C on a Nonius Kappa CCD diffractometer using a Bruker AXS Apex II detector and a graphite monochromator with MoKα radiation (λ = 0.71073Å). Reduced temperatures were maintained by use of an Oxford Cryosystems 600 low-temperature device. A total of 1824 frames of data were collected using ω and ϕ-scans with a scan range of 0.5° and a counting time of 24 seconds per frame. Details of crystal data, data collection and structure refinement are listed in Table A.3. Data reductions were performed using SAINT V8.27B.[1] The structure was solved by direct methods using SHELXT[6] and refined by full-matrix least-squares on F^2 with anisotropic displacement parameters for the non-H atoms using SHELXL-2014/7.[3] Structure analysis was aided by use of the programs PLATON98[4] and WinGX.[5] The hydrogen atoms bound to carbon atoms were calculated in idealized positions.

One of the tetrafluoroborate ions was disordered about two orientations. The disorder was modeled by assigning the variable x to the site occupancy factors of one orientation and (1-x) to the site occupancy factors of the alternate orientation. A common isotropic displacement parameter was refined while refining the variable x. The geometry of the two ions was restrained to be equivalent throughout the refinement. The site occupancy for the major component refined to 63(2) %. The atoms of this ion were refined anisotropically with their displacement parameters restrained to be approximately isotropic.

The refinement showed some of the typical warning signs of twinning. In particular, there were many reflections with large, positive $\Delta(|F_O|^2 - |F_C|^2)$ values. The twin law was determined using TwinRotMat in Platon98. The twin law was -1,0,0; -0.83, 0.66, 0.34; -0.83, 1.66, -0.66. The twin fraction refined to 0.282(3).

The function, $\Sigma w (|F_O|^2 - |F_C|^2)^2$, was minimized, where $w = 1/[(\sigma(F_O))^2 + (5.2461*P)]$ and $P = (|F_O|^2 + 2|F_C|^2)/3$. $R_W(F^2)$ refined to 0.251, with R(F) equal to 0.110 and a goodness of fit, S, = 1.21. Definitions used for calculating R(F), $R_W(F^2)$ and the goodness of fit, S, are given below.[6] The data were checked for secondary extinction but no correction was necessary. Neutral atom scattering factors and values used to calculate the linear absorption coefficient are from the International Tables for X-ray Crystallography (1992).[7] All figures were generated using SHELXTL/PC.[8] Tables of positional and thermal parameters, bond lengths and angles, torsion angles and figures are found elsewhere.

X-RAY EXPERIMENTAL FOR 2.3B [$(C_{23}H_{15}N_3S_2)_2Zn - 2BF_4 - C_3H_6O$]

Crystals grew as long, yellow laths by slow evaporation from acetone. The data crystal was cut from a larger crystal and had approximate dimensions; 0.68 x 0.29 x 0.13

mm. The data were collected at -167 °C on a Nonius Kappa CCD diffractometer using a Bruker AXS Apex II detector and a graphite monochromator with MoKα radiation (λ = 0.71073Å). Reduced temperatures were maintained by use of an Oxford Cryosystems 600 low-temperature device. A total of 1513 frames of data were collected using ω and ϕ-scans with a scan range of 1.0° and a counting time of 41 seconds per frame. Details of crystal data, data collection and structure refinement are listed in Table A.4. Data reduction were performed using SAINT V8.27B.[1] The structure was solved by direct methods using SHELXT[6] and refined by full-matrix least-squares on F^2 with anisotropic displacement parameters for the non-H atoms using SHELXL-2013.[11] Structure analysis was aided by use of the programs PLATON98[4] and WinGX.[5] The hydrogen atoms bound to carbon atoms were calculated in idealized positions.

One of the terminal thiophene rings was disordered. The disorder was minor but was apparent by the shape of the displacement parameter across from the sulfur atom. The disorder was modeled by assigning the variable x to the site occupancy factors for one component of the disorder and (1-x) to the site occupancy factors for the alternate component. A common isotropic displacement parameter was refined for the affected atoms while refining x. The geometry of the two rings was restrained to be equivalent throughout the refinement process. The site occupancy for the major component refined to 90(2) %. The atoms of the major component were refined anisotropically with their displacement parameters restrained to be approximately isotropic in the final refinement model. The atoms of the minor component had their isotropic displacement parameter set to a fixed value.

The function, $\Sigma w (|F_O|^2 - |F_C|^2)^2$, was minimized, where $w = 1/[(\sigma (F_O))^2 + (0.0459*P)^2]$ and $P = (|F_O|^2 + 2|F_C|^2)/3$. $R_W(F^2)$ refined to 0.111, with R(F) equal to 0.0495 and a goodness of fit, S, = 0.991. Definitions used for calculating R(F), $R_W(F^2)$ and the

goodness of fit, S, are given below.[6] The data were checked for secondary extinction but no correction was necessary. Neutral atom scattering factors and values used to calculate the linear absorption coefficient are from the International Tables for X-ray Crystallography (1992).[7] All figures were generated using SHELXTL/PC.[8] Tables of positional and thermal parameters, bond lengths and angles, torsion angles and figures are found elsewhere.

X-RAY EXPERIMENTAL FOR 4.2B ($C_{21}H_9BrN_5O_5Re$)

A single Crystal of the rhenium complex **4.2b**, suitable for X-ray analysis, was grown by slow evaporation of **4.2b** in dichloromethane. The single crystal diffraction data were collected on a Rigaku AFC12 diffractometer with a Saturn 724+ CCD with a Mercury CCD using a graphite monochromator with MoKα radiation (λ = 0.71073 Å). Absorption corrections were applied using Multi-scan. Data reduction were performed using the Rigaku Americas Corporation's Crystal Clear version 1.40.[12] The structures were solved by direct methods using SIR97[9] and refined anisotropically using full-matrix least-squares methods with the SHELX 97 program package.[13] Details of crystal data, data collection and structure refinement are listed in Table A.5. The coordinates of the non-hydrogen atoms were refined anisotropically, while hydrogen atoms were included in the calculation isotropically but not refined. Neutral atom scattering factors and values used to calculate the linear absorption coefficient are from the International Tables for X-ray Crystallography (1992).[7]

X-RAY EXPERIMENTAL FOR 4.2C ($C_{21}H_{10}BrN_4O_3Re$)

Crystals grew as yellow prisms by slow evaporation from dichloromethane. The data crystal had approximate dimensions; 0.14 x 0.09 x 0.07 mm. The data were collected on an Agilent Technologies SuperNova Dual Source diffractometer using a μ-focus Cu Kα

radiation source (λ = 1.5418 Å) with collimating mirror monochromators. A total of 1284 frames of data were collected using ω-scans with a scan range of 1° and a counting time of 3 seconds per frame using a detector offset of ± 41.6° and a counting time of 12 seconds per frame using a detector offset of ± 111.0°. The data were collected at 100 K using an Oxford Cryostream low temperature device. Details of crystal data, data collection and structure refinement are listed in Table A.6. Data collection, unit cell refinement and data reduction were performed using Agilent Technologies CrysAlisPro V 1.171.37.31.[13] The structure was solved by direct methods using SuperFlip[14] and refined by full-matrix least-squares on F^2 with anisotropic displacement parameters for the non-H atoms using SHELXL-2014/7.[3] Structure analysis was aided by use of the programs PLATON98[4] and WinGX.[5] The hydrogen atoms were calculated in ideal positions with isotropic displacement parameters set to 1.2xUeq of the attached atom (1.5xUeq for methyl hydrogen atoms.

A molecule of dichloromethane was found to be badly disordered around a crystallographic mirror plane of symmetry. Attempts to model the disorder were unsatisfactory. The contributions to the scattering factors due to this solvent molecule were removed by use of the utility SQUEEZE[10] in PLATON98. PLATON98 was used as incorporated in WinGX.

The function, $\Sigma w(|F_o|^2 - |F_c|^2)^2$, was minimized, where $w = 1/[(\sigma(F_o))^2 + (0.1075*P)^2 + (45.9963*P)]$ and $P = (|F_o|^2 + 2|F_c|^2)/3$. $R_w(F^2)$ refined to 0.181, with R(F) equal to 0.0633 and a goodness of fit, S, = 1.09. Definitions used for calculating R(F), $R_w(F^2)$ and the goodness of fit, S, are given below.[6] The data were checked for secondary extinction effects but no correction was necessary. Neutral atom scattering factors and values used to calculate the linear absorption coefficient are from the International Tables for X-ray Crystallography (1992).[7] All figures were generated using SHELXTL/PC.[8]

Tables of positional and thermal parameters, bond lengths and angles, torsion angles and figures are found elsewhere.

Table A.1. Crystal data and structure refinement for **2.2a**.

Empirical formula	C38 H30 B2 F8 Fe N6 O2 S2	
Formula weight	896.27	
Temperature	100(2) K	
Wavelength	0.71073 Å	
Crystal system	monoclinic	
Space group	I 2/a	
Unit cell dimensions	a = 10.0749(5) Å	α = 90 °.
	b = 31.8249(16) Å	β = 92.371(2) °
	c = 11.4229(9) Å	γ = 90 °
Volume	3659.4(4) $Å^3$	
Z	4	
Density (calculated)	1.627 mg/m^3	
Absorption coefficient	0.614 mm^{-1}	
F(000)	1824	
Crystal size	0.500 x 0.429 x 0.200 mm^3	
Theta range for data collection	1.896 to 27.963°	
Index ranges	-13<=h<=13, -41<=k<=41, -15<=l<=15	
Reflections collected	32407	
Independent reflections	4403 [R(int) = 0.0439]	
Completeness to theta = 25.242°	100.0 %	
Absorption correction	Semi-empirical from equivalents	
Max. and min. transmission	1.00 and 0.869	
Refinement method	Full-matrix least-squares on F^2	
Data / restraints / parameters	4403 / 501 / 415	
Goodness-of-fit on F^2	1.066	
Final R indices [I>2sigma(I)]	R1 = 0.0307, wR2 = 0.0804	
R indices (all data)	R1 = 0.0368, wR2 = 0.0826	
Largest diff. peak and hole	0.451 and -0.334 $e.Å^{-3}$	

Table A.2. Crystal data and structure refinement for **2.2b**.

Empirical formula	C46 H30 B2 F8 Fe N6 S4	
Formula weight	1024.47	
Temperature	100(2) K	
Wavelength	0.71073 Å	
Crystal system	triclinic	
Space group	P -1	
Unit cell dimensions	a = 12.5480(18) Å	α = 91.688(4) °
	b = 13.6595(18) Å	β = 93.376(4) °
	c = 14.447(2) Å	γ = 114.922(4) °
Volume	2237.7(5) $Å^3$	
Z	2	
Density (calculated)	1.520 mg/m^3	
Absorption coefficient	0.600 mm^{-1}	
F(000)	1040	
Crystal size	0.300 x 0.100 x 0.100 mm^3	
Theta range for data collection	2.197 to 25.349°	
Index ranges	-14<=h<=15, -16<=k<=16, -17<=l<=10	
Reflections collected	25422	
Independent reflections	8052 [R(int) = 0.0876]	
Completeness to theta = 25.242°	98.2 %	
Absorption correction	Semi-empirical from equivalents	
Max. and min. transmission	1.00 and 0.860	
Refinement method	Full-matrix least-squares on F^2	
Data / restraints / parameters	8052 / 48 / 604	
Goodness-of-fit on F^2	1.003	
Final R indices [I>2sigma(I)]	R1 = 0.0677, wR2 = 0.1665	
R indices (all data)	R1 = 0.1451, wR2 = 0.1967	
Largest diff. peak and hole	0.543 and -0.728 $e.Å^{-3}$	

Table A.3. Crystal data and structure refinement for **2.2c**.

Empirical formula	C42 H30 B2 F8 Fe N6 O4 S2	
Formula weight	976.31	
Temperature	106(2) K	
Wavelength	0.71073 Å	
Crystal system	triclinic	
Space group	P -1	
Unit cell dimensions	a = 9.996(3) Å	α= 77.689(10) °
	b = 11.782(4) Å	β= 84.902(13) °
	c = 20.150(8) Å	γ = 66.803(8) °
Volume	2131.1(14) $Å^3$	
Z	2	
Density (calculated)	1.521 mg/m^3	
Absorption coefficient	0.538 mm^{-1}	
F(000)	992	
Crystal size	0.560 x 0.490 x 0.130 mm^3	
Theta range for data collection	1.917 to 25.278°	
Index ranges	-12<=h<=12, -13<=k<=14, -24<=l<=24	
Reflections collected	7613	
Independent reflections	7613 [R(int) = ?]	
Completeness to theta = 25.242°	98.9 %	
Absorption correction	Semi-empirical from equivalents	
Max. and min. transmission	1.00 and 0.759	
Refinement method	Full-matrix least-squares on F^2	
Data / restraints / parameters	7613 / 588 / 635	
Goodness-of-fit on F^2	1.207	
Final R indices [I>2sigma(I)]	R1 = 0.1096, wR2 = 0.2225	
R indices (all data)	R1 = 0.2171, wR2 = 0.2513	
Largest diff. peak and hole	0.719 and -0.527 $e.Å^{-3}$	

Table A.4. Crystal data and structure refinement for **2.3b**.

Empirical formula	C49 H36 B2 F8 N6 O S4 Zn	
Formula weight	1092.07	
Temperature	106(2) K	
Wavelength	0.71073 Å	
Crystal system	triclinic	
Space group	P -1	
Unit cell dimensions	a = 12.3340(8) Å	α = 93.338(2) °
	b = 14.1470(9) Å	β = 93.659(2) °
	c = 14.7989(10) Å	γ = 114.749(2) °
Volume	2330.0(3) $Å^3$	
Z	2	
Density (calculated)	1.557 mg/m^3	
Absorption coefficient	0.785 mm^{-1}	
F(000)	1112	
Crystal size	0.680 x 0.290 x 0.130 mm^3	
Theta range for data collection	1.385 to 27.548°	
Index ranges	-14<=h<=15, -18<=k<=18, -19<=l<=9	
Reflections collected	14897	
Independent reflections	10119 [R(int) = 0.0357]	
Completeness to theta = 25.242°	97.9 %	
Absorption correction	Semi-empirical from equivalents	
Max. and min. transmission	1.00 and 0.790	
Refinement method	Full-matrix least-squares on F^2	
Data / restraints / parameters	10119 / 34 / 656	
Goodness-of-fit on F^2	0.991	
Final R indices [I>2sigma(I)]	R1 = 0.0495, wR2 = 0.0997	
R indices (all data)	R1 = 0.0906, wR2 = 0.1113	
Largest diff. peak and hole	0.647 and -0.460 $e.Å^{-3}$	

Table A.5. Crystal data and structure refinement for **4.2b**.

Empirical formula	C21 H9 Br N5 O5 Re	
Formula weight	677.44	
Temperature	100(2) K	
Wavelength	0.71073 Å	
Crystal system	Triclinic	
Space group	P-1	
Unit cell dimensions	a = 6.5920(10) Å	= 66.926(3) °
	b = 12.742(2) Å	= 87.581(4) °
	c = 13.052(2) Å	= 87.953(3) °
Volume	1007.5(3) $Å^3$	
Z	2	
Density (calculated)	2.233 mg/m^3	
Absorption coefficient	8.061 mm^{-1}	
F (000)	640	
Crystal size	0.14 x 0.13 x 0.08 mm^3	
Theta range for data collection	3.09 to 27.48°	
Index ranges	-8<=h<=28, -16<=k<=16, -16<=l<=16	
Reflections collected	16623	
Max. and min. transmission	0.9686 and 0.9051	
Goodness-of-fit on F^2	1.121	
Final R indices [I>2sigma(I)]	R1 = 0.0609, wR2 = 0.1303	
R indices (all data)	R1 = 0.0810, wR2 = 0.1402	
Largest diff. peak and hole	2.344 and -1.605 $e.Å^{-3}$	

Table A.6. Crystal data and structure refinement for **4.2c**.

Empirical formula	C21 H10 Br N4 O3 Re	
Formula weight	632.44	
Temperature	100(2) K	
Wavelength	1.54184 Å	
Crystal system	monoclinic	
Space group	I 2/m	
Unit cell dimensions	a = 17.5548(9) Å	= 90 °
	b = 12.1265(5) Å	= 91.584(4) °
	c = 19.7341(7) Å	= 90 °
Volume	4199.4(3) $Å^3$	
Z	8	
Density (calculated)	2.001 mg/m^3	
Absorption coefficient	13.811 mm^{-1}	
F (000)	2384	
Crystal size	0.139 x 0.092 x 0.070 mm^3	
Theta range for data collection	3.324 to 75.808°	
Index ranges	-21<=h<=21, -14<=k<=15, -18<=l<=24	
Reflections collected	15462	
Independent reflections	4487 [R(int) = 0.0553]	
Completeness to theta = 67.684°	100.0 %	
Absorption correction	Gaussian	
Max. and min. transmission	1.00 and 0.422	
Refinement method	Full-matrix least-squares on F^2	
Data / restraints / parameters	4487 / 0 / 283	
Goodness-of-fit on F^2	1.091	
Final R indices [I>2sigma(I)]	R1 = 0.0633, wR2 = 0.1787	
R indices (all data)	R1 = 0.0654, wR2 = 0.1810	
Largest diff. peak and hole	3.422 and -2.674 $e.Å^{-3}$	

REFERENCES

1. SAINT V8.27B Bruker AXS Inc, (2012), Madison, WI.
2. Sheldrick, G. M. (2015). SHELXT. *Acta Cryst. A71*, 3-8.
3. Sheldrick, G. M. (2015). SHELXL-2014/7. Program for the Refinement of Crystal Structures. *Acta Cryst. C91*, 9-18.
4. Spek, A. L. (1998). PLATON, A Multipurpose Crystallographic Tool. Utrecht University, The Netherlands.
5. WinGX 1.64. (1999). An Integrated System of Windows Programs for the Solution, Refinement and Analysis of Single Crystal X-ray Diffraction Data. Farrugia, L. J. *J. Appl. Cryst. 32*. 837-838.
6. $R_W(F^2) = \{w(|F_O|^2 - |F_C|^2)^2/w(|F_O|)^4\}^{1/2}$ where w is the weight given each reflection. $R(F) = (|F_O| - |F_C|)/|F_O|\}$ for reflections with $F_O > 4 ((F_O))$. $S = [w(|F_O|^2 - |F_C|^2)^2/(n - p)]^{1/2}$, where n is the number of reflections and p is the number of refined parameters.
7. International Tables for X-ray Crystallography (1992). Vol. C, Tables 4.2.6.8 and 6.1.1.4, A. J. C. Wilson, editor, Boston: Kluwer Academic Press.
8. Sheldrick, G. M. (1994). SHELXTL/PC (Version 5.03). Siemens Analytical X-ray Instruments, Inc., Madison, Wisconsin, USA.
9. SIR97. (1999). A program for crystal structure solution. Altomare A., Burla M.C., Camalli M., Cascarano G.L., Giacovazzo C. , Guagliardi A., Moliterni A.G.G., Polidori G.,Spagna R. *J. Appl. Cryst. 32*, 115-119.
10. Sluis, P. v. d. and Spek, A. L. (1990). SQUEEZE. *Acta Cryst. A46*, 194-201.
11. Sheldrick, G. M. (2008). SHELXL-2013. Program for the Refinement of Crystal Structures. *Acta Cryst. A64*, 112-122.
12. Crystal Clear, 1.40, Rigaku Americas Corporation, The woodlands, Texas, USA, 2008.
13. Sheldrick, G. M. *Acta Cryst.* **2008**, *A64*, 112. SHELXL97: Program for the Refinement of Crystal Structures, University of Gottingen: Gottingen, Germany, 1994.
14. CrysAlisPro. Agilent Technologies (2013). Agilent Technologies UK Ltd., Oxford, UK, SuperNova CCD System, CrysAlicPro Software System, 1.171.37.31.
15. SuperFlip. (2007). A program for crystal structure solution. Palatinus, L. and Chapuis, G. *J. Appl. Cryst. 40*, 786-790.

References

CHAPTER 1

1. Mortimer, R. J.; Dyer, A. L.; Reynolds, J. R. Electrochromic Organic and Polymeric Materials for Display Applications. *Displays* **2006,** *27*, 2-18.
2. Mortimer, R. J. Electrochromic Materials. *Chem. Soc. Rev.* **1997,** *26*, 147-156.
3. Somani, P. R.; Radhakrishnan, S. Electrochromic Materials and Devices: Present and Future. *Mater. Chem. Phys.* **2003,** *77*, 117-133.
4. Runnerstrom, E. L.; Llordes, A.; Lounis, S. D.; Milliron, D. J. Nanostructured Electrochromic Smart Windows: Traditional Materials and NIR-Selective Plasmonic Nanocrystals. *Chem. Commun.* **2014,** *50*, 10555-10572.
5. Granqvist, C. G. Electrochromic Tungsten Oxide Films: Review of Progress 1993-1998. *Sol. Energy Mater. Sol. Cells* **2000,** *60*, 201-262.
6. Niklasson, G. A.; Granqvist, C. G. Electrochromics for Smart Windows: Thin Films of Tungsten Oxide and Nickel Oxide, and Devices Based on These. *J. Mater. Chem.* **2007,** *17*, 127-156.
7. Fang, G. J.; Liu, Z. L.; Wang, Y.; Liu, Y. H.; Yao, K. L. Synthesis and Structural, Electrochromic Characterization of Pulsed Laser Deposited Vanadium Oxide Thin Films. *J. Vac. Sci. Technol. A* **2001,** *19*, 887-892.
8. Lin, Y.-S.; Tsai, T.-H.; Tien, S.-W. Atmospheric Pressure Plasma Jet-Synthesized Electrochromic Organomolybdenum Oxide Thin Films for Flexible Electrochromic Devices. *Thin Solid Films* **2013,** *529*, 248-252.
9. Gao, Q.; Wang, S.; Fang, H.; Weng, J.; Zhang, Y.; Mao, J.; Tang, Y. One-Dimensional Growth of Moox-Based Organic-Inorganic Hybrid Nanowires with Tunable Photochromic Properties. *J. Mater. Chem.* **2012,** *22*, 4709-4715.
10. Mortimer, R. J.; Reynolds, J. R. In Situ Colorimetric and Composite Coloration Efficiency Measurements for Electrochromic Prussian Blue. *J. Mater. Chem.* **2005,** *15*, 2226-2233.
11. Felderhoff, M.; Heinen, S.; Molisho, N.; Webersinn, S.; Walder, L. Molecular Suppression of the Pimerization of Viologens (=4,4'-Bipyridinium Derivatives) Attached to Nanocrystalline Titanium Dioxide Thin-Film Electrodes. *Helv. Chim. Acta* **2000,** *83*, 181-192.
12. Sydam, R.; Deepa, M.; Joshi, A. G. A Novel 1,1'-Bis[4-(5,6-Dimethyl-1H-Benzimidazole-1-yl)Butyl]-4,4'-Bipyridinium Dibromide (Viologen) for a High Contrast Electrochromic Device. *Org. Electron.* **2013,** *14*, 1027-1036.
13. Beaujuge, P. M.; Reynolds, J. R. Color Control in π-Conjugated Organic Polymers for Use in Electrochromic Devices. *Chem. Rev.* **2010,** *110*, 268-320.

14. Berggren, L.; Jonsson, J. C.; Niklasson, G. A. Optical Absorption in Lithiated Tungsten Oxide Thin Films: Experiment and Theory. *J. Appl. Phys.* **2007,** *102*, 083538.

15. Sonmez, G. Polymeric Electrochromics. *Chem. Commun.* **2005**, 5251-5259.

16. Holliday, B. J.; Swager, T. M. Conducting Metallopolymers: The Roles of Molecular Architecture and Redox Matching. *Chem. Commun.* **2005**, 23-36.

17. Whittell, G. R.; Manners, I. Metallopolymers: New Multifunctional Materials. *Adv. Mater.* **2007,** *19*, 3439-3468.

18. Stanley, J. M.; Holliday, B. J. Luminescent Lanthanide-Containing Metallopolymers. *Coord. Chem. Rev.* **2012,** *256*, 1520-1530.

19. Qiu, D.; Bao, X.; Zhao, Q.; Yang, Q.; Feng, Y.; Wang, H.; Yang, C.; Liu, K. Near-IR Electrochromic Film Prepared by Oxidative Electropolymerization of the Cyclometalated Pt(II) Chloride with a Triphenylamine Group. *Inorg. Chem.* **2015,** *54*, 8264-8270.

20. Nie, H.-J.; Zhong, Y.-W. Near-Infrared Electrochromism in Electropolymerized Metallopolymeric Films of a Phen-1,4-Diyl-Bridged Diruthenium Complex. *Inorg. Chem.* **2014,** *53*, 11316-11322.

21. Yao, C.-J.; Yao, J.; Zhong, Y.-W. Metallopolymeric Films Based on a Biscyclometalated Ruthenium Complex Bridged by 1,3,6,8-Tetra(2-Pyridyl)Pyrene: Applications in Near-Infrared Electrochromic Windows. *Inorg. Chem.* **2012,** *51*, 6259-6263.

22. Yao, C.-J.; Zhong, Y.-W.; Nie, H.-J.; Abruña, H. D.; Yao, J. Near-IR Electrochromism in Electropolymerized Films of a Biscyclometalated Ruthenium Complex Bridged by 1,2,4,5-Tetra(2-Pyridyl)Benzene. *J. Am. Chem. Soc.* **2011,** *133*, 20720-20723.

23. Matsuse, R.; Abe, M.; Tomiyasu, Y.; Inatomi, A.; Yonemura, H.; Yamada, S.; Hisaeda, Y. Metallopolymer Films Exhibiting Three-Color Electrochromism in the UV/Vis and Near-IR Region: Remarkable Utility of Trimetallic Clusters Bearing Thienyl Pendants and Their Mixed-Valent Charge Transfer Transitions. *J. Inorg. Organomet. Polym. Mater.* **2012,** *23*, 136-146.

24. Zeng, Q.; McNally, A.; Keyes, T. E.; Forster, R. J. Redox Induced Switching Dynamics of a Three Colour Electrochromic Metallopolymer Film. *Electrochim. Acta* **2008,** *53*, 7033-7038.

25. Satheeshkumar, C.; Park, J.-Y.; Jeong, D.-C.; Song, S. G.; Lee, J.; Song, C. Synthesis and Electronic Properties of N-Heterocyclic Carbene-Containing Conducting Polymers with Coinage Metals. *RSC Adv.* **2015,** *5*, 60892-60897.

26. Powell, A. B.; Bielawski, C. W.; Cowley, A. H. Design, Synthesis, and Study of Main Chain Poly(N-Heterocyclic Carbene) Complexes: Applications in Electrochromic Devices. *J. Am. Chem. Soc.* **2010,** *132*, 10184-10194.

27. Djukic, B.; Seda, T.; Gorelsky, S. I.; Lough, A. J.; Lemaire, M. T. π-Extended and Six-Coordinate Iron(II) Complexes: Structures, Magnetic Properties, and the Electrochemical Synthesis of a Conducting Iron(II) Metallopolymer. *Inorg. Chem.* **2011,** *50*, 7334-7343.

28. Fan, C.; Ye, C.; Wang, X.; Chen, Z.; Zhou, Y.; Liang, Z.; Tao, X. Synthesis and Electrochromic Properties of New Terpyridine-Triphenylamine Hybrid Polymers. *Macromolecules* **2015,** *48*, 6465-6473.

29. Bao, X.; Zhao, Q.; Wang, H.; Liu, K.; Qiu, D. Metallopolymer Electrochromic Film Prepared by Oxidative Electropolymerization of a Fe(II) Complex with Arylamine Functionalized Terpyridine Ligand. *Inorg. Chem. Commun.* **2013,** *38*, 88-91.

30. Liang, Y.; Strohecker, D.; Lynch, V.; Holliday, B. J.; Jones, R. A. A Thiophene-Containing Conductive Metallopolymer Using an Fe(II) Bis(Terpyridine) Core for Electrochromic Materials. *ACS Appl. Mater. Interfaces* **2016,** *8*, 34568-34580.

31. Huang, Z.-F.; Song, J.; Pan, L.; Zhang, X.; Wang, L.; Zou, J.-J. Tungsten Oxides for Photocatalysis, Electrochemistry, and Phototherapy. *Adv. Mater.* **2015,** *27*, 5309-5327.

32. Wojcik, P. J.; Pereira, L.; Martins, R.; Fortunato, E. Statistical Mixture Design and Multivariate Analysis of Inkjet Printed a-WO_3/TiO_2/WO_x Electrochromic Films. *ACS Comb. Sci.* **2014,** *16*, 5-16.

33. Armelao, L.; Quici, S.; Barigelletti, F.; Accorsi, G.; Bottaro, G.; Cavazzini, M.; Tondello, E. Design of Luminescent Lanthanide Complexes: From Molecules to Highly Efficient Photo-Emitting Materials. *Coord. Chem. Rev.* **2010,** *254*, 487-505.

34. Hasegawa, Y.; Nakagawa, T.; Kawai, T. Recent Progress of Luminescent Metal Complexes with Photochromic Units. *Coord. Chem. Rev.* **2010,** *254*, 2643-2651.

35. Yuan, J.; Wang, G. Lanthanide Complex-Based Fluorescence Label for Time-Resolved Fluorescence Bioassay. *J. Fluoresc.* **2005,** *15*, 559-568.

36. Bünzli, J.-C. G. Lanthanide Luminescence for Biomedical Analyses and Imaging. *Chem. Rev.* **2010,** *110*, 2729-2755.

37. Dickins, R. S.; Parker, D.; de Sousa, A. S.; Williams, J. A. G. Closely Diffusing O-H, Amide N-H and Methylene C-H Oscillators Quench the Excited State of Europium Comlexes in Solution. *Chem. Commun.* **1996**, 697-698.

38. Beeby, A.; Clarkson, I. M.; Dickins, R. S.; Faulkner, S.; Parker, D.; Royle, L.; S. de Sousa, A.; Williams, J. A. G.; Woods, M. Non-Radiative Deactivation of the Excited States of Europium, Terbium and Ytterbium Complexes by Proximate Energy-Matched OH, NH and CH Oscillators: An Improved Luminescence Method

for Establishing Solution Hydration States. *J. Chem. Soc., Perkin Trans.* **1999**, 493-504.

39. Werts, M. H. V.; Jukes, R. T. F.; Verhoeven, J. W. The Emission Spectrum and the Radiative Lifetime of Eu^{3+} in Luminescent Lanthanide Complexes. *PCCP* **2002,** *4*, 1542-1548.

40. Amoroso, A. J.; Pope, S. J. A. Using Lanthanide Ions in Molecular Bioimaging. *Chem. Soc. Rev.* **2015,** *44*, 4723-4742.

41. Heffern, M. C.; Matosziuk, L. M.; Meade, T. J. Lanthanide Probes for Bioresponsive Imaging. *Chem. Rev.* **2014,** *114*, 4496-4539.

42. Soini, E.; Kojola, H. Time-Resolved Fluorometer for Lanthanide Chelates-a New Generation of Nonisotopic Immunoassays. *Clin. Chem.* **1983,** *29*, 65-68.

43. Zhang, L.; Wang, Y.; Ye, Z.; Jin, D.; Yuan, J. New Class of Tetradentate β-Diketonate-Europium Complexes That Can Be Covalently Bound to Proteins for Time-Gated Fluorometric Application. *Bioconjugate Chem.* **2012,** *23*, 1244-1251.

44. Sy, M.; Nonat, A.; Hildebrandt, N.; Charbonniere, L. J. Lanthanide-Based Luminescence Biolabelling. *Chem. Commun.* **2016,** *52*, 5080-5095.

45. Nishioka, T.; Yuan, J.; Yamamoto, Y.; Sumitomo, K.; Wang, Z.; Hashino, K.; Hosoya, C.; Ikawa, K.; Wang, G.; Matsumoto, K. New Luminescent Europium(III) Chelates for DNA Labeling. *Inorg. Chem.* **2006,** *45*, 4088-4096.

46. Deng, W.; Jin, D.; Drozdowicz-Tomsia, K.; Yuan, J.; Goldys, E. M. Europium Chelate (BHHCT-Eu^{3+}) and Its Metal Nanostructure Enhanced Luminescence Applied to Bioassays and Time-Gated Bioimaging. *Langmuir* **2010,** *26*, 10036-10043.

47. Yuan, J.; Matsumoto, K.; Kimura, H. A New Tetradentate β-Diketonate-Europium Chelate That Can Be Covalently Bound to Proteins for Time-Resolved Fluoroimmunoassay. *Anal. Chem.* **1998,** *70*, 596-601.

48. Evangelista, R. A.; Pollak, A.; Allore, B.; Templeton, A. F.; Morton, R. C.; Diamandis, E. P. A New Europium Chelate for Protein Labelling and Time-Resolved Fluorometric Applications. *Clin. Biochem.* **1988,** *21*, 173-178.

49. Claudel-Gillet, S.; Steibel, J.; Weibel, N.; Chauvin, T.; Port, M.; Raynal, I.; Toth, E.; Ziessel, R. F.; Charbonnière, L. J. Lanthanide-Based Conjugates as Polyvalent Probes for Biological Labeling. *Eur. J. Inorg. Chem.* **2008,** *2008*, 2856-2862.

50. Starck, M.; Kadjane, P.; Bois, E.; Darbouret, B.; Incamps, A.; Ziessel, R.; Charbonnière, L. J. Towards Libraries of Luminescent Lanthanide Complexes and Labels from Generic Synthons. *Chem. Eur. J.* **2011,** *17*, 9164-9179.

51. Nchimi-Nono, K.; Wegner, K. D.; Linden, S.; Lecointre, A.; Ehret-Sabatier, L.; Shakir, S.; Hildebrandt, N.; Charbonniere, L. J. Activated Phosphonated

Trifunctional Chelates for Highly Sensitive Lanthanide-Based FRET Immunoassays Applied to Total Prostate Specific Antigen Detection. *Org. Biomol. Chem.* **2013,** *11*, 6493-6501.

52. Takalo, H.; Mukkala, V.-M.; Mikola, H.; Liitti, P.; Hemmila, I. Synthesis of Europium(III) Chelates Suitable for Labeling of Bioactive Molecules. *Bioconjugate Chem.* **1994,** *5*, 278-282.

53. de Hoog, P.; Gamez, P.; Driessen, W. L.; Reedijk, J. New Polydentate and Polynucleating N-Donor Ligands from Amines and 2,4,6-Trichloro-1,3,5-Triazine. *Tetrahedron Lett.* **2002,** *43*, 6783-6786.

54. Mitrunen, K.; Pettersson, K.; Piironen, T.; Björk, T.; Lilja, H.; Lövgren, T. Dual-Label One-Step Immunoassay for Simultaneous Measurement of Free and Total Prostate-Specific Antigen Concentrations and Ratios in Serum. *Clin. Chem.* **1995,** *41*, 1115-1120.

55. Saha, A. K.; Kross, K.; Kloszewski, E. D.; Upson, D. A.; Toner, J. L.; Snow, R. A.; Black, C. D. V.; Desai, V. C. Time-Resolved Fluorescence of a New Europium-Chelate Complex: Demonstration of Highly Sensitive Detection of Protein and DNA Samples. *J. Am. Chem. Soc.* **1993,** *115*, 11032-11033.

56. Hovinen, J. Convenient Synthesis of Maleimido-Derivatized Lanthanide(III) Chelates and Their Use in Mercapto Group Conjugation. *Bioconjugate Chem.* **2007,** *18*, 597-600.

57. Ge, P.; Selvin, P. R. Thiol-Reactive Luminescent Lanthanide Chelates: Part 2. *Bioconjugate Chem.* **2003,** *14*, 870-876.

58. Yuan, J.; Matsumoto, K. Synthesis of a New Tetradentate β-Diketonate-Europium Chelate and Its Application for Time-Resolved Fluorimetry of Albumin. *J. Pharm. Biomed. Anal.* **1997,** *15*, 1397-1403.

59. Wu, F.-B.; Han, S.-Q.; Zhang, C.; He, Y.-F. Synthesis of a Highly Fluorescent β-Diketone-Europium Chelate and Its Utility in Time-Resolved Fluoroimmunoassay of Serum Total Thyroxine. *Anal. Chem.* **2002,** *74*, 5882-5889.

60. Wu, F.-B.; Zhang, C. A New Europium β-Diketone Chelate for Ultrasensitive Time-Resolved Fluorescence Immunoassays. *Anal. Biochem.* **2002,** *311*, 57-67.

61. Jingli, Y.; Shinji, S.; Ryosuke, S.; Keiichiro, M.; Kazuko, M. Structure and Luminescence Properties of the Tetradentate β-Diketonate-Europium(III) Complexes. *Chem. Lett.* **2003,** *32*, 492-493.

62. Weibel, N.; Charbonnière, L. J.; Guardigli, M.; Roda, A.; Ziessel, R. Engineering of Highly Luminescent Lanthanide Tags Suitable for Protein Labeling and Time-Resolved Luminescence Imaging. *J. Am. Chem. Soc.* **2004,** *126*, 4888-4896.

63. Tan, M.; Wang, G.; Hai, X.; Ye, Z.; Yuan, J. Development of Functionalized Fluorescent Europium Nanoparticles for Biolabeling and Time-Resolved Fluorometric Applications. *J. Mater. Chem.* **2004,** *14*, 2896-2901.

64. Liu, X.; Ye, Z.; Wei, W.; Du, Y.; Yuan, J.; Ma, D. Artificial Luminescent Protein as a Bioprobe for Time-Gated Luminescence Bioimaging. *Chem. Commun.* **2011,** *47*, 8139-8141.

65. Tian, L.; Dai, Z.; Zhang, L.; Zhang, R.; Ye, Z.; Wu, J.; Jin, D.; Yuan, J. Preparation and Time-Gated Luminescence Bioimaging Applications of Long Wavelength-Excited Silica-Encapsulated Europium Nanoparticles. *Nanoscale* **2012,** *4*, 3551-3557.

66. Zheng, W.; Tu, D.; Huang, P.; Zhou, S.; Chen, Z.; Chen, X. Time-Resolved Luminescent Biosensing Based on Inorganic Lanthanide-Doped Nanoprobes. *Chem. Commun.* **2015,** *51*, 4129-4143.

67. Zheng, W.; Huang, P.; Tu, D.; Ma, E.; Zhu, H.; Chen, X. Lanthanide-Doped Upconversion Nano-Bioprobes: Electronic Structures, Optical Properties, and Biodetection. *Chem. Soc. Rev.* **2015,** *44*, 1379-1415.

68. Mikkelsen, M.; Jorgensen, M.; Krebs, F. C. The Teraton Challenge. A Review of Fixation and Transformation of Carbon Dioxide. *Energy Environ. Sci.* **2010,** *3*, 43-81.

69. Wang, W.-H.; Himeda, Y.; Muckerman, J. T.; Manbeck, G. F.; Fujita, E. CO_2 Hydrogenation to Formate and Methanol as an Alternative to Photo- and Electrochemical CO_2 Reduction. *Chem. Rev.* **2015,** *115*, 12936-12973.

70. Sultana, S.; Sahoo, P. C.; Martha, S.; Parida, K. A Review of Harvesting Clean Fuels from Enzymatic CO_2 Reduction. *RSC Adv.* **2016,** *6*, 44170-44194.

71. Kumar, B.; Brian, J. P.; Atla, V.; Kumari, S.; Bertram, K. A.; White, R. T.; Spurgeon, J. M. New Trends in the Development of Heterogeneous Catalysts for Electrochemical CO_2 Reduction. *Catal. Today* **2016,** *270*, 19-30.

72. Lu, Q.; Jiao, F. Electrochemical CO_2 Reduction: Electrocatalyst, Reaction Mechanism, and Process Engineering. *Nano Energy* **2016,** *29*, 439-456.

73. Benson, E. E.; Kubiak, C. P.; Sathrum, A. J.; Smieja, J. M. Electrocatalytic and Homogeneous Approaches to Conversion of CO_2 to Liquid Fuels. *Chem. Soc. Rev.* **2009,** *38*, 89-99.

74. Qiao, J.; Liu, Y.; Hong, F.; Zhang, J. A Review of Catalysts for the Electroreduction of Carbon Dioxide to Produce Low-Carbon Fuels. *Chem. Soc. Rev.* **2014,** *43*, 631-675.

75. Whipple, D. T.; Kenis, P. J. A. Prospects of CO_2 Utilization Via Direct Heterogeneous Electrochemical Reduction. *J. Phys. Chem. Lett.* **2010,** *1*, 3451-3458.

76. Costentin, C.; Robert, M.; Saveant, J.-M. Catalysis of the Electrochemical Reduction of Carbon Dioxide. *Chem. Soc. Rev.* **2013,** *42*, 2423-2436.

77. Choi, J.; Benedetti, T. M.; Jalili, R.; Walker, A.; Wallace, G. G.; Officer, D. L. High Performance Fe Porphyrin/Ionic Liquid Co-Catalyst for Electrochemical CO_2 Reduction. *Chem. Eur. J.* **2016**, *22*, 14158-14161.

78. Johnson, B. A.; Maji, S.; Agarwala, H.; White, T. A.; Mijangos, E.; Ott, S. Activating a Low Overpotential CO_2 Reduction Mechanism by a Strategic Ligand Modification on a Ruthenium Polypyridyl Catalyst. *Angew. Chem. Int. Ed.* **2016,** *55*, 1825-1829.

79. Portenkirchner, E.; Oppelt, K.; Ulbricht, C.; Egbe, D. A. M.; Neugebauer, H.; Knör, G.; Sariciftci, N. S. Electrocatalytic and Photocatalytic Reduction of Carbon Dioxide to Carbon Monoxide Using the Alkynyl-Substituted Rhenium(I) Complex (5,5'-Bisphenylethynyl-2,2'-Bipyridyl)$Re(CO)_3Cl$. *J. Organomet. Chem.* **2012,** *716*, 19-25.

80. Lim, C.-H.; Holder, A. M.; Musgrave, C. B. Mechanism of Homogeneous Reduction of CO_2 by Pyridine: Proton Relay in Aqueous Solvent and Aromatic Stabilization. *J. Am. Chem. Soc.* **2013,** *135*, 142-154.

81. Froehlich, J. D.; Kubiak, C. P. Homogeneous CO_2 Reduction by Ni(Cyclam) at a Glassy Carbon Electrode. *Inorg. Chem.* **2012,** *51*, 3932-3934.

82. Cole, E. B.; Lakkaraju, P. S.; Rampulla, D. M.; Morris, A. J.; Abelev, E.; Bocarsly, A. B. Using a One-Electron Shuttle for the Multielectron Reduction of CO_2 to Methanol: Kinetic, Mechanistic, and Structural Insights. *J. Am. Chem. Soc.* **2010,** *132*, 11539-11551.

83. Stanton, C. J.; Vandezande, J. E.; Majetich, G. F.; Schaefer, H. F.; Agarwal, J. Mn-NHC Electrocatalysts: Increasing π Acidity Lowers the Reduction Potential and Increases the Turnover Frequency for CO_2 Reduction. *Inorg. Chem.* **2016**.

84. Elgrishi, N.; Chambers, M. B.; Wang, X.; Fontecave, M. Molecular Polypyridine-Based Metal Complexes as Catalysts for the Reduction of CO_2. *Chem. Soc. Rev.* **2017,** *46*, 761-796.

85. Hawecker, J.; Lehn, J.-M.; Ziessel, R. Electrocatalytic Reduction of Carbon Dioxide Mediated by $Re(Bipy)(CO)_3Cl$ (Bipy = 2,2'-Bipyridine). *J. Chem. Soc., Chem. Commun.* **1984**, 328-330.

86. Sullivan, B. P.; Bolinger, C. M.; Conrad, D.; Vining, W. J.; Meyer, T. J. One- and Two-Electron Pathways in the Electrocatalytic Reduction of CO_2 by *fac*-$Re(bpy)(CO)_3Cl$ (bpy = 2,2'-Bipyridine). *J. Chem. Soc., Chem. Commun.* **1985**, 1414-1416.

87. Smieja, J. M.; Kubiak, C. P. Re(Bipy-tbu)$(CO)_3Cl$−Improved Catalytic Activity for Reduction of Carbon Dioxide: IR-Spectroelectrochemical and Mechanistic Studies. *Inorg. Chem.* **2010,** *49*, 9283-9289.

88. Hayashi, Y.; Kita, S.; Brunschwig, B. S.; Fujita, E. Involvement of a Binuclear Species with the Re−C(O)O−Re Moiety in CO_2 Reduction Catalyzed by Tricarbonyl Rhenium(I) Complexes with Diimine Ligands: Strikingly Slow Formation of the Re−Re and Re−C(O)O−Re Species from Re(Dmb)$(CO)_3S$ (Dmb = 4,4'-Dimethyl-2,2'-Bipyridine, S = Solvent). *J. Am. Chem. Soc.* **2003,** *125*, 11976-11987.

89. Agarwal, J.; Fujita, E.; Schaefer, H. F.; Muckerman, J. T. Mechanisms for CO Production from CO_2 Using Reduced Rhenium Tricarbonyl Catalysts. *J. Am. Chem. Soc.* **2012,** *134*, 5180-5186.

90. Sampson, M. D.; Froehlich, J. D.; Smieja, J. M.; Benson, E. E.; Sharp, I. D.; Kubiak, C. P. Direct Observation of the Reduction of Carbon Dioxide by Rhenium Bipyridine Catalysts. *Energy Environ. Sci.* **2013,** *6*, 3748-3755.

91. Keith, J. A.; Grice, K. A.; Kubiak, C. P.; Carter, E. A. Elucidation of the Selectivity of Proton-Dependent Electrocatalytic CO_2 Reduction by *fac*-Re(bpy)$(CO)_3Cl$. *J. Am. Chem. Soc.* **2013,** *135*, 15823-15829.

92. Benson, E. E.; Kubiak, C. P. Structural Investigations into the Deactivation Pathway of the CO_2 Reduction Electrocatalyst Re(bpy)$(CO)_3Cl$. *Chem. Commun.* **2012,** *48*, 7374-7376.

93. Benson, E. E.; Sampson, M. D.; Grice, K. A.; Smieja, J. M.; Froehlich, J. D.; Friebel, D.; Keith, J. A.; Carter, E. A.; Nilsson, A.; Kubiak, C. P. The Electronic States of Rhenium Bipyridyl Electrocatalysts for CO_2 Reduction as Revealed by X-Ray Absorption Spectroscopy and Computational Quantum Chemistry. *Angew. Chem. Int. Ed.* **2013,** *52*, 4841-4844.

94. Machan, C. W.; Yin, J.; Chabolla, S. A.; Gilson, M. K.; Kubiak, C. P. Improving the Efficiency and Activity of Electrocatalysts for the Reduction of CO_2 through Supramolecular Assembly with Amino Acid-Modified Ligands. *J. Am. Chem. Soc.* **2016,** *138*, 8184-8193.

95. Machan, C. W.; Chabolla, S. A.; Yin, J.; Gilson, M. K.; Tezcan, F. A.; Kubiak, C. P. Supramolecular Assembly Promotes the Electrocatalytic Reduction of Carbon Dioxide by Re(I) Bipyridine Catalysts at a Lower Overpotential. *J. Am. Chem. Soc.* **2014,** *136*, 14598-14607.

96. Teesdale, J. J.; Pistner, A. J.; Yap, G. P. A.; Ma, Y.-Z.; Lutterman, D. A.; Rosenthal, J. Reduction of CO_2 Using a Rhenium Bipyridine Complex Containing Ancillary Bodipy Moieties. *Catal. Today* **2014,** *225*, 149-157.

97. Smieja, J. M.; Sampson, M. D.; Grice, K. A.; Benson, E. E.; Froehlich, J. D.; Kubiak, C. P. Manganese as a Substitute for Rhenium in CO_2 Reduction Catalysts: The Importance of Acids. *Inorg. Chem.* **2013,** *52*, 2484-2491.

98. Agarwal, J.; Shaw, T. W.; Stanton, C. J.; Majetich, G. F.; Bocarsly, A. B.; Schaefer, H. F. NHC-Containing Manganese(I) Electrocatalysts for the Two-Electron Reduction of CO_2. *Angew. Chem. Int. Ed.* **2014,** *53*, 5152-5155.

99. Stanton, C. J.; Machan, C. W.; Vandezande, J. E.; Jin, T.; Majetich, G. F.; Schaefer, H. F.; Kubiak, C. P.; Li, G.; Agarwal, J. Re(I) NHC Complexes for Electrocatalytic Conversion of CO_2. *Inorg. Chem.* **2016,** *55*, 3136-3144.

100. Qiao, X.; Li, Q.; Schaugaard, R. N.; Noffke, B. W.; Liu, Y.; Li, D.; Liu, L.; Raghavachari, K.; Li, L.-S. Well-Defined Nanographene-Rhenium Complex as an Efficient Electrocatalyst and Photocatalyst for Selective CO_2 Reduction. *J. Am. Chem. Soc.* **2017,** *139*, 3934-3937.

101. Takeda, H.; Koike, K.; Inoue, H.; Ishitani, O. Development of an Efficient Photocatalytic System for CO_2 Reduction Using Rhenium(I) Complexes Based on Mechanistic Studies. *J. Am. Chem. Soc.* **2008,** *130*, 2023-2031.

CHAPTER 2

1. Holliday, B. J.; Swager, T. M. Conducting Metallopolymers: The Roles of Molecular Architecture and Redox Matching. *Chem. Commun.* **2005**, 23-36.

2. Whittell, G. R.; Manners, I. Metallopolymers: New Multifunctional Materials. *Adv. Mater.* **2007,** *19*, 3439-3468.

3. Stanley, J. M.; Holliday, B. J. Luminescent Lanthanide-Containing Metallopolymers. *Coord. Chem. Rev.* **2012,** *256*, 1520-1530.

4. Chen, X.-Y.; Yang, X.; Holliday, B. J. Photoluminescent Europium-Containing Inner Sphere Conducting Metallopolymer. *J. Am. Chem. Soc.* **2008,** *130*, 1546-1547.

5. Koga, Y.; Yoshida, N.; Matsubara, K. PL and EL Behavior of Near-Red Luminescent Metallopolymer Easily Prepared from Phosphine-Containing Copolymer and Chloro{Bis(1-Phenylisoquinolinato-N,$C^{2'}$)}Iridium(III), and Its Monomeric Analog. *J. Polym. Sci., Part A: Polym. Chem.* **2009,** *47*, 4366-4378.

6. Holliday, B. J.; Stanford, T. B.; Swager, T. M. Chemoresistive Gas-Phase Nitric Oxide Sensing with Cobalt-Containing Conducting Metallopolymers. *Chem. Mater.* **2006,** *18*, 5649-5651.

7. Smith, R. C.; Tennyson, A. G.; Won, A. C.; Lippard, S. J. Conjugated Metallopolymers for Fluorescent Turn-on Detection of Nitric Oxide. *Inorg. Chem.* **2006,** *45*, 9367-9373.

8. Mejía, M. L.; Agapiou, K.; Yang, X.; Holliday, B. J. Seeded Growth of CdS Nanoparticles within a Conducting Metallopolymer Matrix. *J. Am. Chem. Soc.* **2009,** *131*, 18196-18197.

9. Edelman, K. R.; Stevenson, K. J.; Holliday, B. J. Conducting Metallopolymers as Precursors to Fabricate Palladium Nanoparticle/Polymer Hybrids for Oxygen Reduction. *Macromol. Rapid Commun.* **2012,** *33*, 610-615.

10. Djukic, B.; Lemaire, M. T. Hybrid Spin-Crossover Conductor Exhibiting Unusual Variable-Temperature Electrical Conductivity. *Inorg. Chem.* **2009,** *48*, 10489-10491.

11. Djukic, B.; Seda, T.; Gorelsky, S. I.; Lough, A. J.; Lemaire, M. T. π-Extended and Six-Coordinate Iron(II) Complexes: Structures, Magnetic Properties, and the Electrochemical Synthesis of a Conducting Iron(II) Metallopolymer. *Inorg. Chem.* **2011,** *50*, 7334-7343.

12. O'Sullivan, T. J.; Djukic, B.; Dube, P. A.; Lemaire, M. T. A Conducting Metallopolymer Featuring Valence Tautomerism. *Chem. Commun.* **2009**, 1903-1905.

13. Satheeshkumar, C.; Park, J.-Y.; Jeong, D.-C.; Song, S. G.; Lee, J.; Song, C. Synthesis and Electronic Properties of N-Heterocyclic Carbene-Containing Conducting Polymers with Coinage Metals. *RSC Adv.* **2015,** *5*, 60892-60897.

14. Powell, A. B.; Bielawski, C. W.; Cowley, A. H. Design, Synthesis, and Study of Main Chain Poly(N-Heterocyclic Carbene) Complexes: Applications in Electrochromic Devices. *J. Am. Chem. Soc.* **2010,** *132*, 10184-10194.

15. Fan, C.; Ye, C.; Wang, X.; Chen, Z.; Zhou, Y.; Liang, Z.; Tao, X. Synthesis and Electrochromic Properties of New Terpyridine-Triphenylamine Hybrid Polymers. *Macromolecules* **2015,** *48*, 6465-6473.

16. Bao, X.; Zhao, Q.; Wang, H.; Liu, K.; Qiu, D. Metallopolymer Electrochromic Film Prepared by Oxidative Electropolymerization of a Fe(II) Complex with Arylamine Functionalized Terpyridine Ligand. *Inorg. Chem. Commun.* **2013,** *38*, 88-91.

17. Beaujuge, P. M.; Reynolds, J. R. Color Control in π-Conjugated Organic Polymers for Use in Electrochromic Devices. *Chem. Rev.* **2010,** *110*, 268-320.

18. Groenendaal, L.; Zotti, G.; Aubert, P. H.; Waybright, S. M.; Reynolds, J. R. Electrochemistry of Poly(3,4-Alkylenedioxythiophene) Derivatives. *Adv. Mater.* **2003,** *15*, 855-879.

19. Niklasson, G. A.; Granqvist, C. G. Electrochromics for Smart Windows: Thin Films of Tungsten Oxide and Nickel Oxide, and Devices Based on These. *J. Mater. Chem.* **2007,** *17*, 127-156.

20. Han, F. S.; Higuchi, M.; Kurth, D. G. Metallosupramolecular Polyelectrolytes Self-Assembled from Various Pyridine Ring-Substituted Bisterpyridines and Metal

Ions: Photophysical, Electrochemical, and Electrochromic Properties. *J. Am. Chem. Soc.* **2008,** *130*, 2073-2081.

21. Takada, K.; Sakamoto, R.; Yi, S.-T.; Katagiri, S.; Kambe, T.; Nishihara, H. Electrochromic Bis(Terpyridine)Metal Complex Nanosheets. *J. Am. Chem. Soc.* **2015,** *137*, 4681-4689.

22. Shankar, S.; Lahav, M.; van der Boom, M. E. Coordination-Based Molecular Assemblies as Electrochromic Materials: Ultra-High Switching Stability and Coloration Efficiencies. *J. Am. Chem. Soc.* **2015,** *137*, 4050-4053.

23. Friebe, C.; Hager, M. D.; Winter, A.; Schubert, U. S. Metal-Containing Polymers Via Electropolymerization. *Adv. Mater.* **2012,** *24*, 332-345.

24. Scheuble, M.; Goll, M.; Ludwigs, S. Branched Terthiophenes in Organic Electronics: From Small Molecules to Polymers. *Macromol. Rapid Commun.* **2015,** *36*, 115-137.

25. Link, S. M.; Scheuble, M.; Goll, M.; Muks, E.; Ruff, A.; Hoffmann, A.; Richter, T. V.; Navarrete, J. T. L.; Delgado, M. C. R.; Ludwigs, S. Electropolymerized Three-Dimensional Randomly Branched EDOT-Containing Copolymers. *Langmuir* **2013,** *29*, 15463-15473.

26. McEntee, G. J.; Skabara, P. J.; Vilela, F.; Tierney, S.; Samuel, I. D. W.; Gambino, S.; Coles, S. J.; Hursthouse, M. B.; Harrington, R. W.; Clegg, W. Synthesis and Electropolymerization of Hexadecyl Functionalized Bithiophene and Thieno[3,2-b]Thiophene End-Capped with EDOT and EDTT Units. *Chem. Mater.* **2010,** *22*, 3000-3008.

27. Segura, J. L.; Gómez, R.; Reinold, E.; Bäuerle, P. Synthesis and Electropolymerization of a Perylenebisimide-Functionalized 3,4-Ethylenedioxythiophene (EDOT) Derivative. *Org. Lett.* **2005,** *7*, 2345-2348.

28. Akoudad, S.; Roncali, J. Modification of the Electrochemical and Electronic Properties of Electrogenerated Poly(3,4-Ethylenedioxythiophene) by Hydroxymethyl and Oligo(Oxyethylene) Substituents. *Electrochem. Commun.* **2000,** *2*, 72-76.

29. Amb, C. M.; Dyer, A. L.; Reynolds, J. R. Navigating the Color Palette of Solution-Processable Electrochromic Polymers. *Chem. Mater.* **2011,** *23*, 397-415.

30. Dyer, A. L.; Thompson, E. J.; Reynolds, J. R. Completing the Color Palette with Spray-Processable Polymer Electrochromics. *ACS Appl. Mater. Interfaces* **2011,** *3*, 1787-1795.

31. Heuer, H. W.; Wehrmann, R.; Kirchmeyer, S. Electrochromic Window Based on Conducting Poly(3,4-Ethylenedioxythiophene)-Poly(Styrene Sulfonate). *Adv. Funct. Mater.* **2002,** *12*, 89-94.

32. Ponder, J. F.; Österholm, A. M.; Reynolds, J. R. Designing a Soluble PEDOT Analogue without Surfactants or Dispersants. *Macromolecules* **2016,** *49*, 2106-2111.

33. Kumar, A.; Welsh, D. M.; Morvant, M. C.; Piroux, F.; Abboud, K. A.; Reynolds, J. R. Conducting Poly(3,4-Alkylenedioxythiophene) Derivatives as Fast Electrochromics with High-Contrast Ratios. *Chem. Mater.* **1998,** *10*, 896-902.

34. Naseri, Z.; Nemati Kharat, A.; Banavand, A.; Bakhoda, A.; Foroutannejad, S. First Row Transition Metal Complexes of Thienyl Substituted Terpyridine: Structural, Photophysical and Biological Studies. *Polyhedron* **2012,** *33*, 396-403.

35. Hjelm, J.; Handel, R. W.; Hagfeldt, A.; Constable, E. C.; Housecroft, C. E.; Forster, R. J. Conducting Polymers Containing in-Chain Metal Centers: Electropolymerization of Oligothienyl-Substituted {M(Tpy)2} Complexes and in Situ Conductivity Studies, M = Os(II), Ru(II). *Inorg. Chem.* **2005,** *44*, 1073-1081.

36. Beley, M.; Delabouglise, D.; Houppy, G.; Husson, J.; Petit, J. P. Preparation and Properties of Ruthenium (II) Complexes of 2,2':6',2"-Terpyridines Substituted at the 4'-Position with Heterocyclic Groups. *Inorg. Chim. Acta* **2005,** *358*, 3075-3083.

37. Constable, E. C.; Handel, R.; Housecroft, C. E.; Neuburger, M.; Schofield, E. R.; Zehnder, M. Efficient Syntheses of 4'-(2-Thienyl)- and 4'-(3-Thienyl)-2,2':6',2"-Terpyridine: Preparation and Characterization of Fe(II), Ru(II), Os(II) and Co(II) Complexes. *Polyhedron* **2004,** *23*, 135-143.

38. Fillaud, L.; Trippé-Allard, G.; Lacroix, J. C. Synthesis of π-Conjugated 2,2:6',2"-Terpyridine-Substituted Oligomers Based on 3,4-Ethylenedioxythiophene. *Org. Lett.* **2013,** *15*, 1028-1031.

39. Liang, Y.; Strohecker, D.; Lynch, V.; Holliday, B. J.; Jones, R. A. A Thiophene-Containing Conductive Metallopolymer Using an Fe(II) Bis(Terpyridine) Core for Electrochromic Materials. *ACS Appl. Mater. Interfaces* **2016,** *8*, 34568-34580.

40. Raimundo, J.-M.; Blanchard, P.; Gallego-Planas, N.; Mercier, N.; Ledoux-Rak, I.; Hierle, R.; Roncali, J. Design and Synthesis of Push−Pull Chromophores for Second-Order Nonlinear Optics Derived from Rigidified Thiophene-Based π-Conjugating Spacers. *J. Org. Chem.* **2002,** *67*, 205-218.

41. Firstenberg, M.; Shivananda, K. N.; Cohen, I.; Solomeshch, O.; Medvedev, V.; Tessler, N.; Eichen, Y. Harnessing "Click"-Type Chemistry for the Preparation of Novel Electronic Materials. *Adv. Funct. Mater.* **2011,** *21*, 634-643.

42. Gottlieb, H. E.; Kotlyar, V.; Nudelman, A. NMR Chemical Shifts of Common Laboratory Solvents as Trace Impurities. *J. Org. Chem.* **1997,** *62*, 7512-7515.

43. Kharat, A. N.; Bakhoda, A.; Hajiashrafi, T. Catalytic Oxidation of Organosulfides to Sulfoxides Using Two Novel Cu(II) and Ni(II) Complexes with Aqueous H_2O_2:

Effect of TMAO Promoter on Oxidation of Organosulfides. *J. Mol. Catal. A: Chem.* **2010,** *333*, 94-99.

44. Klemens, T.; Switlicka-Olszewska, A.; Machura, B.; Grucela, M.; Schab-Balcerzak, E.; Smolarek, K.; Mackowski, S.; Szlapa, A.; Kula, S.; Krompiec, S.; Lodowski, P.; Chrobok, A. Rhenium(I) Terpyridine Complexes - Synthesis, Photophysical Properties and Application in Organic Light Emitting Devices. *Dalton Trans.* **2016,** *45*, 1746-1762.

45. Presselt, M.; Dietzek, B.; Schmitt, M.; Popp, J.; Winter, A.; Chiper, M.; Friebe, C.; Schubert, U. S. Zinc(II) Bisterpyridine Complexes: The Influence of the Cation on the π-Conjugation between Terpyridine and the Lateral Phenyl Substituent. *J. Phys. Chem. C* **2008,** *112*, 18651-18660.

46. Hunt, R. L.; Ault, B. S. Spectroscopic Influences of Ion Pairing: Infrared Matrix Isolation Spectra of the $M^+BF^-_4$ Ion Pair and Its Chlorine-Fluorine Analogs. *Spectrochim. Acta Mol. Biomol. Spectros.* **1981,** *37*, 63-69.

47. Roncali, J. Conjugated Poly(Thiophenes): Synthesis, Functionalization, and Applications. *Chem. Rev.* **1992,** *92*, 711-738.

48. Muenmart, D.; Tarsang, R.; Jungsuttiwong, S.; Keawin, T.; Sudyoadsuk, T.; Promarak, V. Synthesis and Properties of Fluorene-Oligothiophenes Perylenediimide Triads and Their Electropolymerizations. *J. Mater. Chem.* **2012,** *22*, 14579-14586.

49. Caraway, J. D.; Nguyen, M. T.; Mitchell, L. A.; Holliday, B. J. Incorporation of Thieno[3,2-b]Thiophene Moieties as Novel Electropolymerizable Groups in a Conducting Metallopolymer and Study of the Effect on Photostability. *Macromol. Rapid Commun.* **2015,** *36*, 665-670.

50. Yang, R.; Ruan, C.; Dai, W.; Deng, J.; Kong, J. Electropolymerization of Thionine in Neutral Aqueous Media and H_2O_2 Biosensor Based on Poly(Thionine). *Electrochim. Acta* **1999,** *44*, 1585-1596.

51. Qiu, D.; Zhao, Q.; Bao, X.; Liu, K.; Wang, H.; Guo, Y.; Zhang, L.; Zeng, J.; Wang, H. Electropolymerization and Characterization of an Alternatively Conjugated Donor-Acceptor Metallopolymer: Poly-[Ru(4'-(4-(Diphenylamino)Phenyl)-2,2':6",2"-Terpyridine)$_2$]$^{2+}$. *Inorg. Chem. Commun.* **2011,** *14*, 296-299.

52. Chu, P. K.; Liu, X., *Biomaterials Fabrication and Processing Handbook*. CRC press: 2008; p 339.

53. Marzocchi, M.; Gualandi, I.; Calienni, M.; Zironi, I.; Scavetta, E.; Castellani, G.; Fraboni, B. Physical and Electrochemical Properties of PEDOT:PSS as a Tool for Controlling Cell Growth. *ACS Appl. Mater. Interfaces* **2015,** *7*, 17993-18003.

54. Abd-El-Aziz, A. S.; Manners, I., *Frontiers in Transition Metal-Containing Polymers*. Wiley: Hoboken, NY, 2007.

55. Munzert, S. M.; Schwarz, G.; Kurth, D. G. Kinetic Studies of the Coordination of Mono- and Ditopic Ligands with First Row Transition Metal Ions. *Inorg. Chem.* **2016,** *55*, 2565-2573.

56. Collin, J.-P.; Dixon, I. M.; Sauvage, J.-P.; Williams, J. A. G.; Barigelletti, F.; Flamigni, L. Synthesis and Photophysical Properties of Iridium(III) Bisterpyridine and Its Homologues: A Family of Complexes with a Long-Lived Excited State. *J. Am. Chem. Soc.* **1999,** *121*, 5009-5016.

57. Bechinger, C.; Burdis, M. S.; Zhang, J. G. Comparison between Electrochromic and Photochromic Coloration Efficiency of Tungsten Oxide Thin Films. *Solid State Commun.* **1997,** *101*, 753-756.

58. Yao, D. D.; Rani, R. A.; O'Mullane, A. P.; Kalantar-zadeh, K.; Ou, J. Z. Enhanced Coloration Efficiency for Electrochromic Devices Based on Anodized Nb_2O_5/Electrodeposited MoO_3 Binary Systems. *J. Phy. Chem. C* **2014,** *118*, 10867-10873.

59. Nunes, M.; Araújo, M.; Fonseca, J.; Moura, C.; Hillman, R.; Freire, C. High-Performance Electrochromic Devices Based on Poly[Ni(Salen)]-Type Polymer Films. *ACS Appl. Mater. Interfaces* **2016,** *8*, 14231-14243.

60. Schott, M.; Szczerba, W.; Kurth, D. G. Detailed Study of Layer-by-Layer Self-Assembled and Dip-Coated Electrochromic Thin Films Based on Metallo-Supramolecular Polymers. *Langmuir* **2014,** *30*, 10721-10727.

CHAPTER 3

1. de Sá, G. F.; Malta, O. L.; de Mello Donegá, C.; Simas, A. M.; Longo, R. L.; Santa-Cruz, P. A.; da Silva Jr, E. F. Spectroscopic Properties and Design of Highly Luminescent Lanthanide Coordination Complexes. *Coord. Chem. Rev.* **2000,** *196*, 165-195.

2. Binnemans, K. Lanthanide-Based Luminescent Hybrid Materials. *Chem. Rev.* **2009,** *109*, 4283-4374.

3. Stanley, J. M.; Holliday, B. J. Luminescent Lanthanide-Containing Metallopolymers. *Coord. Chem. Rev.* **2012,** *256*, 1520-1530.

4. Schrader, B. F. Albert Cotton: Chemical Applications of Group Theory, 3rd Ed. John Wiley & Sons: New York, 1990.

5. Armelao, L.; Quici, S.; Barigelletti, F.; Accorsi, G.; Bottaro, G.; Cavazzini, M.; Tondello, E. Design of Luminescent Lanthanide Complexes: From Molecules to Highly Efficient Photo-Emitting Materials. *Coord. Chem. Rev.* **2010,** *254*, 487-505.

6. Lis, S.; Elbanowski, M.; Mkowska, B.; Hnatejko, Z. Energy Transfer in Solution of Lanthanide Complexes. *J. Photochem. Photobiol. A* **2002,** *150*, 233-247.

7. Faulkner, S.; Pope, S. J. A.; Burton-Pye, B. P. Lanthanide Complexes for Luminescence Imaging Applications. *Appl. Spectrosc. Rev.* **2005,** *40*, 1-31.

8. Thibon, A.; Pierre, V. C. Principles of Responsive Lanthanide-Based Luminescent Probes for Cellular Imaging. *Anal. Bioanal. Chem.* **2009,** *394*, 107-120.

9. Zhang, L.; Wang, Y.; Ye, Z.; Jin, D.; Yuan, J. New Class of Tetradentate β-Diketonate-Europium Complexes That Can Be Covalently Bound to Proteins for Time-Gated Fluorometric Application. *Bioconjugate Chem.* **2012,** *23*, 1244-1251.

10. Yuan, J.; Wang, G. Lanthanide Complex-Based Fluorescence Label for Time-Resolved Fluorescence Bioassay. *J. Fluoresc.* **2005,** *15*, 559-568.

11. Nishioka, T.; Yuan, J.; Yamamoto, Y.; Sumitomo, K.; Wang, Z.; Hashino, K.; Hosoya, C.; Ikawa, K.; Wang, G.; Matsumoto, K. New Luminescent Europium(III) Chelates for DNA Labeling. *Inorg. Chem.* **2006,** *45*, 4088-4096.

12. Erostyák, J.; Buzády, A.; Kaszás, A.; Kozma, L.; Hornyák, I. Time-Resolved Study of Intramolecular Energy Transfer in Eu^{3+}, Tb^{3+}/β-Diketone/o-Phenanthroline Complexes in Aqueous Micellar Solutions. *J. Lumin.* **1997,** *72*, 570-571.

13. Halcrow, M. A. The Synthesis and Coordination Chemistry of 2,6-Bis(Pyrazolyl)Pyridines and Related Ligands-Versatile Terpyridine Analogues. *Coord. Chem. Rev.* **2005,** *249*, 2880-2908.

14. Narayana, Y. S. L. V.; Basak, S.; Baumgarten, M.; Müllen, K.; Chandrasekar, R. White-Emitting Conjugated Polymer/Inorganic Hybrid Spheres: Phenylethynyl and 2,6-Bis(Pyrazolyl)Pyridine Copolymer Coordinated to $Eu(tta)_3$. *Adv. Funct. Mater.* **2013,** *23*, 5875-5880.

15. Narayana, Y. S. L. V.; Chandrasekar, R. Triple Emission from Organic/Inorganic Hybrid Nanovesicles in a Single Excitation. *ChemPhysChem* **2011,** *12*, 2391-2396.

16. Basak, S.; Chandrasekar, R. Multiluminescent Hybrid Organic/Inorganic Nanotubular Structures: One-Pot Fabrication of Tricolor (Blue–Red–Purple) Luminescent Parallepipedic Organic Superstructure Grafted with Europium Complexes. *Adv. Funct. Mater.* **2011,** *21*, 667-673.

17. Stanley, J. M.; Zhu, X.; Yang, X.; Holliday, B. J. Europium Complexes of a Novel Ethylenedioxythiophene-Derivatized Bis(Pyrazolyl)Pyridine Ligand Exhibiting Efficient Lanthanide Sensitization. *Inorg. Chem.* **2010,** *49*, 2035-2037.

18. Starck, M.; Kadjane, P.; Bois, E.; Darbouret, B.; Incamps, A.; Ziessel, R.; Charbonnière, L. J. Towards Libraries of Luminescent Lanthanide Complexes and Labels from Generic Synthons. *Chem. Eur. J.* **2011,** *17*, 9164-9179.

19. Stanley, J. M.; King, A. W.; Rack, J. J.; Holliday, B. J. Femtosecond Interligand Dynamics in Highly Luminescent Lanthanide Complexes. *in preparation*.

20. Deng, W.; Jin, D.; Drozdowicz-Tomsia, K.; Yuan, J.; Goldys, E. M. Europium Chelate (BHHCT-Eu^{3+}) and Its Metal Nanostructure Enhanced Luminescence Applied to Bioassays and Time-Gated Bioimaging. *Langmuir* **2010,** *26*, 10036-10043.

21. Elhaïk, J.; Pask, C. M.; Kilner, C. A.; Halcrow, M. A. Synthesis of 2,6-Di(Pyrazol-1-yl)-4-Bromomethylpyridine, and Its Conversion to Other 2,6-Di(Pyrazol-1-yl)Pyridines Substituted at the Pyridine Ring. *Tetrahedron* **2007,** *63*, 291-298.

22. Kai, J.; Parra, D. F.; Brito, H. F. Polymer Matrix Sensitizing Effect on Photoluminescence Properties of Eu^{3+}-β-Diketonate Complex Doped into Poly-β-Hydroxybutyrate (PHB) in Film Form. *J. Mater. Chem.* **2008,** *18*, 4549-4554.

23. Gottlieb, H. E.; Kotlyar, V.; Nudelman, A. NMR Chemical Shifts of Common Laboratory Solvents as Trace Impurities. *J. Org. Chem.* **1997,** *62*, 7512-7515.

24. Lakowicz, J. R., Principles of Fluorescence Spectroscopy. 3rd ed.; Springer: New York, 2006.

25. Xu, H.; Wang, L.-H.; Zhu, X.-H.; Yin, K.; Zhong, G.-Y.; Hou, X.-Y.; Huang, W. Application of Chelate Phosphine Oxide Ligand in Eu(III) Complex with Mezzo Triplet Energy Level, Highly Efficient Photoluminescent, and Electroluminescent Performances. *J. Phys. Chem. B* **2006,** *110*, 3023-3029.

26. Carlos, L. D.; Videira, A. L. L. Emission Spectra and Local Symmetry of the Eu^{3+} Ion in Polymer Electrolytes. *Phys. Rev. B* **1994,** *49*, 11721-11728.

27. Werts, M. H. V.; Jukes, R. T. F.; Verhoeven, J. W. The Emission Spectrum and the Radiative Lifetime of Eu^{3+} in Luminescent Lanthanide Complexes. *Phys. Chem. Chem. Phys.* **2002,** *4*, 1542-1548.

28. Haas, Y. G. S. Radiative and Nonradiative Pathways in Solutions. Excited States of the Europium(III) Ion. *J. Phys. Chem.* **1972,** *76*, 1093-1104.

29. Teotonio, E. E. S.; Brito, H. F.; Felinto, M. C. F. C.; Kodaira, C. A.; Malta, O. L. Luminescence Investigations on Eu(III) Thenoyltrifluoroacetonate Complexes with Amide Ligands. *J. Coord. Chem.* **2003,** *56*, 913-921.

30. Lourenço, A. V. S.; Kodaira, C. A.; Ramos-Sanchez, E. M.; Felinto, M. C. F. C.; Goto, H.; Gidlund, M.; Malta, O. L.; Brito, H. F. Luminescent Material Based on the $[Eu(tta)_3(H_2O)_2]$ Complex Incorporated into Modified Silica Particles for Biological Applications. *J. Inorg. Biochem.* **2013,** *123*, 11-17.

31. Kazakov, V. P.; Voloshin, A. I.; Ostakhov, S. S.; Shavaleev, N. M. The Anomalous Influence of Water on the Intensity and Lifetime of Fluorescence in Tris(Benzoyltrifluoroacetonate)Europium(III). *Mendeleev Commun.* **1998,** *8*, 47-49.

32. Beeby, A.; M. Clarkson, I.; S. Dickins, R.; Faulkner, S.; Parker, D.; Royle, L.; S. de Sousa, A.; Williams, A. G. J.; Woods, M. Non-Radiative Deactivation of the

Excited States of Europium, Terbium and Ytterbium Complexes by Proximate Energy-Matched OH, NH and CH Oscillators: An Improved Luminescence Method for Establishing Solution Hydration States. *J. Chem. Soc., Perkin Trans 2* **1999,** 493-504.

33. Kropp, J. L.; Windsor, M. W. Luminescence and Energy Transfer in Solutions of Rare-Earth Complexes. I. Enhancement of Fluorescence by Deuterium Substitution. *J. Chem. Phys.* **1965,** *42*, 1599-1608.

34. Leung, P. K.; Steig, R. P., Dielectric Constant Measurements: A New, Rapid Method to Characterize Shale at the Wellsite. Society of Petroleum Engineers. Society of Petroleum Engineers: New Orleans, 1992.

35. Halcrow, M. A. Recent Advances in the Synthesis and Applications of 2,6-Dipyrazolylpyridine Derivatives and Their Complexes. *New J. Chem.* **2014,** *38*, 1868-1882.

CHAPTER 4

1. Wang, W-H.; Himeda, Y.; Muckerman, J. T.; Manbeck, G. F.; Fujita, E. CO_2 Hydrogenation to Formate and Methanol as an Alternative to Photo- and Electrochemical CO_2 Reduction. *Chem. Rev.* **2015,** *115*, 12936-12973.

2. Sultana, S.; Sahoo, P. C.; Martha, S.; Parida, K. A Review of Harvesting Clean Fuels from Enzymatic CO_2 Reduction. *RSC Adv.* **2016,** *6*, 44170-44194.

3. Kumar, B.; Brian, J. P.; Atla, V.; Kumari, S.; Bertram, K. A.; White, R. T.; Spurgeon, J. M. New Trends in the Development of Heterogeneous Catalysts for Electrochemical CO_2 Reduction. *Catal. Today* **2016,** *270*, 19-30.

4. Lu, Q.; Jiao, F. Electrochemical CO_2 Reduction: Electrocatalyst, Reaction Mechanism, and Process Engineering. *Nano Energy* **2016,** *29*, 439-456.

5. Benson, E. E.; Kubiak, C. P.; Sathrum, A. J.; Smieja, J. M. Electrocatalytic and Homogeneous Approaches to Conversion of CO_2 to Liquid Fuels. *Chem. Soc. Rev.* **2009,** *38*, 89-99.

6. Qiao, J.; Liu, Y.; Hong, F.; Zhang, J. A Review of Catalysts for the Electroreduction of Carbon Dioxide to Produce Low-Carbon Fuels. *Chem. Soc. Rev.* **2014,** *43*, 631-675.

7. Whipple, D. T.; Kenis, P. J. A. Prospects of CO_2 Utilization Via Direct Heterogeneous Electrochemical Reduction. *J. Phys. Chem. Lett.* **2010,** *1*, 3451-3458.

8. Costentin, C.; Robert, M.; Saveant, J.-M. Catalysis of the Electrochemical Reduction of Carbon Dioxide. *Chem. Soc. Rev.* **2013,** *42*, 2423-2436.

9. Choi, J.; Benedetti, T. M.; Jalili, R.; Walker, A.; Wallace, G. G.; Officer, D. L. High Performance Fe Porphyrin/Ionic Liquid Co-Catalyst for Electrochemical CO_2 Reduction. *Chem. Eur. J.* **2016,** *22*, 14158-14161.

10. Johnson, B. A.; Maji, S.; Agarwala, H.; White, T. A.; Mijangos, E.; Ott, S. Activating a Low Overpotential CO_2 Reduction Mechanism by a Strategic Ligand Modification on a Ruthenium Polypyridyl Catalyst. *Angew. Chem. Int. Ed.* **2016,** *55*, 1825-1829.

11. Portenkirchner, E.; Oppelt, K.; Ulbricht, C.; Egbe, D. A. M.; Neugebauer, H.; Knör, G.; Sariciftci, N. S. Electrocatalytic and Photocatalytic Reduction of Carbon Dioxide to Carbon Monoxide Using the Alkynyl-Substituted Rhenium(I) Complex (5,5′-Bisphenylethynyl-2,2′-Bipyridyl)Re(CO)$_3$Cl. *J. Organomet. Chem.* **2012,** *716*, 19-25.

12. Lim, C.-H.; Holder, A. M.; Musgrave, C. B. Mechanism of Homogeneous Reduction of CO_2 by Pyridine: Proton Relay in Aqueous Solvent and Aromatic Stabilization. *J. Am. Chem. Soc.* **2013,** *135*, 142-154.

13. Froehlich, J. D.; Kubiak, C. P. Homogeneous CO_2 Reduction by Ni(Cyclam) at a Glassy Carbon Electrode. *Inorg. Chem.* **2012,** *51*, 3932-3934.

14. Cole, E. B.; Lakkaraju, P. S.; Rampulla, D. M.; Morris, A, J.; Abelev, E.; Bocarsly, A. B. Using a One-Electron Shuttle for the Multielectron Reduction of CO_2 to Methanol: Kinetic, Mechanistic, and Structural Insights. *J. Am. Chem. Soc.* **2010,** *132*, 11539-11551.

15. Stanton, C. J.; Vandezande, J. E.; Majetich, G. F.; Schaefer, H. F.; Agarwal, J. Mn-NHC Electrocatalysts: Increasing π Acidity Lowers the Reduction Potential and Increases the Turnover Frequency for CO_2 Reduction. *Inorg. Chem.* **2016,** *55*, 9509-9512.

16. Hawecker, J.; Lehn, J.-M.; Ziessel, R. Electrocatalytic Reduction of Carbon Dioxide Mediated by Re(Bipy)(CO)$_3$Cl (Bipy = 2,2'-Bipyridine). *J. Chem. Soc., Chem. Commun.* **1984**, 328-330.

17. Sullivan, B. P.; Bolinger, C. M.; Conrad, D.; Vining, W. J.; Meyer, T. J. One- and Two-Electron Pathways in the Electrocatalytic Reduction of CO_2 by *fac*-Re(bpy)(CO)$_3$Cl (bpy = 2,2'-Bipyridine). *J. Chem. Soc., Chem. Commun.* **1985**, 1414-1416.

18. Smieja, J. M.; Kubiak, C. P. Re(bipy-^{t}bu)(CO)$_3$Cl−Improved Catalytic Activity for Reduction of Carbon Dioxide: IR-Spectroelectrochemical and Mechanistic Studies. *Inorg. Chem.* **2010,** *49*, 9283-9289.

19. Hayashi, Y.; Kita, S.; Brunschwig, B. S.; Fujita, E. Involvement of a Binuclear Species with the Re−C(O)O−Re Moiety in CO_2 Reduction Catalyzed by Tricarbonyl Rhenium(I) Complexes with Diimine Ligands: Strikingly Slow Formation of the Re−Re and Re−C(O)O−Re Species from Re(DMB)(CO)$_3$S (DMB

= 4,4'-Dimethyl-2,2'-bipyridine, S = Solvent). *J. Am. Chem. Soc.* **2003,** *125*, 11976-11987.

20. Agarwal, J.; Fujita, E.; Schaefer, H. F.; Muckerman, J. T. Mechanisms for CO Production from CO_2 Using Reduced Rhenium Tricarbonyl Catalysts. *J. Am. Chem. Soc.* **2012,** *134*, 5180-5186.

21. Portenkirchner, E.; Oppelt, K.; Ulbricht, C.; Egbe, D. A. M.; Neugebauer, H.; Knör, G.; Sariciftci, N. S. Electrocatalytic and Photocatalytic Reduction of Carbon Dioxide to Carbon Monoxide Using the Alkynyl-Substituted Rhenium(I) Complex (5,5′-Bisphenylethynyl-2,2′-Bipyridyl)$Re(CO)_3Cl$. *J. Organomet. Chem.* **2012,** *716*, 19-25.

22. Teesdale, J. J.; Pistner, A. J.; Yap, G. P. A.; Ma, Y.-Z.; Lutterman, D. A.; Rosenthal, J. Reduction of CO_2 Using a Rhenium Bipyridine Complex Containing Ancillary Bodipy Moieties. *Catal. Today* **2014,** *225*, 149-157.

23. Agarwal, J.; Shaw, T. W.; Stanton, C. J.; Majetich, G. F.; Bocarsly, A. B.; Schaefer, H. F. NHC-Containing Manganese(I) Electrocatalysts for the Two-Electron Reduction of CO_2. *Angew. Chem. Int. Ed.* **2014,** *53*, 5152-5155.

24. Clark, M. L.; Grice, K. A.; Moore, C. E.; Rheingold, A. L.; Kubiak, C. P. Electrocatalytic CO_2 Reduction by $M(bpy\text{-}R)(CO)_4$ (M = Mo, W; R = H, ^{t}bu) Complexes. Electrochemical, Spectroscopic, and Computational Studies and Comparison with Group 7 Catalysts. *Chem. Sci.* **2014,** *5*, 1894-1900.

25. Franco, F.; Cometto, C.; Ferrero Vallana, F.; Sordello, F.; Priola, E.; Minero, C.; Nervi, C.; Gobetto, R. A Local Proton Source in a $[Mn(bpy\text{-}R)(CO)_3Br]$-Type Redox Catalyst Enables CO_2 Reduction Even in the Absence of Bronsted Acids. *Chem. Commun.* **2014,** *50*, 14670-14673.

26. Riplinger, C.; Sampson, M. D.; Ritzmann, A. M.; Kubiak, C. P.; Carter E. A. Mechanistic Contrasts between Manganese and Rhenium Bipyridine Electrocatalysts for the Reduction of Carbon Dioxide. *J. Am. Chem. Soc.* **2014,** *136*, 16285-16298.

27. Sampson, M. D.; Kubiak, C. P. Electrocatalytic Dihydrogen Production by an Earth-Abundant Manganese Bipyridine Catalyst. *J. Am. Chem. Soc.* **2015,** *54*, 6674-6676.

28. Stanton, C. J.; Machan, C. W.; Vandezande, J. E.; Jin, T.; Majetich, G. F.; Schaefer, H. F.; Kubiak, C. P.; Li, G.; Agarwal, J. Re(I) NHC Complexes for Electrocatalytic Conversion of CO_2. *Inorg. Chem.* **2016,** *55*, 3136-3144.

29. Machan, C. W.; Yin, J.; Chabolla, S. A.; Gilson, M. K.; Kubiak, C. P. Improving the Efficiency and Activity of Electrocatalysts for the Reduction of CO_2 through Supramolecular Assembly with Amino Acid-Modified Ligands. *J. Am. Chem. Soc.* **2016,** *138*, 8184-8193.

30. Keith, J. A.; Grice, K. A.; Kubiak, C. P.; Carter, E. A. Elucidation of the Selectivity of Proton-Dependent Electrocatalytic CO_2 Reduction by *fac*-Re(bpy)$(CO)_3$Cl. *J. Am. Chem. Soc.* **2013,** *135*, 15823-15829.

31. Benson, E. E.; Kubiak, C. P. Structural Investigations into the Deactivation Pathway of the CO_2 Reduction Electrocatalyst Re(bpy)$(CO)_3$Cl. *Chem. Commun.* **2012,** *48*, 7374-7376.

32. Benson, E. E.; Sampson, M. D.; Grice, K. A.; Smieja, J. M.; Froehlich, J. D.; Friebel, D.; Keith, J. A.; Carter, E. A.; Nilsson, A.; Kubiak, C. P. The Electronic States of Rhenium Bipyridyl Electrocatalysts for CO_2 Reduction as Revealed by X-Ray Absorption Spectroscopy and Computational Quantum Chemistry. *Angew. Chem. Int. Ed.* **2013,** *52*, 4841-4844.

33. Sampson, M. D.; Froehlich, J. D.; Smieja, J. M.; Benson, E. E.; Sharp, I. D.; Kubiak, C. P. Direct Observation of the Reduction of Carbon Dioxide by Rhenium Bipyridine Catalysts. *Energy Environ. Sci.* **2013,** *6*, 3748-3755.

34. Machan, C. W.; Chabolla, S. A.; Yin, J.; Gilson, M. K.; Tezcan, F. A.; Kubiak, C. P. Supramolecular Assembly Promotes the Electrocatalytic Reduction of Carbon Dioxide by Re(I) Bipyridine Catalysts at a Lower Overpotential. *J. Am. Chem. Soc.* **2014,** *136*, 14598-14607.

35. Waterland, M. R.; Gordon, K. C. Electronic Absorption, Resonance Raman and Excited-State Resonance Raman Spectroscopy of Rhenium(I) and Copper(I) Complexes, with Substituted Dipyrido[3,2-a:2′,3′-c]Phenazine Ligands, and Their Electron Reduced Products. *J. Raman Spectrosc.* **2000,** *31*, 243-253.

36. van der Salm, H.; Larsen, C. B.; McLay, J. R. W.; Fraser, M. G.; Lucas, N. T.; Gordon, K. C. Stretching the Phenazine MO in dppz: The Effect of Phenyl and Phenyl-Ethynyl Groups on the Photophysics of Re(I) dppz Complexes. *Dalton Trans.* **2014**, 17775-17785.

37. Kurz, P.; Probst, B.; Spingler, B.; Alberto, R. Ligand Variations in [ReX(Diimine)$(CO)_3$] Complexes: Effects on Photocatalytic CO_2 Reduction. *Eur. J. Inorg. Chem.* **2006,** *2006*, 2966-2974.

38. Bard, A. J.; Faulkner, L. R., *Electrochemical Methods: Fundamentals and Applications*. John Wiley & Sons: New York, 2001; Vol. Chapter 3.

39. Butsch, K.; Gust, R.; Klein, A.; Ott, I.; Romanski, M. Tuning the Electronic Properties of dppz-Ligands and Their Palladium(II) Complexes. *Dalton Trans.* **2010,** *39*, 4331-4340.

40. Waterland, M. R.; Gordon, K. C.; McGarvey, J. J.; Jayaweera, P. M. Spectroscopic and Electrochemical Studies of a Series of Copper(I) and Rhenium(I) Complexes with Substituted Dipyrido[3,2-a:2',3'-c]Phenazine Ligands. *J. Chem. Soc., Dalton Trans.* **1998**, 609-616.

41. Jones, J. E.; Jenkins, R. L.; Hicks, R. S.; Hallett, A. J.; Pope, S. J. A. Water-Soluble, Luminescent Iridium(III)-Ytterbium(III) Complexes Using Dipyrido[3,2-a:2',3'-c]Phenazine Derivatives as Bridging Units. *Dalton Trans.* **2012,** *41*, 10372-10381.

42. Ben-David, H.; Iron, M. A.; Neumann, R. Platinum Complexes of Cationic Ligands for the Aerobic Oxidation of "Inert" Perfluoro-Substituted Alcohols. *Chem. Commun.* **2013,** *49*, 1720-1722.

43. Gottlieb, H. E.; Kotlyar, V.; Nudelman, A. NMR Chemical Shifts of Common Laboratory Solvents as Trace Impurities. *J. Org. Chem.* **1997,** *62*, 7512-7515.

44. Fujita, E.; Szalda, D. J.; Creutz, C.; Sutin, N. Carbon Dioxide Activation: Thermodynamics of Carbon Dioxide Binding and the Involvement of Two Cobalt Centers in the Reduction of Carbon Dioxide by a Cobalt(I) Macrocycle. *J. Am. Chem. Soc.* **1988,** *110*, 4870-4871.

45. Gennaro, A.; Isse, A. A.; Vianello, E. Solubility and Electrochemical Determination of CO_2 in Some Dipolar Aprotic Solvents. *J. Electroanal. Chem. Interfacial Electrochem.* **1990,** *289*, 203-215.

46. Sousa, S. F.; Sampaio, R. N.; Barbosa Neto, N. M.; Machado, A. E. H.; Patrocinio, A. O. T. The Photophysics of *fac*-[$Re(CO)_3(NN)(bpa)$]+ Complexes: A Theoretical/Experimental Study. *Photochem. Photobiol. Sci.* **2014,** *13*, 1213-1224.

47. Dreyse, P.; Isaacs, M.; Calfumán, K.; Cáceres, C.; Aliaga, A.; Aguirre, M. J.; Villagra, D. Electrochemical Reduction of Nitrite at Poly-[$Ru(5\text{-}NO_2\text{-}Phen)_2Cl$] Tetrapyridylporphyrin Glassy Carbon Modified Electrode. *Electrochim. Acta* **2011,** *56*, 5230-5237.

48. Smieja, J. M.; Sampson, M. D.; Grice, K. A.; Benson, E. E.; Froehlich, J. D.; Kubiak, C. P. Manganese as a Substitute for Rhenium in CO_2 Reduction Catalysts: The Importance of Acids. *Inorg. Chem.* **2013,** *52*, 2484-2491.

49. Qiao, X.; Li, Q.; Schaugaard, R. N.; Noffke, B. W.; Liu, Y.; Li, D.; Liu, L.; Raghavachari, K.; Li, L.-S. Well-Defined Nanographene–Rhenium Complex as an Efficient Electrocatalyst and Photocatalyst for Selective CO_2 Reduction. *J. Am. Chem. Soc.* **2017,** *139*, 3934-3937.

APPENDIX: CRYSTAL TABLES

1. SAINT V8.27B Bruker AXS Inc, (2012), Madison, WI.

2. Sheldrick, G. M. (2015). SHELXT. *Acta Cryst. A71*, 3-8.

3. Sheldrick, G. M. (2015). SHELXL-2014/7. Program for the Refinement of Crystal Structures. *Acta Cryst. C91*, 9-18.

4. Spek, A. L. (1998). PLATON, A Multipurpose Crystallographic Tool. Utrecht University, The Netherlands.

5. WinGX 1.64. (1999). An Integrated System of Windows Programs for the Solution, Refinement and Analysis of Single Crystal X-ray Diffraction Data. Farrugia, L. J. *J. Appl. Cryst. 32*. 837-838.

6. $R_W(F^2) = \{w(|F_O|^2 - |F_C|^2)^2/w(|F_O|)^4\}^{1/2}$ where w is the weight given each reflection. $R(F) = (|F_O| - |F_C|)/|F_O|\}$ for reflections with $F_O > 4 ((F_O))$. $S = [w(|F_O|^2 - |F_C|^2)^2/(n - p)]^{1/2}$, where n is the number of reflections and p is the number of refined parameters.

7. International Tables for X-ray Crystallography (1992). Vol. C, Tables 4.2.6.8 and 6.1.1.4, A. J. C. Wilson, editor, Boston: Kluwer Academic Press.

8. Sheldrick, G. M. (1994). SHELXTL/PC (Version 5.03). Siemens Analytical X-ray Instruments, Inc., Madison, Wisconsin, USA.

9. SIR97. (1999). A program for crystal structure solution. Altomare A., Burla M.C., Camalli M., Cascarano G.L., Giacovazzo C. , Guagliardi A., Moliterni A.G.G., Polidori G.,Spagna R. *J. Appl. Cryst. 32*, 115-119.

10. Sluis, P. v. d. and Spek, A. L. (1990). SQUEEZE. *Acta Cryst. A46*, 194-201.

11. Sheldrick, G. M. (2008). SHELXL-2013. Program for the Refinement of Crystal Structures. *Acta Cryst. A64*, 112-122.

12. Crystal Clear, 1.40, Rigaku Americas Corporation, The woodlands, Texas, USA, 2008.

13. Sheldrick, G. M. *Acta Cryst.* **2008**, *A64*, 112. SHELXL97: Program for the Refinement of Crystal Structures, University of Gottingen: Gottingen, Germany, 1994.

14. CrysAlisPro. Agilent Technologies (2013). Agilent Technologies UK Ltd., Oxford, UK, SuperNova CCD System, CrysAlicPro Software System, 1.171.37.31.

15. SuperFlip. (2007). A program for crystal structure solution. Palatinus, L. and Chapuis, G. *J. Appl. Cryst. 40*, 786-790.